Institut für Biochemie und Biologie

Arbeitsgruppe Molekulare Enzymologie

A-Type Carrier Proteins are involved in [4Fe-4S] Cluster insertion into the Radical S-adenosylmethionine (SAM) Protein MoaA and other molybdoenzymes

Muhammad Abrar Hasnat

Dissertation
zur Erlangung des akademischen Grades
"doctor rerum naturalium"
(Dr. rer. nat.)
in der Wissenschaftsdisziplin "Biochemie"

eingereicht an der
Mathematisch-Naturwissenschaftlichen Fakultät
Institut für Biochemie und Biologie
der Universität Potsdam

Published online on the
Publication Server of the University of Potsdam:
https://doi.org/10.25932/publishup-53079
https://nbn-resolving.org/urn:nbn:de:kobv:517-opus4-530791

Publications of the dissertation

Partial results from this work were published with the permission of the Institute for Biochemistry and Biology, represented by the head of the working group Prof. Dr. Silke Leimkühler, in the following articles published in advance:

Publications:

Hasnat, A.M., Zupok, A., Olas, J.J., Müller-Röber, B., Leimkühler, S. (2021) A-type carrier proteins are involved in [4Fe-4S] cluster insertion into the radical SAM protein MoaA for the synthesis of active molybdoenzymes. J. Bacteriol.; doi.org/10.1128/JB.00086-21

Mendel, R.R., Hercher, T.W., Zupok, A., Hasnat, M.A., Leimkühler, S. The Requirement of Inorganic Fe-S Clusters for the Biosynthesis of the Organometallic Molybdenum Cofactor. (2020) Inorganics, 8 (7): doi 10.3390/inorganics8070043

Conference contributions:

Muhammad Abrar Hasnat, Dr. Silke Leimkühler. 'Dissecting the proteins that insert Fe-S clusters into enzymes involved in the biosynthesis of the molybdenum cofactor and into molybdoenzymes in *Escherichia coli.*' Poster presentation, XI Molybdenum & Tungsten Enzyme Conference 2019, Potsdam.

Muhammad Abrar Hasnat, Dr. Silke Leimkühler. 'Dissecting the proteins that insert Fe-S clusters into enzymes involved in the biosynthesis of the molybdenum cofactor or into molybdoenzymes in *Escherichia coli*'. Oral presentation, Iron sulfur cluster for life meeting 2018, Potsdam.

Muhammad Abrar Hasnat, Dr. Silke Leimkühler. 'Dissecting the proteins that insert Fe-S clusters into enzymes involved in the biosynthesis of the molybdenum cofactor or into molybdoenzymes in *Escherichia coli*'. Poster presentation, Iron sulfur cluster for life: Summer school meeting 2017 (Leipzig), 2018 (Freiburg), 2019 (Berlin).

Declaration of Academic Honesty

I Muhammad Abrar Hasnat, hereby declare that I have not carried out this dissertation on anyone else Submitted to the university and prepared it independently and without unauthorized aids and no sources and resources other than those specified have been used by me.

Potsdam, 27.05.2021 Muhammad Abrar Hasnat

Acknowledgment

Foremost, I would like to express my sincere gratitude and thanks to my supervisor, Professor Dr. Silke Leimkühler for the scientific, motivational, and personal support during these years and for giving me the opportunity to work in this exciting project.

Besides that, I want to thank the members of the iron-sulfur cluster for life SPP- 1927 for helping me with different ideas and discussions. Moreover, my sincere thanks to Prof. Dr. Bernd Mueller-Roeber and Dr. Justyna Jadwiga Olas from the Department of Molecular Biology, the University of Potsdam for the tremendous support they gave me for the gene expression experiments.

I would like to thank all the members of my working group Molecular Enzymology, in particular Dr. Arkadiusz Zupok, Dr. Sebastian Keller and Akanksha Moga, for their fantastic help during these years. Moreover, I also thank Jasmin Kurtzke and Angelika Lehmann for their incredible support.

Finally, an enormous thanks to my family members in Bangladesh and all friends in both Germany and Bangladesh. Without your moral support, nothing could be possible.

Summary

Iron-sulfur clusters are essential enzyme cofactors. The most common and stable clusters are [2Fe-2S] and [4Fe-4S] that are found in nature. They are involved in crucial biological processes like respiration, gene regulation, protein translation, replication and DNA repair in prokaryotes and eukaryotes. In *Escherichia coli*, Fe-S clusters are essential for molybdenum cofactor (Moco) biosynthesis, which is a ubiquitous and highly conserved pathway. The first step of Moco biosynthesis is catalyzed by the MoaA protein to produce cyclic pyranopterin monophosphate (cPMP) from 5'GTP. MoaA is a [4Fe-4S] cluster containing radical S-adenosyl-L-methionine (SAM) enzyme. The focus of this study was to investigate Fe-S cluster insertion into MoaA under nitrate and TMAO respiratory conditions using *E. coli* as a model organism. Nitrate and TMAO respiration usually occur under anaerobic conditions, where oxygen is depleted. Under these conditions, *E. coli* uses nitrate and TMAO as terminal electron. Previous studies revealed that Fe-S cluster insertion is performed by Fe-S cluster carrier proteins. In *E. coli*, these proteins are known as A-type carrier proteins (ATC) by phylogenomic and genetic studies. So far, three of them have been characterized in detail in E. coli, namely IscA, SufA, and ErpA. This study shows that ErpA and IscA are involved in Fe-S cluster insertion into MoaA under nitrate and TMAO respiratory conditions. ErpA and IscA can partially replace each other in their role to provide [4Fe-4S] clusters for MoaA. SufA is not able to replace the functions of IscA or ErpA under nitrate respiratory conditions.

Nitrate reductase is a molybdoenzyme that coordinates Moco and Fe-S clusters. Under nitrate respiratory conditions, the expression of nitrate reductase is significantly increased in *E. coli*. Nitrate reductase is encoded in *narGHJI* genes, the expression of which is regulated by the transcriptional regulator, fumarate and nitrate reduction (FNR). The activation of FNR under conditions of nitrate respiration requires one [4Fe-4S] cluster. In this part of the study, we analyzed the insertion of Fe-S cluster into FNR for the expression of *narGHJI* genes in *E. coli*. The results indicate that ErpA is essential for the FNR-dependent expression of the *narGHJI* genes, a role that can be replaced partially by IscA and SufA when they are produced sufficiently under the conditions tested. This observation suggests that ErpA is indirectly regulating nitrate reductase expression via inserting Fe-S clusters into FNR.

Most molybdoenzymes are complex multi-subunit and multi-cofactor-containing enzymes that coordinate Fe-S clusters, which are functioning as electron transfer chains for catalysis. In *E. coli*, periplasmic aldehyde oxidoreductase (PaoAC) is a heterotrimeric molybdoenzyme that

consists of flavin, two [2Fe-2S], one [4Fe-4S] cluster and Moco. In the last part of this study, we investigated the insertion of Fe-S clusters into *E. coli* periplasmic aldehyde oxidoreductase (PaoAC). The results show that SufA and ErpA are involved in inserting [4Fe-4S] and [2Fe-2S] clusters into PaoABC, respectively under aerobic respiratory conditions.

Table of Contents

1 Introduction 1
1.1 Iron in biological systems 1
1.2 Sulfur and L-cysteine desulfurases 2
1.3 Fe-S clusters 6
1.3.1 The ISC system 7
1.3.2 The SUF system 10
1.3.3 Fe-S cluster homeostasis in *E. coli* 11
1.4 Fe-S cluster carrier proteins 13
1.4.1 DNA-binding transcriptional regulator – BolA 13
1.4.2 Glutaredoxins – GrxA, GrxB, GrxC and GrxD 13
1.4.3 P-loop NTPase family protein – Mrp 14
1.4.4 A-type carrier proteins (ATC) – ErpA, IscA, SufA 14
1.4.5 Atypical A-type carrier protein (ATC) – NfuA 16
1.5 Molybdenum cofactor (Moco) biosynthesis and molybdoenzymes 17
1.5.1 Moco biosynthesis 17
1.5.2 Moco sulfuration and insertion into enzymes of the DMSO reductase family . 23
1.5.3 Regulation of Moco biosynthesis 24
1.5.4 Molybdoenzymes 25
1.6 Fumarate and nitrate reduction (FNR) 30
1.7 Aims and Objectives 31
2 Materials and methods 34
2.1 Materials 34
2.1.1 Media and buffers 34
2.1.2 Antibiotics 35
2.1.3 Plasmids 36
2.1.4 Bacterial strains 37
2.1.5 Oligonucleotides 39
2.1.6 Enzymes 39
2.1.7 Markers and dyes 39
2.1.8 Kits 39
2.1.9 Growth curves 40
2.2 Methods 40
2.2.1 Molecular Biology 40
2.2.2 Biochemical Methods 50
3 Results 66
3.1 Analysis of nitrate reductase activity and Moco content 66

3.1.1 The influence of glucose on nitrate reductase activity under anaerobic conditions 66
3.1.2 Nitrate reductase activity under anaerobic conditions of nitrate respiration 67
3.1.3 Moco content and nitrate reductase activity under anaerobic and aerobic conditions 68
3.1.4 Growth curves of the strains under anaerobic conditions of nitrate respiration 71
3.1.5 Nitrate reductase activity in different mutant strains under anaerobic conditions of nitrate respiration 72
3.1.6 Quantification cPMP and Moco in different mutant strains under anaerobic conditions of nitrate respiration 74
3.1.7 Complementation study with *erpA, iscA* and *sufA* expression plasmid 77
3.1.8 Investigation of the expression of the *moaABCDE* operon 79
3.1.9 Immunodetection of MoaC 80
3.1.10 Immunodetection of IscS 81
3.1.11 The expression of IscR and SufA in mutant strains 82
3.1.12 Immunodetection of SufS 85
3.1.13 Detection of relative iron content in *erpA* and *iscA* deleted strains under anaerobic nitrate respiratory conditions 87
3.1.14 Detection of *erpA* and *iscA* transcripts 88
3.1.15 Detection of *sufA* transcripts under anaerobic nitrate respiratory conditions .. 90
3.1.16 Detection of *narG* transcripts under anaerobic nitrate respiratory conditions .. 91
3.2 Fe-S cluster insertion into FNR 92
3.2.1 Insertion of Fe-S clusters into FNR under anaerobic nitrate respiratory conditions 92
3.2.2 Analysis of FNR expression under anaerobic nitrate respiratory conditions ... 94
3.2.3 Analysis of *PpepT-lacZ* expression after complementation with *erpA, sufA,* and *iscA* plasmid under anaerobic respiratory conditions 95
3.3 Analysis of TMAO reductase expression and activities 97
3.3.1 Growth curves of the strains under anaerobic TMAO respiratory conditions .. 97
3.3.2 Quantification of cPMP and Moco under anaerobic TMAO respiratory conditions 99
3.3.3 TMAOR activity under anaerobic conditions of TMAO respiration 101
3.3.4 Expression of *torCAD* under anaerobic TMAO respiratory conditions 102
3.3.5 Immunodetection of TorA 104
3.4 Expression and purification of periplasmic aldehyde oxidase (PaoABC) from different *E. coli* mutant strains 106
3.4.1 Expression of EcPaoABC in *E. coli* mutant strains 107
3.4.2 Size exclusion chromatography (SEC) 107
3.4.3 Characterization of periplasmic aldehyde oxidase 109
3.5 Expression and purification of xanthine dehydrogenase from *R. capsulatus* 117

3.5.1 Expression of RcXDH in mutant strains 117
3.5.2 Ni-NTA affinity and size exclusion chromatography 118
3.5.3 Characterization of purified RcXDH 120
4 Discussion 128
4.1 Fe-S cluster insertion into MoaA and FNR under anaerobic nitrate respiratory conditions 128
4.1.1 Cross-talk between Fe-S and Moco biosynthesis 128
4.1.2 MoaA maturation under anaerobic conditions 129
4.1.3 FNR regulatory network under anaerobic nitrate respiratory conditions 132
4.1.4 The dominant expression of the *isc* operon compared to the *suf* operon under nitrate respiratory conditions 137
4.1.5 The influence of iron content in *erpA*- and *iscA*-deleted strains under nitrate respiratory conditions 141
4.2 Regulation of *torCAD* expression under anaerobic TMAO respiratory conditions 142
4.3 Model for Fe-S clusters insertion under nitrate and TMAO respiratory conditions 143
4.4 Fe-S cluster insertion in MoaA under aerobic conditions 145
4.5 Maturation of EcPaoABC and RcXDH 146
4.5.1 ErpA is essential for the maturation of EcPaoABC 146
4.5.2 Purification of RcXDH from *E. coli* mutant strains 149
4.6 Model for Fe-S clusters insertion into EcPaoABC and RcXDH under aerobic respiratory conditions 150
5 Outlook 153
6 References 155
7 Appendix 199

List of figures

Figure 1-1: The iron intake mechanism by siderophore transporter 1
Figure 1-2: The importance of L-cysteine desulfurase for the biosynthesis of sulfur-containing biomolecules 3
Figure 1-3: Schematic sequence comparisons of two groups of L-cysteine desulfurases 4
Figure 1-4: Reaction mechanism of formation of L-cysteine by L-cysteine desulfurase 5
Figure 1-5: The different forms of naturally abundant Fe-S clusters and their involvement in the biological process 6
Figure 1-6: Assembly of the Fe-S cluster in the Isc system 7
Figure 1-7: The proposed model for chaperone-mediated Fe-S clusters' transfer into the apo-target from the IscS-IscU complex 9
Figure 1-8: Fe-S cluster biogenesis in the Suf system under iron-limiting or oxidative stress condition 10
Figure 1-9: The proposed model for iron-dependent genetic regulation of Fe-S clusters' homeostasis by Isc and Suf systems in *E. coli* 12
Figure 1-10: Amino acid sequence alignment of A-type carrier proteins (ATC), IscA, SufA, and ErpA (YadR) from different organisms 15
Figure 1-11: The operons involved in Moco biosynthesis in *E. coli* 18
Figure 1-12: Biosynthesis of cPMP from 5'GTP catalyzed by MoaA and MoaC 19
Figure 1-13: Schematic diagram of Moco biosynthesis in *E. coli* 21
Figure 1-14: Overall transcriptional regulation of the *moa* and *moe* operon 24
Figure 1-15: Overall transcriptional regulation of the *narGHJI* operon 26
Figure 1-16: Model for the regulation of TMAO reductase in *E. coli* under anaerobic conditions 27
Figure 1-17: Schematic representation of membrane-bound nitrate reductase (NR), TMAO reductase (TMAOR), periplasmic aldehyde oxidase (PaoABC) in *E. coli,* and xanthine dehydrogenase (XDH) from *R. capsulatus* 29
Figure 1-18: Schematic representation of cross-talk between Moco biosynthesis and Fe-S clusters' assembly in *E. coli* 32
Figure 2-1: Site-direct mutagenesis by PCR 48
Figure 2-2: Flow scheme for single-gene knock-out using the λ-red system 49
Figure 2-3: Principle of IMAC (immobilized metal affinity chromatography) 53
Figure 2-4: Scheme for the detection of Moco and cPMP from *E. coli* cell extract 59
Figure 2-5: Determination of nitrate reductase and TMAO reductase activity from the *E. coli* cell lysate 62
Figure 3-1: Analysis of nitrate reductase activity in *E. coli* Wt BW25113 strain 67
Figure 3-2: Analysis of nitrate reductase activity in *E. coli* mutant strains 68
Figure 3-3: Analysis of relative Moco content and nitrate reductase activity in *E. coli* mutant strains 69
Figure 3-4: Analysis of the growth curves of *E. coli* mutant strains 71
Figure 3-5: Analysis of nitrate reductase activity in *E. coli* mutant strains 72
Figure 3-6: Analysis of relative cPMP and Moco content in *E. coli* mutant strains 75
Figure 3-7: Analysis of Moco content and nitrate reductase activity in *E. coli* mutant strains 78
Figure 3-8: Analysis of the expression of a *PmoaA-L-LacZ* fusion in *E. coli* mutant strains . 80
Figure 3-9: Immunodetection of MoaC in *E. coli* mutant strains. 81
Figure 3-10: Immunodetection of IscS in *E. coli* mutant strains. 82
Figure 3-11: Expression of a *PiscR-lacZ* and a *PsufA-lacZ* fusion in *E. coli* mutant strains . 84
Figure 3-12: Immunodetection of SufS in *E. coli* mutant strains. 86
Figure 3-13: Analysis of relative iron saturation in *E. coli* mutant strains 87

Figure 3-14: Analysis of relative expression levels of *erpA* and *iscA* in *E. coli* mutant strains 89
Figure 3-15: Analysis of relative expression levels of *sufA* in *E. coli* mutant strains..... 90
Figure 3-16: Analysis of relative expression levels of *narG* in *E. coli* mutant strains..... 92
Figure 3-17: Expression of a *PpepT-lacZ* fusion in *E. coli* mutant strains 93
Figure 3-18: Expression of a *Pfnr-lacZ* fusion in *E. coli* mutant strains 94
Figure 3-19: Expression of a *PpepT-lacZ* fusion in *E. coli* mutant strains with coexpression of plasmids containing *erpA, iscA,* and *sufA.*..... 96
Figure 3-20: Analysis of the growth curves of *E. coli* mutant strains 98
Figure 3-21: Analysis of relative cPMP and Moco content in *E. coli* mutant strains 100
Figure 3-22: Analysis of TMAOR activity in *E. coli* mutant strains..... 101
Figure 3-23: Expression of a *PtorCAD-lacZ* fusion in *E. coli* mutant strains..... 103
Figure 3-24: Immunodetection of TorA in *E. coli* mutant strains. 104
Figure 3-25: Analysis of predicted FNR binding site at upstream of the *torCAD* operon 105
Figure 3-26: Expression of a *PtorCAD-lacZ* fusion in *E. coli* mutant strains..... 106
Figure 3-27: Gel filtration chromatograms of the purified EcPaoABC expressed in different *E. coli* mutant strains 109
Figure 3-28: Analysis of UV-visible spectrum from purified EcPaoABC expressed in different *E. coli* mutant strains..... 110
Figure 3-29: Analysis of relative molybdenum and iron saturation from EcPaoABC expressed in different *E. coli* mutant strains 112
Figure 3-30: Analysis of relative Moco content from purified EcPaoABC (A) and cell extract (B) in different *E. coli* mutant strains..... 113
Figure 3-31: Analysis of relative FAD content from EcPaoABC expressed in different *E. coli* mutant strains 114
Figure 3-32: Analysis of the specific activity from purified EcPaoABC expressed in different *E. coli* mutant strains..... 115
Figure 3-33: Analysis of CD spectra from purified EcPaoABC expressed in different *E. coli* mutant strains 116
Figure 3-34: Gel filtration chromatograms of the purified RcXDH expressed in different *E. coli* mutant strains 120
Figure 3-35: Analysis of UV-visible spectrum from purified RcXDH expressed in different *E. coli* mutant strains 121
Figure 3-36: Analysis of relative molybdenum and iron saturation from RcXDH expressed in different *E. coli* mutant strains 122
Figure 3-37: Analysis of relative Moco content from purified RcXDH expressed in different *E. coli* mutant strains 124
Figure 3-38: Analysis of relative FAD content from RcXDH expressed in different *E. coli* mutant strains 125
Figure 3-39: Analysis of the specific activity from purified RcXDH expressed in different *E. coli* mutant strains 126
Figure 3-40: Analysis of CD spectra from purified RcXDH expressed in different *E. coli* strains 127
Figure 4-1: The insertion of Fe-S clusters into the MoaA in *E. coli* under nitrate respiratory conditions..... 131
Figure 4-2: The insertion of Fe-S clusters into FNR under nitrate respiratory conditions ... 135
Figure 4-3: Model for apo-IscR regulation of the *suf* operon and degradation of the *isc* operon in the presence of iron..... 137
Figure 4-4: Analysis of iscR expression in the *Δfnr* strain under anaerobic nitrate respiratory conditions..... 138

Figure 4-5: Analysis of the expression of the *suf* operon in the *Δfnr* strain under nitrate respiratory conditions 139
Figure 4-6: Model for Fe-S clusters' insertion into MoaA and FNR under anaerobic nitrate respiratory conditions 144
Figure 4-7: Model for Fe-S clusters' insertion into RcXDH and EcPaoABC under aerobic respiratory conditions 152

List of tables

Table 2-1: The list of media and buffers was used in this study 34
Table 2-2: The list of plasmids was used in this study 36
Table 2-3: The list of strains was used in this study 37
Table 2-4: The list of Kits was used in this study 39
Table 2-5: Composition of PCR reaction for gene amplification 42
Table 2-6: Composition of PCR reaction for gene verification 43
Table 2-7: Reaction composition of restriction digestion 43
Table 2-8: Reaction composition of vector and insert ligation 44
Table 2-9: Composition of PCR reaction for site-directed mutagenesis 47
Table 2-10: Overview of the expressed proteins in this study with expression conditions, plasmids, inducer and respective antibiotics 50
Table 2-11: Components for preparation of separation (12% and 17%) and stacking gel (5%) was used in this study 54
Table 2-12: Molecular weight and extinction coefficient (280 nm, 445 nm and 465 nm) for EcPaoABC and RcXDH 56
Table 2-13: Overview of antibodies and membranes were used for immunodetection of the respective proteins in this study 57
Table 2-14: Reaction composition for measuring NR and TMAOR activity 63
Table 2-15: Reaction composition for measuring EcPaoABC and RcXDH activity 65
Table 3-1: The absorbance ratio between 280 nm and 445 nm of purified EcPaoABC expressed in *E. coli* mutant strains 110
Table 3-2: The absorbance ratio between 280 nm and 445 nm of purified RcXDH expressed in *E. coli* mutant strains 121
Table 7-1: The list of oligonucleotides was used for this study 199

List of abbreviations

°C	degree Celsius
µL, mL, L	microliter, milliliter, liter
ABC	ATP binding cassette
ADP	Adenosine diphosphate
Ala	Alanine
Amp	Ampicillin
AMP	Adenine mono phosphate
AncB/A	Aconitase B/A
AP	Alkaline phosphatase
APS	Ammonium persulfate
ATC	A-type carrier
ATP	Adenosine triphosphate
A_{xxx}	Absorbance with indicated wavelength
BSA	Bovine Serum Albumin
$CaCl_2$	Calcium chloride
Cat	Chloramphenicol
CD	Circular dichroism
cDNA	copy DNA
Cm	Centimetre
CMP	Cytidine monophosphate
cPMP	Cyclic pyranopterin monophosphate
CV	Column volume
Cys	Cysteine
DMSOR	Dimethyl sulfoxide reductase
DNA	Deoxyribonucleic acid
DTT	Dithiothreitol
EDTA	Ethylenediamine-tetra-acetic acid
ErpA	Essential respiratory protein A
FAD	Flavin adenine dinucleotide
Fdh	Format dehydrogenase
Fdn	Formate dehydrogenase
Fdx	Ferredoxin
Fe-S	Iron sulfur

Flp	Flipase
FNR	fumarate and nitrate reductase
dA	Deoxyadenosyl
FXN	Frataxin
g, mg, µg, ng	gram, milligram, microgram, nanogram
GMP	Guanosine monophosphate
Grx	Glutaredoxins
GTP	Guanosine triphosphate
h, min, sec	Hour, minute, second
H_2O_2	Hydrogen peroxide
HCl	Hydrochloric acid
His-tag	Six histidines in a row
HPLC	High pressure liquid chromatography
I_2/KI	Iodine/potassium iodide
ICP-OES	Inductively coupled plasma optical emission spectroscopy
IPP	Isopentenyl diphosphate
IPTG	Isopropyl-β-D-thiogalactopyranoside
ISC	Iron Sulfur Cluster
K(bps)	Kilo (base pairs)
K2HPO4	Potassium biphosphate
Kan	Kanamycine
kDa	Kilo Dalton
KH_2PO_4	Potassium dihydrogen phosphate
KNO_3	Potassium Nitrate
KOH	Potassium hydroxide
kV	Kilo Volt
LB	Luria broth
LipA	Lipoyl synthase A
M, mM, µM, nM	molar, milimolar, micromolar, nanomolar
mA	Milli Ampere
MCD	Molybdopterin-cytosine-dinucleotide
MES	*N*-(morpholino)ethanesulfonic acid
$MgCl_2$	Magnesium chloride
MGD	Molybdopterin-guanine-dinucleotide
$MgSO_4$	Magnesium sulfate

Mo	Molybdenum
Moco	Molybdenum cofactor
MOCS	Molybdenum cofactor synthesis
mol, µmol, mmol, pmol	molar, milimolar, micromolar, nanomolar, picomolar
MPT	Molybdopterin
mRNA	messenger RNA
MW	Molecular Weight
MWCO	Molecular weight cut off
n.d.	Not detectable
Na_2HPO_4	Sodium biphosphate
NaCl	Sodium chloride
NAD	Nicotinamid adenine dinucleotide
NaOH	Sodium hydroxide
Nap	Periplasmic nitrate reductase
Nar	Membrane bound nitrate reductase
NAT	Nitrilotriacetic acid
Ni^{++}	Nickle
Nif	Nitrogen fixation
NR	Nitrate reductase
OD	Optical density
ONPG	Ortho-nitrophenyl-β-D-galactopyranoside
PaoABC	Periplasmic aldehyde oxidase
PCR	Polymerase chain reaction
pepT	Peptidase T
PLP	Pyridoxal-5'-phosphate
QAE	Quaternary ammonium ion exchange
qRT-PCR	Quantitative real time Polymerase chain reaction
RNA	Ribonucleic acid
ROS	Radical oxygen species
Rpm	Rotations per minute
RT	Reverse transcriptase
SAM	S-adenosyl methionine
SDS-PAGE	Sodium dodecyl sulphate polyacrylamide gel electrophoresis
SEC	Size Exclusion chromatography

SO	Sulfite oxidase
Spec	spectinomycin
SUF	Sulfur mobilization
TBS-T	Tris-buffered saline – Tween 20
TMAOR	Trimethylamine N-oxide reductase
TEMED	Tetra methyl ethyl enediamine
U	Unit (of enzyme activity)
v/v	Volume per volume
w/v	Weight per volume
Wt	Wildytpe
XDH	Xanthine dehydrogenase
xg	Gravity
XO	Xanthine Oxidase

1 Introduction

1.1 Iron in biological systems

Iron is an essential element in all forms of life, which involves many kinds of physiological activity (Wang et al., 2019). It is a crucial element for numerous biological reactions such as nitrogen fixation, ATP production, DNA synthesis, oxygen transport, respiration, electron transport, the citric acid cycle, and many other physiological processes (E. S. Boyd et al., 2014; Dixon & Stockwell, 2014; Wang et al., 2019). Iron is the fourth most abundant element on Earth, and appears in two different forms: iron (II) and iron (III) (P. A. Frey & Reed, 2012). Iron (III) is very poorly soluble under physiological conditions. Free iron (II, III) can damage cells or DNA as a result of oxidative stress (Andrews, Robinson, and Rodríguez-Quiñones, 2003; Dixon and Stockwell, 2014). This is known as the Haber–Weiss and Fenton reaction. Free hydroxyl radicals ($^{\cdot}OH$) are generated from hydrogen peroxide (H_2O_2) and superoxide ($^{\cdot}O_2^-$), which is catalysed by free iron (II, III). Free radicals are the main culprit responsible for cellular oxidative stress.

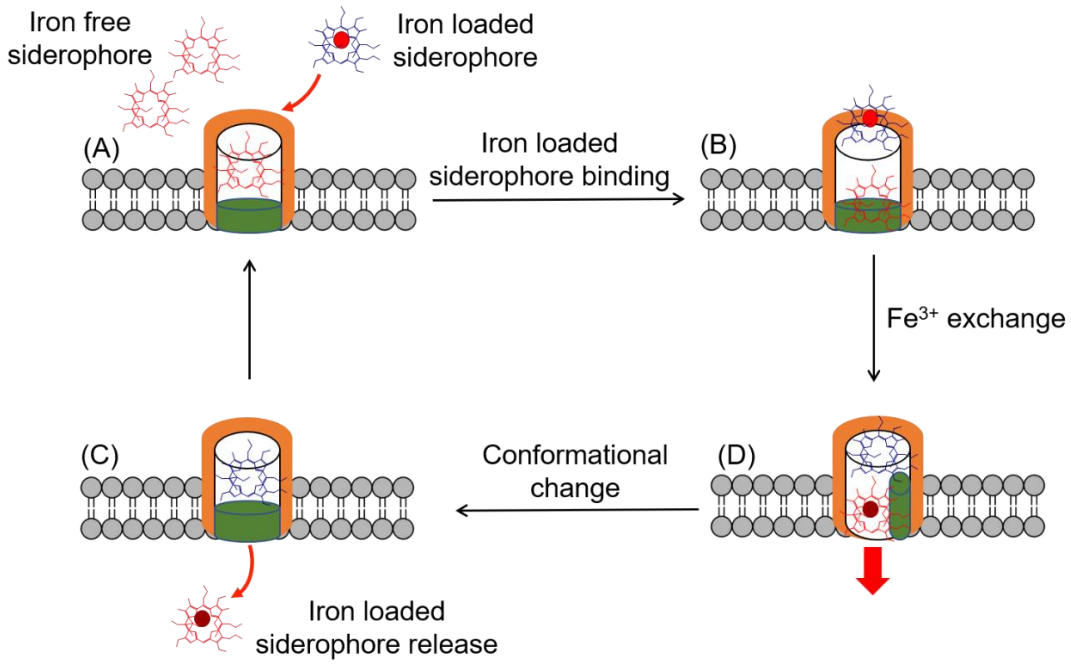

Figure 1-1: The iron intake mechanism by siderophore transporter

The proposed iron exchange mechanism via siderophore transporter in iron intake for gram-negative bacteria (Stintzi et al., 2000). The steps are (A) the iron-loaded siderophore, (B) exchange of Fe^{3+} by a pH gradient, (C) conformational changes of the receptor, and (D) release of the iron to the periplasm

Therefore, the cell has a strict mechanism to avoid potential iron-related toxicity by iron homeostasis. It regulates iron uptake and storage depending upon the availability of iron in nature (Andrews, Robinson, and Rodríguez-Quiñones, 2003). In *E. coli*, iron uptake is performed by the high-affinity iron (III) siderophores, associated with a transport system. Iron uptake takes place in four steps: a) iron (III) loaded siderophore, b) iron (III)-siderophore exchange by pH gradient, c) conformational change of receptor, and d) release of iron into the periplasmic space (Stintzi et al., 2000).

The siderophore is highly specific to iron (III) and makes an Fe^{3+}-siderophore complex (Andrews et al., 2003; Neilands, 1981). Fe^{3+} is exchanged by the binding protein and is attached to the multifunctional receptor. An ATP-dependent reaction takes place to transport the complex into the cytosol (Köster, 2001; Krewulak & Vogel, 2008), where the iron (III) is converted to iron (II) by iron (III) reductase and released from the receptor (Fontecave, 2006). The iron-free siderophore can then be exported and is available for the next cycle (Cowart, 2002; Furrer et al., 2002).

1.2 Sulfur and L-cysteine desulfurases

Sulfur is an essential element in living organisms and is present in cofactors, nucleotides, amino acids, vitamins, and other components (Kessler, 2006; Mueller, 2006). Sulfur has a unique characteristic, acting both as an electrophile (e.g., disulfides) and as a nucleophile (e.g., thiols) (Beinert, 2000a, 2000b). Sulfur is present in cysteine and methionine amino acids, where it plays an important role in protein folding, conformation, coordination of metal, and other functions (Kessler, 2006; Nagahara et al., 2009). Sulfur is present as persulfide, bound to a cysteine residue (Kessler, 2006; Mueller, 2006). The cells absorb sulfur as sulfate (SO_4^{2-}) from nature and consequently reduce it to sulfite (SO_3). Sulfite is further reduced into hydrosulfide (HSO_3) and converted into L-cysteine from O-acetylserine (Sekowska, Danchin, and Risler, 2000; Hullo et al., 2007). L-cysteine is the major source of sulfur in cells. It is used for the formation of a variety of sulfur-containing compounds such as molybdenum cofactor (Moco), biotin, thiamin, lipoic acid, and thionucleosides, Fe-S clusters, ribonucleic acid, and others (Kessler, 2006). The persulfide is bound to a cysteine in proteins that protects sulfur against destabilization and oxidation in the cell.

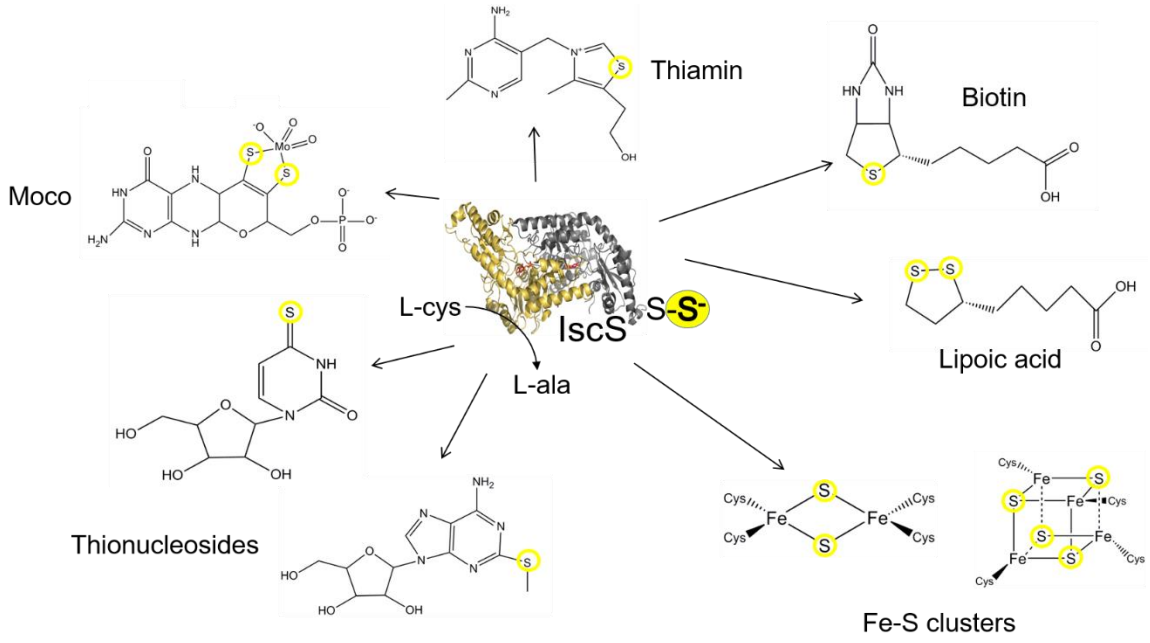

Figure 1-2: The importance of L-cysteine desulfurases for the biosynthesis of sulfur-containing biomolecules

The L-cysteine desulfurase mobilizes the sulfur as persulfide from L-cysteine; the persulfide functions as a source of sulfur for the biosynthesis of vitamins (biotin, thiamine), cofactors (Moco, Fe-S clusters, lipoic acid) and thionucleosides; IscS: PDB – 3LVM

In *E. coli*, sulfur atom mobilization is performed by L-cysteine desulfurases, which belong to the class of sulfurtransferase (Westley et al., 1983; Hidese, Mihara, and Esaki, 2011). The first L-cysteine desulfurase was characterized as NifS (nitrogen fixation) for nitrogen fixation in *Azotobacter vinelandii* by Dean and coworkers (Jacobson et al., 1989; L. Zheng et al., 1994). The enzyme catalyzes the conversion of L-cysteine to L-alanine via the formation of a cysteine persulfide (Jacobson et al., 1989; L. Zheng et al., 1994). The transfer of terminal sulfur to a cysteine residue in the acceptor protein provides sulfur in the biosynthesis of various sulfur-containing compounds such as Fe-S clusters, Moco, biotin, and thiamin (Kessler, 2006). L-cysteine desulfurases are homodimers and contain pyridoxal-5'-phosphate (PLP) as a cofactor (L. Zheng et al., 1994). In *E. coli*, three different NifS homologs have been identified, namely IscS, SufS, and CsdA (Flint, 1996; Mihara et al., 1997). Sequence analysis has shown that NifS has around 25-40% amino acid sequence homology with IscS (iron–sulfur cluster), SufS (sulfur mobilization), and CsdA (Mihara et al., 1999). The L-cysteine desulfurases can be divided into two groups based on their specific amino acid sequence characteristics. NifS and IscS belong to group 1 L-cysteine desulfurases, and group 2 consists of SufS and CsdA (Mihara et al., 1997, 1999). Group 1 can be characterized by a conserved flexible long-loop motif with a unique

cysteine residue. On the other hand, group 2 represents a smaller and structurally rigid loop (Mihara et al., 1997; Cupp-Vickery, Urbina, and Vickery, 2003; Kessler, 2006).

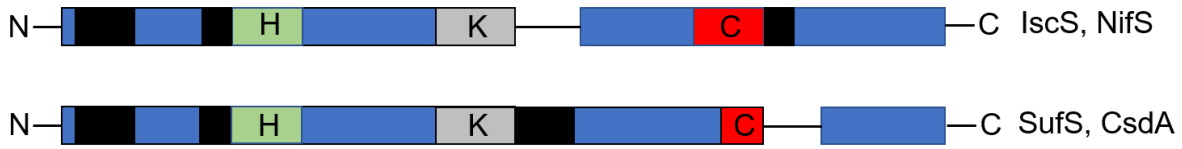

Figure 1-3: Schematic sequence comparisons of two groups of L-cysteine desulfurases

The high variability of sequence regions is shown in black, the gaps in sequences are bridged; the amino acid residues histidine (H), lysine (K), and cysteine (C) are physiologically essential; the conserved lysine (K) binds to the PLP cofactor

The formation of a persulfide from L-cysteine is a precise multistep mechanism with the direct involvement of the PLP cofactor of the L-cysteine desulfurases (L. Zheng et al., 1993).

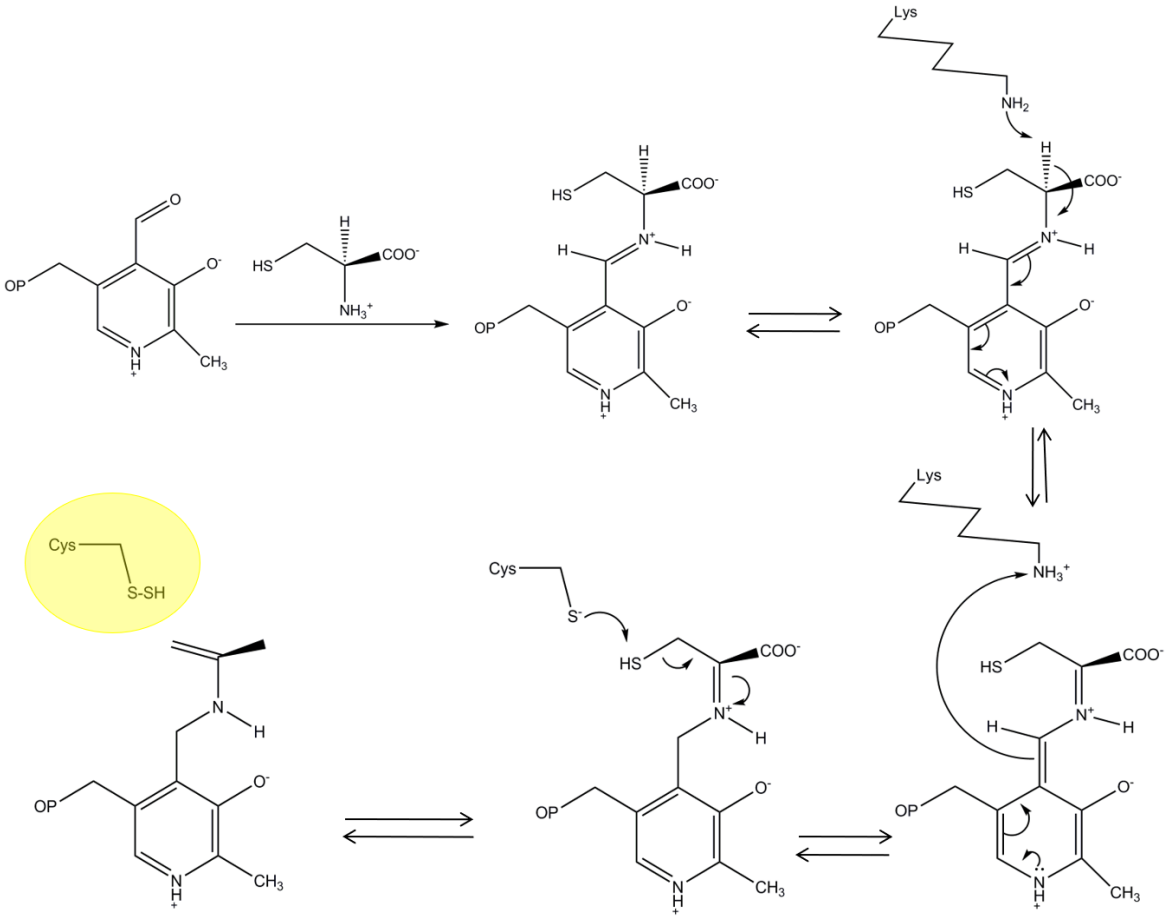

Figure 1-4: Reaction mechanism of formation of L-cysteine by L-cysteine desulfurases

Sulfur is mobilized by L-cysteine desulfurases as a form of persulfide by conversion of L-cysteine to L-alanine. The reaction starts with binding the PLP cofactor to lysine, which binds the substrate L-cysteine, resulting in the formation of an external aldimine. The ketamine intermediate is formed in the next step, which is further attacked by the thiolate-anion of cysteine to the electrophilic sulfur atom and form protein-bound persulfide (-Cys-S-S-). L-alanine is formed for another turnover and release of persulfide sulfur.

The formation of the persulfide is performed in five steps: a) the PLP cofactor binds on to a conserved lysine, which binds the substrate L-cysteine to start the reaction, b) formation of external aldimine, c) conversion of ketamine intermediate from aldimine (L. Zheng et al., 1993), d) the thiolate anion of cysteine attacks the electrophilic sulfur atom of the ketamine in an intermediate step and this leads to the formation of the protein-bound persulfide (-Cys-S-S-) novel ketamine (Lima, 2002; L. Zheng et al., 1994), and e) the formation of L-alanine for the next turnover by hydrolysis of a novel ketamine (Behshad et al., 2004; Mihara et al., 2000; L. Zheng et al., 1994).

1.3 Fe-S clusters

Iron–sulfur clusters are among the most ancient and functionally diverse prosthetic groups present in all forms of life, acting as a cofactor in multiple enzymes involved in critical metabolic pathways in prokaryotes and eukaryotes (Fontecave, 2006). They involve various functions in diverse cellular and vital biological processes, including electron transfer, respiration, photosynthesis, metabolism of nitrogen, sulfur, carbon, hydrogen, biosynthesis of antibiotics, gene regulation, protein translation replication, DNA repair, protection from oxidizing agents, and neurotransmission (Ayala-Castro et al., 2008; Beinert et al., 1997; Fuss et al., 2015; Lill et al., 2006; Mettert & Kiley, 2015; Roche et al., 2013).

(A)

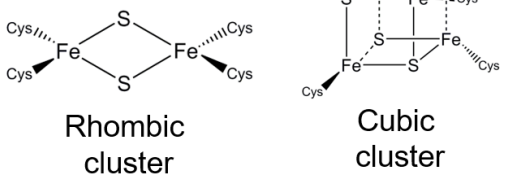

Rhombic cluster

Cubic cluster

(B)

Respiration	37%
Protein maturation	3%
Fe-S cluster biosynthesis	6%
DNA repair	4%
Amino acid biosynthesis	6%
Unknown functions	11%

Figure 1-5: The different forms of naturally abundant Fe-S clusters and their involvement in the biological process.

(A) the [2Fe-2S] as rhombic shape and [4Fe-4S] cluster as cubic shape; (B) the known Fe-S clusters containing proteins and their respective functions in *E. coli*

The abundance of Fe and S facilitates their recruitment as a cofactor in the early stage of life. Over 165 proteins have been identified that contain Fe-S clusters as a cofactor (Py & Barras, 2010). Different types of iron–sulfur cluster are found in nature, such as the [2Fe-2S] cluster which has a rhombic shape, as well as [3Fe-4S] and [4Fe-4S] clusters with a cubic shape. Moreover, [7Fe-8S] and [8Fe-8S] clusters also exist in nature (Beinert, 2000). Free iron and sulfide can spontaneously form Fe-S clusters under reducing conditions (Malkin & Rabinowitz, 1966). However, Fe-S cluster biosynthesis does not spontaneously occur in biological systems; it requires precise multistep mechanisms with specific scaffold proteins. Finally, the assembled Fe-S cluster is transferred by means of chaperones and insertion into the target apo-protein (Roche et al., 2013). In prokaryotes, three different systems have been identified for Fe-S cluster biosynthesis, namely the NIF (nitrogen fixation), ISC (iron–sulfur cluster), and SUF (sulfur mobilization) systems (D. C. Johnson

et al., 2005). ISC and SUF are also found in eukaryotes as homologous proteins and have been identified in mitochondria and chloroplasts (Lill, 2009; Wayne Outten, 2015).

1.3.1 The ISC system

In *E. coli*, the ISC system is expressed from the *isc* operon containing the *iscRSUAhscBAfdx* genes. The ISC system is the housekeeping system for Fe-S cluster biosynthesis under normal cellular conditions (Mettert & Kiley, 2015; L. Zheng et al., 1998). IscR regulates transcription of the *isc* operon in the presence or absence of cellular iron (Giel et al., 2006; Schwartz et al., 2001).

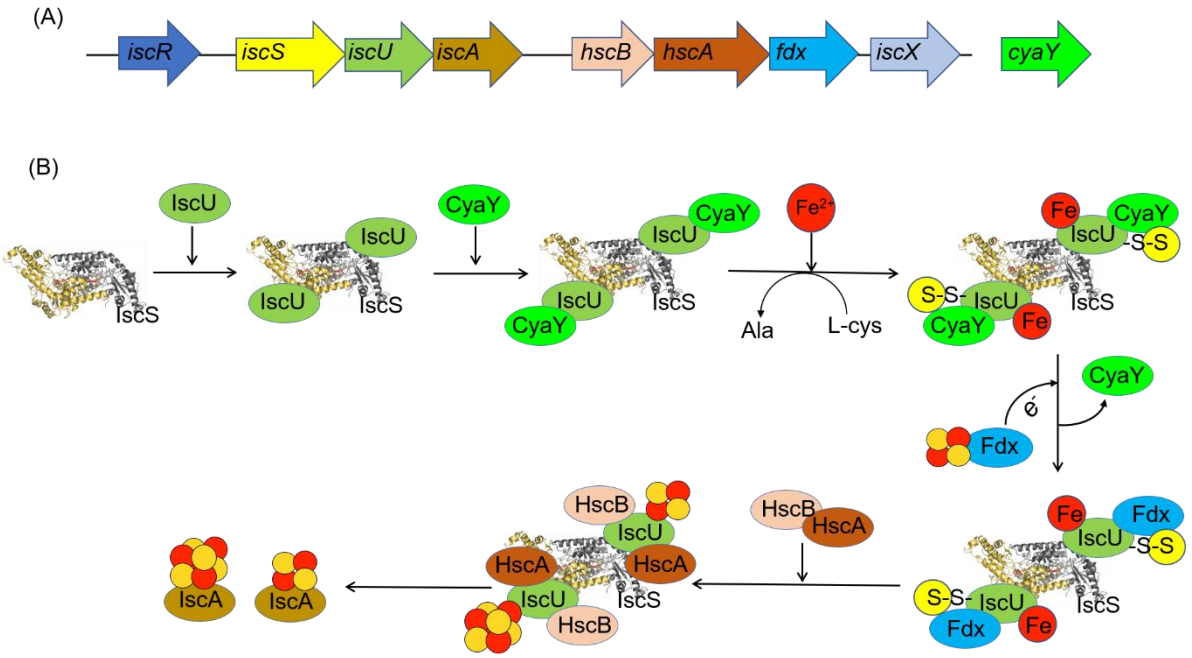

Figure 1-6: Assembly of the Fe-S clusters in the ISC system

(A) the *isc* operon encodes the genes for the proteins required for Fe-S cluster biosynthesis, except for *cyaY*; (B) the proposed model for Fe-S cluster biosynthesis in the ISC system, whereby CyaY binds to the IscS-IscU complex to regulate the introduction of iron, the IscS provides sulfur to the IscS-IscU complex as persulfide from the conversion of L-cysteine to alanine, ferredoxin (Fdx) replaces the CyaY in the complex and provides the electron for Fe-S clusters' biogenesis; the chaperone proteins HscB and HscA replace the ferredoxin (Fdx) and assist the clusters' release from the IscS-IscU complex to the apo-target through IscA; IscS: PDB – 3LVM

Fe-S cluster biosynthesis starts with the formation of a persulfide by IscS. IscS-catalyzed L-cysteine to L-alanine conversion and serves as the sulfur source for assembly (Beinert, 2000b). Assembly is performed on a scaffold protein called IscU, in which the IscS and IscU interaction has been reported both in vivo and in vitro (Kato et al., 2002; Raulfs et al., 2008; Shi et al., 2010). The IscU-IscS macromolecular complex is characterized as an S-

shaped structure, where the IscU monomer binds to the C-terminus end of the IscS subunit (Shi et al., 2010). The IscU-IscS complex facilitates the Fe-S cluster assembly in the presence of iron and sulfur from IscS. The iron donor in this complex is still unknown, with various candidates having been suggested such as CyaY, IscX, and IscA (Blanc, Gerez, and de Choudens, 2015). It has been proposed that CyaY, a prokaryotic homolog of eukaryotic frataxin (Huynen et al., 2001), is involved in iron donation together with iscX (Kim et al., 2014). It has been shown that CyaY has a strong affinity in binding ferric iron (III) (Adamec et al., 2000; Layer et al., 2006). However, deletion of both genes leads to a slight loss of activity for Fe-S clusters containing enzymes (Li et al., 1999; Tokumoto and Takahashi, 2001; Vivas, Skovran, and Downs, 2006; Pohl et al., 2007; Kim et al., 2014). The function of CyaY is still quite unclear since it is involved in regulation of Fe-S cluster biosynthesis by competing for the binding site of IscS with other proteins like IscX and in slowing down the activity of IscS (Adinolfi et al., 2009a; Kim et al., 2013, 2014; Prischi et al., 2010; Shi et al., 2010). It has been shown that the binding of CyaY induces conformational changes in the IscS-IscU complex and reduction of Fe-S cluster biosynthesis (Adinolfi et al., 2009a; Tsai & Barondeau, 2010). The sulfur is reduced to sulfide to bind with iron to form an Fe-S cluster, where the electron is provided by ferredoxin (Fdx). Ferredoxin is encoded in the *isc* operon and contains a [2Fe-2S] cluster as a cofactor (Lange et al., 2000). Under physiological conditions, it has been shown that each dimer of IscU contains a [2Fe-2S] cluster (Shimomura et al., 2008). However, an in vitro experiment reported that each dimer of IscU contains two [2Fe-2S] clusters or one [4Fe-4S] cluster (Agar et al., 2000). Therefore, the [4Fe-4S] cluster assembly is replaced by a second [2Fe-2S] cluster biosynthesis in the IscU dimer. The $[4Fe\text{-}4S]^{2+}$ cluster is formed by means of reductive coupling between two $[2Fe\text{-}2S]^{2+}$ clusters on the IscU dimer, where ferredoxin provides the electron (Chandramouli et al., 2007; Chandramouli & Johnson, 2006).

1.3.1.1 Release of the Fe-S cluster from the IscU complex

The assembled [2Fe-2S] or [4Fe-4S] clusters are released from the IscU dimer and subsequently transferred to the apo-target proteins with the aid of the chaperones called HscB and HscA. Both HscB and HscA are encoded in the *isc* operon, which assist in releasing Fe-S clusters from IscU in an ATP-dependent system (Bonomi et al., 2008, 2011; Kim, Tonelli, Frederick, et al., 2012).

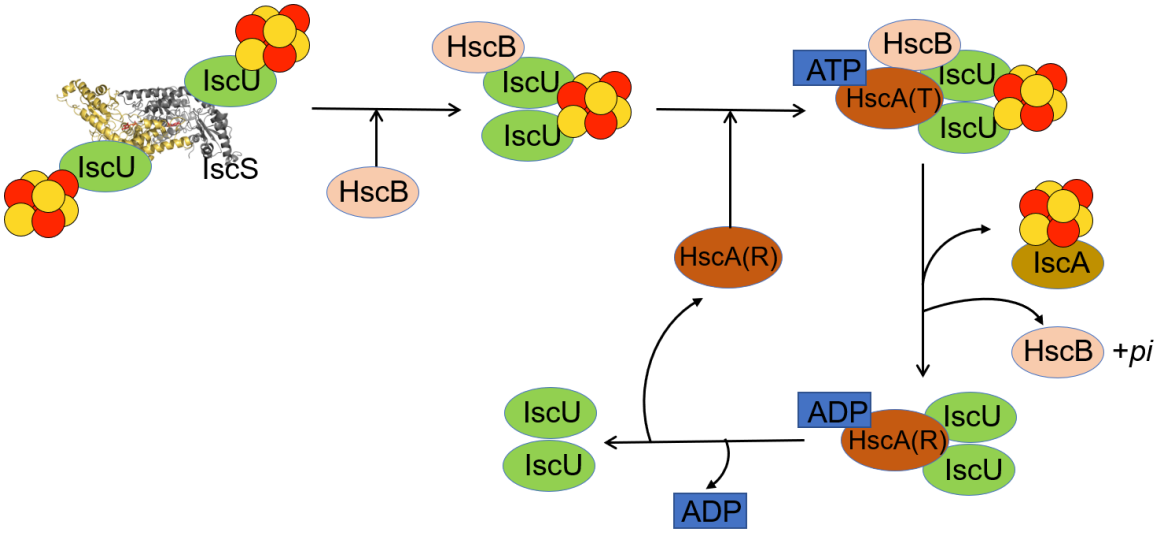

Figure 1-7: The proposed model for chaperone-mediated Fe-S cluster transfer into the apo-target from the IscS-IscU complex

The HscB binds to an Fe-S cluster containing IscU, which triggers the recruitment of ATP-HscA(T-state) and forms an HscA-HscB-holo-IscU complex; ATP hydrolysis facilitates the release of the Fe-S cluster to the IscA protein, leading to the formation of an ADP-HscA(R-state)-apo-IscU complex; the apo-IscU and HscA(R) are released from the complex and engaged in a new cycle; T and R are denoted as transition and resting states; IscS: PDB – 3LVM

The process is initiated with the binding of HscB to the IscU and the formation of the HscB-IscU complex. HscA (T) and HscA (R) are denoted as the transition and resting states of the protein, indicating ATP- and ADP-bound states respectively. The substrate-binding domain (SBD) of HscA (T) binds to the conserved LPPCK sequence motif in IscU and makes a transient IscU-HscB-HscA complex. The binding of HscA induces the ATPase activity of the chaperone (Silberg and Vickery, 2000; Hoff, Cupp-Vickery, and Vickery, 2003; Cupp-Vickery, Peterson, et al., 2004; Tapley, Cupp-Vickery, and Vickery, 2006). The transient IscU-(Fe-S)-HscA-HscB complex is delivered by the Fe-S cluster to an apo-target protein such as IscA, induced by the ATP hydrolysis and then changes the conformation of the IscU scaffold protein (Chandramouli & Johnson, 2006). Consequently, ADP-bound HscA also undergoes a conformational change after the ATP-dependent reaction and forms HscA (R) to engage in a new cycle of cluster transfer from the IscU complex (Kim, Tonelli, & Markley, 2012; Kim, Tonelli, Frederick, et al., 2012).

1.3.2 The SUF system

The *suf* operon is encoded by the *sufABCDSE* genes and regulated by IscR, OxyR, and Fur (J. H. Lee et al., 2004; Outten et al., 2004; Yeo et al., 2006). The operon is only expressed under oxidative stress and iron-limiting conditions (Lee, Yeo, and Roe, 2004; Yeo et al., 2006; Jang and Imlay, 2010).

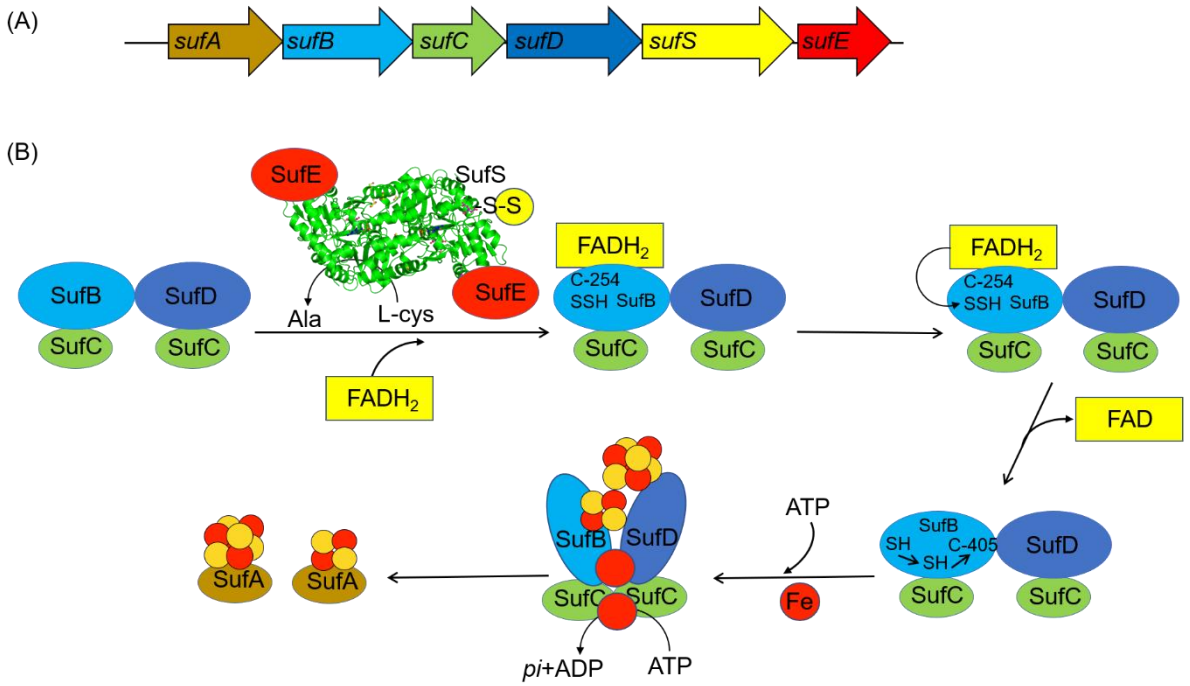

Figure 1-8: Fe-S cluster biogenesis in the SUF system under iron-limiting or oxidative stress condition

(A) the *suf* operon encodes the genes for the proteins that are required for Fe-S cluster biosynthesis; (B) the proposed model for Fe-S cluster biosynthesis by the Suf system, whereby the $SufBC_2D$ complex is required for the biosynthesis of the cluster, sulfur is transferred as persulfide by L-cysteine desulfurase from the SufE-SufS complex to SufB, SufD regulates the access of iron in the $SufBC_2D$ complex, the oxidation of $FADH_2$ provides the electron, and ATP hydrolysis facilitates the formation of Fe-S clusters in the $SufBC_2D$ complex and is then transferred to the SufA protein for inserting into the apo-target; SufS: PDB – 6O10

The SUF system is quite similar to the ISC system, whereby the SufS is the L-cysteine desulfurase, functioning in conjunction with SufE. SufS belongs to group 2 of L-cysteine desulfurase, catalyzes L-cysteine to L-alanine conversion, and provides sulfur as persulfide for Fe-S cluster biogenesis. It has been shown that SufE binds to SufS and induces the activity of SufS by a conformational change (Loiseau et al., 2003; Outten et al., 2003). SufE binding facilitates the less flexible active-site loop of SufS to become more exposed (Lima, 2002; G. Liu et al., 2009). SufE has structural homology with IscU but

lacks conserved sequence motifs to bind Fe-S clusters and interact with HscB and HscA (Goldsmith-Fischman et al., 2004). In the Suf system, SufB functions as a scaffold protein that binds a [4Fe-4S] cluster (Chahal et al., 2009; Wollers et al., 2010), while 2xSufC and SufD also interact with SufB and form a $SufBC_2D$ complex for Fe-S cluster biosynthesis (Saini et al., 2010). SufD is a SufB paralog that involves introducing iron into the complex (Saini et al., 2010). In vitro, it has been shown that the SufSE and $SufBC_2D$ complexes interact with each other, which also stimulates the L-cysteine desulfurase activity of SufS (Layer et al., 2007; Outten et al., 2003). The role of SufC is still unclear; however, it is required for the interaction between the SufB and SufSE complexes to enhance the activity of the $SufBC_2D$ complex (Layer et al., 2007). Overall the sulfur is transferred from SufS to $SufBC_2D$ through SufE in the Fe-S cluster biosynthesis complex (Layer et al., 2007). With SufSE and SufD in the $SufBC_2D$ complex, sulfur and iron are provided to form Fe-S clusters. However, the iron donor is still unknown. A flavin-based cofactor provides the required electrons to the $SufBC_2D$ complex (Wollers et al., 2010). Further, the assembled Fe-S cluster is released from the $SufBC_2D$ complex and transferred to A-type carrier proteins-like SufA for final delivery to the targeted apo-protein (de Choudens, Sanakis, and Fontecave, 2004; Chahal et al., 2009).

1.3.3 Fe-S cluster homeostasis in *E. coli*

Under oxidative stress and iron-limiting conditions, Fe-S clusters are oxidized and further degraded (Imlay, 2003; Jang & Imlay, 2010), leading to a reduction in iron (II) concentration in the cell and followed by cell death. The cellular iron level must be regulated to avoid this scenario (Andrews, Robinson, and Rodríguez-Quiñones, 2003). In *E. coli*, regulation of iron availability is performed by Fur (ferric uptake regulator) (Fillat, 2014). Fur is an iron sensor; a homodimeric protein that contains two Zn^{2+} (Althaus et al., 1999) molecules, each subunit able to bind one iron (II) (Bags & Neilands, 1987). The DNA-binding and metal-binding domains are located at the N- and C-termini, respectively. Fur is involved in regulating siderophores, ABC transporters, iron storage proteins, and Fe-S cluster biosynthesis (Fillat, 2014).

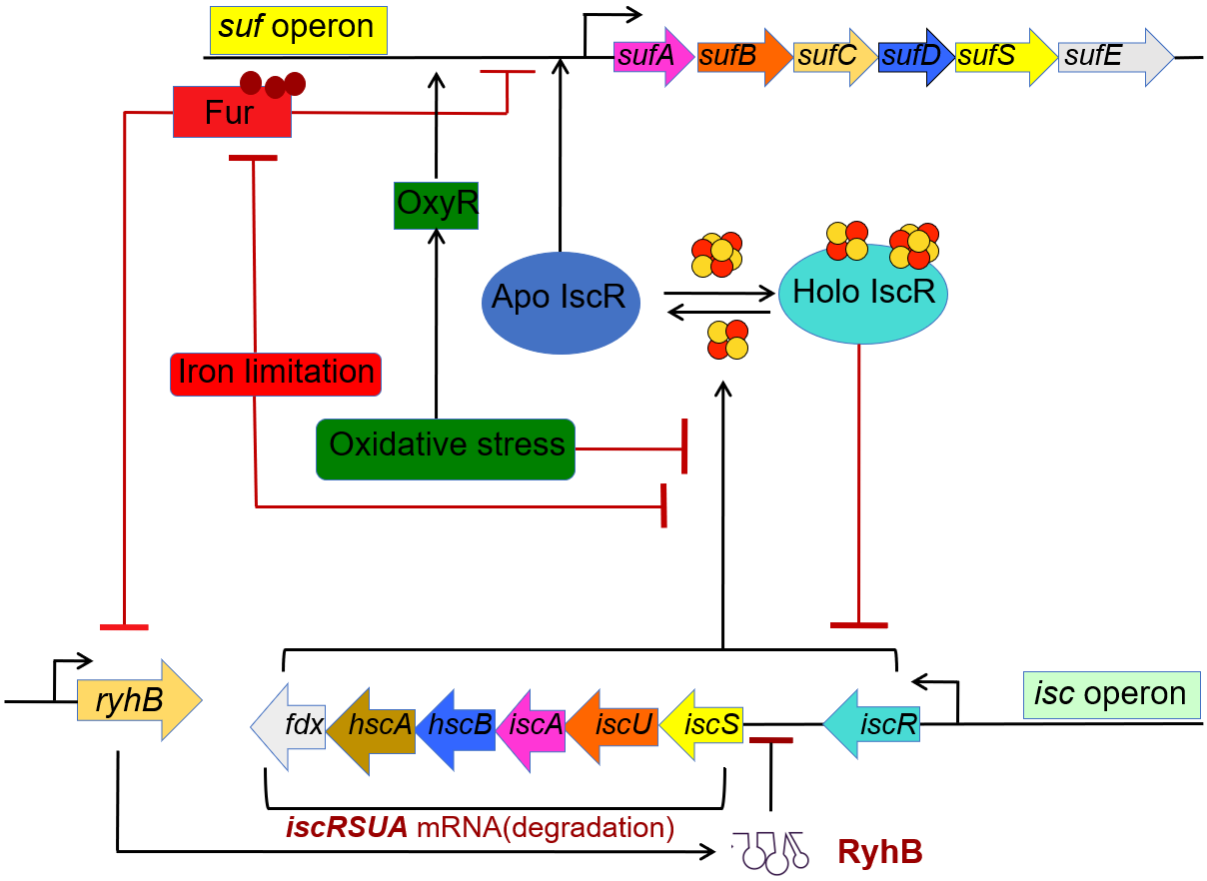

Figure 1-9: The proposed model for iron-dependent regulation of Fe-S cluster homeostasis by ISC and SUF systems in *E. coli*

Under normal conditions, the ISC system is involved in Fe-S cluster biogenesis; the *isc* operon is regulated indirectly by Fe^{2+}-Fur through a small non-coding RNA called *rhyB,* and holo-IscR, which regulates the expression of operon by an autoregulatory circuit in the presence of Fe-S clusters; the *suf* operon is influenced by apo-Fur, OxyR and apo-IscR under iron-limiting condition where the Fur repression is abolished and *rhyB* gene expressed, which leads to a degradation in the mRNA of the *isc* operon except for *iscR*, the apo-IscR regulator recruits the *suf* operon for Fe-S cluster biosynthesis; under oxidative stress condition, OxyR activates expression of the *suf* operon; the activation and repression are shown as black and red lines

The Fe^{2+}-Fur complex represses the *suf* operon by downregulating the expression of *rhyB*. *rhyB* is a small RNA, the expression of which is negatively regulated by the Fur protein (Massé and Gottesman, 2002; Massé, Vanderpool, and Gottesman, 2005). It is a 90-nucleotide small RNA, expressed only under low iron concentrations. *rhyB* reduces the stability of the mRNA of the *isc* operon, since after binding of *rhyB* to the mRNA of *iscSUA,* its degradation is stimulated (Desnoyers et al., 2009). However, it has been shown that *iscR* mRNA remains intact and IscR in its apo-form then binds to the promoter region of the *sufABCDE* operon in its [2Fe-2S] cluster-bound form. Holo IscR represses transcription of the *isc* operon (Giel et al., 2006). Therefore, under iron-limiting conditions,

cells use the SUF system and not the ISC system for Fe-S cluster assembly. (Desnoyers et al., 2009; Massé & Gottesman, 2002). IscR is a transcription factor that belongs to the *isc* operon (Schwartz et al., 2001). IscR is highly conserved in bacteria and regulates at least 40 different genes (Giel et al., 2006).
Under oxidative stress conditions in the presence of superoxide or reactive oxygen species, *suf* operon expression is activated by the transcription factor OxyR (M. Zheng et al., 2001). OxyR is activated by oxidation of the two conserved cysteine residues (Cys-199, Cys-208) (C. Lee et al., 2004) and induces the transcription of the *suf* operon by binding to the promoter region (M. Zheng et al., 2001).

1.4 Fe-S cluster carrier proteins

In the final step of Fe-S cluster biosynthesis, the produced Fe-S clusters are released from the IscU scaffold protein with the aid of HscB and HscA chaperones (Mühlenhoff et al., 2003; Wu, Mansy, and Cowan, 2005; Chandramouli and Johnson, 2006) and further delivered to the targeted apo-protein. The insertion of Fe-S clusters is performed by Fe-S cluster carrier proteins such as BolA, GrxA/B/C/D, and A-type carrier proteins (ATC) (Py, Moreau, and Barras, 2011).

1.4.1 DNA-binding transcriptional regulator – BolA

BolA was first identified as a transcription factor that plays a vital role in cell morphology in the stationary phase under conditions of starvation (Aldea et al., 1989; Santos et al., 2002). BolA also plays a role in the maturation of complex-I since the deletion of *bolA* leads to loss of the binuclear Fe-S cluster N1b and a partially disturbed assembly of the complex (Burschel et al., 2019). It has been reported that the glutaredoxin (Grlx-3)-BolA2 complex acts as a chaperone to transfer [2Fe-2S] clusters into the apo-protein in human cells (A. G. Frey et al., 2016). Moreover, the Grlx-3-BolA2-[2Fe-2S] cluster complex is also involved in sensing the cellular iron status in eukaryotes (H. Li et al., 2012).

1.4.2 Glutaredoxins – GrxA, GrxB, GrxC and GrxD

Glutaredoxins are ubiquitous and catalyze the reduction of disulfides via reduced glutathione (GSH) (Begas et al., 2017). It has been reported that *E. coli* contains four different types of glutaredoxin, namely GrxA, GrxB, GrxC, and GrxD. GrxA, GrxB, and GrxC contain a dithiol active site, whereas GrxD has a monothiol active site (Åslund et al.,

1996; Fernandes et al., 2005). It has been proposed that GrxD physically interacts with the iron–sulfur cluster assembly and acts as an Fe-S cluster carrier protein for the SUF system (Bolstad et al., 2010; Bolstad & Wood, 2010). In vitro studies have shown the interaction of GrxD and NfuA are involved in the maturation of apo-MiaB (Boutigny et al., 2013). Moreover, dimeric GrxD is involved in transferring [2Fe-2S] clusters into the apo-ferredoxin (Yeung et al., 2011).

1.4.3 P-loop NTPase family protein – Mrp

Mrp is reported as a Fe-S cluster carrier protein, which binds and rapidly transfer Fe-S clusters to apoprotein (J. M. Boyd et al., 2008). It belongs to the Mrp/Nbp35 subfamily of the P-loop NTPases (Leipe et al., 2002). It is proposed initially to have a role in thiamine biosynthesis (Petersen & Downs, 1996). It has been reported that the archaeal ApbC/Nbp35 homolog was functioning as a carrier protein (J. M. Boyd, Drevland, et al., 2009). ApbC is a Mrp ortholog from *Salmonella typhimurium* (J. M. Boyd et al., 2008; J. M. Boyd, Sondelski, et al., 2009)

1.4.4 A-type carrier proteins (ATC) – ErpA, IscA, SufA

Phylogenomic and genetic analysis by Frédéric Barras and coworkers has shown that A-type carrier proteins (ATC) originated in the Last Bacterial Common Ancestor and were conserved in most bacteria (Daniel Vinella et al., 2009). Eukaryotes and archaea further acquired this via horizontal gene transfer (Daniel Vinella et al., 2009). The genome analysis of proteobacteria also indicates the presence of two distinct ATC. Moreover, the ATC phylogeny shows another sub-family of ATCs that is involved in nitrogenase maturation. The ATCs are divided into three sub-families based on evolutionary criteria and phylogenomic study: ATC-I, ACT-II, and ATC III, where only ErpA belongs to ATC-I, whereas the IscA and SufA are ATC-II (Daniel Vinella et al., 2009). The ATC-III encoding genes are involved in nitrogenase maturation, since they are surrounded by genes of the *nif* operon (Daniel Vinella et al., 2009).

IscA and SufA belong to the *isc* and *suf* operons, respectively, whereas *erpA* is a single transcriptional unit in the chromosome (Loiseau et al., 2007; Daniel Vinella et al., 2009). In *E. coli*, three ATCs share around 30% sequence identity (Loiseau et al., 2007) with three conserved cysteine residues at Cys-50, Cys-114, and Cys-116 (Wada et al., 2005), that facilitate the binding of Fe-S clusters. Moreover, SufA and IscA also share around 48% sequence similarities (Bilder, Ding, and Newcomer, 2004; Cupp-Vickery, Silberg et

al., 2004; Wada et al., 2005). ErpA shares 40% with IscA and 34% with SufA amino acid sequence identity (Loiseau et al., 2007).

In *E. coli,* the ATCs can bind with both [2Fe-2S] and [4Fe-4S] clusters. It has been reported that an *iscA/sufA* double mutant is not viable under aerobic conditions (Butland et al., 2008; Mettert et al., 2008) but survive under the anaerobic conditions in the presence of ErpA (Mettert et al., 2008). In contrast, the deletion of *erpA* is lethal under aerobic and anaerobic conditions (Loiseau et al., 2007). Aerobic and anaerobic respiration depends on quinones' requirement as electron carriers, which is derived from isopentenyl diphosphate (IPP). The biosynthesis of IPP is directly dependent on IspG and IspH proteins, which contain [4Fe-4S] clusters. Maturation of IspG and IspH requires ErpA and IscA under both aerobic and anaerobic conditions. Therefore, deletion of these genes leads to defective growth and respiration for the strains. To avoid this situation, mutant strains have been introduced with the eukaryotic mevalonate-dependent pathway for biosynthesis of IPP (Gräwert et al., 2004; Wolff et al., 2003).

All the observations are due to the lack of maturation of the IspG/H enzyme (Daniel Vinella et al., 2009), which is essential for the biosynthesis of isopentenyl diphosphate (IPP) (Gräwert et al., 2004; Wolff et al., 2003).

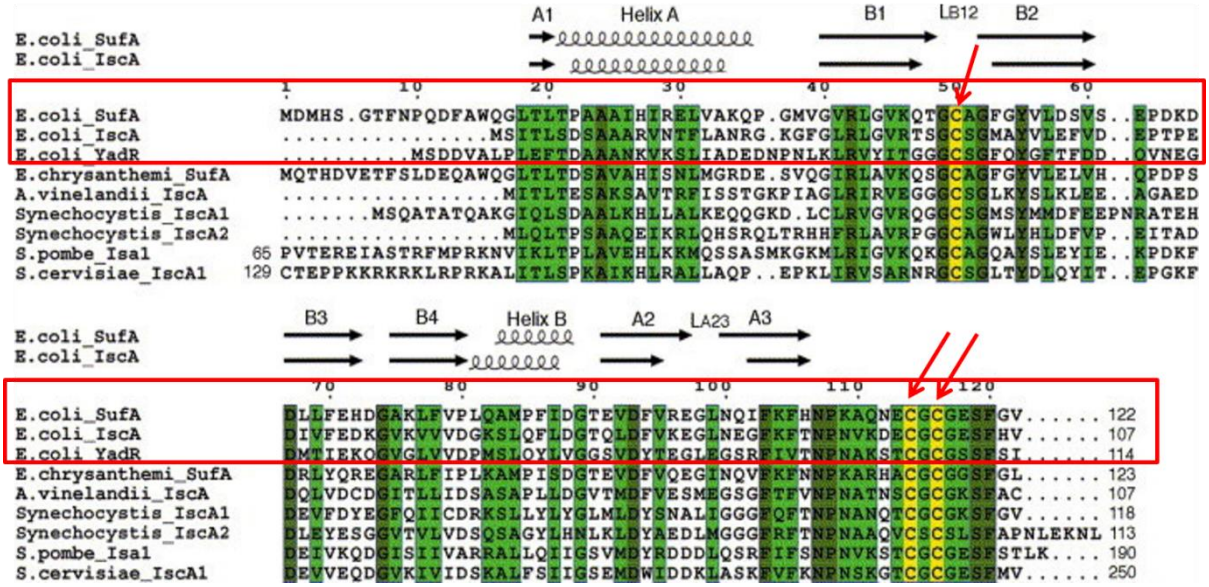

Figure 1-10: Amino acid sequence alignment of A-type carrier proteins (ATC), IscA, SufA, and ErpA (YadR) from different organisms

The three cysteine variants at C-50, C-114, and C-116 are highlighted in yellow; other conserved residues are shown in dark green, and variant residues in light green (Wada et al., 2005)

The maturation model of IspG/H by Frédéric Barras and coworkers has shown that the Fe-S cluster is transferred to ErpA before insertion into the final apo-target under both aerobic and anaerobic conditions. Under anaerobic conditions, IscA can directly deliver the cluster to the final apo-target, but IscA requires ErpA under aerobic conditions (Daniel Vinella et al., 2009). In *E. coli,* IscA and SufA are functionally redundant; under aerobic conditions, the *iscA/sufA* double mutant can survive by exogenous overexpression of either *iscA* or *sufA* (Lu et al., 2008). Both SufA and IscA potentially receive Fe-S clusters from the IscU scaffold protein or the $SufBC_2D$ complex and are further delivered to ErpA (Daniel Vinella et al., 2009). Moreover, under anaerobic conditions, ErpA and IscA might be functionally redundant since both can receive the Fe-S clusters from IscU and deliver these to the IspG/H, as demonstrated by Barras and his team (Daniel Vinella et al., 2009). It has been reported that the ErpA and IscA are involved in the maturation of formate: hydrogen lyase, the hydrogen-oxidizing [NiFe]-hydrogenase (Pinske & Sawers, 2012b), and IspG/H (Daniel Vinella et al., 2009) by inserting Fe-S clusters into them. The nitrate reductase, formate dehydrogenase-N, and format dehydrogenase-O activity are significantly reduced in the *iscA* deleted strain, whereas no activity has been observed in the *erpA* mutant strain (Pinske & Sawers, 2012a). Moreover, no hydrogenase 1 and hydrogenase 2 activity has been observed in either the *iscA*- or *erpA*-deleted mutant (Pinske & Sawers, 2012b). It has also been shown that SufA is able to insert a [2Fe-2S] cluster into ferredoxin and Aconitase-A (Gupta et al., 2009).

1.4.5 Atypical A-type carrier protein (ATC) – NfuA

NfuA is another Fe-S cluster carrier protein known as atypical A-type carrier protein (Py et al., 2012). NfuA can potentially receive Fe-S clusters from the IscU-HscBA or $SufBC_2D$ complexes and further deliver them to typical ATCs like SufA or IscA (Py et al., 2012). *E. coli* NfuA belongs to the Nfu-I sub-family of Nfu-like proteins (Angelini et al., 2008). However, NfuA does not contain a typically conserved cysteine residue at the N-terminus like the ATCs. However, this degenerated domain has shown efficient Fe-S cluster transfer to apo-target proteins. It has been reported that the C-terminus of NfuA is able to bind a [4Fe-4S] cluster (Angelini et al., 2008; Py et al., 2012). The deletion of *nfuA* is not lethal under both anaerobic and aerobic conditions (McCarthy & Booker, 2017; Palchevskiy & Finkel, 2006). NfuA is involved in the maturation of apo-aconitase (AncA and AncB) (Angelini et al., 2008), and the NuoG-a subunit of NADH dehydrogenase I (Py et al., 2012). In vitro studies have shown that NfuA also performs maturation of LipA

(McCarthy and Booker, 2017) and apo-MiaB (Boutigny et al., 2013). Moreover, Py and her team have demonstrated that NfuA plays a vital role in repairing damaged or oxidized Fe-S clusters under aerobic conditions. It has been proposed that NfuA interacts directly with ErpA for Fe-S cluster insertion to the target apo-protein under oxidative stress conditions (Py et al., 2018).

1.5 Molybdenum cofactor (Moco) biosynthesis and molybdoenzymes

1.5.1 Moco biosynthesis

Molybdoenzymes are essential for biological processes, and play a crucial role in sulfur, carbon, and nitrogen metabolism (Hille, 1996). These enzymes participate in critical redox reactions that are required for fundamental physiological processes (Zhang and Gladyshev, 2008; Madsen, 2011; Carpenter, Archer, and Beale, 2012). In most molybdoenzymes, electron transfer is mediated by Fe-S clusters, FMN/FAD, or cytochrome to or from a molybdenum cofactor (Moco) (Iobbi-Nivol & Leimkühler, 2013; Yokoyama & Leimkuhler, 2015). To date, more than 60 different molybdoenzymes have been identified in prokaryotes and 5 in eukaryotes (Hille, Hall, and Basu, 2014). About 19 different molybdoenzymes are present in *E. coli*, which have been studied in great detail (Iobbi-Nivol & Leimkühler, 2013). Molybdoenzymes contain a molybdenum cofactor. The molybdenum atom is involved in electron transfer during redox reactions, which exist as IV, V and VI oxidation states (Hille, 2002). The molybdoenzymes are classified into three different families depending on the configuration of ligands around the molybdenum atom. The three different families are: a) the xanthine oxidase (XO), b) sulfite oxidase (SO), and c) dimethyl sulfoxide (DMSO) reductase families (Hille, 1996). Enzymes of the DMSO reductase family are only present in prokaryotes (Leimkühler, 2020).

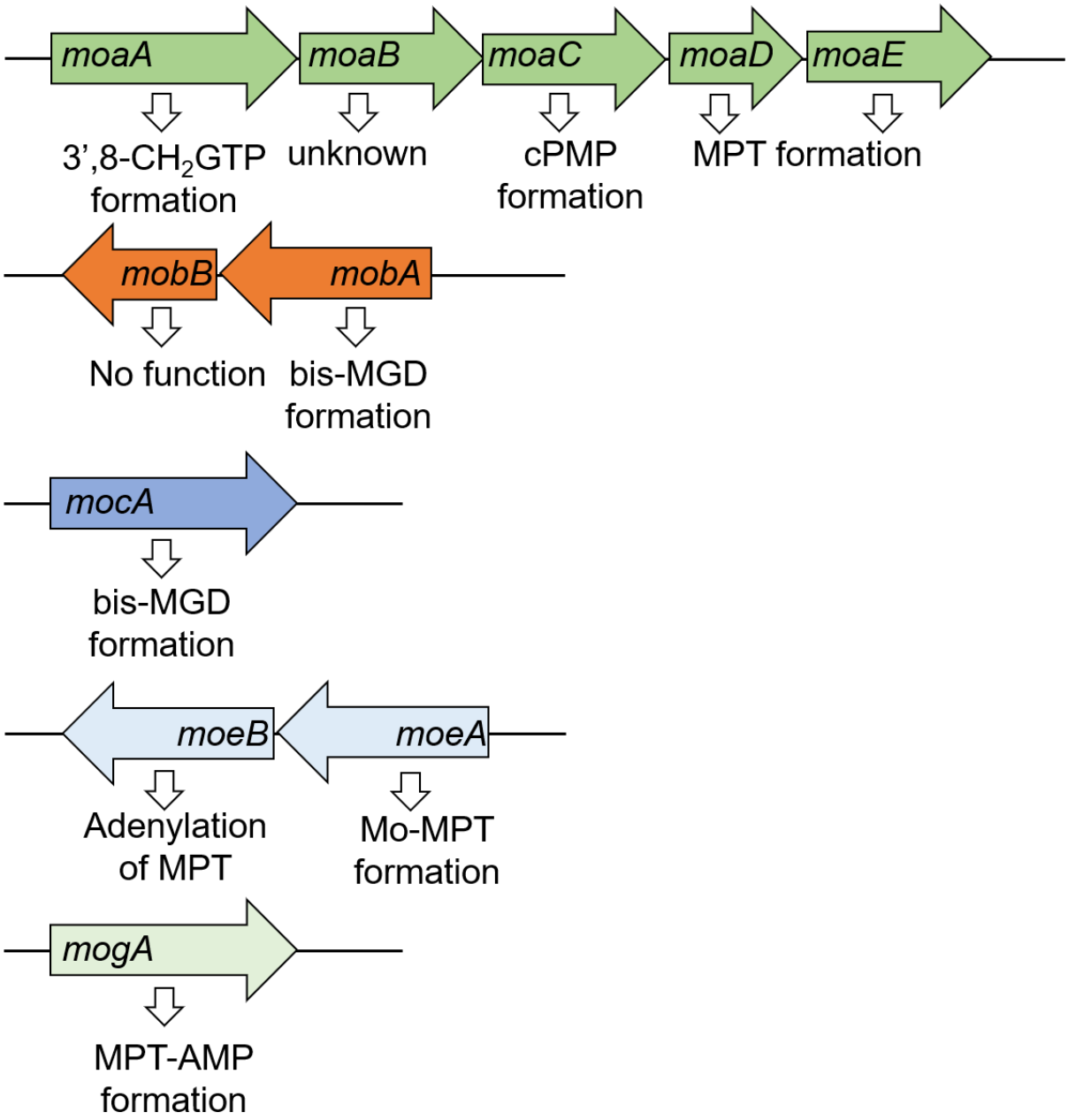

Figure 1-11: The operons involved in Moco biosynthesis in *E. coli*

A total of 5 different gene loci and 11 different organizations of genes are directly involved in Moco biosynthesis that are encoded in *moa, mob, moc, moe,* and *mog* operons, with the individual role of each protein from the respective gene in different steps in Moco biosynthesis

Molybdenum enzymes are composed of a tricyclic pyranopterin ring. The molybdenum atom is coordinated by a unique dithiolene moiety (Johnson and Rajagopalan, 1982; Rajagopalan, Johnson, and Hainline, 1982). The nature of its chemical structure was established by Rajagopalan and Johnson (Rajagopalan & Johnson, 1992). The biosynthesis pathway of Moco is highly conserved from prokaryotes to eukaryotes (R R Mendel & Leimkuhler, 2015; Ralf R. Mendel, 2013). In *E. coli,* the biosynthesis of Moco

has been extensively studied, where 11 different genes in 5 different loci, namely *moa, moe, mob, moc,* and *mog* have been identified as being involved in Moco biosynthesis (Shanmugam et al., 1992; Neumann et al., 2009). The biosynthesis of Moco is divided into four steps in bacteria (Rajagopalan, 1996; Mendel and Leimkuhler, 2015): a) cyclic pyranoptrein monophosphate (cPMP) formation from 5'GTP, b) formation of molybdopterin (MPT) by sulfur incorporation into cPMP, c) formation of Mo-MTP by the insertion of a molybdate atom to the dithiolene group, and d) further modification of Mo-MTP to form bis-MGD (molybdopterin guanine dinucleotide) and MCD (molybdopterin cytosine dinucleotide) by attachment of GMP and CMP respectively.

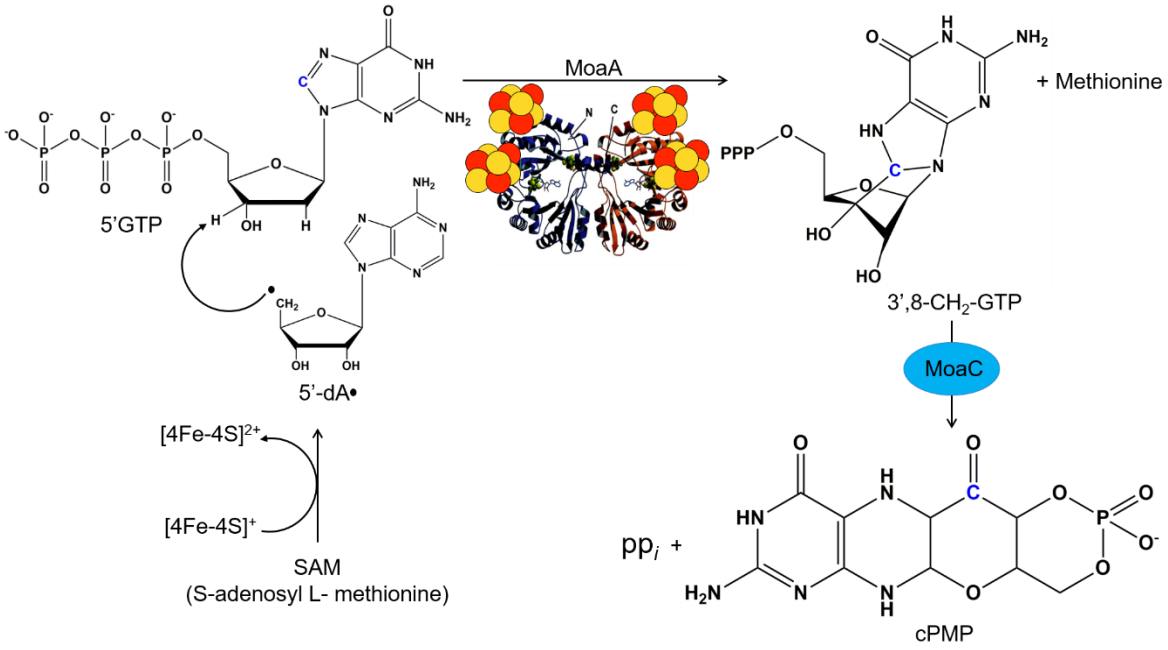

Figure 1-12: Biosynthesis of cPMP from 5'GTP catalyzed by MoaA and MoaC

MoaA catalyzes the conversion of 5'GTP to 3',8-CH_2GTP intermediates, where the C8 (blue) atom of guanine is inserted between C2 and C3 of ribose and forms 3',8-CH_2GTP intermediates, here the SAM is reductively cleaved to 5'-dA, which further abstracts the H atom in 5'GTP; cPMP is formed by cleaving of a pyrophosphate group from 3',8-CH_2GTP intermediates, and the reaction is catalyzed by MoaC; MoaA:PDB – 1TV7

The first step of Moco biosynthesis is performed by the conversion of cPMP from 5'GTP. The reaction is catalyzed by two enzymes, namely MoaA and MoaC (Hover et al., 2013, 2015; Hover & Yokoyama, 2015; Wuebbens & Rajagopalan, 1995). In vitro studies have demonstrated that 5'GTP is the initial substrate for Moco biosynthesis. MoaA is a homodimeric enzyme that belongs to the superfamily of radial S-adenosyl methionine (SAM) dependent enzymes (Hanzelmann & Schindelin, 2004; Sofia et al., 2001). It binds

two [4Fe-4S] clusters in each monomer, where one at the C-terminus binds the substrate 5'GTP and the other one at the N-terminus binds SAM to initiate the reaction (Hänzelmann and Schindelin, 2004, 2006). The reaction starts with the interaction of the N-terminus [4Fe-4S] cluster of MoaA with SAM, in which the SAM is reductively cleaved and forms 5'-deoxyadenosyl radical (5'-dA.), and an electron is provided from the oxidation of the [4Fe-4S] cluster (Frey, Hegeman, and Ruzicka, 2008). Consequently, the C8 guanine is opened and inserted between C2 and C3 carbon of ribose (Hover et al., 2013; Mehta, Abdelwahed, and Begley, 2013) to produce a 3'-8-CH2-GTP. Further, this 3'-8-CH_2-GTP intermediate is converted into the cPMP by MoaC. It has been demonstrated that the formation of cPMP is catalyzed by the cleavage of the pyrophosphate group (Hover et al., 2013, 2015).

The second step of Moco biosynthesis is molybdopterin (MPT) formation from cPMP by incorporating two sulfur atoms from MPT synthase (Pitterle and Rajagopalan, 1989, 1993; Pitterle, Johnson, and Rajagopalan, 1993; Rudolph et al., 2001). MPT synthase is a heterotetrameric complex of two $(MoaE)_2$ and $(MoaD)_2$ subunits (Pitterle & Rajagopalan, 1989). The isolated MTP synthase from *E. coli* demonstrates that MoaE is a central dimer, where one subunit of MoaD is located at each end (Daniels et al., 2008; Rudolph et al., 2001). The reaction starts with the insertion of the thiocarboxylate sulfur atom from the MoaD to the C2 position of cPMP and formation of hemisulfurated intermediate (Daniels et al., 2008) before the dissociation of MoaD from the MPT synthase complex (Daniels et al., 2008; Wuebbens & Rajagopalan, 2003). The second thicarboylate attacks the C1 position of cPMP and forms molybdopterin (MPT) (Daniels et al., 2008). The regeneration of MoaD with sulfur is performed by MoeB, which interacts with the C-terminus end of MoaD (Leimkuhler & Rajagopalan, 2001). IscS donates the sulfur atom as a form of persulfide (Mihara et al., 2000; Leimkuhler and Rajagopalan, 2001; Leimkuhler, Wuebbens, and Rajagopalan, 2001). The MoaD-AMP receives the sulfur from the L-cysteine desulfurases to the $(MoaD\text{-}MoeB)_2$ complex, where the sulfur is transferred by the TusA to the MoaD and forms MoaD-SH (persulfide) (Leimkühler, 2017).

The third step of Moco biosynthesis involves the addition of a molybdate atom to the unique dithiolene moiety and formation of Mo-MPT (Grunden & Shanmugam, 1997). The reaction is catalyzed by MoeA and MogA (Grunden & Shanmugam, 1997), where MogA is a homotrimer (M. T. W. Liu et al., 2000) and MoeA is a dimer (Schrag et al., 2001; Xiang et al., 2001). It has been demonstrated that the addition of the molybdenum atom is performed in two steps (J. Nichols & Rajagopalan, 2002), where MogA catalyzes the

formation of MPT-adenylate species under low physiological molybdate concentrations (J. D. Nichols & Rajagopalan, 2005; J. Nichols & Rajagopalan, 2002). This reaction is Mg^{2+}- and ATP-dependent (Kuper et al., 2004). In the next step, the MoeA catalyzes the molybdenum ligation to the MPT structure and Mo-MPT is formed (Nichols and Rajagopalan, 2005; Leimkuhler, Wuebbens, and Rajagopalan, 2011). Mo-MPT functions as a basic form of Moco that can be directly inserted into molybdoenzymes that belong to the sulfite oxidase family (SO) (Brokx et al., 2005; Havelius et al., 2011).

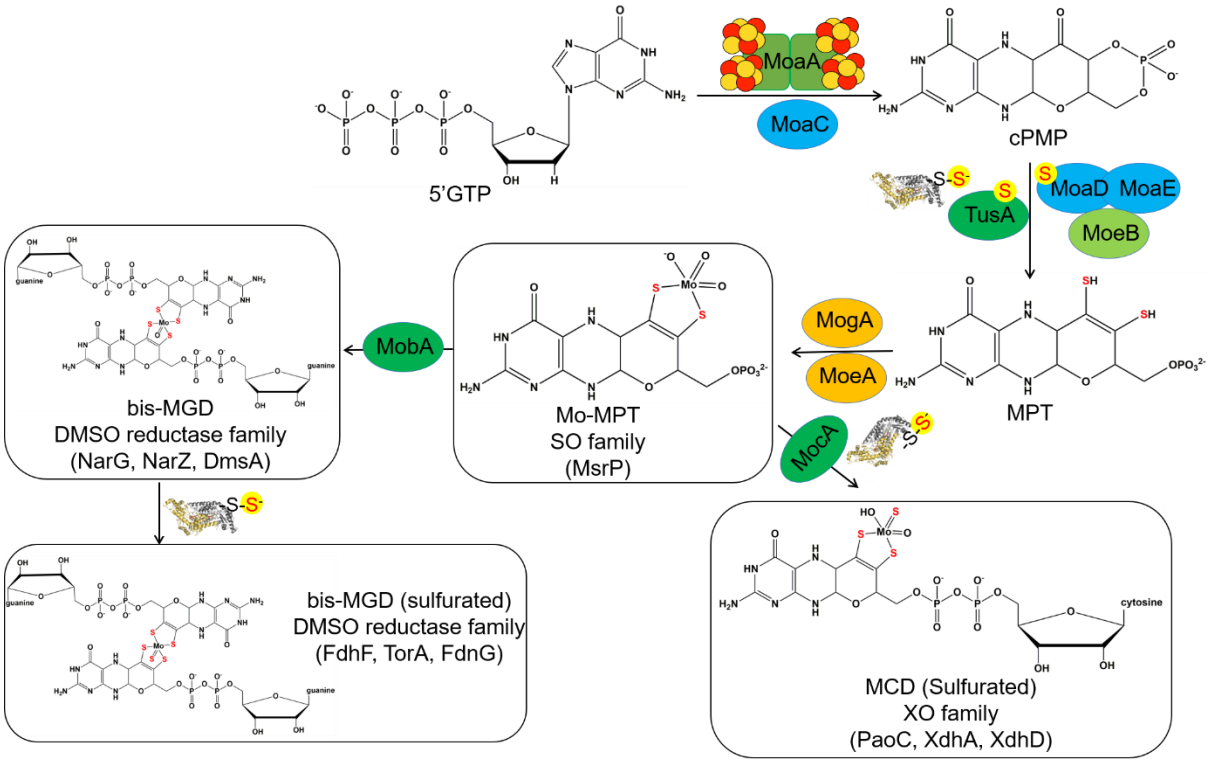

Figure 1-13: Schematic diagram of Moco biosynthesis in *E. coli*

Moco biosynthesis starts with the conversion of 5'GTP to cPMP catalyzed by MoaA and MoaC; MPT is formed in the second step by incorporation of sulfur atoms; sulfur is provided by L-cysteine desulfurase as a form of persulfide, which is further mobilized by TusA through MoeB, and the reaction is catalyzed by MPT synthase (MoaD/MoaE); in the third step, Mo-MPT is formed by incorporation of a molybdenum atom in the presence of MogA and MoeA, and the Mo-MPT can be directly inserted into the sulfite oxidase family of enzymes (SO and mARC). In *E. coli*, Mo-MPT can be further modified into MCD and a bis-MGD cofactor, and the addition of cytosine nucleotide in Mo-MPT is catalyzed by MocA to form a molybdopterin cytosine dinucleotide (MCD) cofactor that contains an equatorial sulfur ligand coordinate to the Mo atom; the MCD cofactors are present in all the xanthine oxidase (XO) enzyme family; the bis-MGD cofactor belongs to the whole DMSO reductase (DMSOR) enzyme family, where the Mo-MPT is modified by the addition of two guanosine dinucleotides that are catalyzed by MobA to form bis-MGD; bis-MGD can be further modified with an addition of a sulfur ligand at the molybdenum center

Mo-MPT can be further modified into bis-MGD (Hille et al., 2014). The formation of bis-MGD is performed by adding GMP to the phosphate group of each Mo-MPT (Leimkühler, 2017). The reaction is catalyzed by MobA, which exists as a monomer and contains two domains. The crystal structure of MobA demonstrates that the N-terminus contains a GTP-binding Rossmann fold, and the MPT binding site is located at the C-terminus end (Lake et al., 2000; Stevenson et al., 2000). The conversion of bis-MGD from Mo-MTP is carried out in two steps (Reschke et al., 2013). In the first step, the Mo-MTP is used as a substrate for MobA to form bis-Mo-MPT. In the next step, the GMP molecules from GTP hydrolysis bind to the C4 phosphate of bis-Mo-MPT and facilitate the formation of bis-MGD (Lake et al., 2000; Palmer et al., 1996). One molybdate is released from the two combined Mo-MPT molecules during the reaction (Leimkühler, 2020).

Mo-MTP can also be modified as MCD and inserted into the xanthine oxidase family of molybdoenzymes in *E. coli* (Neumann et al., 2009; Iobbi-Nivol and Leimkühler, 2013). The formation of MCD from Mo-MTP is catalyzed by MocA (Leimkühler & Neumann, 2011). The reaction is catalyzed by the addition of CMP to the C4 phosphate of Mo-MTP, where the MPT and CMP covalently link to each other by the release of pyrophosphate (Neumann et al., 2009a, 2009b).

Moco is sulfurated in molybdoenzymes that belong to the xanthine oxidase (XO) family (Hille, 1996; Hille, Hall, and Basu, 2014). Sulfuration of the Mo-MPT cofactor of xanthine dehydrogenase from *Rhodobacter capsulatus* has been investigated in particular detail (Neumann et al., 2007a). Moreover, the sulfurated MCD cofactor has also been observed in periplasmic aldehyde oxidase (PaoABC) (Iobbi-Nivol & Leimkühler, 2013; Neumann, Mittelstädt, et al., 2009). In Moco sulfuration, the molybdenum oxygen ligand is replaced by a sulfur atom, where the L-cysteine desulfurase provides the sulfur. In *R. capsulatus* XDH, this sulfur incorporation is performed by the direct association of XdhC, where it interacts with L-cysteine desulfurases (NifS4) and mobilizes the sulfur as persulfide by catalyzing the conversion of L-cysteine to L-alanine. This further facilitates the replacement of one oxygen ligand by a sulfur ligand (Neumann et al., 2007a). It has been demonstrated that XdhC also protects the oxidation of Mo-MPT until the terminal sulfur is inserted (Leimkühler, 2020; Neumann et al., 2007a). Moreover, the XdhC chaperone also plays a role in Moco insertion into the target apo-protein and further interacts with the apo-target to facilitate proper folding after the insertion of Moco (Leimkühler & Klipp, 1999). PaoD and YqeB also belong to this XdhC chaperone family. It is believed that the PaoD

also performs an identical role to XdhC in sulfur-ligand incorporation in MCD for the PaoABC enzyme (Iobbi-Nivol & Leimkühler, 2013; Neumann et al., 2007a).

1.5.2 Moco sulfuration and insertion into enzymes of the DMSO reductase family

The addition of sulfur in Moco has also been observed in some DMSO reductase family enzymes, such as periplasmic nitrate reductase from *Cupriavidus necator* (Coelho et al., homologous to NapA from *Desulfovibrio desulfuricans* (Najmudin et al., 2008). It has been established recently that the TMAO reductase (Kaufmann et al., 2018) and formate dehydrogenase (FdhF) (Thome et al., 2012) from *E. coli* both carry a sulfur ligand in place of the molybdenum–oxygen ligand. It has been reported that the absence of FdhD leads to the production of inactive FdhF, which can be restored by chemical sulfuration (Thome et al., 2012). Therefore, this indicates that sulfuration of FdhF requires the presence of FdhD, which acts as a chaperone for inserting a sulfur atom in bis-MGD (Thome et al., 2012), a role similar to that played by XdhC for xanthine dehydrogenase.

In *E. coli*, most molybdoenzymes of the DMSO reductase family harbor a specific chaperone for Moco insertion (Iobbi-Nivol & Leimkühler, 2013) such as NarJ for NarGHI (Blasco et al., 1998), NarW for NARZYV (Blasco et al., 1992), NapD for NapA (Dow et al., 2014), TorD for TorA (Genest et al., 2005, 2006), and FdhD for FdhF (Thome et al., 2012), as well as FdnGHI and FdoGHI. Moco insertion into a target apo-protein has been extensively studied for the TMAO reductase enzyme in *E. coli*, where TorD functions as a chaperone for apo-TorA maturation (Genest et al., 2005). It has been reported that TorD binds both TorA and MobA during the insertion process, where it binds to the signal peptide in apo-TorA and inserts the bis-MGD (Genest et al., 2008; Genest, Méjean, and Iobbi-Nivol, 2009; Iobbi-Nivol and Leimkühler, 2013). TorD also accomplishes the correct folding of holo-TMAO reductase (Genest et al., 2008) before the periplasmic translocation by cleavage of the signal peptide (Iobbi-Nivol & Leimkühler, 2013). It has been shown that TorD plays an important role in the binding to the TorA-Tat-leader peptide (Genest, Méjean, and Iobbi-Nivol, 2009; Leimkuhler and Iobbi-Nivol, 2016). The Tat (twin-arginine translocation) pathway is essential for translocation of the folded protein to the periplasm (Jack et al., 2004; Berks, Palmer, and Sargent, 2005). Insertion of the bis-MGD and conformational change of TorA induces the dissociation of TorD from the complex and exposes the Tat-leader peptide to the Tat-machinery for facilitating the translocation of mature TMAO reductase (Pommier et al., 1998). The Tat-consensus motif has been

identified for DMSO reductase (DmsA and DmsB), format dehydrogenase (FdnG/H, FdoG/H), TMAO reductase (TorA), and periplasmic oxidoreductase (PaoA) (Berks et al., 2005; Ize et al., 2009).

1.5.3 Regulation of Moco biosynthesis

In *E. coli*, FNR (fumarate and nitrate reduction) is a dual transcriptional regulator, which needs a [4Fe-4S] cluster under anaerobic condition to regulate the activation or repression of different genes (Green & Guest, 1993; S Spiro & Guest, 1990; Unden et al., 2002). Transcription of the *moaABCDE* and *moeAB* operons are up- and downregulated respectively, by FNR (Anderson et al., 2000; Hasona, Self, and Shanmugam, 2001; Zupok et al., 2019).

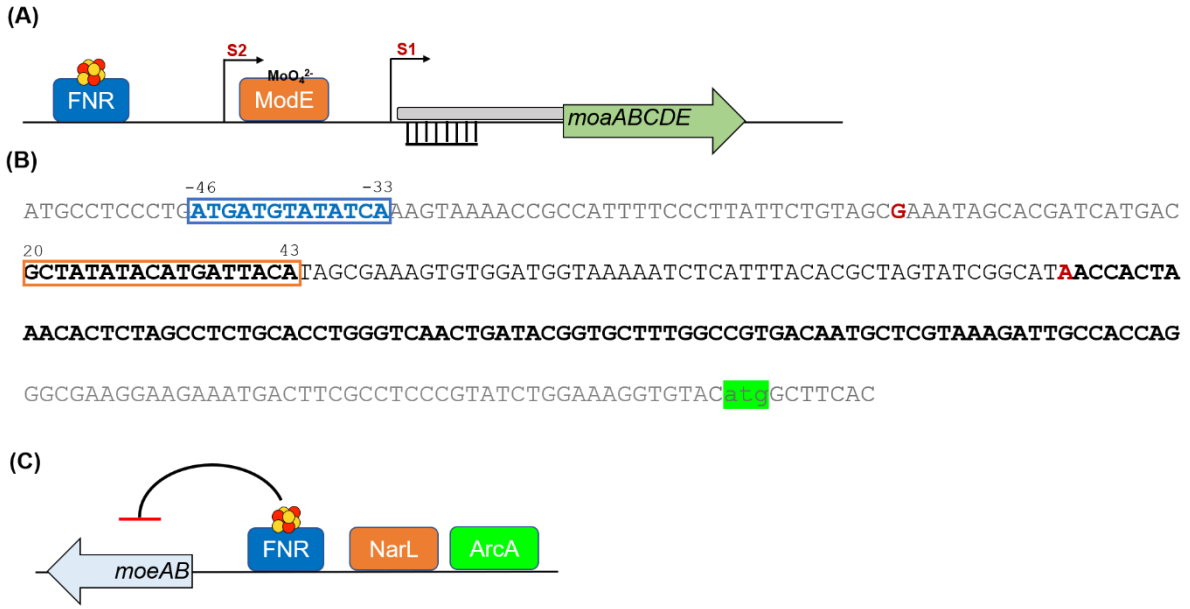

Figure 1-14: Overall transcriptional regulation of the *moa* and *moe* operon

Depicted is the promoter region upstream of the *moaABCDE* operon (A) the binding sites of regulators schematically: FNR (blue), ModE (orange), Moco riboswitch region (black) binding site, transcription start sites: S1 and S2. The biding sequence of transcriptional activator and repressor (B) show as FNR (-46 to -33), ModE (+20 to +43), Moco riboswitch region (bold). The promoter region of *moeAB* operon (C) which is expressed by NarL and repress by holo-FNR

FNR is itself also autoregulated by [4Fe-4S]-FNR (Mettert & Kiley, 2007). Moreover, ArcA and Fur also downregulate FNR expression (Compan & Touati, 1994; Gunsalus & Park, 1994; Kumar & Shimizu, 2011).

1.5.4 Molybdoenzymes

1.5.4.1 Nitrate reductase

Nitrate reductase is a molybdoenzyme that belongs to the DMSO reductase family (Miralles-Robledillo et al., 2019). Dependent upon the growth condition and presence of nitrate in the medium, three different types of nitrate reductases are encoded in the genome of *E. coli* (Cole, 2006; Yokoyama & Leimkuhler, 2015), namely NarGHI and NarZYV which are oriented towards the cytoplasm, but anchored in the membrane (Stewart, 1988; Chang et al., 1999), and NapAB localized in the periplasm (Brondijk et al., 2004). All these types of nitrate reductase consist of bis-MGD as a form of Moco (Yokoyama & Leimkuhler, 2015). The expression of membrane-bound NarGHI is induced at a high concentration of nitrate in the medium, further localized at the cytoplasm (Stewart, 1988). In contrast, periplasmic NapAB is produced under a low nitrate concentration (Brondijk et al., 2004). NarZYV is produced regardless of the presence of nitrate at the early stationary phase (Chang et al., 1999). NarGHI is the most predominantly expressed nitrate reductase, and is involved in cellular respiration under anaerobic conditions, where it functions as a terminal electron acceptor from the quinone pool and facilitates the conversion of nitrate to nitrite (Berks et al., 1995; Unden & Bongaerts, 1997). Nitrate reductase is a heterotrimer consisting of NarG, NarH, and NarI subunits (Forget, 1974; Enoch and Lester, 1975; Clegg, 1976; Coleman, Cornish-Bowden, and Cole, 1978; Sodergren, Hsu, and DeMoss, 1988). The oxidation of quinol provides the electron for the reaction at the cellular level, which is transferred through the heme in NarI, through one [3Fe-4S] and three [4Fe-4S] clusters in NarH, and one [4Fe-4S] cluster in NarG to the bis-MGD catalytic site for performing the reduction of nitrate to nitrite (Rothery et al., 1999, 2001, 2004; Zhao et al., 2003). The NarGH subunit is located in the inner membrane of the cytoplasm, where it binds with a membrane-bound fraction of NarI through hydrophobic interaction. In vitro study has shown that NarGHI exits in homodimer form (Bertero et al., 2003). A chaperone protein, namely NarJ, performs bis-MGD incorporation in the NarG. The *narJ* belongs to the *narGHJI* operon, which coexpresses with *narGHI* during transcription (Blasco et al., 1992, 1998; Dubourdieu & DeMoss, 1992).

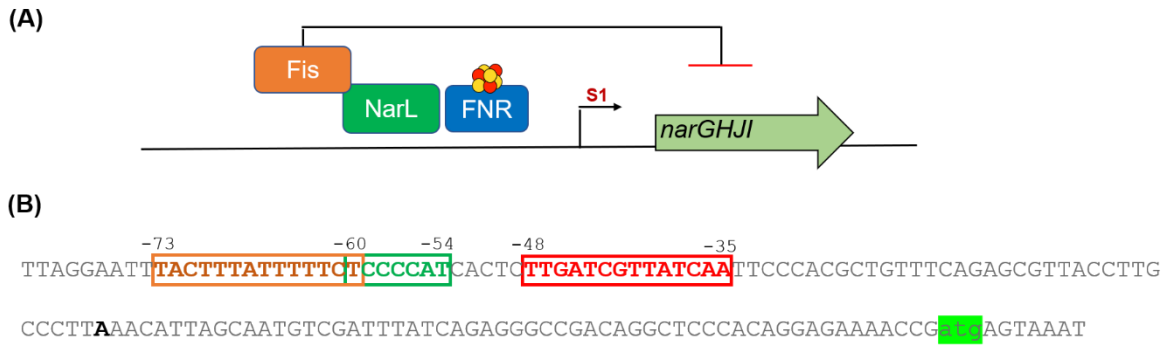

Figure 1-15: Overall transcriptional regulation of the *narGHJI* operon

Depicted is the promoter region upstream of the *narGHJI* operon (A) the binding sites of regulators schematically: FNR (blue), NarL (green) and Fis (orange), transcription start sites: S1. The biding sequence of transcriptional activator and repressor (B) show as FNR (-48 to -35), NarL (-60 to -54) and Fis (-73 to -60), transcriptional starting site atg (green)

The *narGHJI* operon is regulated by FNR (Lamberg & Kiley, 2000; Melville & Gunsalus, 1996; Stewart, 1982) and NarL (Stewart, 1982; Li, Kustu, and Stewart, 1994). Holo-FNR is required for the activation of *narGHJI* expression under anaerobic conditions (Schroder, Darie, and Gunsalus, 1993). It has been reported that holo-FNR binds to the upstream of the *narGHJI* operon at the -48 to -35 region (Melville and Gunsalus, 1996; Lamberg and Kiley, 2000). Moreover, NarL is essential for nitrate- and molybdate-dependent activation of the *narGHJI* operon under anaerobic conditions (Iuchi and Lin, 1987a; Kalman and Gunsalus, 1990; Chiang, Cavicchioli, and Gunsalus, 1992). Under nitrate respiratory conditions, NarL is phosphorylated to NarL-P (Rabin & Stewart, 1993) and positively regulates operon expression by binding to the -60 to -54 region, upstream of the *narGHJI* operon (Stewart, 1982; Rabin, Collins, and Stewart, 1992; Li, Kustu, and Stewart, 1994). However, NarL expression is downregulated by FNR in the presence of Fe-S in cells (Myers, Yan, Ong, Chung, Liang, Tran, Keles, et al., 2013). In addition, Fis protein is involved in the downregulation of *narGHJI* expression (Bradley et al., 2007).

1.5.4.2 TMAO reductase

TMAO reductase belongs to only those few DMSO reductase family members that do not contain an Fe-S cluster (McCrindle, Kappler, and McEwan, 2005). TMAO reductase functions as a terminal electron acceptor like nitrate reductase during anaerobic respiration in the presence of TMAO (Cox et al., 1980; Cox & Knight, 1981). *E. coli* harbors two different types of TMAO reductase, namely TorCA and TorYZ (Gon et al., 2000). However, the *torCAD* operon is induced in the presence of TMAO (Ansaldi et al., 2007).

It has been reported that TMAO reductase is one of the few molybdoenzymes that is expressed in the presence of oxygen (Carey et al., 2018; Kaufmann et al., 2018; Roggiani & Goulian, 2015). TMAO reductase catalyzes the reduction of TMAO to TMA. TMAO reductase consists of two main subunits, TorA and TorC (McCrindle, Kappler, and McEwan, 2005). TorC is an inner-membrane-bound anchor protein (Iobbi-Nivol et al., 1994; Méjean et al., 1994; Gon et al., 2001), which is considered as a hydrophilic protein with a small hydrophobic amino acid portion at the N-terminus (Méjean et al., 1994). Five heme prosthetic groups are present in TorC, four of which are located at the N-terminus of TorC and one at the C-terminus. Electron transfer occurs from the quinone pool through the hemes of membrane-bound TorC and transfers to the catalytic site of periplasmic TorA for reduction (Gon et al., 2001). The TorA subunit contains the bis-MGD cofactor to convert TMAO to TMA (Genest et al., 2008; Méjean et al., 1994; L. Zhang et al., 2008). The bis-MGD is inserted into the TorA subunit with the help of TorD (Genest et al., 2008; Méjean et al., 1994).

TMAO reductase expression is regulated by TorT, TorS, TorR, and TorC (Simon et al., 1994; Gon et al., 2001; Baraquet et al., 2006). It has been reported that the expression of *torCAD* is influenced by phosphorylated TorR, where it positively regulates the expression of the operon (Jourlin et al., 1995; Simon et al., 1994).

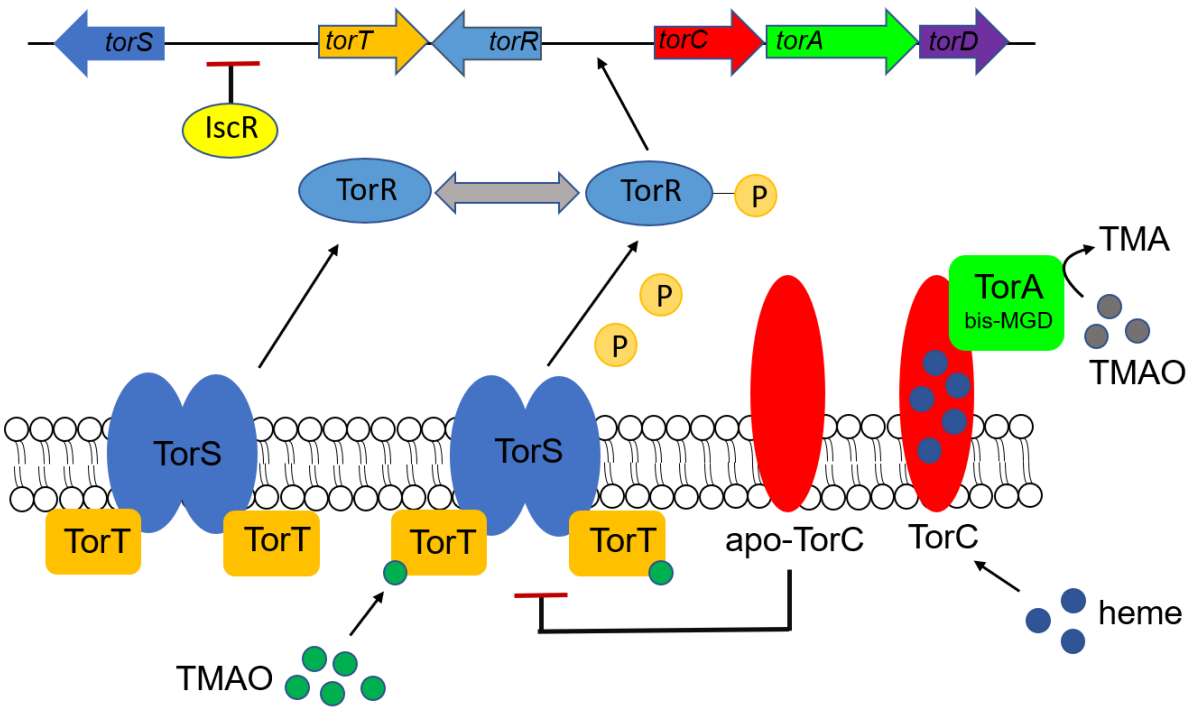

Figure 1-16: Model for the regulation of TMAO reductase in *E. coli* under anaerobic conditions

TorA contains bis-MGD, a terminal electron acceptor under TMAO respiration and catalyzes the conversion of TMAO to TMA; TorC is a membrane-bound *c*-type cytochrome, TMAO reductase expression depends upon the presence of TMAO. The operon is activated through a signaling system that is composed of three proteins: TorT: senses the presence of TMAO in the periplasm, TorS: interacts with TorT and phosphorylates TorR, phosphorylated TorR: activates *torCAD* expression; apo-TorC interacts with TorS and prevents it from phosphorylating TorR and negatively regulate its expression; the expression of *torT* and *torS* is regulated by oxygen through IscR transcription that binds to a shared regulator site between the two genes and represses their transcription

In the presence of TMAO, the TorST complex induces the phosphorylation of TorR, which stimulates the expression of *torCAD* (Jourlin et al., 1996; Simon et al., 1994). Furthermore, membrane-bound TorC also plays a vital role in the expression of the operon. In the absence of heme, apo-TorC negatively regulates *torCAD* expression by interacting with TorS sensory kinase, which prevents the phosphorylation of TorR (Ansaldi et al., 1999; Gon, Jourlin-Castelli, et al., 2001). The formation of holo-TorC is dependent on the availability of iron and the presence of Fe-S clusters in the cells. Under anaerobic conditions, heme biosynthesis is directly influenced by the Fe-S cluster and further regulates expression of the *torCAD* operon. It has been reported that the aminolevulinic acid dehydratase is a [4Fe-4S] cluster containing an enzyme that is involved in the conversion of the second step in heme biosynthesis (Gon et al., 2001). Therefore, the lack of an Fe-S cluster leads to impaired heme biosynthesis and this consequently represses *torCAD* expression. Besides this, *torCAD* expression is also significantly reduced by IscR in the presence of oxygen (Schwartz et al., 2001). The abundance of IscR under the aerobic condition compared to the anaerobic condition facilitates the binding of the IscR between the *torS* and *torT* at the promoter region and represses transcription (Roggiani & Goulian, 2015). TorT and TorS are regulators that positively influence *torCAD* transcription (Simon et al., 1994; Gon et al., 2001). Therefore, the absence of oxygen leads to a reduction in IscR production and positively influences the expression of *torCAD*.

1.5.4.3 Periplasmic aldehyde oxidase (PaoABC)

The xanthine oxidase family of molybdoenzymes is characterized as molybdopterin (MPT)-$Mo^{VI}OS(OH)$ in the oxidation state with one MPT equivalent coordinated to the metal (Hille, 1996). The inactive desulfo-enzyme is formed by removing sulfur from the active molybdenum site, where the oxygen can replace the sulfur.

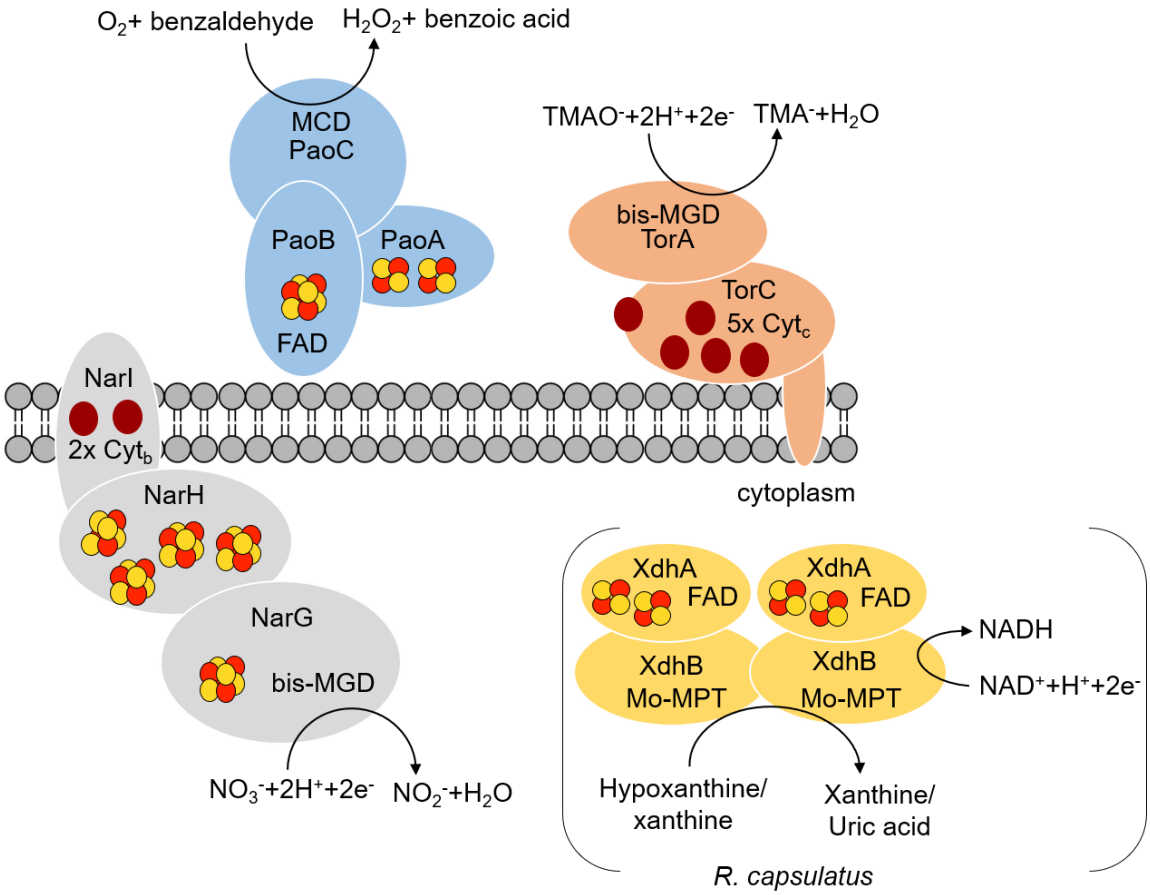

Figure 1-17: Schematic representation of membrane-bound nitrate reductase (NR), TMAO reductase (TMAOR), periplasmic aldehyde oxidase (PaoABC) in *E. coli,* and xanthine dehydrogenase (XDH) from *R. capsulatus*

The *E. coli* membrane-bound NarGHI (NR) contains three subunits: NarI, where the membrane anchor subunit consists of Cyt_b, one [3Fe-4S], three [4Fe-4S] clusters in NarH, and one [4Fe-4S] cluster, bis-MGD in the NarG subunit, which catalyzes the conversion of nitrate to nitrite; TAMOR consists of two subunits, namely TorC and TorA – the TorC subunit contains heme, bis-MGD present in the TorA subunit for catalyzing TMAO to TMA; PaoABC belongs to the xanthine oxidase family (XO) and consists of three subunits: PaoA contains two [2Fe-2S] clusters, one [4Fe-4S] cluster and flavin (FAD) cofactor in PaoB and MCD present in the PaoC subunit to catalyze the aldehydes to their respective acids; xanthine dehydrogenase (XDH) from *R. capsulatus* consists of two subunits: two [2Fe-2S] clusters and a flavin (FAD) cofactor in XdhA, and XdhB contains an Mo-MPT cofactor that catalyzes the formation of xanthine or uric acid and NAD^+ from NADH

The xanthine oxidase family enzymes use oxygen by taking part in two-electron transfer hydroxylation or oxo-transfer reactions with water (Wahl & Rajagopalan, 1982). In *E. coli*, periplasmic aldehyde oxidase (PaoABC) is one of the three enzymes in the xanthine oxidase family. The other two are xanthine dehydrogenase XdhABC and uncharacterized XdhD (Leimkühler & Neumann, 2011). PaoABC is a heterotrimer, with a size of 135.0 kDa, and consists of the Moco-containing large subunit PaoC (78.1 kDa), FAD and one [4Fe-

4S] cluster containing a medium subunit PaoB (33.9 kDa), and a small subunit PaoA (21.0 kDa) that binds two [2Fe-2S] clusters. PaoA contains the Tat-leader peptide that is involved in the periplasmic localization of the enzyme. The PaoD subunit is not part of the mature enzyme but belongs to the operon (Neumann et al., 2009). PaoD has around ~40% amino acid sequence homology to the XdhC in *R. capsulatus* (Neumann et al., 2007b). Therefore, it is believed that PaoD is involved in sulfuration of Moco and further insertion into the PaoC subunit (Iobbi-Nivol & Leimkühler, 2013; Neumann et al., 2007b). The enzyme oxidizes a broad spectrum of aldehydes to their respective carboxylic acids (Neumann et al., 2009).

1.5.4.4 Xanthine dehydrogenase (XDH)

Xanthine dehydrogenase (XDH) is a molybdoflavo-enzyme involved in the oxidation of purine using NAD^+, or a molecular oxygen electron acceptor (Leimkühler et al., 1998, 2003). An autosomal recessive disease identified by hyperuricemia and xanthinuria can be due to a deficiency of xanthine dehydrogenase. The enzyme catalyzes the formation of uric acid from hypoxanthine or xanthine and is excreted through urine. The inactivation or lack of XDH expression reduces cellular xanthine metabolism (Beedham, 2010; Hille, 2007). The XDH from *R. capsulatus* was heterologously expressed in *E. coli* strains in our study. *R. capsulatus* is a heterotetrameric enzyme with a size of 275 kDa, located in the cytoplasm (Leimkühler et al., 2003). The XDH contains two subunits, with the large subunit XDHB at 83.0 kDa containing Moco as a form of MCD, and the relatively small subunit XdhA at 50.0 kDa which consists of FAD and two [2Fe-2S] clusters (Leimkühler et al., 1998, 2003).

1.6 Fumarate and nitrate reduction (FNR)

FNR is a global regulator under anaerobic conditions, which regulates the transcription of hundreds of different genes by activation or repression (Kang et al., 2005; Salmon et al., 2003). FNR stands for fumarate and nitrate reduction (Lambden and Guest, 1976), and regulates the expression of genes with the functions of chemotaxis, cell structure, and signaling, molecular biosynthesis, and others (Kang et al., 2005; Salmon et al., 2003). The activation or repression of FNR regulation is oxygen-dependent (Sutton et al., 2004), whereas FNR requires a [4Fe-4S] cluster under anaerobic conditions (Moore & Kiley, 2001). This leads to a conformational change, and dimerization of protein takes place. Consequently, it becomes activated and able to bind at the promoter site to regulate its

transcription (Moore & Kiley, 2001). The [4Fe-4S]-FNR binds to the respective operon at a specific palindromic consensus sequence TTGATNNNNATCAA (Eiglmeier et al., 1989; Gerasimova et al., 2001). The G and the first T of each FNR half-site appear to interact with the FNR residues Glu-209 and Ser-212 (S Spiro & Guest, 1990). The active FNR can bind to the transcription site at two different promoter regions; class I is located at -61, -71, -82, and -92, and class II is located at -41.5 (Wing, Williams, and Busby, 1995). Under anaerobic conditions, [4Fe-4S]-FNR exists in a homodimeric form (Crack et al., 2014), where the sensory domain is located in the N-terminus end, and the DNA-binding domain at the C-terminus end contains a dimerization motif (Körner, Sofia, and Zumft, 2003). The [4Fe-4S] cluster binds at the N-terminus end containing 5 conserved cysteine residues (Green et al., 1993). FNR inactivation is performed via oxygen, where the [4Fe-4S] cluster is oxidized to [3Fe-4S], followed by the [2Fe-2S] cluster and consequent disassembly of the dimer takes place (Khoroshilova, Beinert, and Kiley, 1995; Lazazzera et al., 1996; Sutton et al., 2004; Jervis et al., 2009; Crack, Thomson, and Le Brun, 2017). The prolonged exposure results in the destruction of [2Fe-2S] clusters and the formation of apo-FNR (Reinhart et al., 2008; Sutton et al., 2004).

1.7 Aims and Objectives

Recently a direct connection between Moco biosynthesis and Fe-S clusters assembly has been discovered. In the first step of Moco biosynthesis, MoaA requires two [4Fe-4S] clusters to catalyze the formation of cPMP from 5'GTP. Besides, molybdoenzymes such as nitrate reductase, formate dehydrogenase, and periplasmic aldehyde oxidoreductase require either [2Fe-2S] or [4Fe-4S] or both clusters for their activity. These observations indicate that Moco biosynthesis or the activity of most molybdoenzymes directly depends on the presence or assembly of Fe-S clusters. The critical gaps in our knowledge are how the Fe-S clusters are inserted into their target apo-enzymes and with what specificity this process is ensured. Therefore, this study focuses on identifying the proteins that insert Fe-S clusters into MoaA and nitrate reductase and how the process is achieved at the cellular level in *E. coli*. Moreover, TMAO reductase is used in our study as a control instead of nitrate reductase since TMAO reductase is devoid of Fe-S clusters. Selected *E. coli* mutant strains in Wt MG1655, *ΔmoeB*, *ΔerpA*, *ΔiscA*, *ΔsufA*, *ΔnfuA*, *ΔiscAΔnfuA*, *ΔiscA/ΔerpA*, *ΔiscA/ΔsufA*, *ΔsufA/ΔerpA*, *Δfnr*, and *ΔiscA/ΔsufA*/*ΔerpA* will be tested for their ability to synthesize Moco, cPMP or to produce an active nitrate reductase or TMAO reductase under anaerobic nitrate or TMAO respiration.

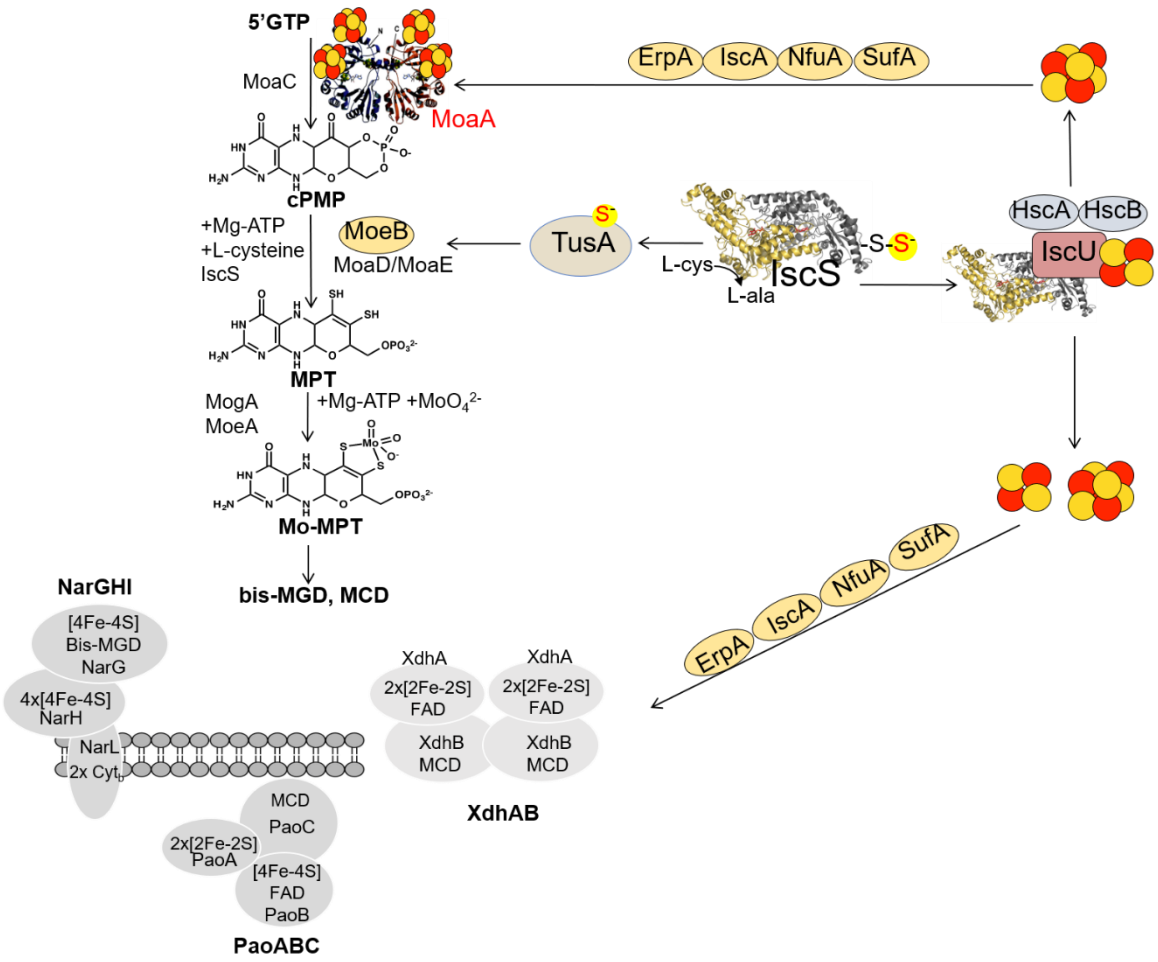

Figure 1-18: Schematic representation of cross-talk between Moco biosynthesis and Fe-S cluster assembly in *E. coli*

Conserved Moco biosynthesis requires four steps: cPMP formation from 5'GTP, MPT formation by sulfur incorporation, the addition of a molybdenum atom, and the modification of Mo-MPT to MCD and bis-MGD cofactors; the Fe-S cluster is required for activation of MoaA in the first step of Moco biosynthesis and intramolecular electron transfer into the molybdoenzymes; the A-type carrier proteins (ATCs)-IscA, SufA, ErpA, and NfuA are the potential candidates for Fe-S cluster transfer into the MoaA and other molybdoenzymes; IscS: PDB – 3LVM; MoaA:PDB – 1TV7

Some genes are involved in Moco biosynthesis and most of the genes encoded in molybdoenzyme expression in *E. coli* are regulated by the transcriptional regulator FNR. Activation of FNR directly depends on the presence of [4Fe-4S] clusters under anaerobic conditions. Therefore, in the absence of an Fe-S cluster, Moco biosynthesis and the expression of molybdoenzymes are inhibited. Therefore, the second objective of our study is to understand FNR regulation in the expression of molybdoenzymes and to identify the particular proteins that insert Fe-S clusters into FNR at the cellular level under anaerobic conditions of nitrate respiration.

Molybdoenzymes such as periplasmic aldehyde oxidase (PaoABC) and xanthine dehydrogenase (XDH) belong to the xanthine oxidase (XO) family. The only difference between these two enzymes lies in the form of the Fe-S clusters present, where the PaoABC contains additional [4Fe-4S] clusters along with 2x[2Fe-2S] clusters, which is absent in XDH (Leimkühler et al., 1998, 2003; Neumann et al., 2009; Otrelo-Cardoso et al., 2014). Therefore, the third objective of our study was to identify the carrier proteins that insert the different Fe-S clusters into the EcPaoABC and RcXDH. Thus, we will express the EcPaoABC and RcXDH in the selected *E. coli* mutant strains in the Wt MG1655, *ΔerpA*, *ΔiscA*, *ΔsufA*, *ΔnfuA* mutant strains, purified, to characterize the enzymes.

2 Materials and methods

2.1 Materials

2.1.1 Media and buffers

All the standard buffers were prepared with deionized Milli-Q water (Merck EMD Millipore Corporation, Billerica, MA). The pH of solutions was adjusted using a glass pH sensor S 100 NE (Knick Elektronische Messgeräte, Berlin) with either HCl or KOH. The solutions were further sterilized with a 0.2 µm sterile filter. The media components were dissolved with deionized water and further sterilized by autoclaving at 121°C, 1 bar for 20 min.

Table 2-1: The list of media and buffers was used in this study

Media and buffers	compositions	pH
LB media	10 g/L of tryptone, 5 g/L of yeast extract, 10 g/L of NaCl	
LB media (overexpression)	10 g/L of peptone, 5 g/L of yeast extract, 10 g/L of NaCl	
MES buffer	500 mM 2-(*N*-morpholino) ethane sulfonic acid, 30 mM $CaCl_2xH_2O$, 22 mM $MnCl_2xH_2O$, 10% Glycerol	6.3
TES buffer	10 mM Tris, 10 mM EDTA, 0.5% SDS	
TAE buffer	1 mM EDTA, 40 mM Tris, 20 mM acetic acid	
Resuspension buffer (1)	50 mM sodium phosphate, 300 mM NaCl	8.0
Resuspension buffer (2)	50 mM Tris-HCl	7.5
Resuspension buffer (3)	100 mM Tris-HCl	7.2
Wash buffer (1)	10 mM imidazole, 50 mM sodium phosphate, 300 mM NaCl	8.0
Wash buffer (2)	20 mM imidazole, 50 mM sodium phosphate, 300 mM NaCl	8.0
Elution buffer (1)	250 mM imidazole in 50 mM sodium phosphate, 300 mM NaCl	8.0
Elution buffer (2)	50 mM Tris-HCl, 200 mM NaCl, 1 mM EDTA	7.5
	50 mM Tris-HCl, 200 mM NaCl, 2.5 mM DTT, 1 mM EDTA	7.5

Dialysis buffer (1)	50 mM Tris, 1 mM EDTA	7.5
Dialysis buffer (2)	50 mM Tris-HCl, 2.5 mM DTT, 1 mM EDTA	7.5
Transfer buffer	25 mM Tris-HCl, 200 mM glycine, 20% methanol	
TBS-T buffer	50 mM Tris-HCl, 150 mM NaCl, 0.1% (w/v) Tween-20	7.4
Solution A	100 µL 250 mM luminol, 44 µL 90 mM p-coumaric acid, 8.85 mL H_2O	
Solution B	1 ml 1 M Tris-HCl, pH 8.5, 6 µL 30% H_2O_2, 9 mL of H_2O	
Acidic iodine	914 µL I_2/KI+86 µL 37% HCl	
Potassium phosphate buffer	10 mM KH_2PO_4	3.0
Potassium phosphate buffer (2)	33.7 mM K_2HPO_4, 66.3 mM KH_2PO_4	6.5
Buffer Z	40 mM NaH_2PO4, 10 mM KCl, 1 mM MgSO4, 0.05 β-mercaptoethanol	7.0
Reaction buffer (XDH)	50 mM Tris-HCl, 1 mM EDTA	8.0
McIlvaine buffer	200 mM Na_2HPO_4, 100 mM citric acid	6.5
SDS-PAGE buffer	192 mM glycine, 25 mM Tris, 0.1 % (w/v) SDS	8.2
Coomassie staining solution	40% (v/v) MeOH, 10 % (v/v) acetic acid, 0.25 (w/v) Coomassie	

2.1.2 Antibiotics

The antibiotic stock solutions were prepared with either Millipore water or 97% ethanol and sterilized with a 0.2 µm sterile filter. The following concentration of antibiotics was used in experiments: 150 µg/mL for Ampicillin, 50 µg/mL for Kanamycin, 50 µg/mL for Chloramphenicol in 97% (w/v) ethanol and 50 µg/mL for Spectinomycin, and 50 µg/mL for Tetracycline in 97% (w/v) ethanol.

2.1.3 Plasmids

Table 2-2: The list of plasmids was used in this study

Plasmids	Genotype or relevant characteristics	Source or reference
pmoaABCDE	*moaABCDE* coding region cloned into HindIII/XhoI of *pCDF-duet1*, Spec^r	This study
pnarGHJI	*narGHJI* coding region cloned into *pTrcHis* NdeI/SalI, Amp^r	This study
pMN100	*paoABCD* coding region cloned into *pTrcHis* NdeI/SacI, Amp^r	(Neumann, Mittelstädt, et al., 2009)
pSL207	*RcxdhABC* coding region cloned into *pTrcHis* NdeI/HindIIII, Amp^r	(Leimkühler et al., 2003)
pfnr	*fnr coding region cloned into pTrcHis*	This study
pLAS-A	*sufA* coding region cloned into EcoRI/XhoI of *pBAD-I*, Amp^r	(Daniel Vinella et al., 2009)
pLAI-A	*iscA* coding region cloned into EcoRI/XhoI of *pBAD-I*, Amp^r	(Daniel Vinella et al., 2009)
pLAE-A	*erpA* coding region cloned into EcoRI/XhoI of *pBAD-I*, Amp^r	(Daniel Vinella et al., 2009)
psufA	*sufA* coding region cloned into BamHI/XhoI of *pCDF-Duet1*, spec^r	This study
piscA	*iscA* coding region cloned into NdeI/XhoI of *pCDF-Duet1*, spec^r	This study
perpA	*erpA* coding region cloned into BamHI/XhoI of *pCDF-duet1*, spec^r	This study
PtorCAD-lacZ	Gene region -276 bp to -1 bp upstream of *torC* transcriptional start cloned into smaI site of *pGE593*, Amp^r	(Jourlin et al., 1995)
pJD84	Gene region -200 bp to -1 bp upstream of *pepT* transcriptional start cloned into EcoRI/BamHI sites of *pGE593*, Amp^r	(Dahl, Radon, Buhning, et al., 2013)

Pfnr-lacZ	Gene region -200 bp to -1 bp upstream of *fnr* transcriptional start cloned into BamHI site of *pGE593*, Amp^r	This study
PmoaA-L-lacZ	Gene region -477 bp to -1 bp upstream of *moaA* transcriptional start cloned into EcoRI/BamHI sites of *pGE593*, Amp^r	(Zupok et al., 2019)
pGE593	*pBR322Δtet lacZ lacY'*	(Zupok et al., 2019)
pTrcHis	Expression vector *pTrcdel* containing the His_6-Tag and *trc* promotor, Amp^r	(Temple et al., 2000)
pCDF-duet1	T7-RNA polymerase-based expression vector, CloDF13 origin, Spec^r	Novagen

2.1.4 Bacterial strains

Table 2-3: The list of strains was used in this study

Strains	Genotype characteristics	Sources or references
DH5α	F-, supE44, Δlac U169, (φ80*lacZ* ΔM15), hsdR17, endA1, gyrA96, thi-1, relA1, recA56	(Hanahan, 1983)
MG1655 MVA+	Parental strain, MG1655 derivative carrying the MVA pathway genes in the chromosome	(Daniel Vinella et al., 2009)
Δ*moeB*	MG1655 derivative, Δ*moeB::cat*, MVA+	This study
Δ*erpA* (DV1094)	MG1655 derivative, Δ*erpA::cat*, MVA+	(Daniel Vinella et al., 2009)
Δ*iscA* (DV700)	MG1655 derivative, Δ*iscA::kan,* MVA+	(Daniel Vinella et al., 2009)
Δ*nfuA* MVA+	MG1655 derivative, Δ*nfuA::kan,* MVA+	(Py et al., 2018a)
Δ*sufA* MVA+	MG1655 derivative, Δ*sufA*::cat, MVA+	This study
Δ*nfuA*/Δ*iscA* MVA+	MG1655 derivative, Δ*nfuA::*Δ*iscA::cat*; MVA+	(Daniel Vinella et al., 2009)

Δ*iscA*/Δ*erpA* (DV1217)	MG1655 derivative, Δ*iscA*::Δ*erpA::cat*; MVA+	(Daniel Vinella et al., 2009)
Δ*sufA*/Δ*iscA* (DV1219)	MG1655 derivative, Δ*sufA*::Δ*iscA::cat*; MVA+	(Daniel Vinella et al., 2009)
Δ*sufA*/Δ*erpA* (DV1220)	MG1655 derivative, Δ*sufA*::Δ*erpA::cat*; MVA+	(Daniel Vinella et al., 2009)
Δ*sufA*/Δ*iscA*/Δ*erpA* (DV1285)	MG1655 derivative, Δ*sufA*::Δ*iscA*::Δ*erpA::cat*; MVA+	(Daniel Vinella et al., 2009)
Δ*fnr*	MG1655 derivative, Δ*fnr::kan*, MVA+	This study
Δ*moaA*	BW25113 derivative, Δ*moaA::kan*	(Baba et al., 2006)
Δ*sufS*	BW25113 derivative, Δ*sufS::kan*	(Baba et al., 2006)
Δ*iscS*	BW25113 derivative, Δ*iscS*::kan	(Baba et al., 2006)
Δ*moaC*	BW25113 derivative, Δ*moaC::kan*	(Baba et al., 2006)
Δ*torA*	BW25113 derivative, Δ*torA::kan*	(Baba et al., 2006)
Δ*iscA*	BW25113 derivative, Δ*iscA::kan*	(Baba et al., 2006)
Δ*sufA*	BW25113 derivative, Δ*sufA::kan*	(Baba et al., 2006)
Δ*nfuA*	BW25113 derivative, Δ*nfuA::kan*	(Baba et al., 2006)
Δ*bolA*	BW25113 derivative, Δ*bolA::kan*	(Baba et al., 2006)
Δ*grxA*	BW25113 derivative, Δ*grxA::kan*	(Baba et al., 2006)
Δ*grxB*	BW25113 derivative, Δ*grxB::kan*	(Baba et al., 2006)
Δ*grxC*	BW25113 derivative, Δ*grxC::kan*	(Baba et al., 2006)

2.1.5 Oligonucleotides

Different oligonucleotides were used in this study for qRT-PCR (Quantitative Real time PCR), verification PCR, antibiotic cassette amplification PCR, and cloning. All the oligonucleotides were purchased from Eurofins Genomics GmbH and are listed in appendix Table 7-1.

2.1.6 Enzymes

All the restriction enzymes for this study (NdeI, EcoRI, XhoI, BamHI, SalI and HindIII) and T4 ligase were purchased from New England Biolabs and Thermo Fisher Scientific. The DNA polymerase Herculase II was purchased from Agilent Technologies.

2.1.7 Markers and dyes

The agarose and SDS loading dyes were prepared as

6X Agarose loading dye	30% (w/v) glycerol, 0.25% (w/v) Bromophenol Blue, water
5X SDS loading dye	250 mM Tris/HCl pH 6.8, 0.5% Bromophenol blue, 10% (w/v) SDS, 50% (w/v) glycerol, 500 mM 2-mercaptoethanol

2.1.8 Kits

Table 2-4: The list of Kits was used in this study

NucleoSpin Plasmid Purification	Macherey & Nagel (Düren, Germany)
NucleoSpin Gel and PCR Clean Up	Macherey & Nagel (Düren, Germany)
High Pure RNA Isolation Kit	Roche Applied Biosystems (Mannheim, Germany)
Quantitect reverse transcription kit	Qiagen (Hilden, Germany)
Quick change site-directed mutagenesis	Agilent technology (Waldbronn, Germany)
Power SYBR Green PCR Master Mix	Applied Biosystems, Darmstadt, Germany

2.1.9 Growth curves

The growth curve was measured to analyze the growth pattern of the strains since deletion of essential genes leads to growth defects for the strains. The precultures were prepared from the single colony of *E. coli* strains and incubated at 37°C in the presence of 1 mM mevalonate and 15 mM potassium nitrate or TMAO under anaerobic conditions with appropriate antibiotics. The main cultures were prepared by inoculating the precultures in 50 mL LB media in the presence of 1 mM mevalonate and 15 mM potassium nitrate or TMAO with the starting cell density (OD_{600}) of 0.05 at 37°C anaerobically. Afterward, 1 mL culture suspension was aliquoted every hour in a cuvette, and OD_{600nm} was measured using a spectrophotometer for 12 h.

2.2 Methods

2.2.1 Molecular Biology

2.2.1.1 Cultivation

The *E. coli* MG1655 strains were cultivated in LB media in the presence of suitable antibiotics. Anaerobic cultivation was undertaken anaerobically for 8 h with the supplement of 15 mM potassium nitrate or 15 mM TMAO as an alternative electron acceptor in the presence of 1 mM mevalonate. All the protein expressions were performed at either 22°C (EcPaoABC) or 30°C (RcXDH) for 24 h under a semi-aerobic cultivation condition, where tryptone was replaced by peptone (10 g/L) in presences of 20 µM IPTG.

2.2.1.2 Preparation of competent cells

2.2.1.2.1 Chemical competent cells

The chemical competent cells were prepared according to Dagert and Ehrlich (1979) for the transformation of extrachromosomal plasmid DNA. To obtain the competent cells, a respective single colony of *E. coli* strain was incubated in 50 mL of LB media with the supplement of 20 mM $MgSO_4$ and suitable antibiotics for 3-4 h at 37°C until a cell density (OD_{600nm}) of 0.7-0.9 was reached. After cooling at 4°C for 30 min, the cells underwent harvesting at 727xg for 12 min. The pellets were further resuspended in an MES buffer (500 mM 2-(*N*-morpholino) ethane sulfonic acid, 30 mM $CaCl_2xH_2O$, 22 mM $MnCl_2xH_2O$,

10% Glycerol, pH 6.3) and incubated for 10 min at 4°C. The centrifugation process was repeated, and cells were further resuspended in a 2 mL MES buffer. Afterward, the 100 µL separated aliquots were prepared and stored at -80°C for future use.

2.2.1.2.2 Electrocompetent cells

The electrocompetent cells were prepared to transform linear DNA into the *E. coli* strain by electroporation (Gonzales et al., 2013). This method is widely used for selective gene deletion using the lambda-red recombination technique. The respective colony from the *E. coli* strain containing pkD46 plasmid was cultivated in 5 mL LB media in the presence of an appropriate antibiotic for 3-4 h with 10 mM L-arabinose until a cell density of 0.6-0.7 was reached. Further, the cells were harvested at 4000xg for 10 min and resuspended twice with 5 mL sterile water for washing. After resuspension, the centrifugation process was repeated twice, and the supernatant discarded. The pellets were again resuspended twice with 10% (v/v) glycerol and further centrifuged at 4000xg for washing. Afterward, the pellets were resuspended in 100 µL 10% (v/v) glycerol, which was used for electroporation.

2.2.1.3 Cloning

2.2.1.3.1 Isolation of genomic DNA

Genomic DNA was isolated from the wild-type *E. coli* MG1655, which was used for the amplification by PCR for cloning purposes. The *E. coli* strain was cultivated in 5 mL LB media at 37°C overnight. Afterward, the cells were harvested at 11000xg for 1 min and washed twice with a TES buffer (10 mM Tris, 10 mM EDTA, 0.5% SDS). After the final centrifugation step, the cells were resuspended with 800 µL of TES buffer. About 20 µL of 20% SDS-lysed were added to the cell suspension and incubated for 30 min at RT. Further, 300 µL of phenol was added to the batch and centrifuged at 12000xg for 10 min. Then 300 µL of phenol was again added to obtain the upper phase, and this step was repeated four times. Afterward, the equivalent volume of isopropanol was added with the obtained upper phase, and the genomic DNA was incubated for 1 h at -20°C for precipitation. Centrifugation was conducted at 15000xg for 20 min at 4°C to obtain the pellet, which was further washed twice with 1 mL 70% ethanol. After centrifugation, the ethanol was completely removed and dried at 37°C for 20 min. The pellets were

resuspended with 100 µL TES buffer and incubated at 37°C for 1 h. The concentration of genomic DNA was measured at 260 nm and further stored at -20°C.

2.2.1.3.2 Polymerase chain reaction (PCR)

PCR was carried out to amplify particular genes, which were intended to be cloned into a specific plasmid for expression. It was also used for amplification of antibiotic cassette for selective gene knock-out using lambda-red recombination.

2.2.1.3.3 Amplification of genes

The amplification of the selected gene was performed by means of a polymerase chain reaction (PCR). The volume of the reaction was 50 µL.

Table 2-5: Composition of PCR reaction for gene amplification

Components	Volume [µL]
5x Herculase buffer	10
10 mM dNTP	1
DMSO	2.5
50 pmol/µL forward primer	1.25
50 pmol/µL reverse primer	1.25
1 U/µL Herculase II	1
250 ng/µL DNA template	1-2
Water	To make the volume 50 µL

The standard protocol of amplification PCR depends on the annealing temperate at step 3, which is directly influenced by the melting temperature of primers. The elongation temperature also varies according to the size of the fragments, which can be 1000 bps per minute. The standard PCR program contained following steps:

Step 1	Denaturation	4 min at 95°C	
Step 2	Denaturation	30 s at 95°C	34X
Step 3	Annealing of primers	30 s at primer melting temperature (Tm)	
Step 4	elongation	1 min/1000 bps at 72°C	
Step 5	Final elongation	6 min at 72°C	

2.2.1.3.4 Verification of genes

The presence or absence of selected gene fragments can be evaluated using verification polymerase chain reaction (PCR). This method is widely used to verify knock-out for a selected gene. PCR was performed using a single colony or pre-culture instead of pure DNA fragments. The final volume of this PCR reaction was 25 µL.

Table 2-6: Composition of PCR reaction for gene verification

Components	Volume [µL]
5x Herculase buffer	5
10 mM dNTP	0.5
DMSO	1.25
50 pmol/µL forward primer	0.75
50 pmol/µL reverse primer	0.75
1 U/µL Herculase II	0.5
DNA template	Colony fractions or 1 µL culture
Water	To make the volume 25µL

The standard protocol for verification PCR was identical to the amplification PCR, which has been previously described.

2.2.1.3.5 Restriction digestion

Restriction double digestion was performed during the cloning for introducing the specific (sticky) ends for both vector and insert, which allows the ligation of a suitable (insert) gene in the vector. The final volume of the restriction double digestion reaction was 20 µL. The reaction was performed for 2-3 h with suitable restriction enzymes, except for high fidelity (HF) restriction enzymes, which were used for 10-15 min. During vector digestion, FastAP was used to avoid re-ligation of the end after the cleavage by enzymes.

Table 2-7: Reaction composition of restriction digestion

Components	Vector digestion [µL]	Insert digestion [µL]
DNA	10	10
Water	5	6
10x Reaction buffer	2	2

Restriction enzyme 1	1	1
Restriction enzyme 2	1	1
Fast AP	1	

2.2.1.3.6 Agarose gel electrophoresis

Agarose gel electrophoresis was used to isolate the DNA fragments according to their respective sizes. In this study, 1% (w/v) agarose gel was used, which contains 1% (w/v) ethidium bromide. The gel was run at 90-100 V in a 1% TAE buffer (1 mM EDTA, 40 mM Tris, 20 mM acetic acid). The DNA or PCR product was combined with DNA-loading dye and a 1 Kbs DNA ladder was deployed to identify the size of DNA fragments.

2.2.1.3.7 Isolation of DNA fragment from the agarose gel

The DNA fragment was isolated from the gel and further purified for use as a template in cloning and gene knock-out. The extraction of purified DNA fragments was performed using the NucleoSpin Extract II Kit (Macherey-Nagel) and eluted with 20-50 µL of water at 70°C.

2.2.1.3.8 Ligation

Ligation was conducted for tying the suitable gene fraction to a vector. The ligation was carried out at 16°C overnight with the T4 ligase enzyme. The reaction was stopped at 65°C for 20 min. The 5-fold higher insert DNA to vector DNA ratio was used during the ligation reaction. The final volume of the reaction was 20 µL.

Table 2-8: Reaction composition of vector and insert ligation

Components	Volume [µL]
Insert DNA (4-6 µg)	10
Vector DNA (1 µg)	2
10x T4 ligase buffer	2
1 U T4 ligase	1
Water	5

2.2.1.4 Transformation

2.2.1.4.1 Heat shock transformation

Heat shock was performed for the transformation of the circular plasmid DNA into the *E. coli* strain. Around 1-2 µL of plasmid DNA was added to the competent cells and further incubated in ice for 30 min. Afterward, the mixture of cells and plasmid DNA was heat-shocked at 42°C for 0.5 min and again incubated in ice for 2 min. Around 800 µL of LB media was added to the cells and further incubated at 37°C for 1 h. About 200 µL of aliquots were spread on an agar plate with appropriate antibiotics.

2.2.1.4.2 Electroporation

Electroporation was applied for the transformation of linear DNA into the *E. coli* strains. About 1 µg of purified linear DNA fragment was added to the electrocompetent cells prepared fresh according to the preparation of the electrocompetent cells outlined above at 2.2.1.2.2. Further, the DNA and cell mixture were transferred into the electroporation cuvette and electroporate at 2.5 kV. Afterward, 1 mL of warm LB media was added to the mixture and incubated for 2 h at 37°C. Then, 200 µL of aliquots were spread on the agar plate in the presence of appropriate antibiotics.

2.2.1.5 RNA extraction

The total RNA was extracted from the *E. coli* Wt MG1655 and mutant strains, which were grown with 15 mM potassium nitrate at 37° for 8 h anaerobically. The extraction was performed using the High Pure RNA Isolation Kit (Roche Applied Biosystem) according to the specifications of manufacturer. The total RNA concentration and purity were determined by its absorption at 230 nm and A230/A260, respectively, using Nanodrop (Shimadzu Scientific).

2.2.1.6 Reverse transcription

Reverse transcription was performed to produce cDNA from the extracted mRNA. This cDNA was further used in RT-qPCR to analyze the expression of respective genes. The conversion of cDNA from mRNA was executed by a reverse transcript kit (Qiagen). The concentration and purity of the produced cDNA were measured by its absorption at 260 nm and A260/A230, respectively, using Nanodrop (Shimadzu Scientific).

2.2.1.7 qRT-PCR

qRT-PCR was conducted to analyze the relative expression of selective genes under a specific growth condition. In our study, the strains were grown anaerobically with 15 mM potassium nitrate for 8 h at 37°C. Quantitative real-time PCR (qRT-PCR) was performed in a final volume of 10 µL according to the instructions of Power SYBR Green PCR Master Mix (Applied Biosystems, Darmstadt, Germany) using the CFX96 system (Bio-Rad, Munich, Germany). The reaction was performed with 2-4 biological replicates for each strain.

2.2.1.8 Construction of mutants

2.2.1.8.1 Removal of antibiotic cassette

The removal of the antibiotic cassette was necessary to construct double or triple mutant strains from the single mutant strain to avoid the antibiotic selection problem. Cassette removal was executed by Flp-recombinase, whose gene is encoded in pCB20 plasmid. The *E. coli* strain that contains the antibiotic cassette was transformed with plasmid pCB20 by heat-shock transformation and further incubated at 30°C with LB media since pCB20 is a temperature-sensitive plasmid. Afterward, 200 µL of aliquot was spread in the LB amp-agar plate and incubated at 30°C overnight to express the Flp recombinase. Further, several colonies were picked from the LB amp-agar plate and patched two times on new LB amp-plates at 30°C to ensure complete removal of the antibiotic cassette. Then, several colonies were picked and subsequently patched at least three times at 43°C on LB plates containing no antibiotics. Afterward, one single colony from the LB plate was struck out on (a) LB plates without any antibiotics, (b) antibiotic plates that were intended to be removed, and (c) LB amp-plates, to remove any traces of the plasmid. The colonies were exclusively grown in LB plates without antibiotics, and no colonies were observed on the other two plates. Furthermore, the single colonies were tested with verification PCR to confirm the removal of the antibiotic cassette.

2.2.1.8.2 Site-directed mutagenesis

Site-directed mutagenesis was performed by using a polymerase chain reaction (PCR). Based on the site-directed mutagenesis quick-change method (Braman et al., 1996), the Quick-change Lighting site-directed mutagenesis kit from Agilent Technology was used.

The primers were designed for this PCR reaction as homologous to the cDNA template with a mutation to the base pair in the sequence.

Table 2-9: Composition of PCR reaction for site-directed mutagenesis

Components	Volume [µL]
10x reaction buffer	5
10 mM dNTP	1
100 ng DNA template	1.5
50pmol/µL forward primer	1.25
50pmol/µL reverse primer	1.25
2.5U/µL Pfu Ultra HF DNA polymerase	1
Water	To make the volume 50µL

The PCR program for site-directed mutagenesis contained following steps:

Step 1	Denaturation	30 s at 95°C	
Step 2	Denaturation	30 s at 95°C	18X
Step 3	Annealing of primers	1 min at primer melting temperature (Tm)	
Step 4	Elongation	1 min/1000 bps at 68°C	
Step 5	Final elongation	10 min at 68°C	

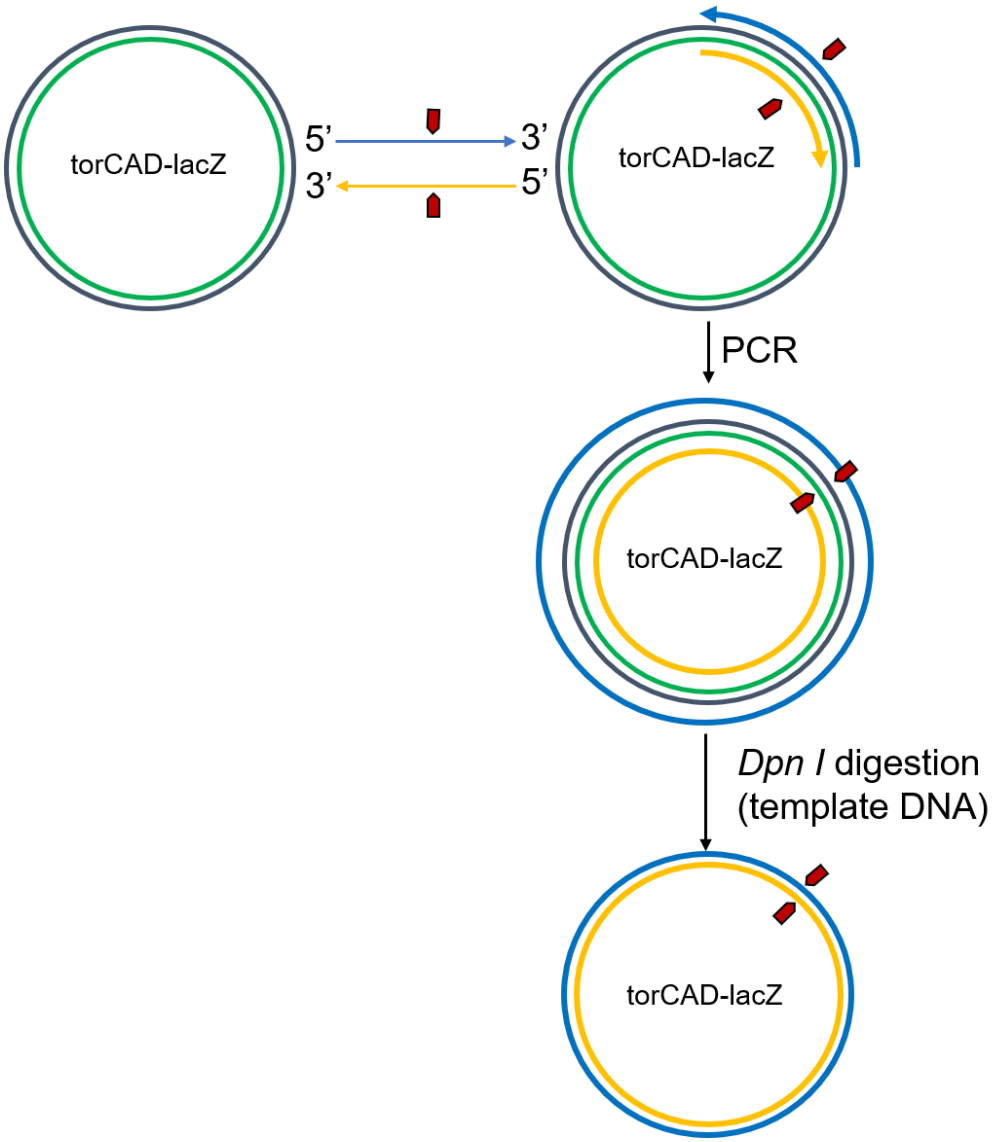

Figure 2-1: Site-direct mutagenesis by PCR

Mutagenesis of a single base by using mutagenic primers; the *Dpn I* is used for digestion of parenteral DNA

After the PCR reaction, 1 µL of 10 U/µL *DnpI* restriction enzyme was added to the PCR mixture and incubated at 37°C for 1 h. *DnpI* is specific for methylated DNA. The template plasmid that was biosynthesized in *E. coli* had been digested, while the mutated plasmid, which was generated in vitro and unmethylated, had been left undigested. Afterward, the PCR product was transformed into a DH5α and further plaited with the appropriate antibiotics. The single colony was picked on the following day, and mini prep was performed. The extracted plasmid was sent for sequencing to identify the single point mutation.

2.2.1.8.3 Selective gene knock-out

Gene knock-out was performed using the single-gene knock-out technique by means of the λ-red system, adapted from Datsenko and Wanner (2000). The selective gene to be knocked out was replaced by an antibiotic cassette as a selection marker. The lambda-red system works by homologous recombination in vivo in *E. coli*. This allows for choosing the homologous arm at 50 bps upstream and downstream of the selected gene, which can easily be added to the functional cassette by long PCR primers (70-80 bps). The pKD3 and pKD4 templates were used to amplify chloramphenicol and kanamycin cassette, respectively, with 50 bps upstream and downstream homology with the selective gene. The host *E. coli* strain requires a pKD46 plasmid, which further expresses the lambda-red (RecE and RecT) recombinase enzyme under the induction with 10 mM L-arabinose. These enzymes are facilitated in the exchange between the gene to be knocked out and the antibiotic cassette.

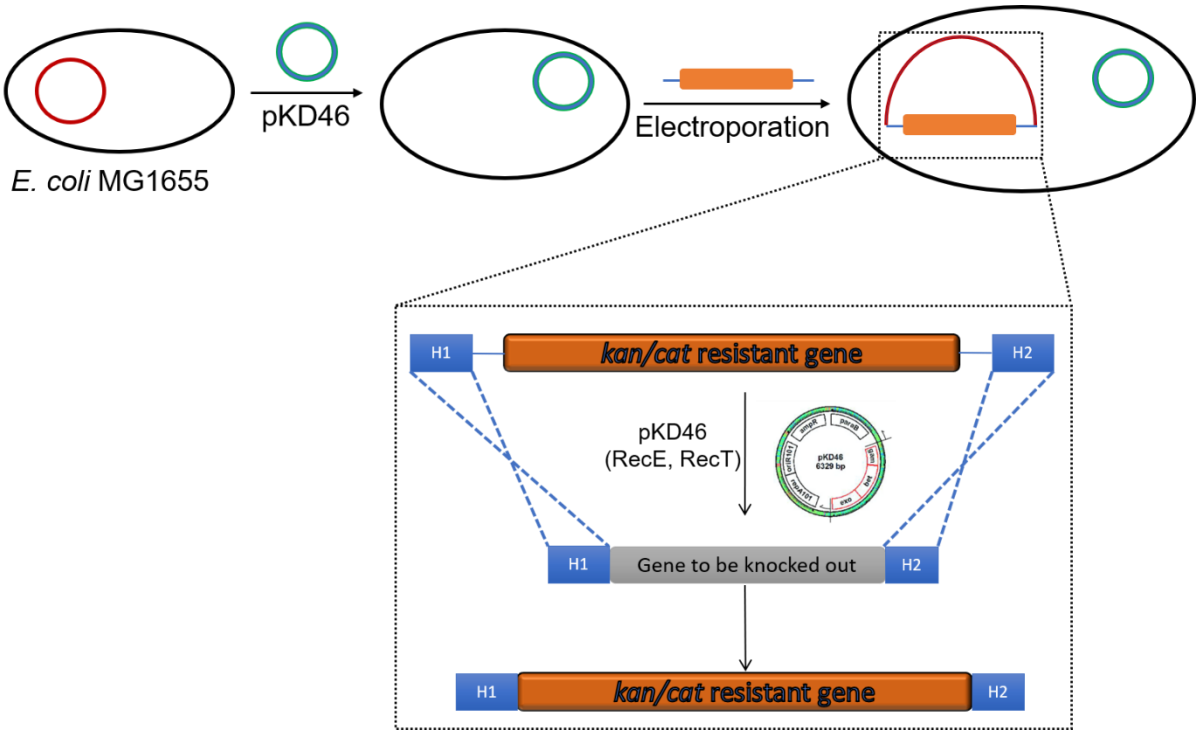

Figure 2-2: Flow scheme for single-gene knock-out using the λ-red system

The strain was transformed with pKD46 plasmid, which contains recombinase enzymes. RecT and RecE function as recombinase enzymes, which are induced using L-arabinose at 30°C; H1 and H2 refer to the homologous arm around 50-70 bps

For this experiment, the pKD3 and pKD4 template DNA was amplified using the PCR gene amplification protocol according to 2.2.1.3.3. In addition, the PCR product containing

chloramphenicol (cat) or kanamycin (kan) cassette was purified from the agarose gel according to 2.2.1.3.7. The single colony of pKD46 containing the host *E. coli* strain was grown in LB at 30°C for 2-3 h with 10 mM L-arabinose to induce the expression of lambda-red recombinase (RecE and RecT). Afterward, electrocompetent cells were prepared with the grown host *E. coli* strain according to 2.2.1.2.2. Furthermore, the transformation of PCR product (cat or kan cassette) was performed by electroporation at 2.5 kV, and 1000 µL of LB media was added to the cells and incubated at 37°C for 2 h according to 2.2.1.4.2. About 200 µL of aliquots were spread on an agar plate with appropriate antibiotics. Afterward, deletion of the selective gene was verified by colony verification PCR.

2.2.2 Biochemical Methods

2.2.2.1 Overexpression of proteins

Overexpression of proteins was performed after the transformation of plasmid by either heat shock or electroporation of the gene of interest into the selective *E. coli* strain. In general, the strain containing the selective plasmid was incubated aerobically in LB media in the presence of appropriate antibiotics at 130 rpm. Expression was induced with either 20 µM IPTG or 0.2% L-arabinose regarding the protomers for transcription. The cells were harvested by centrifugation at 8000xg for 5 min and resuspended in a suitable buffer before storage at -20°C. On the other hand, anaerobic expression was performed in the presence of 15 mM potassium nitrate or 15 mM TMAO. The cells were incubated in a 50 mL falcon tube without any shaking at 37°C. The anaerobic overexpression of the *narGHJI* and *moa* operons was performed at 24°C and 37°C for 24 h and 8 h respectively in the presence of 20 µM IPTG and 0.2% L-arabinose, respectively. All the purified proteins in this work are listed in Table 2-10 including their expression condition, the plasmids, strains used for expression, and respective antibiotics.

Table 2-10: Overview of the expressed proteins in this study with expression conditions, plasmids, inducer and respective antibiotics

Proteins	Plasmid	Condition	Inducer	Antibiotics
Nitrate reductase	endogenous	8 h, 37°C, anaerobic	15mM KNO_3	
TMAO reductase	endogenous	8 h, 37°C, anaerobic	15 mM TMAO	

Nitrate reductase	*narGHJI (pTri-His)*	24 h, 24°C, anaerobic	20 µM IPTG	Ampicillin
MoaABCDE	*moaABCDE (pCDF-duet1)*	8 h, 30°C, anaerobic	0.2% L-arabinose	Spectinomycin
Periplasmic aldehyde oxidase	*paoABCD (pMN100)*	24 h, 22°C, 130rpm	20 µM IPTG	Ampicillin
Xanthine dehydrogenase	*xdhABC (pSL207)*	24 h, 30°C, 130 rpm	20 µM IPTG	Ampicillin
SufA	*pLAS-A (pBAD-I)*	8 h, 37°C, anaerobically	15 mM KNO_3, 0.2% L-arabinose	Ampicillin
IscA	*pLAI-A (pBAD-I)*	8 h, 37°C, anaerobically	15 mM KNO_3, 0.2% L-arabinose	Ampicillin
ErpA	*pLAE-A (pBAD-I)*	8 h, 37°C, anaerobically	15 mM KNO_3, 0.2% L-arabinose	Ampicillin
SufA	*PsufA (pCDF-duet1)*	8 h, 37°C, anaerobically	15 mM KNO_3, 0.2% L-arabinose	Spectinomycin
IscA	*PiscA (pCDF-duet1)*	8 h, 37°C, anaerobically	15 mM KNO_3, 0.2% L-arabinose	Spectinomycin
ErpA	*PerpA (pCDF-duet1)*	8 h, 37°C, anaerobically	15 mM KNO_3, 0.2% L-arabinose	Spectinomycin

2.2.2.2 Cell lysis

Lysis was performed using the harvested cells, which were stored at -20°C. Cell lysis was carried out using either a cell disruptor or with an ultrasonic method by sonification.

2.2.2.2.1 Cell disruptor

The cells were thawed and further resuspended with 10 mM imidazole, 50 mM sodium phosphate, 300 mM NaCl, pH 8.0. DNase (1 µg/mL) was added to the cell suspension before lysis. The resuspended cells were lysed two times mechanically using high pressure and shear force in a pre-cooled (12°C) cell disruptor (TS Benchtop Series, Constant Systems Ltd) at 1.35 kbar. The cell debris was separated from the cytosolic materials by centrifuging at 4°C, 13500xg for 45 min. The separated supernatant contained the protein that was to undergo further purification. The complete process was performed at 4°C to minimize protease activity.

2.2.2.2.2 Sonification

Sonification was conducted to disrupt the anaerobically grown cells using the ultrasound method. The procedure was performed in a 1.5 mL Eppendorf tube at 4°C to neutralize heat generation as a result of sonification. The cell pellets were resuspended using 1 mL 50 mM Tris-HCl, pH 7.5, and further lysed using 20% amplitude with 2 sec on and 2 sec off for 30 sec. For the anaerobically *narGHJI*- and *moa*-operon overexpressed culture, cell lysis was undertaken using 25% amplitude with 2 sec on and 2 sec off for 1 min. After sonification, the cell debris was removed by centrifugation at 4°C, 13500xg for 30 min. The supernatant was collected and further used for activity study and cofactor analysis.

2.2.2.3 Purification of protein

The collected crude extract after the centrifugation was used to purify the expressed protein. The purification was performed in the following two steps.

2.2.2.3.1 Affinity purification

Affinity purification was done by immobilized metal ion affinity chromatography (IMAC) using a Ni^{++}-NTA matrix, in which the Ni^{++}-ion competitively binds with 6x histidine of the expressed protein. Ni^{++}-NTA is a complex of Ni^{++}-ions with nitrilotriacetic acid (NTA). The elution of protein was performed using a high concentration of competitors such as imidazole.

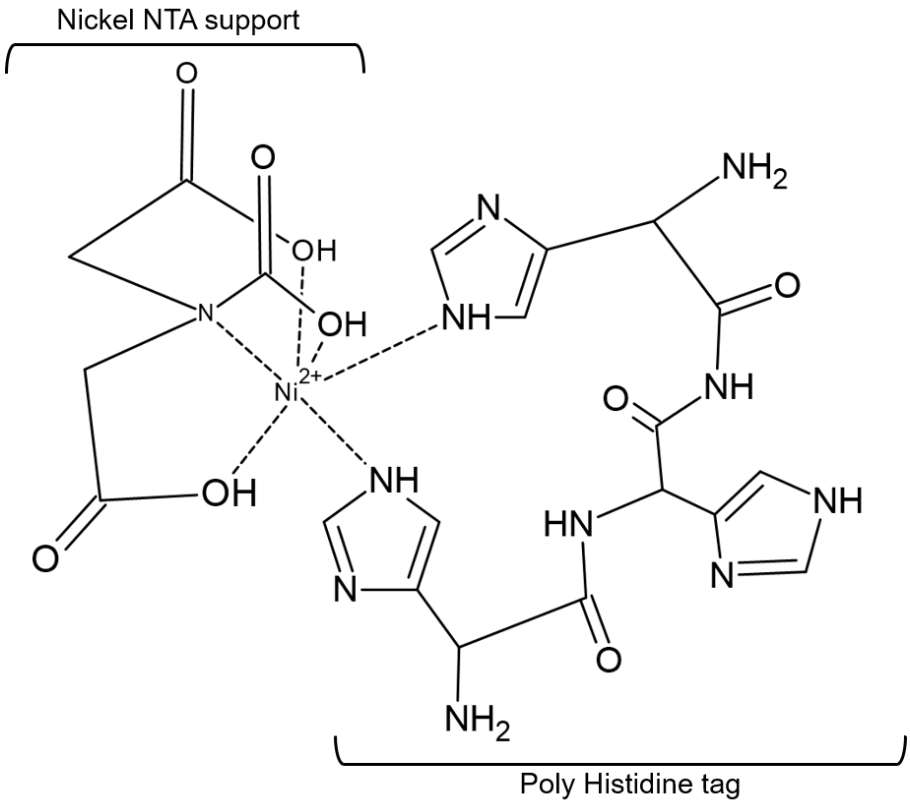

Figure 2-3: Principle of IMAC (immobilized metal affinity chromatography)

A specific coordinate covalent bond between Ni^{++} and an imidazole ring of histidine; here nitrilotriacetic acid (NTA) is shown as a spacer, which connects with the resin (beads)

The Ni^{++}-NTA matrix was pre-equilibrated with 50 mL of 10 mM imidazole, 50 mM sodium phosphate, 300 mM NaCl, pH 8.0. Afterward, the collected crude extract from the lysed cells was poured into the Ni^{++}-NTA matrix (0.5 mL/L of culture volume), allowing the histidine-containing protein to bind the Ni^{++}-ions. Then, the resin was washed with 20 CV of 10 mM imidazole, 50 mM sodium phosphate, 300 mM NaCl, pH 8.0 and, after this, with 20 CV of 20 mM imidazole, 50 mM sodium phosphate, 300 mM NaCl, pH 8.0. The protein was eluted with 2-3 CV of 250 mM imidazole in 50 mM sodium phosphate, 300 mM NaCl, pH 8.0. Further, the purity of the eluted protein was analyzed by SDS-PAGE. The eluted protein was dialyzed (10 kDa membrane) overnight against 50 mM Tris, 1 mM EDTA, pH 7.5 at 4°C to eliminate excess imidazole. The dialyzed protein was then concentrated by means of ultrafiltration, using Centriprep YM-50 concentrators with a 50 kDa cut-off membrane. The concentrated protein was further used in gel filtration.

2.2.2.3.2 Size exaltation chromatography (SEC)

The eluted protein after Ni^{++}-NTA was further purified by using SEC. The protein with different sizes can be separated with SCE, in which the small protein molecules diffuse through the porous tunnel gel using the superose-6 column. Therefore, migration is comparatively slower in complex pathways compared to the case with large protein molecules. As a result, the large protein molecules elute faster than the small ones. The protein was eluted using 50 mM Tris-HCl, 200 mM NaCl, 1 mM EDTA, pH 7.5, and further concentrated by means of ultrafiltration using Centriprep YM-50 concentrators with a 50 kDa cut-off membrane. Eluted protein was collected in fractions and analyzed by SDS-PAGE as well as with UV-Vis spectroscopy at 280 nm, 445 nm, and 550 nm for purity.

2.2.2.4 Analytical methods

2.2.2.4.1 Sodium dodecyl sulfate-polyacrylamide gel electrophoresis (SDS-PAGE)

The purity of the protein can be analyzed using SDS-PAGE, where the mixture of protein molecules is separated according to their mass. SDS facilitates the denaturation and reduction of the proteins according to their molecular weight in discontinuous Tris/glycine-SDS gels. Therefore, the mixture of protein molecules is separated in an applied electric field according to their mass but not to their net charge. The high negative charge of SDS enhances the movement of the proteins, which leads to the slow movement of large protein molecules.

Table 2-11: Components for preparation of separation (12% and 17%) and stacking gel (5%) was used in this study

Compositions	12 % Separation gel (mL)	17 % Separation gel (mL)	5% Stacking gel (mL)
Water	1.75	0.85	1.16
4x Lower Tris	1.25	1.25	
4x Upper Tris			0.50
30% (w/v) Acrylamid/ 0.8% (w/v) Bisacrylamid	2.00	2.85	0.34
TMED	0.0025	0.0025	0.0020
10% (w/v) APS	0.025	0.025	0.010

The samples were mixed with 5xSDS-loading dye and incubated at 95°C for 5 min. For the separation of proteins, gels were run at a constant 15 mA for 75 min at room temperature. In this study, 12% and 17% gels were used to obtain an effective separation of the proteins.

2.2.2.4.2 Coomassie staining

Coomassie Brilliant Blue R-250 was used to stain the separated protein molecules in SDS-PAGE. The Coomassie Blue binds with the basic amino acids of the protein molecules in an acidic environment such as lysin, arginine, and histidine. The gel was incubated with staining solution for around 1 h at room temperature after the SDS-PAGE. Subsequently, the gel was destained using a destaining solution containing methanol: acetic acid: water (4:1:5) until the excess stain was removed. Further, the gel was documented in Gel doc from Bio-Rad.

2.2.2.4.3 Determination of protein concentration

2.2.2.4.3.1 Photometric protein concentration

The concentration of purified protein was determined by the extinction coefficient at 280 nm using the Lambert-Beer law. The concentration was calculated from the following equation:

$$c\left(\frac{mol}{L}\right) = \frac{A_{280}}{\varepsilon_{280(M^{-1}cm^{-1})}} * d(cm)$$

A = Absorbance at specific wavelength
ε = specific molar extinction coefficient
d = path length of cuvette
c = concentration of protein

The extinction coefficient at 280 nm was calculated using the ProtParam (ExPASy) tool with the respective amino acid sequences. Moreover, the concentration of Flavin cofactor-containing proteins was also determined by the extinction coefficient at 445 nm.

Table 2-12: Molecular weight and extinction coefficient (280 nm, 445 nm and 465 nm) for EcPaoABC and RcXDH

Protein	MW (kDa)	$\varepsilon_{280}(M^{-1}cm^{-1})$	$\varepsilon 445(M^{-1}cm^{-1})$	$\varepsilon 465(M^{-1}cm^{-1})$
EcPaoABC	135	93835	23686	
RcXdhAB	135	107270		31600

2.2.2.4.3.2 Bradford

The overall protein concentration from the crude cell extract was determined by the Bradford method. The experiment was performed using Bradford assay solutions, where the Coomassie reagent binds with basic and aromatic amino acids such as arginine, tryptophan, or tyrosine. The crude extracts were diluted 1:500-800 with 0.9% NaCl solution and incubated at 1:1 with the Bradford reagent for 10 min or until the color had developed at room temperature. Further, the formed color complex was measured phototactically at 595 nm. The BSA was used as a standard for this experiment.

2.2.2.4.4 Immunodetection

The experiment was performed to detect the specific protein with an antibody that interacts with it specifically in a mixture of different proteins. The Wt MG1655 and all the mutant strains were cultivated with 15 mM potassium nitrate or 15 mM TMAO for 8 h anaerobically at 37°C. The *moa*-operon overexpressing strains were cultivated for 8 h at 30°C with 20 µM IPTG. Afterward, the cells were harvested and resuspended with 50 mM Tris-HCl, pH 7.5. Furthermore, cell lysis was performed by sonification (2.2.2.2.2) and centrifuged to remove the cell debris. The concentration of protein was determined by Bradford from the cell extract. About 50 µg of protein was loaded to the 12% (SufS, IscS, and TorA) or 17% (MoaC) SDS-PAGE gel and, subsequently, proteins were separated according to their mass. Furthermore, the protein was transferred to the PVDF (IscS, TorA, and MoaC) or nitrocellulose (SufS) membrane. The PVDF was activated by 20% methanol with a transfer buffer containing 25 mM Tris-HCl, 200 mM glycine, 20% methanol for 2 min. The transfer of protein to the membrane was performed using 90 V for 90 min. Afterward, the membrane was blocked with 5% (w/v) milk powder in TBS-T solution (50 mM Tris-HCl, 150 mM NaCl, 0.1% (w/v) Tween-20, pH 7.4) for 1 h at room temperature. The excess milk powder was rinsed three times using TBS-T. Next, the membrane was incubated overnight at 4°C with slight agitation (20 rpm) with a primary antibody diluted with TBS-T.

On the following day, the membranes were again washed three times with TBS-T and incubated at room temperature for 1 h with horseradish peroxidase (HRP)-conjugated goat anti-rabbit (IscS, TorA, and MoaC) and goat anti-chicken (SufS) secondary antibodies. Then, the unbound antibodies were washed three times with TBS-T before the protein bands were visualized by chemiluminescence. For this purpose, the membrane was treated with a 1:1 mixture of solution A (100 µL 250 mM luminol, 44 µL 90 mM p-coumaric acid, 8.85 mL H_2O) and solution B (1 ml 1 M Tris-HCl, pH 8.5, 6 µL 30% H_2O_2, 9 mL of H_2O) according to the recommended amount supplied by the device manufacturer (FUSION FX7, Vilber) given optimal exposure time (5-45 sec) that the chemiluminescence recorded. A pre-stained protein molecular weight marker from 20.0 to 120.0 kDa (Fermentas) was used.

Table 2-13: Overview of antibodies and membranes were used for immunodetection of the respective proteins in this study

Proteins	Primary antibody	Secondary antibody	Membrane
IscS	Rabbit anti-IscS (1:5000)	goat anti-rabbit (1:10000)	PVDF
SufS	Goat anti-SufS (1:2000)	goat anti-chicken (1:5000)	Nitrocellulose
TorA	Rabbit anti-TorA (1:500)	goat anti-rabbit (1:10000)	PVDF
MoaC	Rabbit anti-MoaC (1:1000)	goat anti-rabbit (1:10000)	PVDF

2.2.2.4.5 Characterization of purified protein with UV-vis spectrum

The purity of the purified protein can be estimated by photometric measurement using the Lambert-Beer law. The Lambert-Beer equation is as follows:

$$A = \varepsilon * c * d$$

A = Absorbance at specific wavelength
ε = specific molar extinction coefficient
d = path length of cuvette
c = concentration of protein

In this study, the spectrum of purified EcPaoABC and RcXDH proteins was measured. 1000 µL of 10 µM purified protein was used in a range of 250 nm-800 nm on a Shimadzu

UV-2401PC spectrophotometer at room temperature. The absorption was measured for prosthetic FAD cofactor at 445 nm and 465 nm for EcPaoABC and RcXDH.

2.2.2.4.6 Metal content determination by ICP-OES

Inductively coupled plasma optical emission spectrometry (ICP-OES) with an Optima 2100 DV (PerkinElmer Life and Analytical Sciences, Waltham, MA) was used to quantify the metal contents in purified EcPaoABC and RcXDH. The ICP-OES can detect and quantify any trace metal elements. It uses an inductively coupled plasma in a very high temperature at a high-frequency field to excite the analyte metals or atoms. Those that are emitted in electromagnetic radiation in specific wavelengths characterize the selected metal. The intensity of a specific wavelength is directly proportional to the content of the elements.

The metal content was quantified for purified EcPaoABC and RcXDH, and expressed in Wt MG1655 and other single mutant strains. 500 µL of 10 µM of purified protein was incubated with an equal volume of 65% HNO_3 at 100°C overnight for denaturation. Then, the samples were diluted with 4 mL of millipore water and a 6.5% HNO_3-treated buffer was used as a reference. The detection was performed at wavelengths of 203.845 nm, 202.031 nm, and 204.597 nm for molybdenum and 238.204 nm, 239.562 nm, and 259.939 nm for iron. A standard was used to calibrate and quantify the detected metals (standard solution XVI; Merck Millipore, Darmstadt, Germany). The relative molybdenum content was estimated as 1 mole for both of the proteins. 8 and 4 moles' iron content were estimated for EcPaoABC and RcXDH, respectively.

2.2.2.4.7 Cofactor detection and quantification

2.2.2.4.7.1 Moco and cPMP content detection

The Moco can be detected as FormA on a C18 reversed-phase HPLC column, where the molybdopterin (MPT) can be oxidized with acidic iodine, and FormA is produced. The total Moco content was quantified from the crude cell extract of the Wt MG1655 and all the mutant strains that were grown anaerobically with 15 mM potassium nitrate or 15 mM TMAO for 8 h at 37°C. The cells were harvested, washed twice with 100 mM Tris-HCl, pH 7.2 and further lysed by sonification. The cell debris was separated by centrifugation at 13200xg for 30 min, and the crude extract was collected. Subsequently, 400 µL of the crude cell extract was isolated, oxidized with 150 µL of iodine solution that contains 1% I_2

(w/v) and 2% KI (w/v) and 50 µL of acidic iodine (914 µL I_2/KI+86 µL 37% HCl) for 30 min at 95°C. The denatured protein was removed by centrifugation at 13200xg for 30 min, and 400µL of supernatant was collected in a new tube. The excess iodine was removed by adding 100 µL 1% (w/v) ascorbic acid, which resulted in the formation of a transparent solution. 1 M Tris was added to the solution to adjust the pH at 8.3. Finally, the FormA was obtained by removing the phosphate group with 40 µL $MgCl_2$, 2 µL of 1 U Fast AP, and further incubated for 2 h at room temperature. Purifying of FormA was done by loading the sample onto a 500 µL QAE ion exchange resin (Sigma), which was equilibrated with 5 CV millipore water. After the FormA had bound with the resin, the column was washed by 10 CV millipore water and 1.3 mL of 10 mM acetic acid. The FormA was eluted in six fractions with 10 mM acetic acid, in which the eluent in each fraction was 500 µL. All the fractions were separated on a C18 reversed-phase HPLC column (4.6 x 250 mm ODS Hypersil, particle size 5 µm), equilibrated with 5 mM ammonium acetate and 15% (v/v) methanol at a flow rate of 1 mL/min. The injection volume for each sample in HPLC was 100 µL. An Agilent 1100 series fluorescence detector monitored elution of FormA with an excitation at 383 nm and emission at 450 nm. The total FormA content was normalized to the growth of cells at $OD_{600\ nm}$.

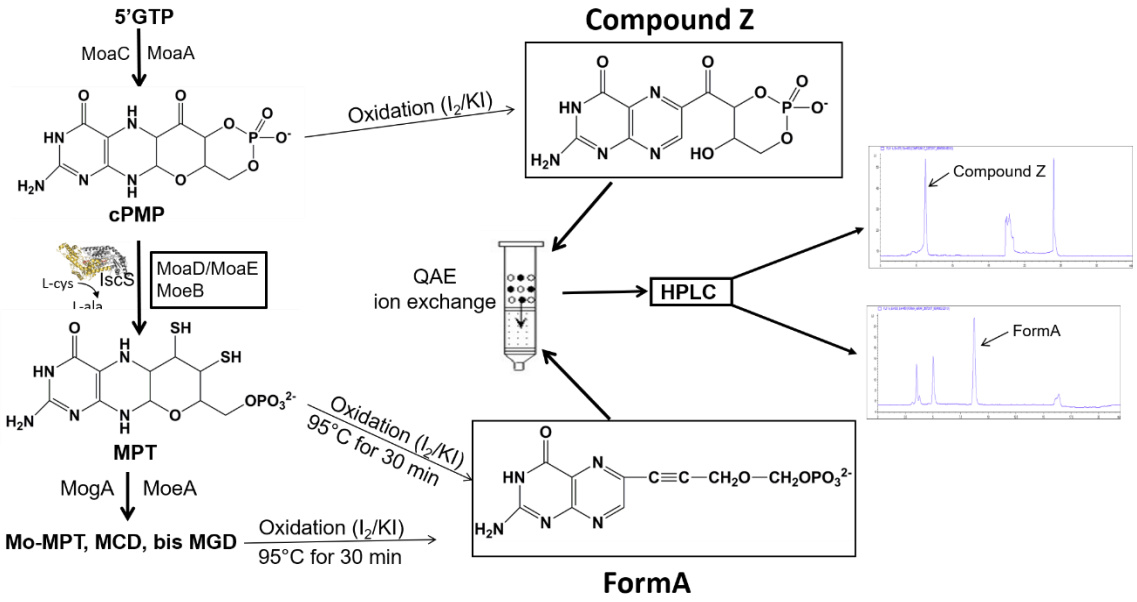

Figure 2-4: Scheme for the detection of Moco and cPMP from *E. coli* cell extract

The Moco and cPMP are detected as their fluorescence derivatives FormA and compound Z respectively and analyzed by means of a C18 reversed-phase column in HPLC with an excitation at 383 nm and emission at 450 nm; IscS: PDB – 3LVM

In this study, the Moco content was also estimated from the purified EcPaoABC and RcXDH, where 10 µM of 400 µL purified protein was used for oxidation. The complementation study was also performed with the Wt MG1655 and respective mutant strains, whereby the plasmid *moa* operon, *sufA*, *iscA*, and *erpA* were introduced and expressed in the presence of 0.2% L-arabinose, 15 mM potassium nitrate at 37°C (for *sufA*, *iscA*, and *erpA*) or 30°C (*moa* operon) for 8 h. Further, the cells were harvested, and the Moco content was measured as described above.

The cPMP was detected as an oxidized fluorescent derivative called compound Z, whereby the cPMP was oxidized with acidic iodine and further analyzed in the C18 reversed-phase HPLC column. The detection and quantification of compound Z were performed from the identical crude-cell extract from which the Moco was identified. The oxidation of 400 µL crude extract was performed with 150 µL of Iodine solution that contained 1% I_2 (w/v) and 2% KI (w/v) and 50 µL of acidic iodine (914 µL I2/KI+ 86 µL 37% HCl), which was further incubated for 16 h in the dark at room temperature. The denatured proteins were separated by centrifugation at 13200xg for 30 min. Then, the 400 µL of supernatant was collected into another tube. The removal of excess iodine and adjustment of pH at 8.3 was performed as described above for Moco extraction. Purifying of compound Z was done by using 500 µL QAE ion exchange resin (Sigma) as described above. However, before the elution of compound Z, the column was washed with 10 CV of millipore water and 10 mM acetic acid. Afterward, compound Z was eluted as 5x1000 µL with 100 mM HCl. The fractions were separated on a C18 reversed-phase HPLC column (4.6 x 250 mm ODS Hypersil, particle size 5 µm) equilibrated with 10 mM potassium dihydrogen phosphate (pH 3.0), 1% (v/v) methanol at a flow rate of 1 mL/min. A fluorescence detector monitored compound Z elution with an excitation at 383 nm and emission at 450 nm. The total Compound Z content was normalized to the growth of cells at $OD_{600\ nm}$.

2.2.2.4.7.2 The detection and quantification of FAD

The detection and quantification of flavin cofactor were performed photometrically at 450 nm using purified EcPaoABC and RcXDH. The 10 µM of 500 µL purified protein was incubated with 150 µL of 50% (w/v) trichloroacetic acid for 10 min on ice. As a result, the protein was denatured, and the FAD cofactor was released into the solution. The

denatured protein was centrifuged at 13200xg for 20 min, and the supernatant was collected into another tube. The pellet was resuspended with 200 µL of 5% (w/v) trichloroacetic acid and incubated in ice for 10 min. Subsequently, the resuspended solution was centrifuged for 10 min at 13200xg, and the supernatant collected. Both the supernatants were combined with the addition of 300 µL of 2 M K_2HPO_4. The released FAD was detected photometrically on a Shimadzu UV-2401 PC photometer (Shimadzu Europa, Duisburg, Germany) at 450 nm. FAD concentration was calculated from the specific extinction coefficient of free FAD (11300 M^{-1} cm^{-1} at 450 nm) and normalized to the concentration of the purified protein that was expressed in the wild-type Wt MG1655 and in the respective mutant strains.

2.2.2.5 Enzyme activity

2.2.2.5.1 Nitrate and TMAO reductase activity

Nitrate and TMAO reductase are molybdoenzymes that belong to the DMSOR family, where both enzymes function as electron acceptors under anaerobic respiratory conditions. Nitrate and TMAO reductase are able to reduce the nitrate to nitrite and the TMAO to TMA, respectively, under anaerobic conditions. Enzyme activity was measured from the crude cell extract in the anaerobic chamber. The Wt MG1655 and all the mutant strains were cultivated anaerobically with 15 mM potassium nitrate or 15 mM TMAO for 8 h at 37°C. The cells were harvested at 8000xg for 10 min and subsequently washed two times with 50 mM Tris-HCl, pH 7.5 and phosphate buffer, pH 6.5 for nitrate- and TMAO-induced culture. Finally, the cell pellets were resuspended with 1000 µL of 50 mM Tris-HCl, pH 7.5 and phosphate buffer, pH 6.5 for nitrate and TMAO reductase activity before the cells were lysed. Cell lysis was performed by sonification according to 2.2.2.2.2. The cell lysates were subsequently transferred into the anaerobic condition and incubated at 4°C for 3-4 h before measurements started.

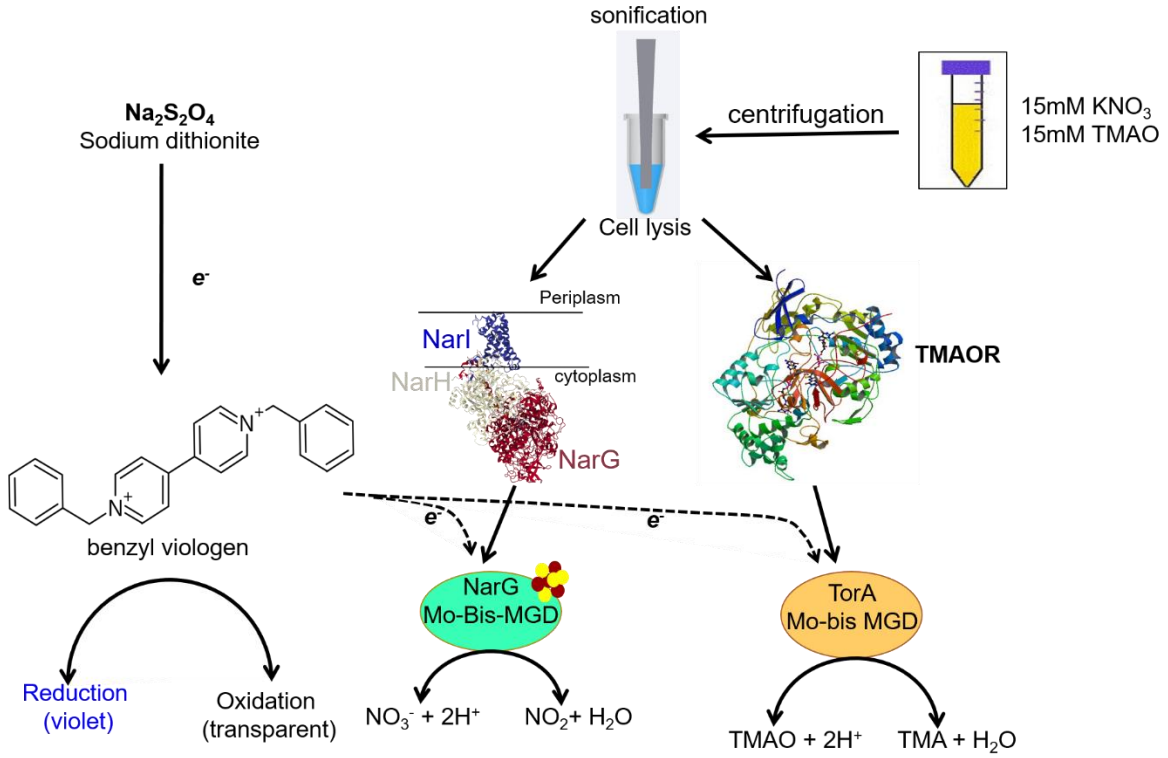

Figure 2-5: Determination of nitrate reductase and TMAO reductase activity from the *E. coli* cell lysate

The cells were cultivated anaerobically with 15 mM KNO_3 or 15 mM TMAO, 1 mM mevalonate for 8 h respectively, and cell lysis was performed by sonification; the sodium dithionite provides the electron for the reaction; NR: PDB - 1Q16; TMAOR: PDB - 1TMO

In 4 mL of final reaction volume that contains 0.3 mM benzyl viologen, 10 mM potassium nitrate or 5 mM TMAO in a water or phosphate buffer, pH 6.5 respectively, about 50 µL of cell lysate was used for analyzing the nitrate reductase and TMAOR activity. The reaction was initiated with the addition of sodium dithionate in the reaction mixture, which provides electrons for the reaction, and subsequent oxidation of benzyl viologen takes place, resulting in a purple to transparent color change recorded at 600 nm for 30 sec. The activity was calculated according to the following equation:

$$U = 0.5x \left[\frac{\Delta Ab_{600nm/min}}{\varepsilon_{600nm\ (Benzyl\ viologen)}}\right]\Big/_{V}$$

ΔAb = Absorbance at $_{600nm}$/min

ε_{600nm} = molar extinction coefficient of benzyl viologen

V = volume of the reaction mixture (mL)

U = enzyme activity

The molar extinction coefficient for benzyl viologen of 7.4 $mmol^{-1}$ cm^{-1} was used for calculation. One unit is defined as the oxidation of 1 µM-reduced benzyl viologen per minute. The activity was normalized to the $OD_{600\ nm}$ of the cells before harvesting.

Table 2-14: Reaction composition for measuring NR and TMAOR activity

Components	NR assay	TMAOR assay
1 M KNO_3 or TMAO	40 µL	40 µL
1 M Tris-HCl pH 6.8	80 µL	80 µL
15 mM benzyl viologen	80 µL	80 µL
Water or 100 mM phosphate buffer (pH 6.5)	3750 µL	3750 µL
Cell lysate	50 µL	50 µL
Sodium dithionate	Add x µL to make final volume 4 mL	

Exclusion of the FNR regulation study was performed with the expression of *narGHJI* plasmid in Wt MG1655 and all the mutant strains anaerobically at 24°C for 36 h with 20 µM IPTG. Moreover, the complementation study was performed by anaerobic expression of exogenous *sufA*, *iscA*, and *erpA* in wild-type MG1655 and the mutant strains (*ΔiscA*, *ΔerpA*, and *ΔiscA/ΔerpA*) with 0.2% L-arabinose for 8h at 37°C. Further, the cells were harvested, and nitrate reductase activity was carried out as described above.

2.2.2.5.2 The β-galactosidase activity

The β-galactosidase activity was performed to evaluate the transcriptional level of a respective gene under a particular condition. The promoter region of this respective gene is cloned before the lacZ reporter gene in a plasmid. Under a particular condition or in a mutant strain, the promoter region is induced or repressed, leading to increased or decreased β-galactosidase enzyme production. This enzyme catalyzes the formation of the yellow dye o-nitrophenol from ortho-nitrophenyl-β-D galactopyranoside. The product can be further measured photometrically at 420 nm.

In this study, the expression of *moaA*, *fnr*, *sufA*, *iscR*, *torCAD*, and *pepT* was analyzed in Wt MG1655 and the respective mutant strains. Therefore, *PmoaA-L-lacZ*, *Pfnr-lacZ*, *PsufA-lacZ*, *PtorCAD-lacZ*, and *PpepT-lacZ* plasmids were individually transformed into all the respective strains. The strains were cultivated with 15 mM potassium nitrate for 8

h at 37°C, except for the strains containing *PtorCAD-lacZ*. These strains were cultivated with 15 mM TMAO under conditions identical to those outlined above. After cultivation, the cells were diluted with a freshly prepared buffer Z (40 mM NaH2PO4, 10 mM KCl, 1 mM MgSO4, 0.05 β-mercaptoethanol, pH 7.0), in which the dilution can be 1:5 to 1:10 depending on the strong or weak activation of the promoter region. Subsequently, 25 µL of 0.1% SDS and 50 µL of chloroform were added to the cell dilution and incubated for 5 min at 28°C. The reaction was initiated with the addition of 100 µL of 4 mg/mL ortho-nitrophenyl-β-D-galactopyranoside (ONPG) and was stopped when the development of sufficient yellow color either in the wild-type strain or in any of the mutant strains was detected. The reaction was stopped by the addition of 250 µL 1 M Na_2CO_3. The amount of formed ortho-nitrophenol was measured photometrically at 420 nm, corrected for light scattering at 550 nm, and normalized to the cells' optical density at 600nm. The activity was calculated as a Miller unit with the following equation:

$$Miller\ unit\ (MU) = 1000 * \frac{[A_{420} - 1.75 * A_{550}]}{v\ (mL) * t\ (\min) * OD_{600}}$$

$A_{420/550nm}$ = Absorbance at 420 nm and 550 nm
v = volume of cell lysate (mL)
t = time of the reaction (min)
OD_{600nm} = Optical density of cells at 600nm

For each strain, a respective blank reaction containing cells transformed with the vector control was subtracted.

2.2.2.5.3 Periplasmic aldehyde oxidase (Ec paoABC) and Xanthine dehydrogenase (RcXDH) activity

The specific activity of purified RcXDH and EcPaoABC was determined spectrophotometrically at room temperature under aerobic conditions. 10 µL of 5 µM purified enzyme was used for the reaction. Oxygen and xanthine were used as electron acceptors, for EcPaoABC and RcXDH respectively. The specific activity of EcPaoABC was determined as U/mg, which is defined as 1 µmol of benzaldehyde that was oxidized min^{-1} mg^{-1}, with a molar extinction coefficient of ε = 1321 mM^{-1} cm^{-1}. On the other hand, the specific enzyme activity of RcXDH was determined as U/mg, which is defined as 1

µmol of xanthine oxidized min^{-1} mg^{-1}, with a molar extinction coefficient for NADH of ε NADH = 6.22 mM^{-1} cm^{-1}.

Table 2-15: Reaction composition for measuring EcPaoABC and RcXDH activity

Components	EcPaoABC	RcXDH
Buffer	McIlvaine buffer (Citrate phosphate), pH 6.5	50 mM Tris-HCl, 1 mM EDTA, pH 8
Electron acceptor	Oxygen	50 mM Xanthine
Substrate	50mM Benzaldehyde	75 mM NAD+
Enzyme	5 µM	
Absorption	290 nm	340 nm

2.2.2.6 Circular dichroism (CD) spectroscopy

UV-visible circular dichroism is a method of absorption spectroscopy, where the measurement takes place based on the difference of absorption in right- and left-circularly polarized light by a substance. It is widely used to evaluate the structural integrity of protein molecules. In our study, a CD spectrometer was used to detect the presence of different forms of Fe-S clusters in the purified protein. About 20 µM of 1000 µL purified protein (EcPaoABC and RCXDH) in 50 mM Tris-HCl, 1 mM EDTA, pH 7.5 was used for the analysis by means of a Jasco J-715 CD spectrophotometer at room temperature. The spectra were recorded in the range of 300-600 nm as an average of three runs with sensitivity set to standard. The scanning mode was set with a step width of 1 nm at a scan speed of 10 nm/s, and each measurement was repeated three times. N2 flow was set to 6-8 L/min.

3 Results

3.1 Analysis of nitrate reductase activity and Moco content

3.1.1 The influence of glucose on nitrate reductase activity under anaerobic conditions

At the cellular level, Fe-S cluster insertion into the target apo-protein is still one of the open questions in this field. This study focuses on identifying the carrier proteins that are involved in the maturation of MoaA. Fe-S cluster transfer is performed by carrier proteins such as IscA, SufA, or ErpA (Vinella et al., 2009; Zheng et al., 1998; Outten, Djaman, and Storz, 2004; Tanaka et al., 2016). IscA and ErpA were shown to deliver an Fe-S cluster to the formate: hydrogen lyase and hydrogen oxidizing [NiFe]-hydrogenase (Pinske & Sawers, 2012b). Also, NfuA (Angelini et al., 2008), BolA, and GrxA/B/C/D are known as Fe-S cluster carrier proteins (Begas et al., 2017; Burschel et al., 2019; A. G. Frey et al., 2016). The Fe-S cluster carrier proteins were identified by using knock-out strains of selected genes in which nitrate reductase activity and Moco content were measured. In this study, we wanted to first identify the growth conditions that are suitable for assaying nitrate reductase activity and Moco formation. After an initial screening, we wanted to exclude the proteins that are not essential for the production of Moco.

Nitrate reductase activity was measured to evaluate the influence of glucose, whereby the cells were cultivated with 15 mM potassium nitrate in the presence or absence of 0.2% glucose anaerobically at 37°C for 8 h.

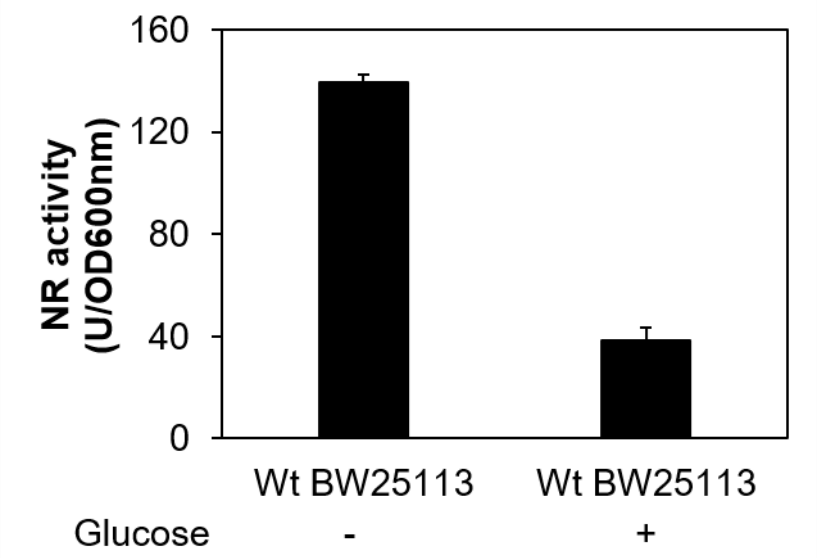

Figure 3-1: Analysis of nitrate reductase activity in *E. coli* Wt BW25113 strain

Nitrate reductase activity was determined in Wt BW25113 strains, which were grown in the presence of 15 mM potassium nitrate, with and without 0.2% glucose under anaerobic conditions; nitrate reductase activities were normalized to OD_{600} nm; Standard deviations were calculated from three biological replicates

Figure 3-1 shows that the nitrate reductase activity was ~80% reduced in the presence of glucose as compared to the BW25113 strain grown under anaerobic nitrate respiratory conditions without glucose. This shows that nitrate reductase is repressed under anaerobic fermentative conditions as repeated before (Stephen Spiro & Guest, 1987).

3.1.2 Nitrate reductase activity under anaerobic conditions of nitrate respiration

E. coli harbors three different types of nitrate reductase, NarGHI, NarZYV, and NapAB, with NarGHI being the most predominant of the three under nitrate respiratory conditions (Leimkühler, 2020). To confirm that, under nitrate respiratory conditions, only the activity of NarGHI is measured and not that of the other two nitrate reductases; nitrate reductase activity was determined in the mutant strains *ΔnarG*, *ΔnapA*, and *ΔnarZ* in comparison to the corresponding Wt BW25113 strain. The strains were grown anaerobically in the presence of 15 mM potassium nitrate for 8 h at 37°C.

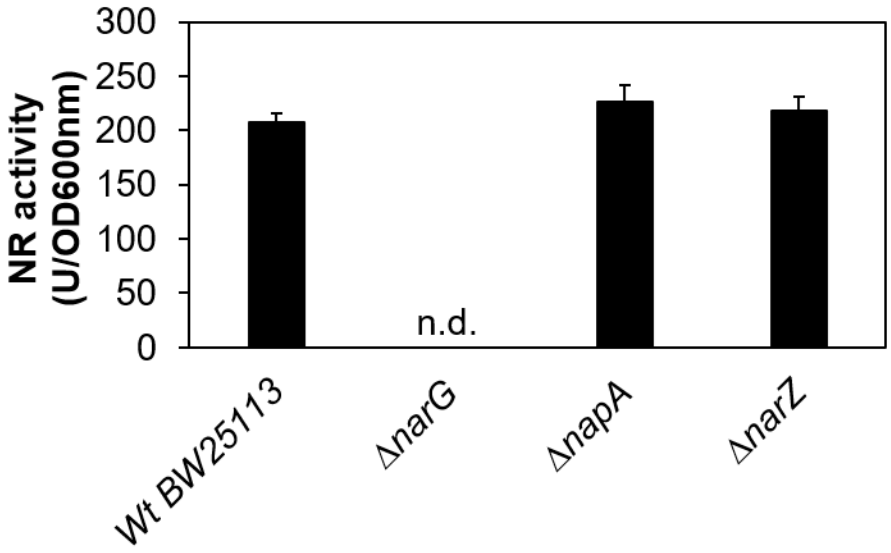

Figure 3-2: Analysis of nitrate reductase activity in *E. coli* mutant strains

Nitrate reductase activity was determined in Wt BW25113, *ΔnarG, ΔnapA* and *ΔnarZ* strains, which were grown in the presence of 15 mM potassium nitrate under anaerobic conditions; nitrate reductase activities were normalized to OD_{600} nm; Standard deviations were calculated from three biological replicates

Figure 3-2 shows that nitrate reductase activity was absent in the *ΔnarG* strain, whereas the activities in the *ΔnapA* and *ΔnarZ* strains were almost similar to the parenteral Wt BW25113 strain. The complete absence of nitrate reductase activity in the *ΔnarG* strain suggests that, under nitrate respiratory conditions, NarGHI mainly contributes to the nitrate reductase activities that can be detected.

3.1.3 Moco content and nitrate reductase activity under anaerobic and aerobic conditions

In order to identify the carrier protein that inserts the Fe-S clusters into the MoaA or nitrate reductase, the Wt BW25113, *ΔiscA*, *ΔnufA*, *ΔsufA*, *ΔbolA*, *ΔgrxA*, *ΔgrxB*, and *ΔgrxC* strains were cultivated under aerobic and anaerobic condition with 15 mM potassium nitrate for 8 h at 37°C. The Moco was quantified as FormA after separation on a C18 reversed-phase HPLC column.

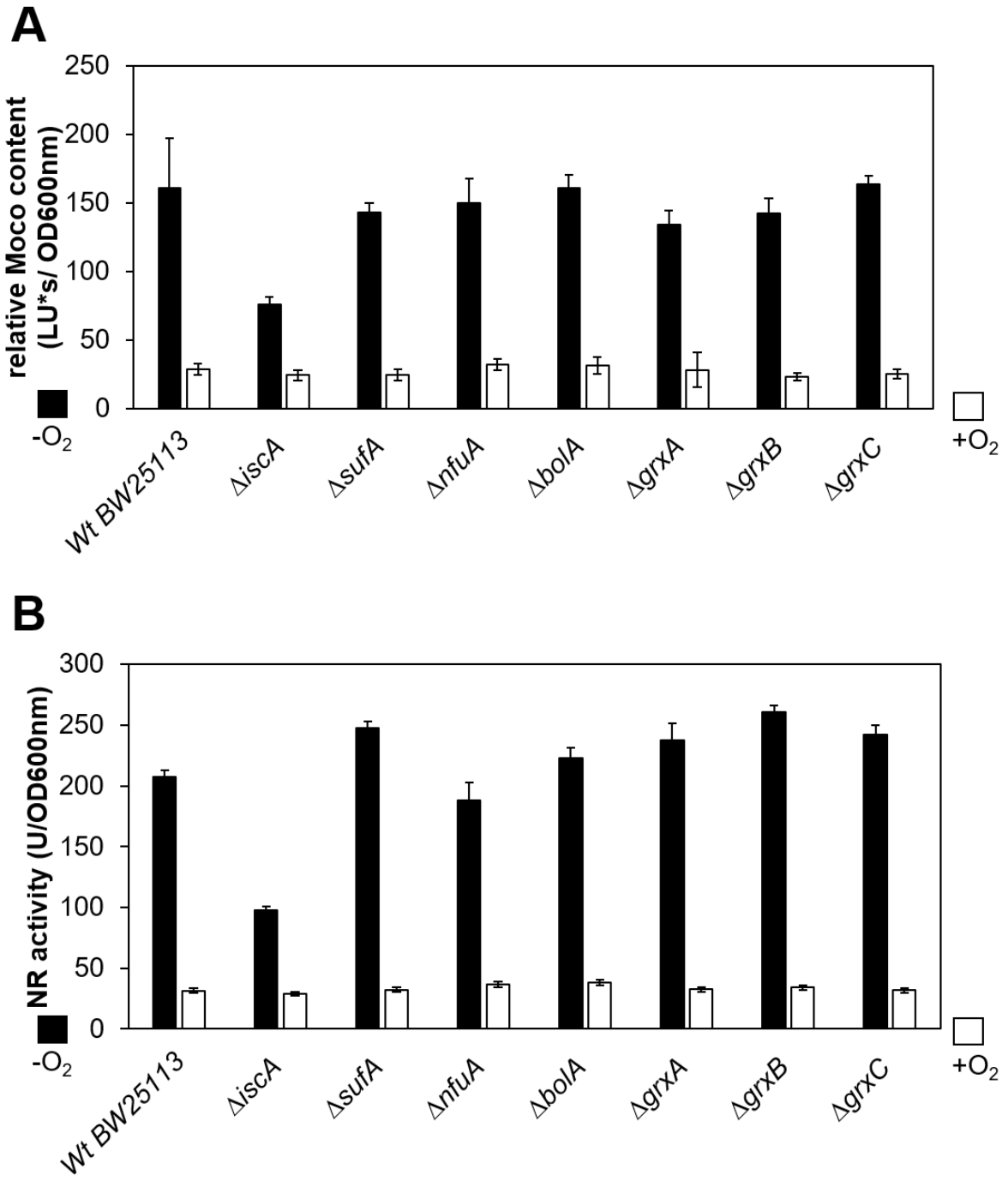

Figure 3-3: Analysis of relative Moco content and nitrate reductase activity in *E. coli* mutant strains

Relative Moco content (A) and nitrate reductase activities (B) were determined in *E. coli* Wt BW25113, *ΔiscA, ΔsufA, ΔnfuA, ΔbolA, ΔgrxfA, ΔgrxB,* and *ΔgrxC* strains, the strains were grown under anaerobic (black bar) and aerobic (white bar) conditions in the presence of 15 mM potassium nitrate; Moco content and nitrate reductase activity were normalized to OD_{600} nm. Standard deviations were calculated from three biological replicates.

Figure 3-3 show that under anaerobic conditions, the Moco content and nitrate reductase activity for all the mutant strains were quite similar in comparison to the Wt BW25113 strain, with the exception of the *ΔiscA* strain under anaerobic conditions, where both Moco content and nitrate reductase activity were reduced by about ~53% and ~40%, respectively. Moreover, the Moco content and nitrate reductase activity under aerobic conditions were comparable in all the mutant strains. Both Moco content and nitrate reductase activity were reduced by around ~80% when the cells were cultivated aerobically compared to under anaerobic cultivation. This significant measured difference suggests that the nitrate reductase- and Moco-producing ability of the strains were much more favorable under anaerobic conditions than under the aerobic condition based on FNR regulation. Therefore, the rest of our study was carried out under anaerobic conditions in the presence of potassium nitrate. The *ΔerpA* strain was not a part of this measurement because the strain was only available in the MG1655 MVA^+ background. Therefore, all the strains were changed to MG1655 MVA^+ from BW25113 for the rest of this study. The Wt MG1655, *ΔmoeB*, *ΔerpA*, *ΔiscA*, Δ*nufA*, *ΔsufA*, *Δfnr*, the double mutant *ΔnfuA/ΔiscA*, *ΔerpA/ΔiscA*, *ΔsufA/ΔiscA*, *ΔsufA/ΔerpA* strains, and the triple mutant *ΔsufA/ΔiscA/ΔerpA* strain were used for the rest of the study. The *moeB*-deleted strain was used as a negative control for the Moco quantification since MoeB is involved in the formation of MPT from cPMP in Moco biosynthesis. The strains were either constructed by the lambda-red method or received from Béatrice Py (Daniel Vinella et al., 2009). The *erpA*- and *iscA*-deleted strains are lethal under anaerobic or aerobic respiratory conditions based on the requirement of quinones as electron carriers, which is derived from isopentenyl diphosphate (IPP) (Gräwert et al., 2004; Wolff et al., 2003). IPP biosynthesis depends on [4Fe-4S] containing IspG and IspH proteins, which are dependent on ErpA and IscA for their maturation. Therefore, deletion of these genes leads to a defective respiration of these strains. To ensure growth, the mutant strains were introduced with a eukaryotic mevalonate-dependent pathway for biosynthesis of IPP (Gräwert et al., 2004; Wolff et al., 2003) and restoration of the defective respiration (Daniel Vinella et al., 2009). The *E. coli* MG1655 strains were always cultivated in the presence of 1 mM mevalonate in this study. Moreover, the *bolA*, *grxA*, *grxB*, and *grxC* deleted strains were not further used in our study since deletion of these genes did not impact either the Moco content or the nitrate reductase activity.

3.1.4 Growth curves of the strains under anaerobic conditions of nitrate respiration

Growth curves were measured for all the strains to determine their growth patterns, since deletion of essential genes leads to growth defects for the strains. The strains were cultivated anaerobically with 15 mM potassium nitrate and 1 mM mevalonate at 37°C. The samples were taken every hour for measuring the optical density at 600 nm for 12 h.

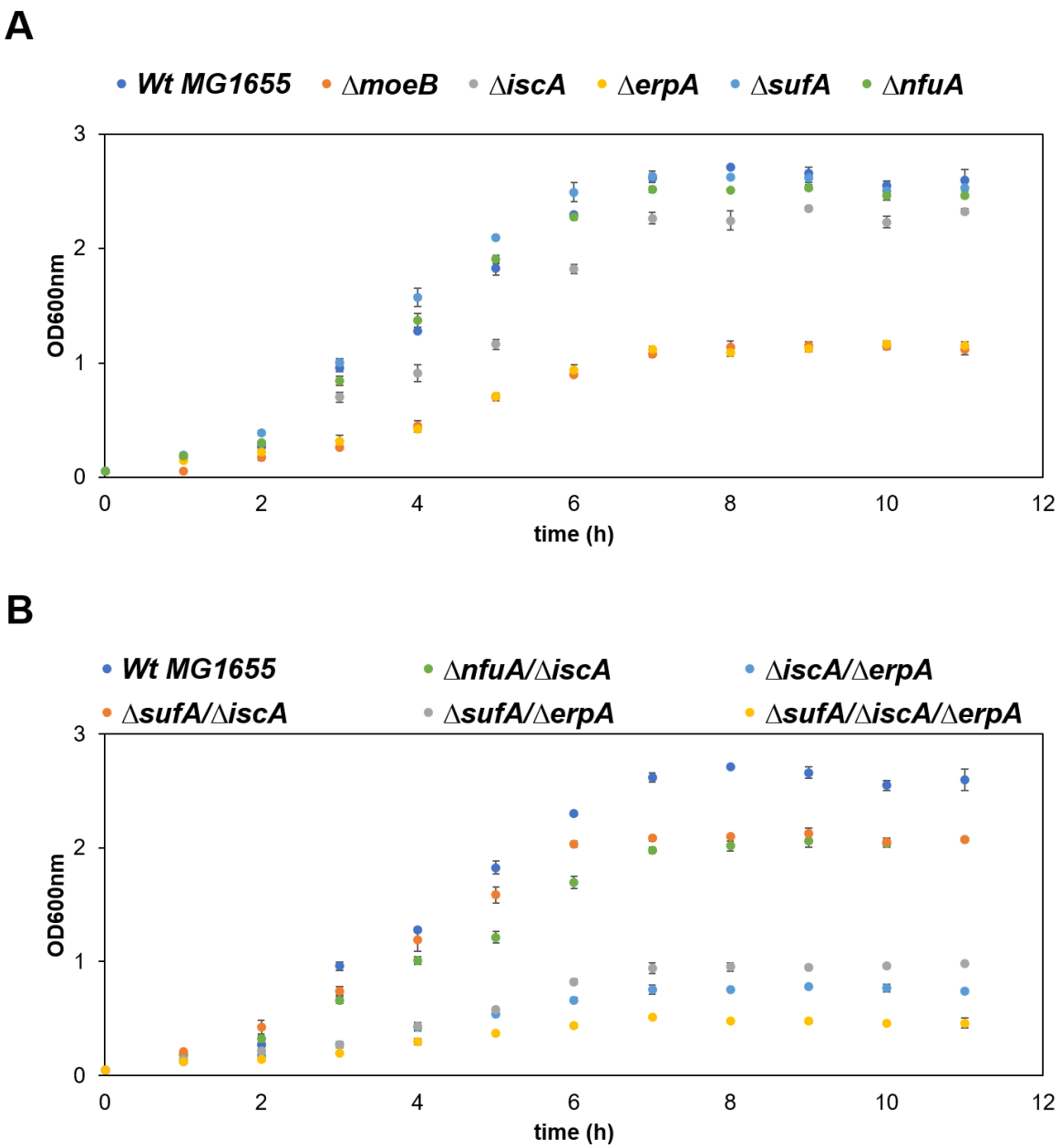

Figure 3-4: Analysis of the growth curves of *E. coli* mutant strains

The growth curves were measured for *E. coli* Wt MG1655, Δ*moeB,* Δ*erpA,* Δ*iscA,* Δ*sufA,* Δ*nfuA* (A), Wt MG1655, Δ*nfuA*/Δ*iscA,* Δ*iscA*/Δ*erpA,* Δ*iscA*/Δ*sufA,* Δ*sufA*/Δ*erpA* and Δ*iscA*/Δ*sufA*/Δ*erpA* (B) mutant strains; the cells were grown in 50 mL LB medium

supplemented with 15 mM potassium nitrate and 1 mM mevalonate. The start OD_{600} nm was 0.05 and recorded for 12 h. Standard deviations were calculated from three biological replicates

Figure 3-4 show that the cell growth was significantly reduced for the *ΔmoeB*, *ΔerpA*, *ΔiscA/ΔerpA*, *ΔsufA/ΔerpA*, and *ΔsufA/ΔiscA/ΔerpA* strains as compared to the Wt MG1655 under nitrate respiratory conditions. All the strains reached the stationary phase at 8 h, despite a growth defect of some mutant strains. Therefore, the cells were harvested at the late exponential phase at 8 h for this study to measure Moco content, nitrate reductase, and β-galactosidase activity.

3.1.5 Nitrate reductase activity in different mutant strains under anaerobic conditions of nitrate respiration

The *E. coli* active nitrate reductase requires Fe-S clusters together with the bis-MGD cofactor. The strains were cultivated under anaerobic conditions with 15 mM potassium nitrate for 8 h at 37°C supplemented with 1 mM mevalonate. Activity was measured from the crude cell extract.

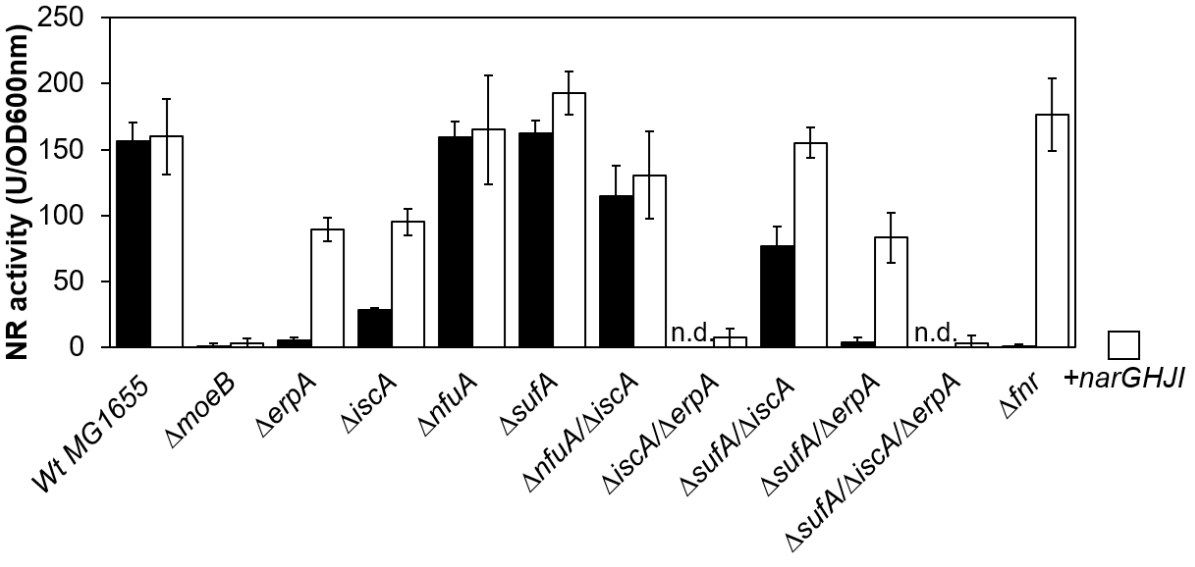

Figure 3-5: Analysis of nitrate reductase activity in *E. coli* mutant strains

Nitrate reductase activity was determined in Wt MG1655, *ΔmoeB, ΔerpA, ΔiscA, ΔnfuA, ΔsufA, ΔnfuA/ΔiscA, ΔiscA/ΔerpA, ΔiscA/ ΔsufA, ΔsufA/ΔerpA, ΔsufA/ΔiscA/ΔerpA,* and *Δfnr* strains (black bars) and the same mutant strains transformed with a *narGHJI* plasmid under the control of an IPTG inducible promoter (white bars) in the presence of 15 mM potassium nitrate, 20 µM IPTG and 1 mM mevalonate under anaerobic conditions; nitrate reductase

activities were normalized to OD_{600} nm; Standard deviations were calculated from three biological replicates, n.d.: not detectable

Figure 3-5 show that nitrate reductase activity almost remained constant in all the single mutant strains, except the strains containing a deletion of *iscA*, where the activity was significantly reduced compared to the Wt MG1655 strain. In contrast, all the *erpA*-deleted strains completely lost nitrate reductase activity. The *ΔerpA* single mutant and *ΔsufA*/*ΔerpA* double mutant strains showed almost no nitrate reductase activity. On the other hand, the single *ΔiscA* mutant strain retained only ~20% of nitrate reductase activity compared to the Wt MG1655 strain. Surprisingly, the *ΔnfuA/ΔiscA* and *ΔsufA/ΔiscA* double mutant strains showed comparatively higher nitrate reductase activity, of about ~65% and ~50% respectively, compared to the Wt MG1655 strain. Moreover, no nitrate reductase activity was detected in the *Δfnr*, the *ΔiscA/ΔerpA* double mutant strain, or the *ΔsufA/ΔiscA/ΔerpA* triple mutant strain.

The nitrate reductase expression (*narGHJI* operon) is strictly dependent on the activation by FNR (Lamberg & Kiley, 2000). It has been reported that the deletion of the *iscRSUAhscBAfdx* operon significantly reduces FNR activity. FNR activity can be restored by the plasmid-borne *suf* operon expression in the *isc* operon deleted strain (Mettert et al., 2008). FNR regulation was avoided by constructing a *narGHJI* expression plasmid under the control of an IPTG inducible promoter and transforming it into the Wt MG1655 and other mutant strains. The *narGHJI* plasmid-containing strains were induced by 20 µM IPTG for 36 h at 24°C under anaerobic conditions in the presence of 1 mM mevalonate and 1 mM Na_2MoO_4.

When the *narGHJI* plasmid was expressed from an IPTG inducible promoter in these mutant strains, a restoration of nitrate reductase activity was observed in the *ΔerpA* single mutant and *ΔsufA*/*ΔerpA* double mutant strains, up to almost ~55% and ~50% respectively, in comparison to the Wt MG1655 strain. The restoration of nitrate reductase activity in *erpA*-deleted strains indicates that ErpA is not required for nitrate reductase activity. Furthermore, nitrate reductase activity in the *ΔiscA* single mutant strain also increased around ~3-fold, while in the *ΔerpA/ΔiscA* double mutant strain and the *ΔsufA/ΔiscA/ΔerpA* triple mutant strain, nitrate reductase activity remained undetectable.

Moreover, nitrate reductase activity was restored in the *Δfnr* strains when the *narGHJI* was exogenously expressed, which indicates the requirement of FNR in nitrate reductase expression, but not for the activity. The other single mutants possessed a quite similar nitrate reductase activity as compared to the Wt MG1655 strain.

3.1.6 Quantification cPMP and Moco in different mutant strains under anaerobic conditions of nitrate respiration

In order to identify the carrier protein that inserts Fe-S clusters into MoaA, the cPMP- and Moco-producing ability was investigated for the single mutant strains *ΔmoeB* (as a negative control), *ΔerpA*, *ΔiscA*, Δ*nufA*, *ΔsufA*, *Δfnr*, the double mutant strains *ΔerpA/ΔiscA*, *ΔsufA/ΔiscA*, *ΔsufA/ΔerpA*, the triple mutant strain *ΔsufA/ΔiscA/ΔerpA*, and the Wt MG1655 strain. The cPMP measurement was used as a control in our study. The cPMP content reflects the cellular MoaA activity. The strains were cultivated under anaerobic conditions for 8 hours with 15 mM potassium nitrate and 1 mM mevalonate.

The cPMP and Moco content were quantified from the crude extracts in the form of their fluorescence derivatives as Compound Z and FormA, respectively, in which the conversion was performed by oxidation using KI and I_2. Furthermore, the compounds were separated on a C18 reversed-phase HPLC column.

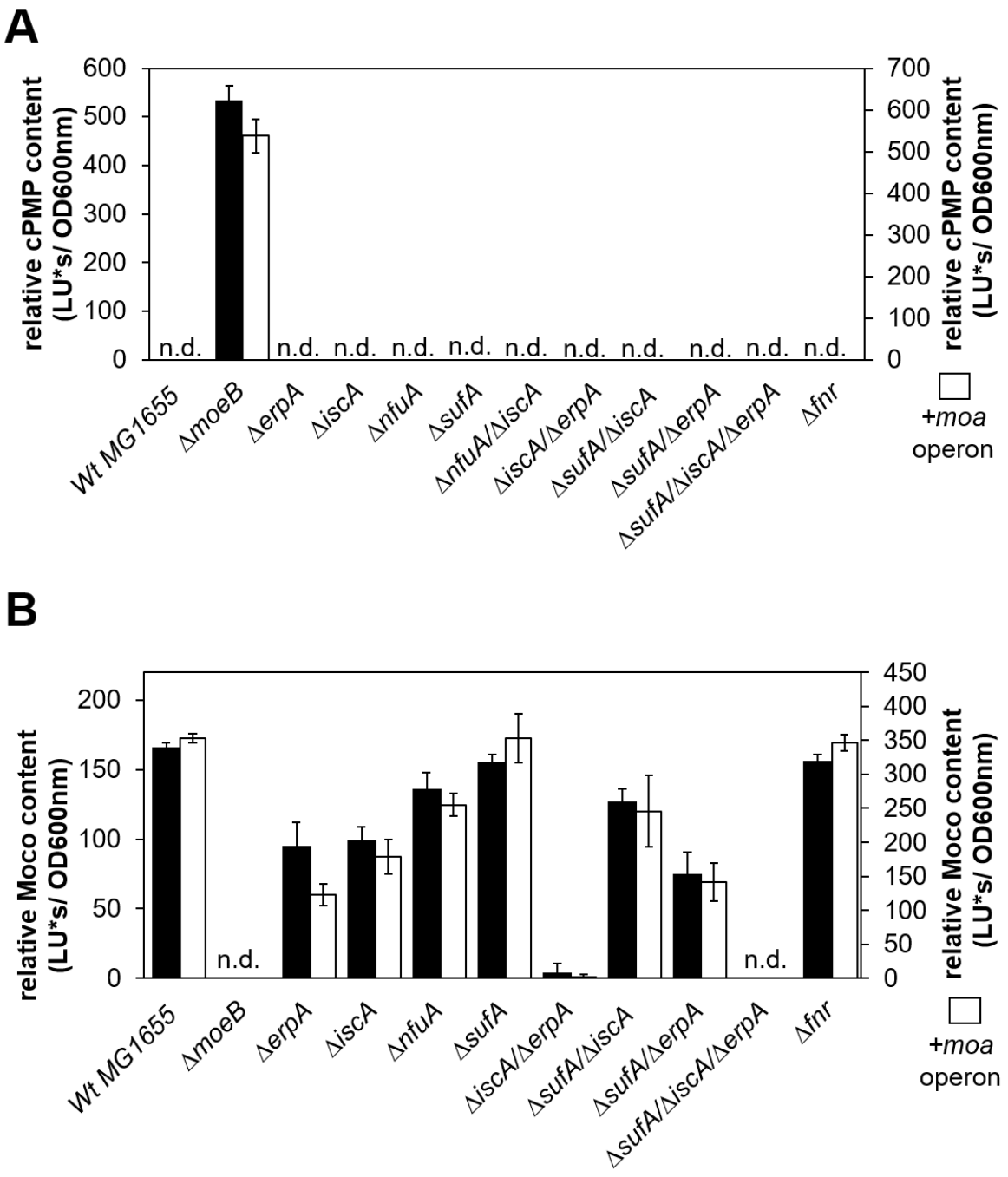

Figure 3-6: Analysis of relative cPMP and Moco content in *E. coli* mutant strains

Relative cPMP (A) and Moco content (B) were determined in Wt MG1655, *ΔmoeB, ΔerpA, ΔiscA, ΔnfuA, ΔsufA, ΔnfuA/ΔiscA, ΔiscA/ΔerpA, ΔiscA/ΔsufA, ΔsufA/ΔerpA, ΔsufA/ΔiscA/ΔerpA,* and *Δfnr* strain (black bar) and the same mutant strains transformed with a *moaABCDE* plasmid under the control of an arabinose inducible promoter (white bars) in the presence of 15 mM potassium nitrate, 0.2% L-arabinose and 1 mM mevalonate under anaerobic conditions; the Compound Z (cPMP) and FormA (Moco) were monitored by fluorescence of extinction at 383 nm and an emission at 450 nm using HPLC; the relative amounts of cPMP and Moco were normalized to the OD_{600} nm. Standard deviations were calculated from three biological replicates, n.d.: not detectable

Figure 3-6 shows that cPMP was only accumulated in the *ΔmoeB* strain under nitrate respiration. This was expected since the deletion of *moeB* leads to inhibition in the production of MPT from cPMP. The absence of cPMP accumulation in other mutant strains suggests that either MoaA was completely inactive, which indicates that no cPMP was produced, or that MoaA was active and all cPMP was converted to MPT/Moco.

Furthermore, the Moco content was analyzed in all the respective mutant strains. As expected, the results show that no Moco was detected in the *ΔmoeB* mutant in the presence of nitrate, whereas mutant strains containing deletions in either *iscA* or *erpA* showed a reduced Moco content. In the single Δ*erpA* and Δ*iscA* mutants, the Moco content was ~40% reduced, whereas no Moco was detectable in the *ΔiscA/ΔerpA* double mutant strain or the *ΔsufA/ΔiscA/ΔerpA* triple mutant strain as compared to the Wt MG1655 strain. Furthermore, the respective Moco contents in the *ΔnfuA/ΔiscA* and *ΔsufA/ΔiscA* strains were almost ~13% and ~24% reduced in comparison to the Wt MG1655 strain. This had not been predicted since the double mutant strains produced higher Moco content than the respective *ΔiscA* single mutant strain, as it was ~40% reduced.

On the other hand, the *ΔsufA/ΔerpA* double mutant strain produced an almost similar amount of Moco in comparison to the *ΔerpA* and *ΔiscA* single mutant strains. The other single mutant strains showed almost identical Moco content as the Wt MG1655 strain. Under nitrate respiratory conditions, the Moco-producing ability of the *Δfnr* strain was almost identical when compared to the Wt MG1655 strain.

It has been reported that the Moco biosynthesis pathway is regulated by FNR, where it positively regulates the *moa* operon but negatively regulates the *moe* operon. (Rivers et al., 1993; Zupok et al., 2019; Anderson et al., 2000; Hasona, Self, and Shanmugam, 2001). The additional *moaABCDE* operon was introduced on a replicative plasmid under the control of an arabinose inducible promoter into the respective mutant strains to exclude the effect of regulation by FNR. The *moaABCDE* operon was overexpressed under anaerobic conditions in the presence of 1 mM mevalonate and 0.2% L-arabinose for 8 h at 37°C.

After the *moaABCDE* overexpression, no major changes were observed in comparison to the chromosomal *moaABCDE* expression from the endogenous promoter. However, the overall Moco content increased about ~2-fold after the exogenous operon expression. The Moco content in the *ΔnfuA/ΔiscA* and *ΔsufA/ΔiscA* double mutant strains was,

respectively, almost ~43% and ~32% reduced in comparison to the Wt MG1655 strain. Simultaneously, the *ΔsufA/ΔerpA* double mutant strain showed a ~58% reduction in Moco content compared to the Wt MG1655 strain. Furthermore, the Moco content was reduced to almost ~67% in the *ΔerpA* and ~50% in the *ΔiscA* mutant strain compared to in the Wt MG1655 strain. This result confirmed the importance of IscA and ErpA for Moco biosynthesis. No Moco content was detectable in the *ΔiscA/ΔerpA* double mutant and *ΔsufA/ΔiscA/ΔerpA* triple mutant strains in the presence or absence of exogenous *moaABCDE* expression under nitrate respiratory conditions. Overall, after uncoupling the *moa*-operon expression from the control of FNR and other cellular regulations, the overall cellular Moco content matched the nitrate reductase activity measured for the respective mutant strains.

3.1.7 Complementation study with *erpA, iscA* and *sufA* expression plasmid

ErpA and IscA play an important role in the maturation of nitrate reductase and MoaA under anaerobic nitrate respiratory conditions, as shown above. A complementation study was conducted to analyze the functional replacement of Fe-S cluster carrier proteins that play a role in MoaA and FNR maturation. The experiment was performed using *iscA*, *sufA*, and *erpA* overexpressing plasmids under the control of an arabinose inducible promoter. EcoRI and XhoI were used to digest the *iscA*, *sufA*, and *erpA* PCR product. Further, the digested PCR product was ligated into the *pBAD-I* vector and produced *pLAI-A* for *iscA*, *pLAS-A* for *sufA*, and *pLAE-A* for *erpA*, respectively. The *pLAI-A*, *pLAS-A*, and *pLAE-A* overexpressing plasmids were transformed into Wt MG1655, *ΔiscA*, *ΔerpA*, and *ΔiscA/ΔerpA* strains and further cultivated anaerobically with 15 mM potassium nitrate, 1 mM mevalonate and 0.2% L-arabinose for 8 h at 37°C. The complementation effect was analyzed by performing nitrate reductase activity and measuring overall Moco content in the cell extract.

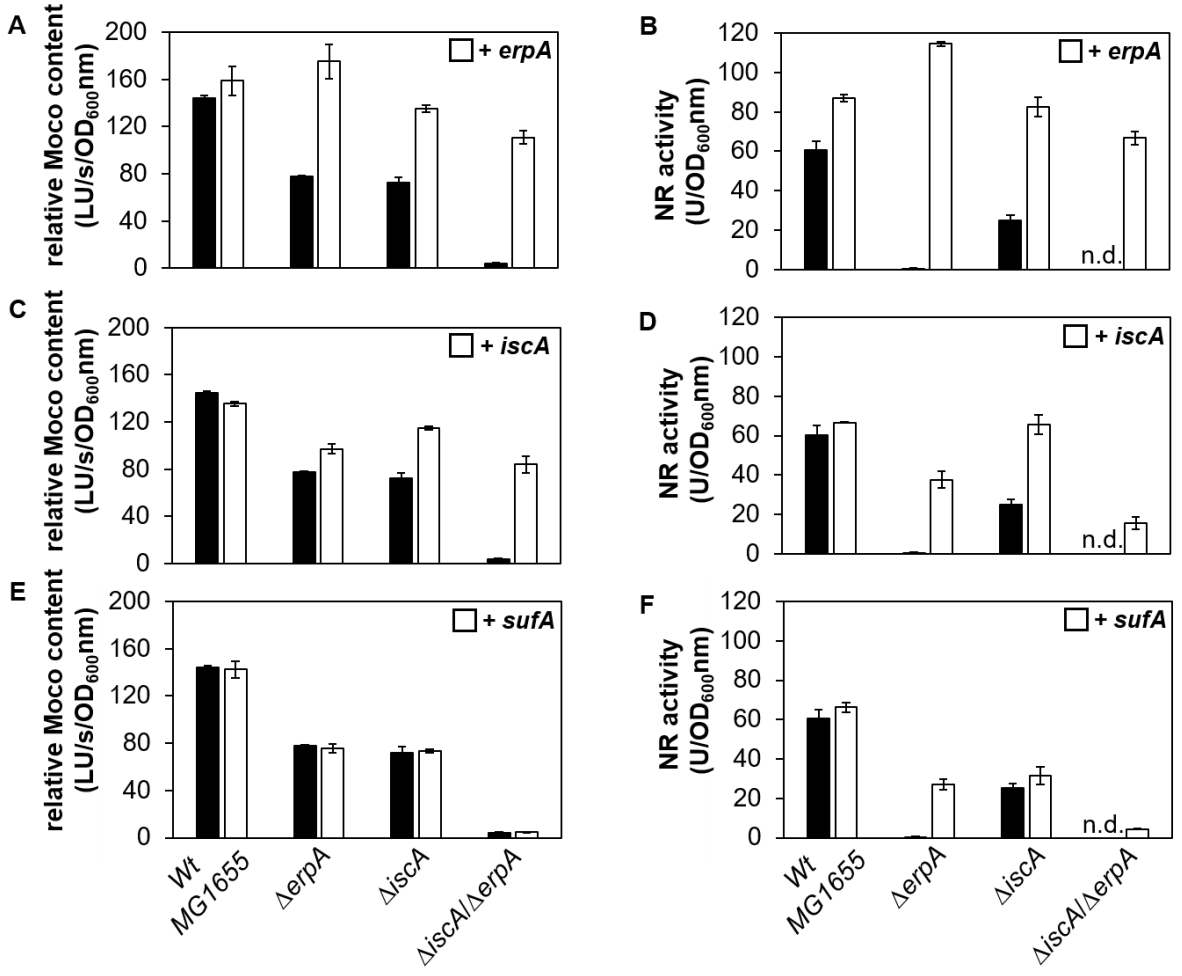

Figure 3-7: Analysis of Moco content and nitrate reductase activity in *E. coli* mutant strains

Relative Moco content (A, C, E) were determined in Wt MG1655, *ΔerpA, ΔiscA,* and *ΔiscA/ΔerpA* strains. FormA (Moco) was monitored by fluorescence of extinction at 383 nm and an emission at 450 nm using HPLC; the relative amounts of Moco were normalized to the OD_{600} nm; Nitrate reductase activities (B, D, F) were determined in Wt MG1655, *ΔerpA, ΔiscA,* and *ΔiscA/ΔerpA* strains; nitrate reductase activities were normalized to OD_{600} nm, the strains were grown anaerobically in the presence of 15 mM potassium nitrate, 0.2% L-arabinose, and 1 mM mevalonate for 8 h. Standard deviations were calculated from three biological replicates. Black bars correspond to the indicated mutant strains; white bars correspond to the same mutant strains containing either a plasmid expressing *erpA* (A+B), *iscA* (C+D), or *sufA* (E+F); n.d.: not detectable

Figure 3-7 shows no alteration of Moco content under exogenous *sufA* overexpression in the mutant strains. This indicates that SufA could not replace ErpA or IscA in the maturation of MoaA by inserting Fe-S clusters into it. However, nitrate reductase activity was restored in *ΔerpA* strains, indicating that plasmid-borne *sufA* expression could replace ErpA when produced in sufficient amounts. No nitrate reductase activity in *ΔiscA/ΔerpA* strains was detected due to the absence of Moco. On the other hand, the

overexpression of *iscA* slightly increased the Moco content in the *ΔerpA* and *ΔiscA/ΔerpA* strains, at around ~20% and ~50% respectively, compared to the Wt MG1655 strain. Moreover, nitrate reductase activity in the *ΔerpA* strain increased up to ~55% compared to the Wt MG1655 strain. This shows that exogenously produced IscA could replace the role of ErpA. Furthermore, nitrate reductase activity in the *ΔiscA*/*ΔerpA* double mutant strain was around ~35% compared to the Wt MG1655 strain. Finally, the Moco content was significantly increased in the *ΔiscA*, *ΔerpA, ΔiscA*/*ΔerpA* strains as compared to the Wt MG1655 strain after *erpA* overexpression. The nitrate reductase activity in the *ΔiscA*/*ΔerpA* strain was increased to ~85% compared to the Wt MG1655 strain. After the overexpression of *erpA*, an increased Moco content and a higher nitrate reductase activity were observed under nitrate respiratory conditions.

3.1.8 Investigation of the expression of the *moaABCDE* operon

The unaltered expression of *moaA* is important for Moco biosynthesis in *E. coli*. However, the expression of *moaA* is controlled by FNR and can be altered due to the deletion of A-type carrier proteins. Therefore, it was necessary to evaluate the expression level of *moaA* in the *ΔerpA*, *ΔiscA*, *ΔsufA*, and *ΔnufA* mutant strains and to compare it to the Wt MG1655 strain.

In this study, the *PmoaA-L-LacZ* fusion plasmid was used, including a 477 bps fragment upstream of the *moaA* ATG start codon containing the reported FNR binding sites (Zupok et al., 2019). The *E. coli* Wt MG1655, *ΔerpA, ΔiscA*, Δ*nufA*, *ΔsufA*, and *Δfnr* strains were grown under anaerobic conditions in the presence of 15 mM potassium nitrate and 1 mM mevalonate.

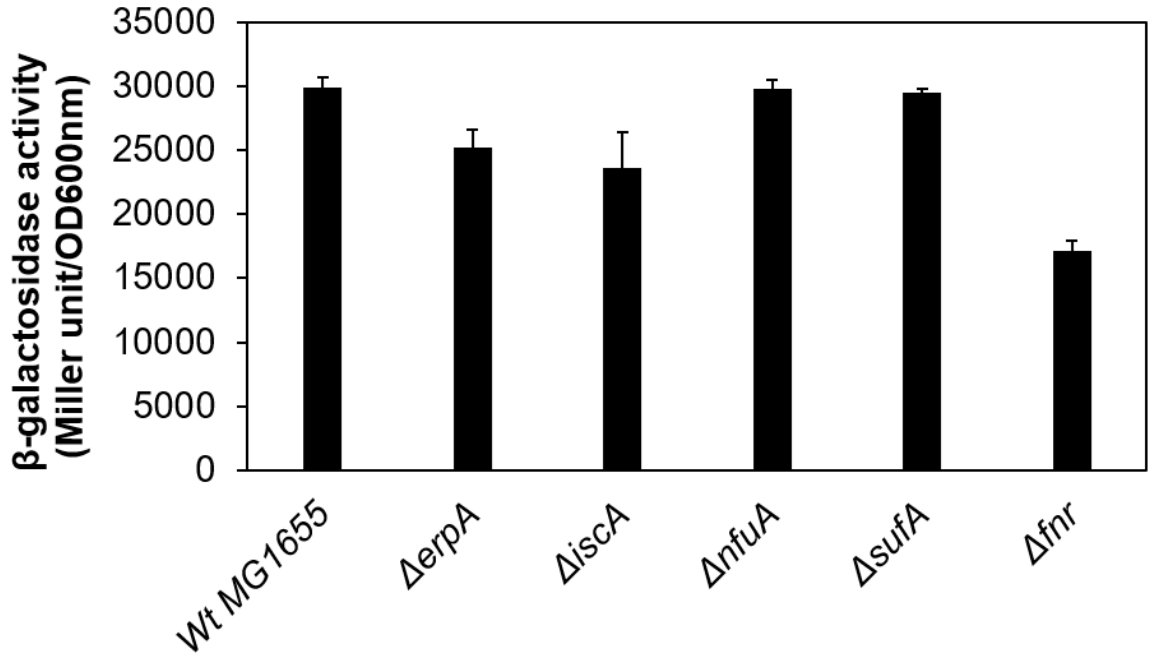

Figure 3-8: Analysis of the expression of a *PmoaA-L-LacZ* fusion in *E. coli* mutant strains

β-galactosidase activities in Miller units were determined for the *PmoaA-L-LacZ* fusion in Wt MG1655, *ΔerpA, ΔiscA, ΔnfuA, ΔsufA, Δfnr* mutant strains. Strains were grown anaerobically in 15 mM potassium nitrate and 1 mM mevalonate for 8 h. *β*-galactosidase activities were normalized to OD_{600} nm. Standard deviations were calculated from three biological replicates.

Figure 3-8 shows that β-galactosidase activity under nitrate respiratory conditions was reduced to almost ~40% in the *Δfnr* mutant strain. This was consistent with the previous report, indicating that FNR acts as a transcriptional activator of the operon, but is not entirely essential for its expression (Zupok et al., 2019). In comparison, the *ΔiscA* and *ΔerpA* mutant strains showed around ~20% and ~15% reduced β-galactosidase activity, respectively. The β-galactosidase activity remained comparable in the *ΔsufA* and *ΔnfuA* mutant strains to the Wt MG1655 strain. The slightly reduced expression of the operon in the *ΔiscA* and *ΔerpA* mutant strains might indicate that these two proteins are also involved in Fe-S cluster insertion into FNR, as suggested from the results shown above (Mettert et al., 2008).

3.1.9 Immunodetection of MoaC

The *moaABCDE* operon overexpression was performed to avoid the effects of FNR regulation under nitrate respiratory conditions. To confirm that the protein levels of protein

expressed from the *moaABCDE* operon are not altered in the various mutant strains used, we performed immunoblot analysis using an antiserum raised against MoaC.

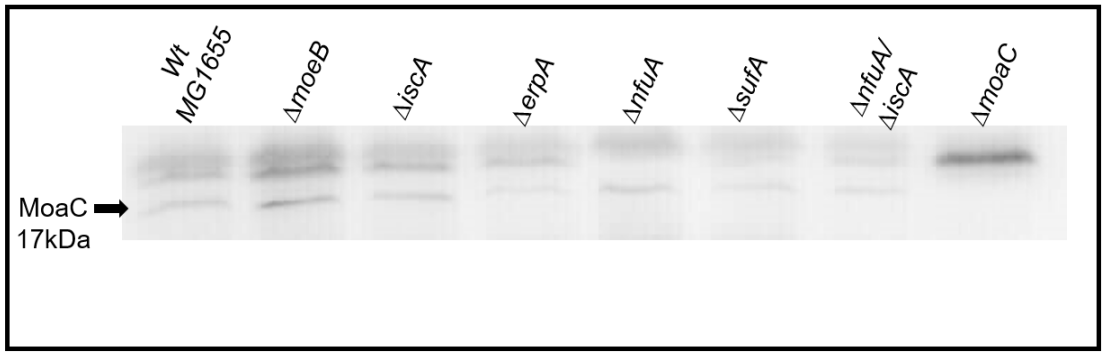

Figure 3-9: Immunodetection of MoaC in *E. coli* mutant strains.

50 µg of total protein fractions of cell extract of Wt MG1655*, ΔmoeB, ΔiscA, ΔerpA, ΔsnfuA, ΔsufA,* and *ΔnfuA/ΔiscA* strains were separated by 17% SDS-PAGE and transferred onto a PVDF membrane. A MoaC specific antiserum (1:1000 dilution) was used and visualized by enhanced chemiluminescence; the *ΔmoaC* cell extract served as a negative control; the strains were grown anaerobically in the presence of 15 mM potassium nitrate, 0.2% L-arabinose, and 1 mM mevalonate for 8 h.

Figure 3-9 shows that MoaC was detectable in similar amounts in the different mutant strains, with the exception of the *ΔmoeB* strain, where the MoaC expression was slightly increased. The presence of the MoaC band confirmed the sufficient expression of the exogenous *moaABCDE* operon in Wt MG1655 and in the mutant strains.

3.1.10 Immunodetection of IscS

The IscS protein is essential for Fe-S cluster biosynthesis and provides sulfur as a form of persulfide in Moco biosynthesis. Therefore, it was also important to establish that the cellular levels of IscS were not affected by Fe-S cluster carrier proteins like IscA, SufA, ErpA, or NfuA. Otherwise, the absence of Moco in these strains will be based on the absence of IscS since it provides sulfur in MPT. In this study, the effect of cellular IscS levels was analyzed in all the single mutant strains, in the *ΔiscA/ΔerpA*, *ΔsufA/ΔiscA*, and *ΔsufA/ΔerpA* double mutant strains, and in a *ΔerpA*/*ΔsufA/ΔiscA* triple mutant strain by immunodetection using antisera derived against IscS. The Wt MG1655 and other mutant strains were grown anaerobically for 8 h in LB medium supplemented with 15 mM potassium nitrate and 1 mM mevalonate.

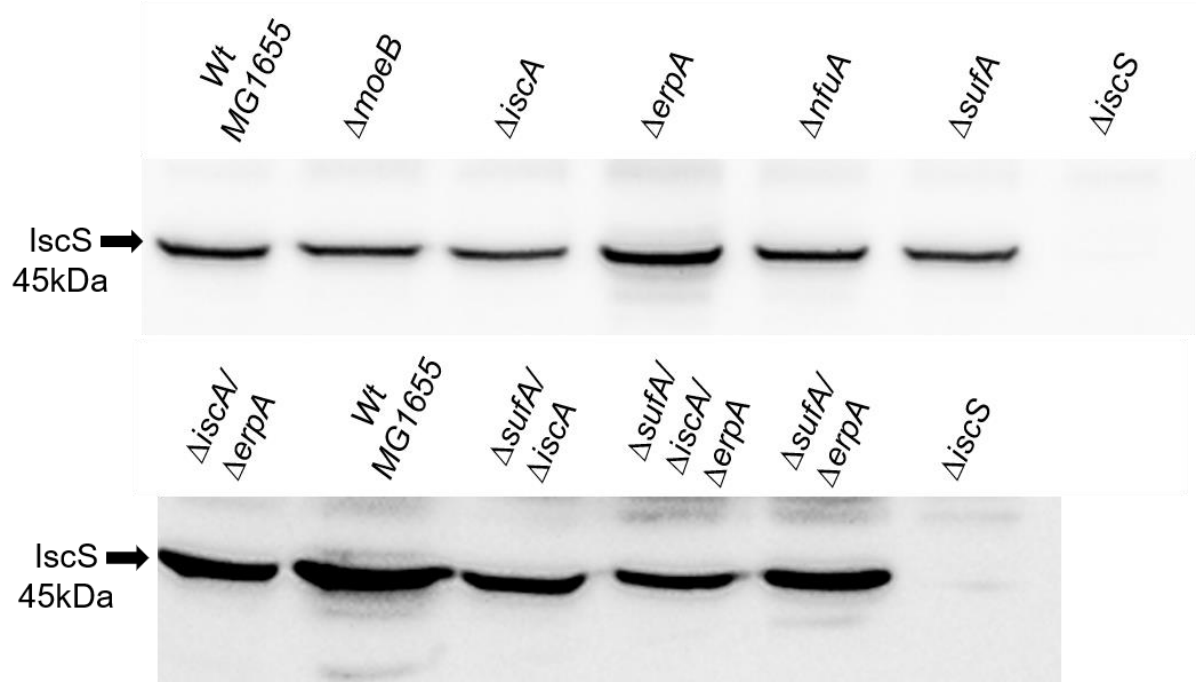

Figure 3-10: Immunodetection of IscS in *E. coli* mutant strains.

50 µg of total protein fractions of the cell extract of Wt MG1655, *ΔmoeB, ΔiscA, ΔerpA, ΔnfuA, ΔsufA, ΔiscA/ΔerpA, ΔiscA/ΔsufA, ΔsufA/ΔerpA, ΔsufA/ΔiscA/ΔerpA* strains were separated by 12% SDS-PAGE and transferred onto a PVDF membrane. An IscS specific antiserum (1:5000 dilution) was used and visualized by enhanced chemiluminescence; the *ΔiscS* cell extract served as a negative control; the strains were grown anaerobically in the presence of 15 mM potassium nitrate, and 1 mM mevalonate for 8 h.

Figure 3-10 shows that IscS was detectable in almost similar amounts in most mutant strains but was slightly lower in the *ΔiscA*, *ΔnfuA*, and *ΔsufA* single mutant strains. Conclusively, the reduced Moco content in the A-type carrier protein deleted strain, in the *ΔiscA/ΔerpA*, *ΔsufA/ΔiscA*, and *ΔsufA/ΔerpA* double mutant strains, and in the *ΔerpA*/*ΔsufA/ΔiscA* triple mutant strain was generally not based on the absence of IscS.

3.1.11 The expression of IscR and SufA in mutant strains

In *E. coli,* the *iscRSUA-hscBA-fdx-iscX* and *sufABCDSE* operons are involved in Fe-S cluster assembly, where the *isc* operon functions as a housekeeping system and the *suf* operon expresses under iron-limiting conditions (Zheng et al., 1998; Outten, Djaman, and Storz, 2004; Ayala-Castro, Saini, and Outten, 2008; Tanaka et al., 2016). The expression of the *iscRSUA-hscBA-fdx-iscX* and the *sufABCDSE* operons are regulated by IscR, a protein that represses the expression of *iscRSUA-hscBA-fdx-iscX* in the presence of a

[2Fe-2S] cluster and activates the expression of *sufABCDSE* in its apo-form (Giel et al., 2006; Schwartz et al., 2001). In this study, the expression of a *PiscR-lacZ* fusion and a *PsufA-lacZ* fusion was analyzed in the Wt MG1655, *ΔerpA*, *ΔiscA*, Δ*nufA*, *ΔsufA*, and *Δfnr* single mutant strains, and in the *ΔnfuA/ΔiscA*, *ΔerpA/ΔiscA*, *ΔsufA/ΔiscA*, and *ΔsufA/ΔerpA* double mutant strains. The experiment was performed to determine the expression level of the *isc* operon and further compare it to the expression of the *suf* operon under anaerobic nitrate respiratory conditions. The strains were grown under anaerobic conditions with 15 mM potassium nitrate and 1 mM mevalonate for 8 h.

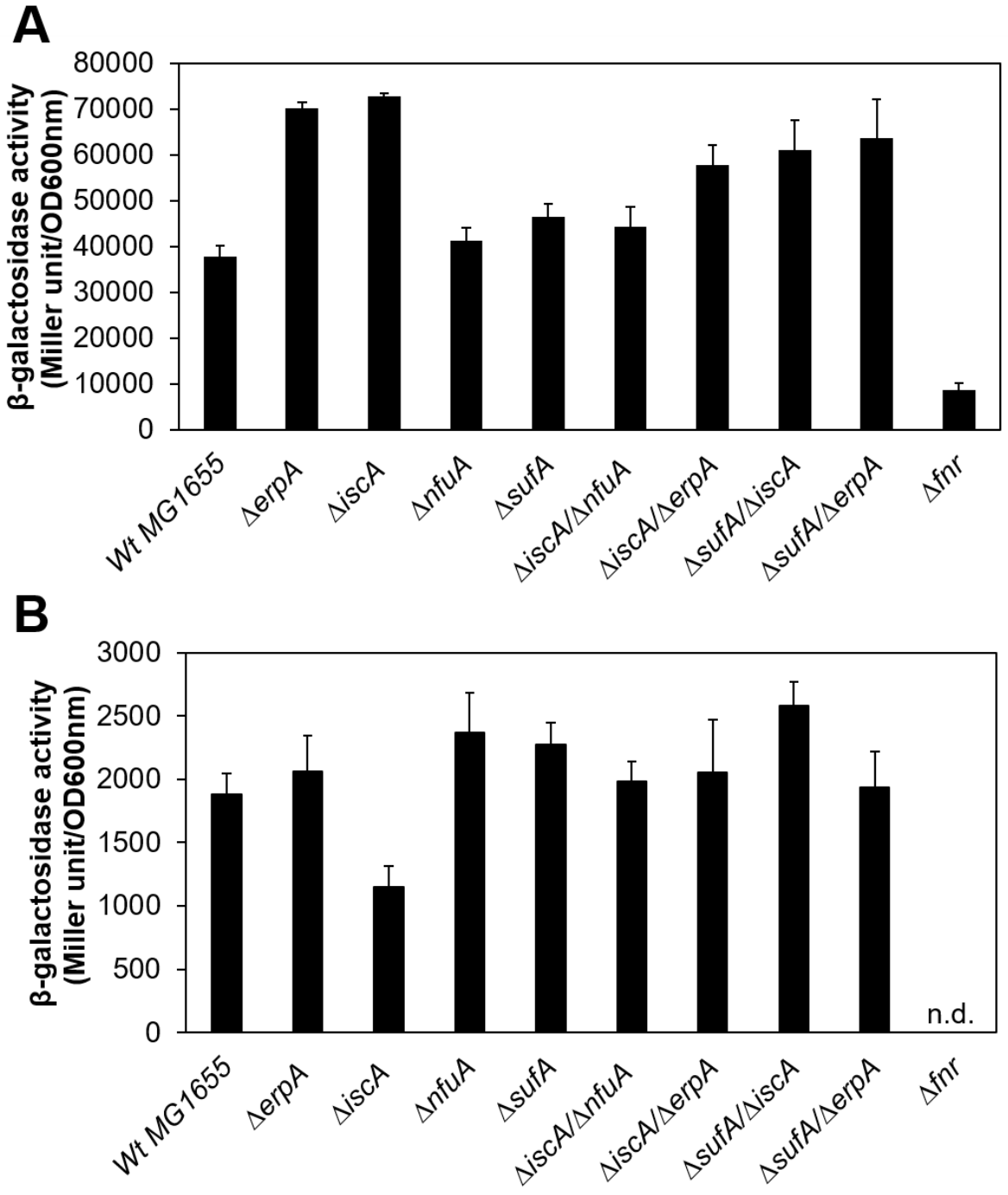

Figure 3-11: Expression of a *PiscR-lacZ* and a *PsufA-lacZ* fusion in *E. coli* mutant strains

β-galactosidase activities in Miller units were determined for the *PiscR-lacZ* (A) and the *PsufA-lacZ* (B) fusion in Wt MG1655, *ΔerpA, ΔiscA,* Δ*nufA, ΔsufA, ΔnfuA/ΔiscA, ΔerpA/ΔiscA, ΔsufA/ΔiscA, ΔsufA/ΔerpA,* and *Δfnr* strains. The strains were grown anaerobically in the presence of 15 mM potassium nitrate and 1 mM mevalonate for 8 h; *β*-galactosidase activities were normalized to OD_{600} nm; standard deviations were calculated from three biological replicates; n.d.: not detectable

Figure 3-11 show that β-galactosidase activity was increased in *erpA*- and *iscA*-deleted strains in the presence of *PiscR-lacZ*, in which the expression of *iscR* was increased almost 2-fold in the *ΔerpA* and *ΔiscA* mutant strains as compared to the Wt MG1655 strain. Moreover, the expression was also increased almost 1.7-fold in *ΔsufA/ΔiscA* and *ΔsufA/ΔerpA* compared to the Wt MG1655 strain. The *ΔsufA*, *ΔnfuA*, and *ΔnfuA/ΔiscA* strains showed slightly increased *iscR* expression as compared to the Wt MG1655 strain. However, *iscR* expression significantly decreased to ~80% in the *Δfnr* mutant strain compared to the Wt MG1655 strain.

On the other hand, a slightly increased β-galactosidase activity was observed in all the single and double mutant strains compared to the Wt MG1655 strain for *PsufA-lacZ* fusion, except in the *ΔiscA* strains, where β-galactosidase activity was reduced by around ~40%. Moreover, undetected β-galactosidase activity in the *Δfnr* mutant strain compared to the Wt MG1655 reflects the finding that *sufA* was not expressed in the absence of FNR protein. Overall, the expression of *sufA* was almost 20 times lower than the expression of *iscR* under anaerobic nitrate respiratory conditions.

3.1.12 Immunodetection of SufS

Under nitrate respiratory conditions, it has been shown that SufA did not play any role in FNR or MoaA maturation at the cellular level. The experiment was performed to determine the *suf* operon expression under nitrate respiratory conditions by immunodetection using SufS antiserum. For these experiments, the cells were cultivated under anaerobic conditions with 15 mM potassium nitrate and 1 mM mevalonate for 8 h at 37°C. Immunodetection using SufS antiserum was performed with the crude cell lysate, where 50 µg of protein was used for detection.

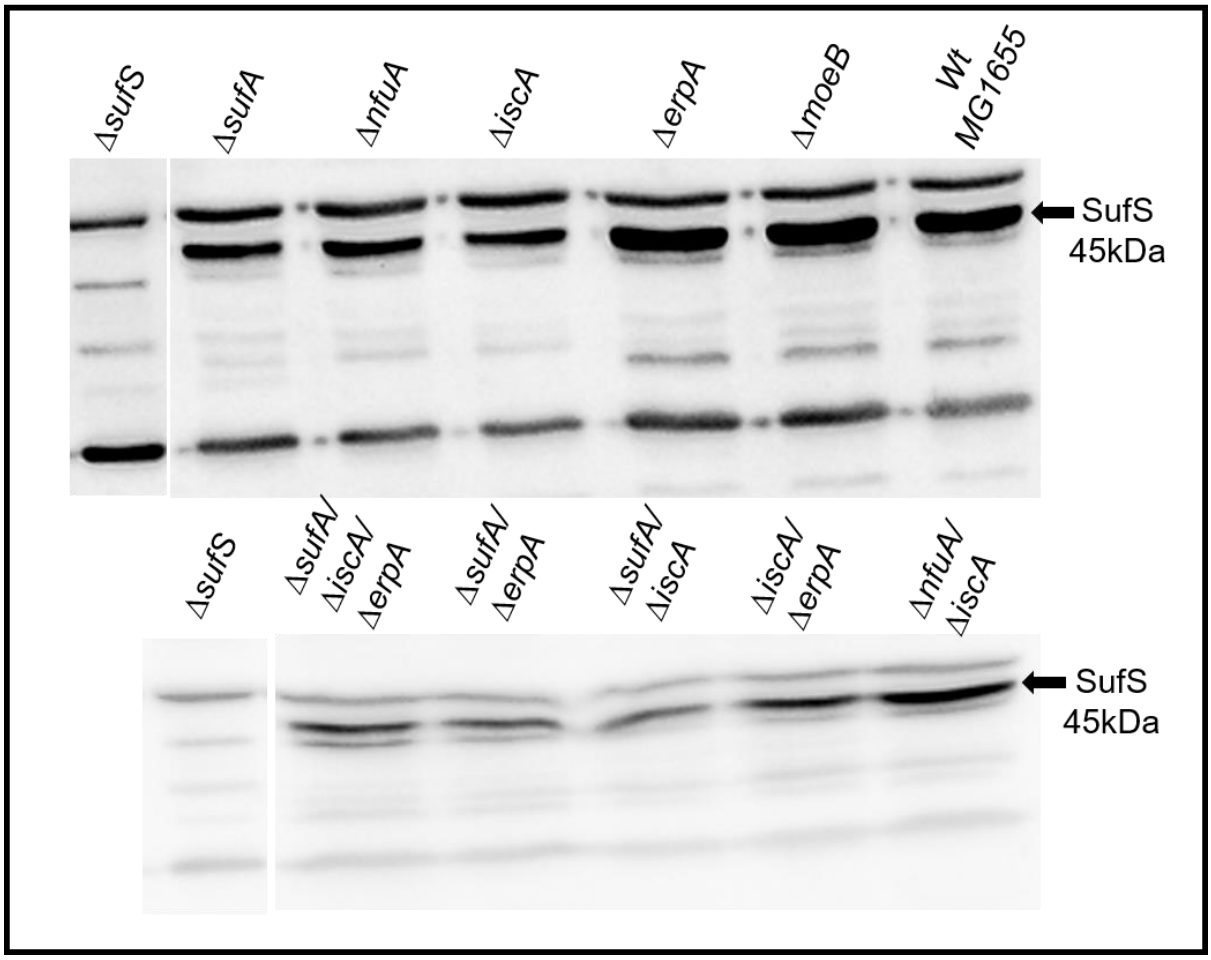

Figure 3-12: Immunodetection of SufS in *E. coli* mutant strains.

50 µg of total protein fractions of the cell extract of Wt MG1655, *ΔmoeB, ΔiscA, ΔerpA, ΔnfuA, ΔsufA, ΔnfuA/ΔiscA, ΔiscA/ΔerpA, ΔiscA/ΔsufA, ΔsufA/ΔerpA, ΔsufA/ΔiscA/ΔerpA* strains were separated by 12% SDS-PAGE and transferred onto a nitrocellulose membrane. A SufS specific antiserum (1:2000 dilution) was used and visualized by enhanced chemiluminescence; the *ΔsufS* cell extract served as a negative control; the strains were grown anaerobically in the presence of 15 mM potassium nitrate, and 1 mM mevalonate for 8 h.

Immunodetection (Figure 3-12) showed that SufS detection was almost similar in all the mutant strains compared to the Wt MG1655 strain. However, the SufS amount was slightly enhanced in the *ΔerpA* mutant strains and reduced in the *ΔiscA*, *ΔsufA/ΔiscA*, and *ΔsufA/ΔerpA* mutant strains.

3.1.13 Detection of relative iron content in *erpA* and *iscA* deleted strains under anaerobic nitrate respiratory conditions

The availability of Fe is required for Fe-S cluster biosynthesis, where the source of iron is still unknown. Yang et al. (2015) reported that IscA might be functioning as an Fe chaperone in Fe-S cluster biosynthesis. Therefore, it was of interest to determine the Fe content in *ΔiscA* and *ΔerpA* strains; otherwise, the lack of Moco content could be based on a lack of iron content in these strains. The iron content was quantified in Wt MG1655, and in the *ΔiscA* and *ΔerpA* strains, by inductively coupled plasma optical emission spectrometry (ICP-OES). The measurement was performed using a reference standard (Solution XVI, Merck) for the exact quantification of iron content. The strains were cultivated anaerobically with 15 mM potassium nitrate and 1 mM mevalonate for 8 h.

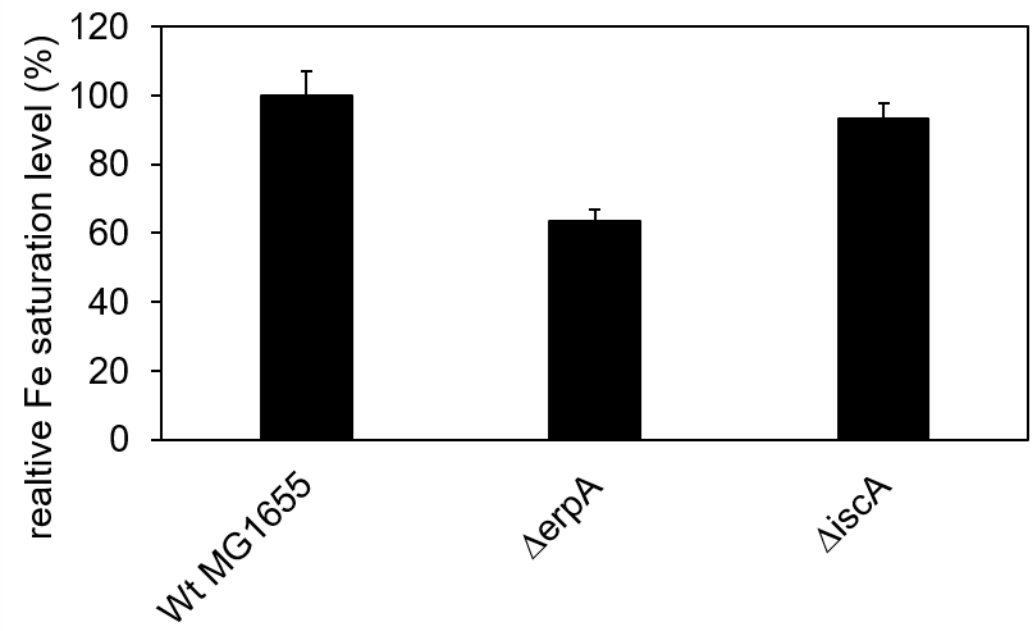

Figure 3-13: Analysis of relative iron saturation in *E. coli* mutant strains

The ICP-OES analysis for the determination of relative iron saturation in Wt MG1655, *ΔerpA,* and *ΔiscA* strains; the strains were cultivated anaerobically with 15 mM potassium nitrate and 1 mM mevalonate for 8 h at 37°C; 50 µM total protein extract was used the analysis; the following wavelengths were used to analyze for iron: 238.204 nm, 238.562 nm, 259.939 nm; A baseline was measured using 100 mM Tris, pH 7.5; the iron concentrations were determined by using the Standard XVI (Merck)

Figure 3-13 shows that the iron content was almost similar for the *ΔiscA* strain and was reduced by around ~25% in the *ΔerpA* strain compared to in the Wt MG1655 strain.

Therefore, the reduced Moco content in the *ΔerpA* and *ΔiscA* strains was generally not based on the absence of Fe-S cluster formation since the iron content was comparable in these mutant strains.

3.1.14 Detection of *erpA* and *iscA* transcripts

The previous results showed that together ErpA and IscA are involved in the Fe-S cluster insertion into MoaA in the Moco biosynthesis pathway. However, the double mutant strains containing either *iscA* or *erpA* (except for the *ΔerpA/ΔiscA* double mutant strain) also showed higher Moco content and nitrate reductase activity in comparison to their respective single mutant strains such as the *ΔiscA* strain. This indicates that ErpA and IscA could probably replace each other in their role in [4Fe-4S] cluster insertion into MoaA or FNR. Therefore, it was important to quantify gene expression in the respective single and double mutant strains. The strains were grown under anaerobic conditions with 15 mM potassium nitrate and 1 mM mevalonate for 8 h at 37°C. qRT-PCR was performed to quantify the transcript levels of *erpA* and *iscA* in the mutant strains.

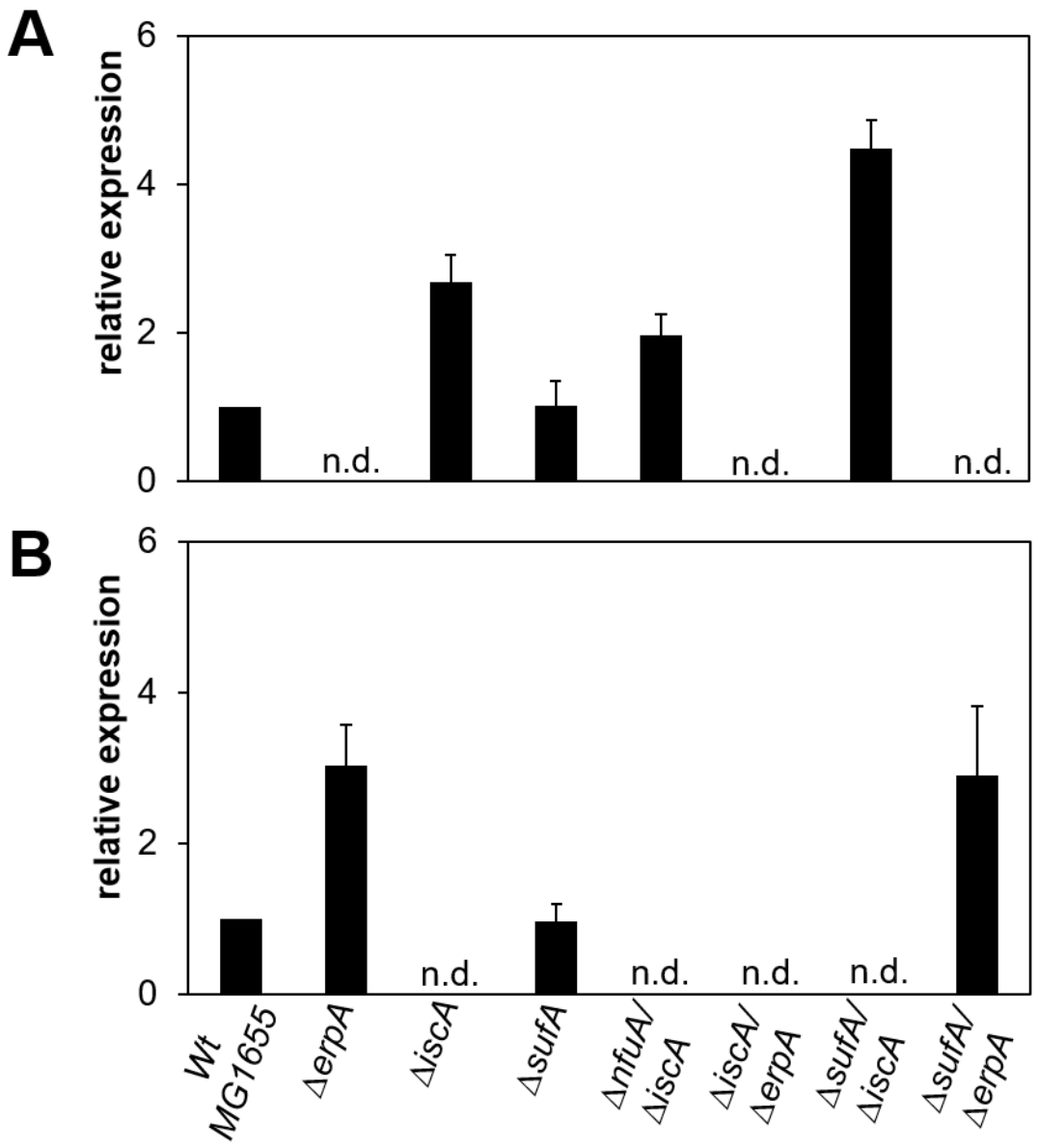

Figure 3-14: Analysis of relative expression levels of *erpA* and *iscA* in *E. coli* mutant strains

Relative expression was carried out using qRT-PCR; the expression levels of *erpA* (A) and *iscA* (B) in Wt MG1655, Δ*erpA,* Δ*iscA,* Δ*sufA,* Δ*nfuA*/Δ*iscA,* Δ*iscA*/Δ*erpA,* Δ*iscA*/Δ*sufA,* and Δ*sufA*/Δ*erpA* strains. The strains were grown in the presence of 15 mM potassium nitrate and 1 mM mevalonate; Y-axis denotes the relative expression value in the log of fold changes to Wt MG1655, standard deviations were calculated from three biological replicates; n.d.: not detectable

Figure 3-14 show the transcript levels of *erpA* in the respective mutant strains. No *erpA* transcript was detected in the *erpA*-deleted single and double mutant strains. The transcription level of *erpA* was increased about ~2.6-fold in the *ΔiscA* single mutant and

about ~4.6-fold in the *ΔiscA*/*ΔsufA* double mutant strain as compared to in the Wt MG1655 strain. Moreover, the *ΔnfuA*/*ΔiscA* double mutant strain showed a ~2-fold increased *erpA* expression compared to the Wt MG1655 strain. This higher expression of *erpA* in the *ΔnfuA*/*ΔiscA* and *ΔiscA*/*ΔsufA* double mutant strains might explain the increased nitrate reductase activity and Moco content in these strains in comparison to the *ΔiscA* single mutant strain, and shows that higher ErpA levels result in a better substitution of the role of IscA in these strains.

Similar results were obtained for the *iscA* transcript levels, in which the *iscA* transcript level was almost ~3-fold higher in the *ΔerpA and ΔsufA*/*ΔerpA* mutant strains while, as expected, no *iscA* transcripts were detected in the *ΔiscA*, *ΔnfuA*/*ΔiscA*, and *ΔiscA*/*ΔerpA* mutant strains. This result shows that IscA protein levels should be higher in *ΔerpA* mutant strains.

3.1.15 Detection of *sufA* transcripts under anaerobic nitrate respiratory conditions

The expression level of *sufA* in Wt MG1655 and other mutant strains was determined under nitrate respiratory conditions by qRT-PCR. The cells were cultivated under anaerobic conditions with 15 mM potassium nitrate and 1 mM mevalonate for 8 h at 37°C. For the qRT-PCR expression analysis, cDNA was used from the extracted mRNA from the respective strains.

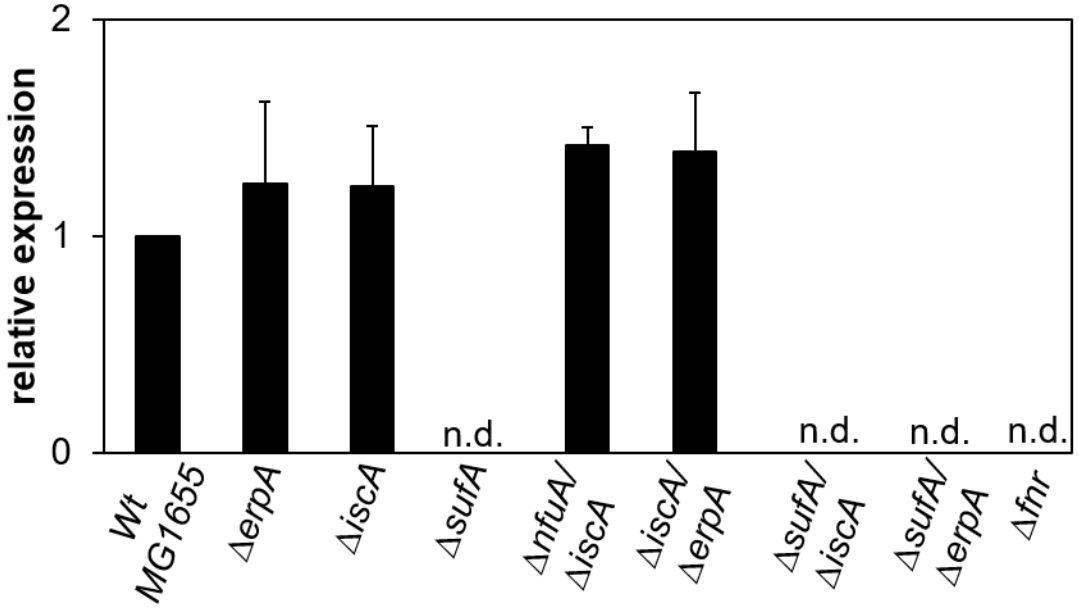

Figure 3-15: Analysis of relative expression levels of *sufA* in *E. coli* mutant strains

Relative expression was carried out using qRT-PCR; the expression levels of *sufA* in Wt MG1655*,* ∆*erpA,* ∆*iscA,* ∆*sufA,* ∆*nfuA/*∆*iscA,* ∆*iscA/*∆*erpA,* ∆*iscA/*∆*sufA,* ∆*sufA/*∆*erpA* and ∆*fnr* strains. The strains were grown in the presence of 15 mM potassium nitrate and 1 mM mevalonate; Y-axis denotes the relative expression value in the log of fold changes to Wt MG1655, standard deviations were calculated from three biological replicates; n.d.: not detectable

The qRT-PCR result (Figure 3-15) shows the transcript levels of *sufA* in the respective mutant strains. No *sufA* transcript was detected in the *sufA*-deleted single and double mutant strains. Moreover, the transcription level of *sufA* was almost similar in *ΔiscA*, the *ΔerpA* single mutant strain, and the *ΔiscA/ΔerpA* and *ΔnfuA*/*ΔiscA* double mutant strains as compared to the Wt MG1655 strain. Furthermore, *sufA* was also not detectable in the *Δfnr* strain. Conclusively, no enhanced expression of *sufA* was observed under nitrate respiratory conditions.

3.1.16 Detection of *narG* transcripts under anaerobic nitrate respiratory conditions

qRT-PCR analysis was performed to analyze the transcript level of *narG* in the Wt MG1655, the *ΔerpA*, *ΔiscA*, and Δ*fnr* single mutant strains, and in the *ΔnfuA/ΔiscA*, *ΔerpA/ΔiscA*, *ΔsufA/ΔiscA*, and *ΔsufA/ΔerpA* double mutant strains. This experiment was conducted to understand nitrate reductase expression in the mutant strains since *erpA*-deleted strains were shown to be devoid of nitrate reductase activity. The strains were cultivated for 8 h at 37°C with 15 mM potassium nitrate and 1 mM mevalonate.

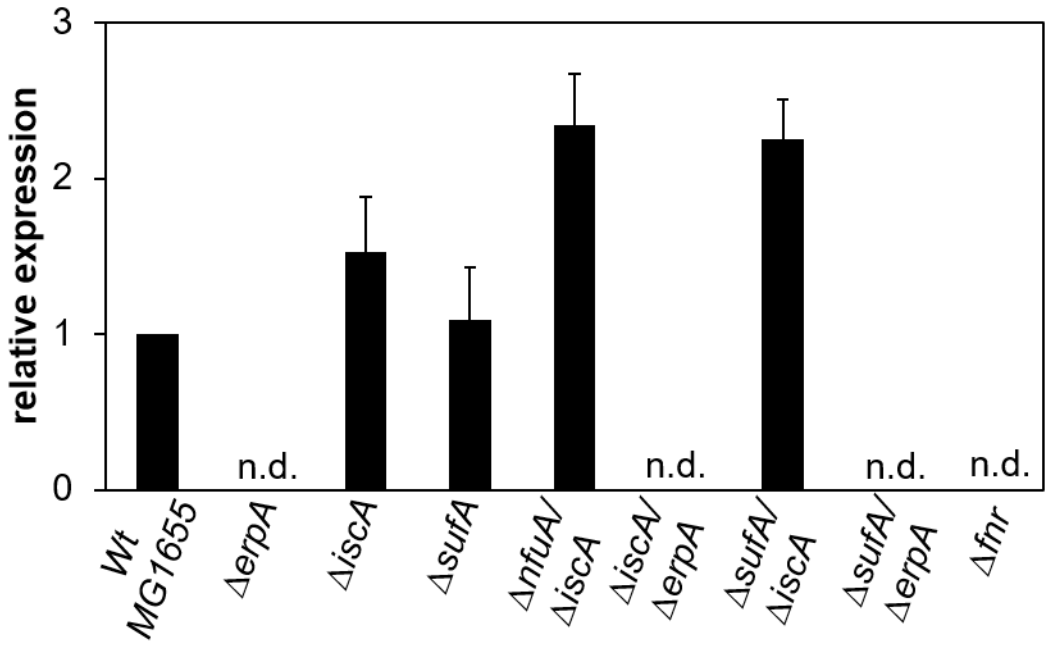

Figure 3-16: Analysis of relative expression levels of *narG* in *E. coli* mutant strains

Relative expression was carried out using qRT-PCR; the expression levels of *narG* in Wt MG1655*,* Δ*erpA,* Δ*iscA,* Δ*sufA,* Δ*nfuA/*Δ*iscA,* Δ*iscA/*Δ*erpA,* Δ*iscA/*Δ*sufA,* Δ*sufA/*Δ*erpA* and Δ*fnr* strains. The strains were grown in the presence of 15 mM potassium nitrate and 1 mM mevalonate; Y-axis denotes the relative expression value in the log of fold changes to Wt MG1655, standard deviations were calculated from three biological replicates; n.d.: not detectable

Figure 3-16 shows that the transcript level of *narG* increased almost ~1.2- and 2.2-fold in the *ΔiscA* and in the *ΔnfuA/ΔiscA*, *ΔiscA/ΔsufA* mutant strains, respectively. In contrast, no *narG* transcripts were detected in the *ΔerpA*, *ΔiscA/ΔerpA*, *ΔerpA/ΔsufA*, and *Δfnr* mutant strains.

3.2 Fe-S cluster insertion into FNR

3.2.1 Insertion of Fe-S clusters into FNR under anaerobic nitrate respiratory conditions

From the previous results, it can be assumed that FNR maturation is performed by the A-type carrier proteins like ErpA or IscA by inserting Fe-S clusters into it. This experiment was performed to investigate the activity of FNR in the different strains, including the Wt MG1655 strain, the *ΔerpA*, *ΔiscA*, Δ*nufA*, *ΔsufA*, and *Δfnr* single mutant strains, in addition to the double mutant strains *ΔerpA/ΔiscA*, *ΔsufA/ΔiscA*, and *ΔsufA/ΔerpA.* In this experiment, the analysis of the expression of a *PpepT-lacZ* fusion was performed since

pepT expression is solely dependent on FNR (Constantinidou et al., 2006; Myers, Yan, Ong, Chung, Liang, Tran, Keleş, et al., 2013), without the involvement of other transcriptional regulators (Dahl et al., 2013). The *pepT* gene codes for peptidase T, a tripeptidase that cleaves the amino-terminal leucine, lysine, methionine, or phenylalanine residue from certain tripeptides (Sussman and Gilvarg, 1970; Simmonds, Szeto, and Fletterick, 1976; Hermsdorf, 1978). The strains were cultivated for 8 h at 37°C in the presence of 15 mM potassium nitrate and 1 mM mevalonate.

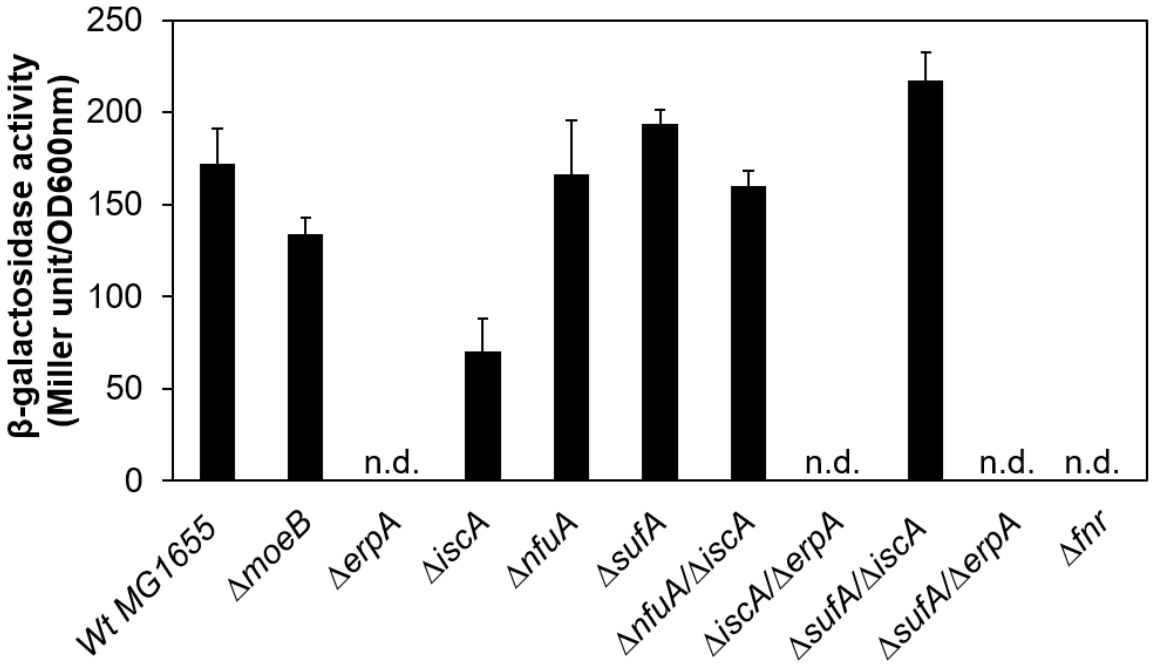

Figure 3-17: Expression of a *PpepT-lacZ* fusion in *E. coli* mutant strains

β-galactosidase activities in Miller units were determined for the *PpepT-lacZ* fusion in Wt MG1655, *ΔmoeB, ΔerpA, ΔiscA,* Δ*nufA, ΔsufA, ΔnfuA/ΔiscA, ΔerpA/ΔiscA, ΔsufA/ΔiscA, ΔsufA/ΔerpA,* and *Δfnr* strains. The strains were grown anaerobically in the presence of 15 mM potassium nitrate and 1 mM mevalonate for 8 h; *β*-galactosidase activities were normalized to OD_{600} nm; standard deviations were calculated from three biological replicates; n.d.: not detectable

Figure 3-17 shows no β-galactosidase activity was detected either for *erpA*-deleted strains such as the *ΔerpA* single mutant, or for the *ΔiscA/ΔerpA* and *ΔsufA/ΔerpA* double mutant strains as compared to the Wt MG1655 strain. Moreover, β-galactosidase activity was not detectable in the *Δfnr* strain, confirming that FNR activates the expression of *pepT*. Furthermore, β-galactosidase activity was reduced to almost ~60% in the *ΔiscA* mutant strain compared to the Wt MG1655 strain. The other single and double mutant strains,

including *ΔnfuA/ΔiscA* and *Δsuf/ΔiscA*, showed unaltered β-galactosidase activity compared to the Wt MG1655 strain.

3.2.2 Analysis of FNR expression under anaerobic nitrate respiratory conditions

This experiment was conducted to analyze the *fnr* expression level in different mutant strains. To exclude the lack of expression of the *PpepT-lacZ* fusion based on undetectable β-galactosidase activity in the *ΔerpA* mutant strains, this additional investigation was performed to quantify the expression of a *Pfnr-lacZ* fusion in Wt MG1655, as well as in the *Δfnr*, *ΔerpA*, *ΔiscA*, *ΔnufA*, and *ΔsufA* single mutant strains. The expression of *fnr* has been described previously as being repressed by a [4Fe-4S] cluster containing FNR. Cultivation was carried out under anaerobic conditions with 15 mM potassium nitrate supplemented with 1 mM mevalonate for 8 h at 37°C.

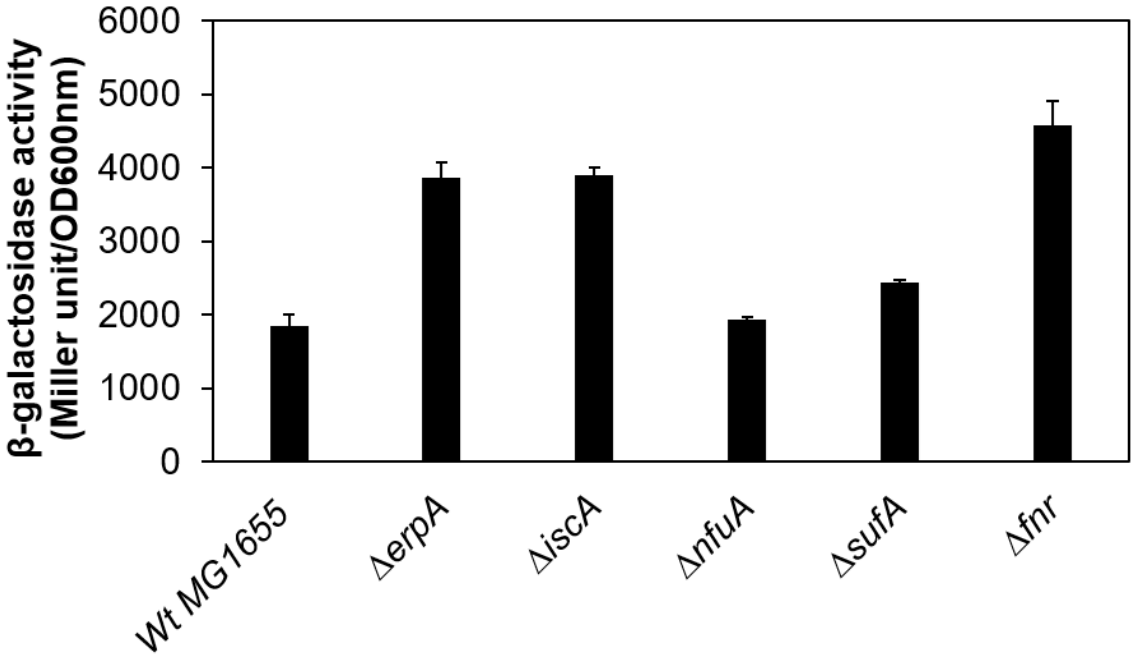

Figure 3-18: Expression of a *Pfnr-lacZ* fusion in *E. coli* mutant strains

β-galactosidase activities in Miller units were determined for the *Pfnr-lacZ* fusion in Wt MG1655*, ΔerpA, ΔiscA,* Δ*nufA, ΔsufA,* and *Δfnr* strains. The strains were grown anaerobically in the presence of 15 mM potassium nitrate and 1 mM mevalonate for 8 h; *β*-galactosidase activities were normalized to OD_{600} nm; standard deviations were calculated from three biological replicates

Figure 3-18 shows that β-galactosidase activity was increased to comparable levels in the *Δfnr*, *ΔerpA*, and *ΔiscA* mutant strains, while activity in the *ΔnufA* and *ΔsufA* single mutant strains was similar to that in the Wt MG1655 strain. This result indicates that in the *ΔerpA* and *ΔiscA* mutant strains, *fnr* was expressed but likely inactive based on a lack of Fe-S clusters in these strains. The increased expression level was also observed in the *Δfnr* strain since apo-FNR cannot bind to the promoter region of FNR to repress its expression (Mettert & Kiley, 2007).

3.2.3 Analysis of *PpepT-lacZ* expression after complementation with *erpA, sufA,* and *iscA* plasmid under anaerobic respiratory conditions

The experiment was performed to analyze the Fe-S cluster insertion into the FNR regulator using *erpA*, *iscA*, and *sufA* plasmids coexpressed with *PpepT-lacZ* in Wt MG1655 and in the *ΔerpA*, *ΔiscA*, and *ΔiscA/ΔerpA* strains. This study helps to understand the functional replacement of Fe-S cluster carrier proteins in FNR maturation. The cloning was performed for overexpressing the *iscA*, *sufA*, and *erpA* gene, where the NdeI/XhoI enzymes digested the PCR product of *iscA*, BamHI/XhoI, for *sufA*, and *erpA*. Further, the digested PCR product was ligated into the *pcdf-duet1* vector to construct *piscA*, *psufA*, and *perpA* plasmids. The *perpA*, *piscA*, and *psufA* overexpressing plasmids were transformed into *PpepT-lacZ* containing Wt MG1655, *ΔiscA*, *ΔerpA*, and *ΔiscA/ΔerpA* strains, and were further cultivated anaerobically with 15 mM potassium nitrate, 0.2% L-arabinose for 8 h at 37°C. The complementation effect was analyzed by measuring the β-galactosidase activity.

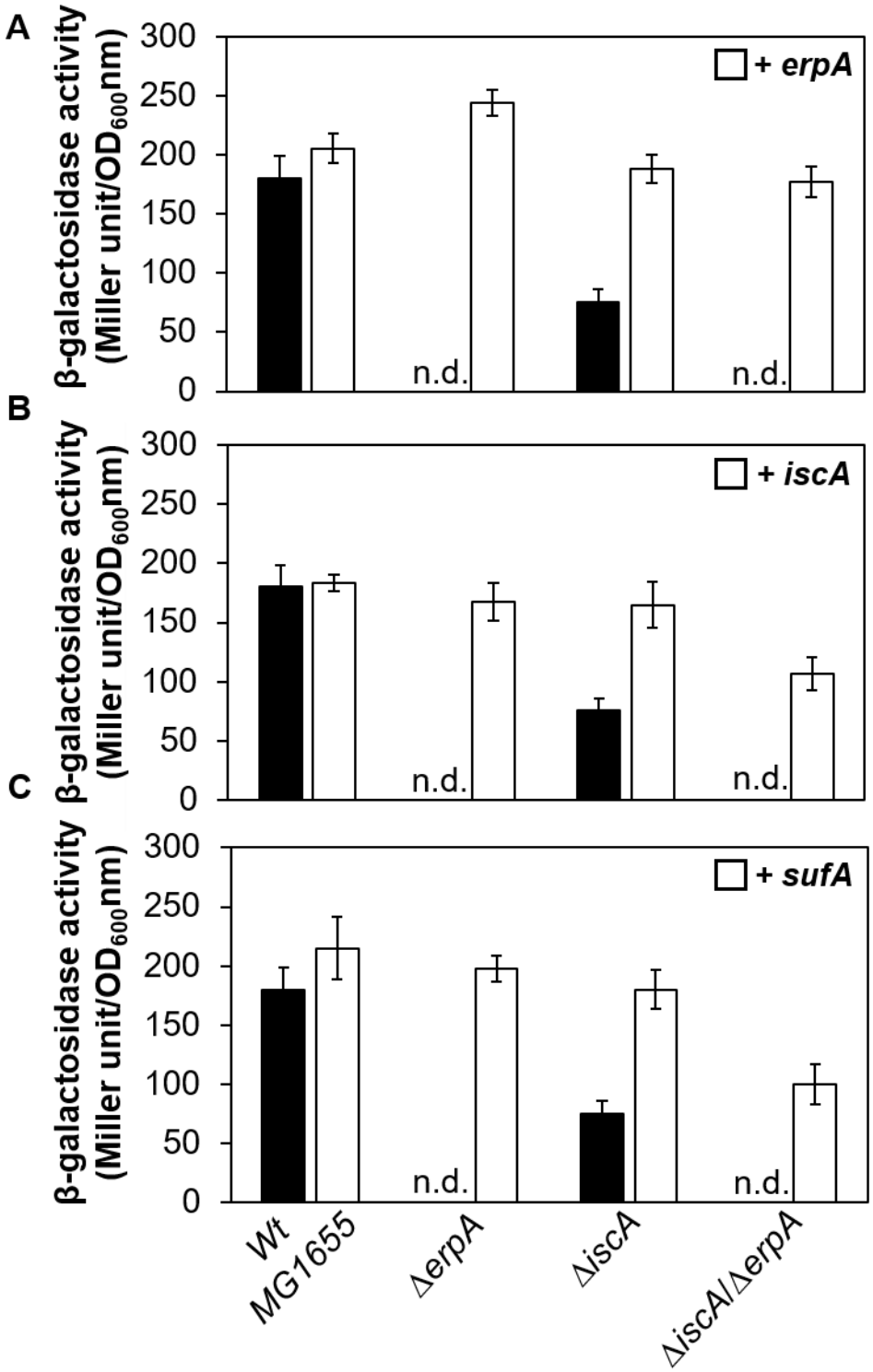

Figure 3-19: Expression of a *PpepT-lacZ* fusion in *E. coli* mutant strains with coexpression of plasmids containing *erpA, iscA,* and *sufA.*

β-galactosidase activities in Miller units were determined for the *PpepT-lacZ* fusion in Wt MG1655*, ΔerpA, ΔiscA,* and Δ*iscA/ΔerpA* strains. The strains were grown anaerobically in 15 mM potassium nitrate, 0.2% L-arabinose, and 1 mM mevalonate for 8 h; *β*-galactosidase activities were normalized to OD_{600} nm; standard deviations were calculated from three biological replicates. Black bars correspond to the indicated mutant strains; white bars

correspond to the same mutant strains containing either a plasmid expressing *erpA* (A), *iscA* (B), or *sufA* (C); n.d.: not detectable

Figure 3-19 show that β-galactosidase activity was restored after the expression of *perpA*, *piscA*, and *psufA* in all the mutant strains compared to the Wt MG1655 strain. This indicates that sufficient production of IscA and SufA could replace the function of ErpA for the insertion of Fe-S clusters into FNR. β-galactosidase activity slightly increased after overexpression of *erpA* in the *ΔerpA* strain compared to in the Wt MG1655 strain. In contrast, the expression of *iscA* and *sufA* was able to restore activity in all the mutant strains, except for the *ΔiscA/ΔerpA* double mutant strain, where β-galactosidase activity was slightly reduced as compared to the Wt MG1655 strain. Moreover, the plasmid-encoded copies of *erpA* showed increased β-galactosidase activity in the *ΔiscA/ΔerpA* double mutant strain compared to the expression of *sufA* and *iscA*. This result indicates the preference for ErpA as an Fe-S cluster carrier protein in FNR maturation since deletion of *erpA* leads to inactivation of FNR, and *iscA* or *sufA* is not able to compensate for this role under nitrate respiratory conditions at the cellular level. However, the plasmid-encoded copies of *iscA* and *sufA* were able to replace the function of ErpA in FNR maturation.

3.3 Analysis of TMAO reductase expression and activities

TMAO reductase functions as a terminal electron acceptor like nitrate reductase during anaerobic respiration in the presence of TMAO (Cox et al., 1980; Cox & Knight, 1981). It belongs to only a few DMSO reductase family members of molybdoenzyme that do not contain any Fe-S cluster (McCrindle, Kappler, and McEwan, 2005). It has been reported that the TMAO reductase enzyme escapes FNR regulation. Therefore, we have selected the TMAO reductase enzyme as a control in this study along with nitrate reductase to avoid Fe-S cluster-related regulations.

3.3.1 Growth curves of the strains under anaerobic TMAO respiratory conditions

The growth curve was measured for all strains to evaluate their growth in the presence of TMAO since deletion of essential genes leads to growth defects for the strains. The strains were cultivated anaerobically with 15 mM TMAO and 1 mM mevalonate at 37°C. The samples were taken every hour for measuring the optical density at 600 nm for 12 h.

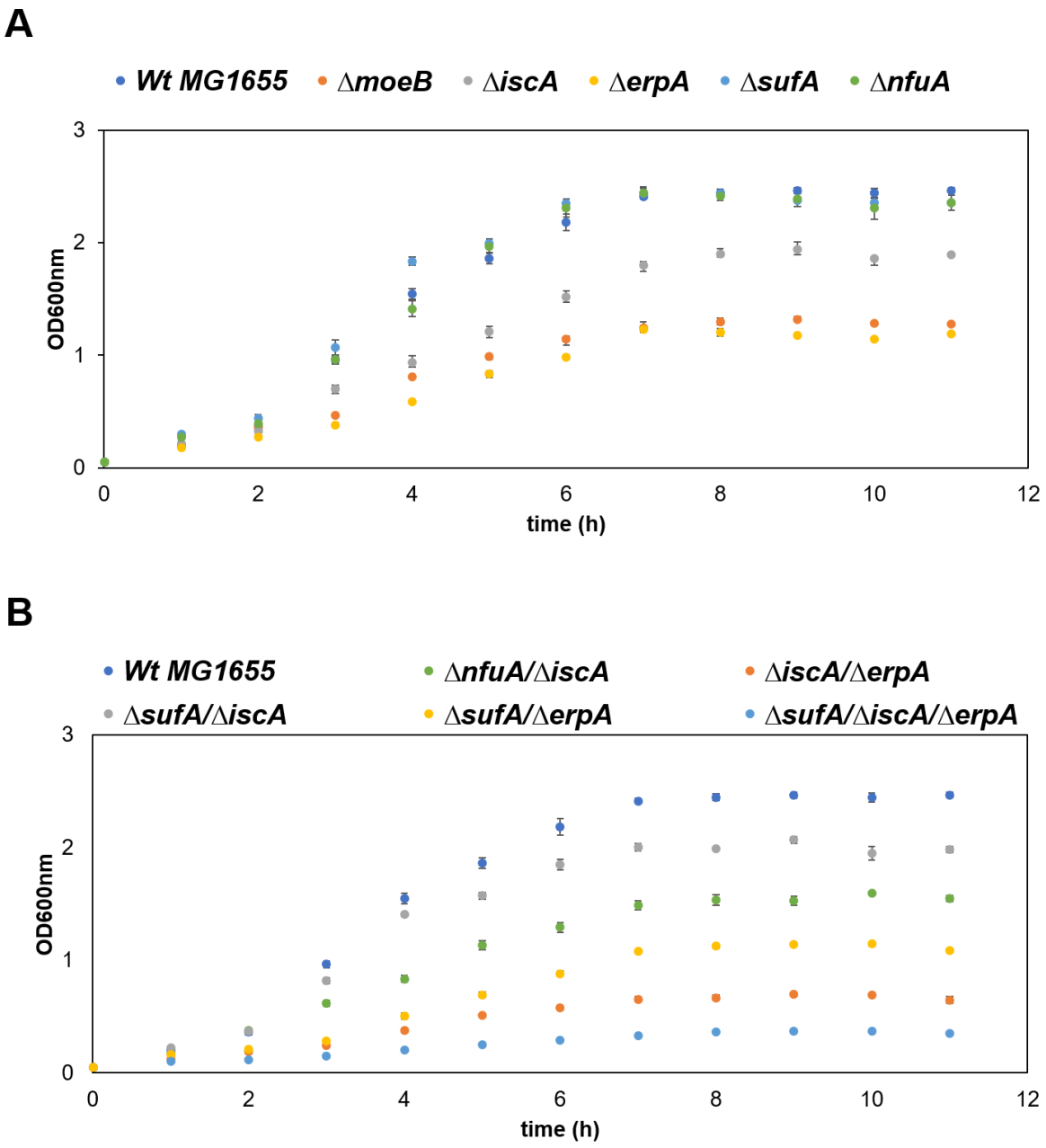

Figure 3-20: Analysis of the growth curves of *E. coli* mutant strains

The growth curves were measured for Wt MG1655, Δ*moeB,* Δ*erpA,* Δ*iscA,* Δ*sufA,* Δ*nfuA* (A), Wt MG1655, Δ*nfuA*/Δ*iscA,* Δ*iscA*/Δ*erpA,* Δ*iscA*/Δ*sufA,* Δ*sufA*/Δ*erpA* and Δ*iscA*/Δ*sufA*/Δ*erpA* (B) mutant strains; the cells were grown in 50 mL LB medium supplemented with 15 mM TMAO and 1 mM mevalonate. The start OD_{600} nm was 0.05 and recorded for 12 h. Standard deviations were calculated from three biological replicates.

Figure 3-20 shows that under TMAO respiration, cell growth was significantly reduced for the *ΔmoeB*, *ΔerpA*, *ΔiscA/ΔerpA*, *ΔsufA/ΔerpA*, and *ΔsufA/ΔiscA/ΔerpA* strains, which was quite comparable under nitrate respiratory conditions. All the strains reached the stationary phase at 8 h. Therefore, cells were harvested at the late exponential phase at

8 h for this study to measure Moco content, TMAO reductase, and β-galactosidase activity.

3.3.2 Quantification of cPMP and Moco under anaerobic TMAO respiratory conditions

In this experiment, the Moco- and cPMP-producing ability of the single mutant strains *ΔmoeB* (as a negative control), *ΔerpA, ΔiscA*, Δ*nufA*, and *ΔsufA*, the double mutant strains *ΔerpA/ΔiscA*, *ΔsufA/ΔiscA*, and *ΔsufA/ΔerpA*, as well as the triple mutant strain *ΔsufA/ΔiscA/ΔerpA* and the Wt MG1655 strain, was determined in the presence of TMAO. This experiment confirmed the Moco content of the mutant strains grown in the presence of potassium nitrate since both nitrate reductase and TMAO reductase contain bis-MGD as a cofactor. The strains were cultivated under the anaerobic condition for 8 h with 15 mM TMAO and 1 mM mevalonate. The cPMP and Moco were quantified from the crude extract in the form of fluorescence derivatives as Compound Z and FormA, respectively, which were derived by oxidation using KI and I_2.

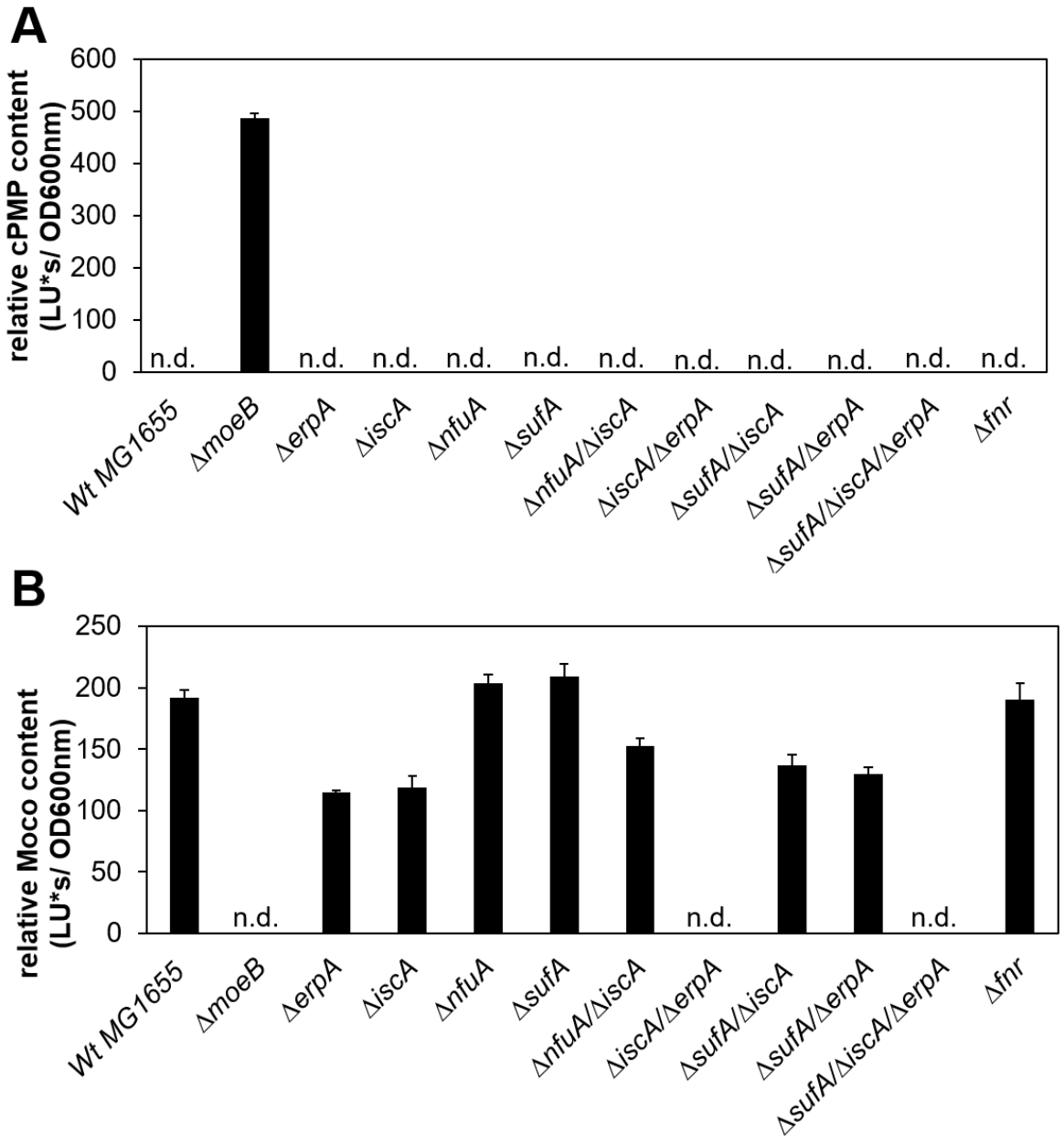

Figure 3-21: Analysis of relative cPMP and Moco content in *E. coli* mutant strains

Relative cPMP (A) and Moco content (B) were determined in Wt MG1655, *ΔmoeB, ΔerpA, ΔiscA, ΔnfuA, ΔsufA, ΔnfuA/ΔiscA, ΔiscA/ΔerpA, ΔiscA/ΔsufA, ΔsufA/ΔerpA, ΔsufA/ΔiscA/ΔerpA,* and *Δfnr* strain. The strains were grown in the presence of 15 mM TMAO, and 1 mM mevalonate under anaerobic conditions; the Compound Z (cPMP) and FormA (Moco) were monitored by fluorescence of extinction at 383 nm and an emission at 450 nm using HPLC; the relative amounts of cPMP and Moco were normalized to the OD_{600} nm. Standard deviations were calculated from three biological replicates, n.d.: not detectable

A similar result (Figure 3-21) was obtained under TMAO respiration, where cPMP was only accumulated in the *ΔmoeB* strain, identical to nitrate respiration. This was expected since deletion of *moeB* leads to an inhibition in the production of MPT from cPMP.

Under conditions of TMAO respiration, all mutant strains containing deletions of either *iscA* or *erpA* also showed a reduced Moco content similar to that for nitrate respiration. Particularly, in the *ΔerpA* and *ΔiscA* single mutant strains, the Moco content was ~40% reduced. No Moco was detected in the *ΔerpA/ΔiscA* double mutant or the *ΔsufA/ΔiscA/ΔerpA* triple mutant strains. The Moco content for the other single mutant strains *ΔsufA* and *ΔnfuA* was quite similar to that of the Wt MG1655 strain. Moreover, the Moco content in *ΔnfuA/ΔiscA* and *ΔsufA/ΔiscA*, as well as in the *ΔsufA/ΔerpA* double mutant strain, was reduced almost ~20% and ~30%, respectively, in comparison to the Wt MG1655 strain. The Moco content in the *Δfnr* strain was almost identical to that in the Wt MG1655 strain, indicating that the absence of FNR does not influence Moco production under the anaerobic condition of TMAO respiration.

3.3.3 TMAOR activity under anaerobic conditions of TMAO respiration

TMAO reductase contains only a molybdenum cofactor as a form of bis-MGD but no Fe-S clusters. TMAOR activity was measured to quantify the Moco content of all the mutant strains in the presence of TMAO. The strains were cultivated under anaerobic conditions with 15 mM TMAO for 8 h at 37°C supplemented with 1 mM mevalonate. Activity was measured from the crude cell extract inside the anaerobic chamber.

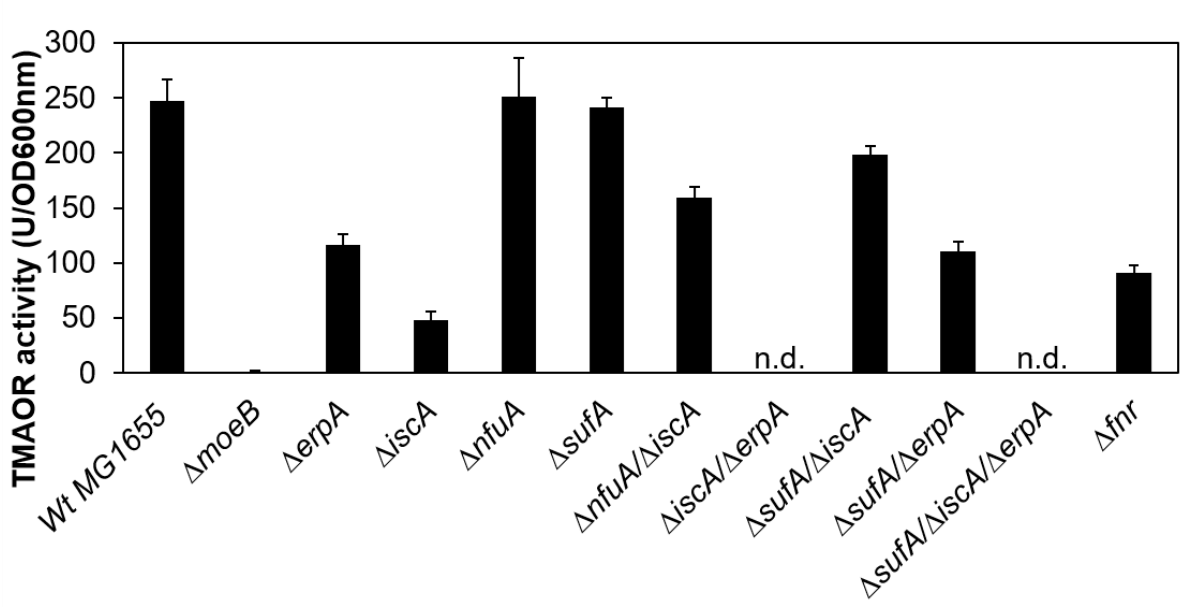

Figure 3-22: Analysis of TMAOR activity in *E. coli* mutant strains

TMAOR activity was determined in Wt MG1655, *ΔmoeB, ΔerpA, ΔiscA, ΔnfuA, ΔsufA, ΔnfuA/ΔiscA, ΔiscA/ΔerpA, ΔiscA/ ΔsufA, ΔsufA/ΔerpA, ΔsufA/ΔiscA/ΔerpA,* and *Δfnr* strains.

The strains were grown in the presence of 15 mM TMAO and 1 mM mevalonate under anaerobic conditions; TMAO reductase activities were normalized to OD_{600} nm; Standard deviations were calculated from three biological replicates, n.d.: not detectable

Figure 3-22 shows a comparable TMAOR activity that matches the cellular Moco content under TMAO respiration. TMAO reductase activity was reduced ~54% and ~80% in the *ΔerpA* and *ΔiscA* mutant strains respectively and almost undetectable in the *ΔerpA/ΔiscA* double mutant and the *ΔsufA/ΔiscA/ΔerpA* triple mutant strains. Moreover, TMAO reductase activity for the *ΔnfuA/ΔiscA* and *ΔsufA/ΔiscA* double mutant strains shows relatively similar results to the nitrate reductase activity, in which a comparatively higher level of activity was observed for those double mutant strains as compared to in the *ΔiscA* single mutant strain. Overall, the findings were identical to the results obtained for the cellular Moco content in these strains. However, TMAOR activity in the *Δfnr s*train was reduced ~65% compared to the activity in the Wt MG1655 strain. This indicates that FNR is important for the active TMAO reductase. However, it has been reported that TMAOR enzyme expression is not dependent on FNR (Pascal, Burini, and Chippaux, 1984; Iuchi and Lin, 1988; Spiro and Guest, 1990).

3.3.4 Expression of *torCAD* under anaerobic TMAO respiratory conditions

The expression of *torCAD* was determined in the Wt MG1655, the *ΔerpA*, *ΔiscA*, *ΔnfuA*, *ΔsufA*, and Δ*fnr* single mutant strains in addition to the double mutant strains *ΔnfuA/ΔiscA*, *ΔerpA/ΔiscA*, *ΔsufA/ΔiscA*, and *ΔsufA/ΔerpA* by using the *PtorCAD-lacZ* plasmid. This experiment was conducted to understand the regulation of *torCAD* transcription in *fnr*-, *erpA*-, and *iscA*-deleted strains since TMAOR activity was reduced in these strains. The cells were cultivated under the anaerobic condition with 15 mM TMAO and 1 mM mevalonate for 8 h at 37°C.

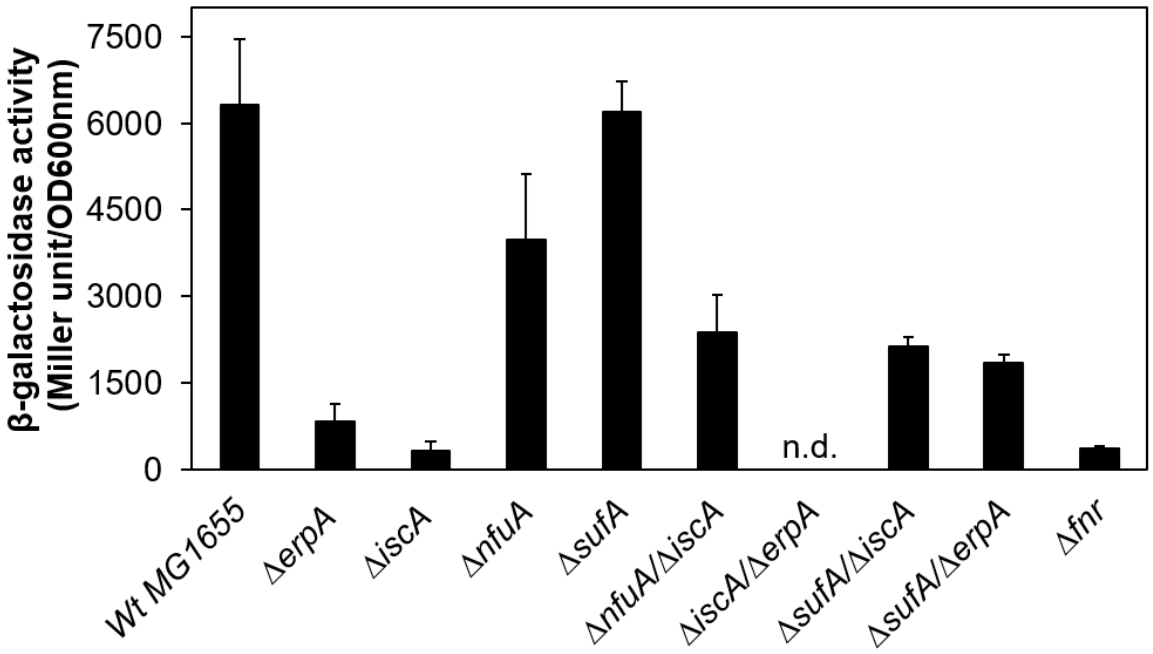

Figure 3-23: Expression of a *PtorCAD-lacZ* fusion in *E. coli* mutant strains

β-galactosidase activities in Miller units were determined for the *PtorCAD-lacZ* fusion in Wt MG1655*, ΔiscA, ΔerpA, ΔnfuA, ΔsufA, ΔnfuA/ΔiscA, ΔiscA/ΔerpA, ΔiscA/ ΔsufA, ΔsufA/ΔerpA,* and *Δfnr* strains. The strains were grown anaerobically in the presence of 15 mM TMAO and 1 mM mevalonate for 8 h; *β*-galactosidase activities were normalized to OD_{600} nm; standard deviations were calculated from three biological replicates, n.d.: not detectable

Figure 3-23 shows that β-galactosidase activity was significantly reduced in the *erpA*- and *iscA*-deleted strains compared to in the Wt MG1655 strain, which might be due to lack of Moco content in the *ΔerpA* and *ΔiscA* strains. The expression was also remarkably decreased in *fnr*-deleted strains. The reduced expression in the *erpA*- and *iscA*-deleted strains could be due to an indirect regulation in FNR maturation since ErpA and IscA proteins insert the Fe-S cluster into FNR. Moreover, expression of *torCAD* was not observed in the *ΔiscA/ΔerpA* double mutant. However, a relatively higher β-galactosidase activity was observed in the *ΔsufA/ΔiscA* and *ΔsufA/ΔerpA* double mutant strains as compared to in the *ΔiscA* or *ΔerpA* single mutant strains. Furthermore, the *ΔnfuA* strain expression was reduced around ~25% compared to in the Wt MG1655 strain. No significant change in β-galactosidase activity was observed in the *ΔsufA* strain compared to in the Wt MG1655 strain.

3.3.5 Immunodetection of TorA

Immunodetection of TorA using an antiserum was carried out to quantify cellular TorA levels. This experiment was performed to determine the production level of TMAO reductase in different mutant strains.

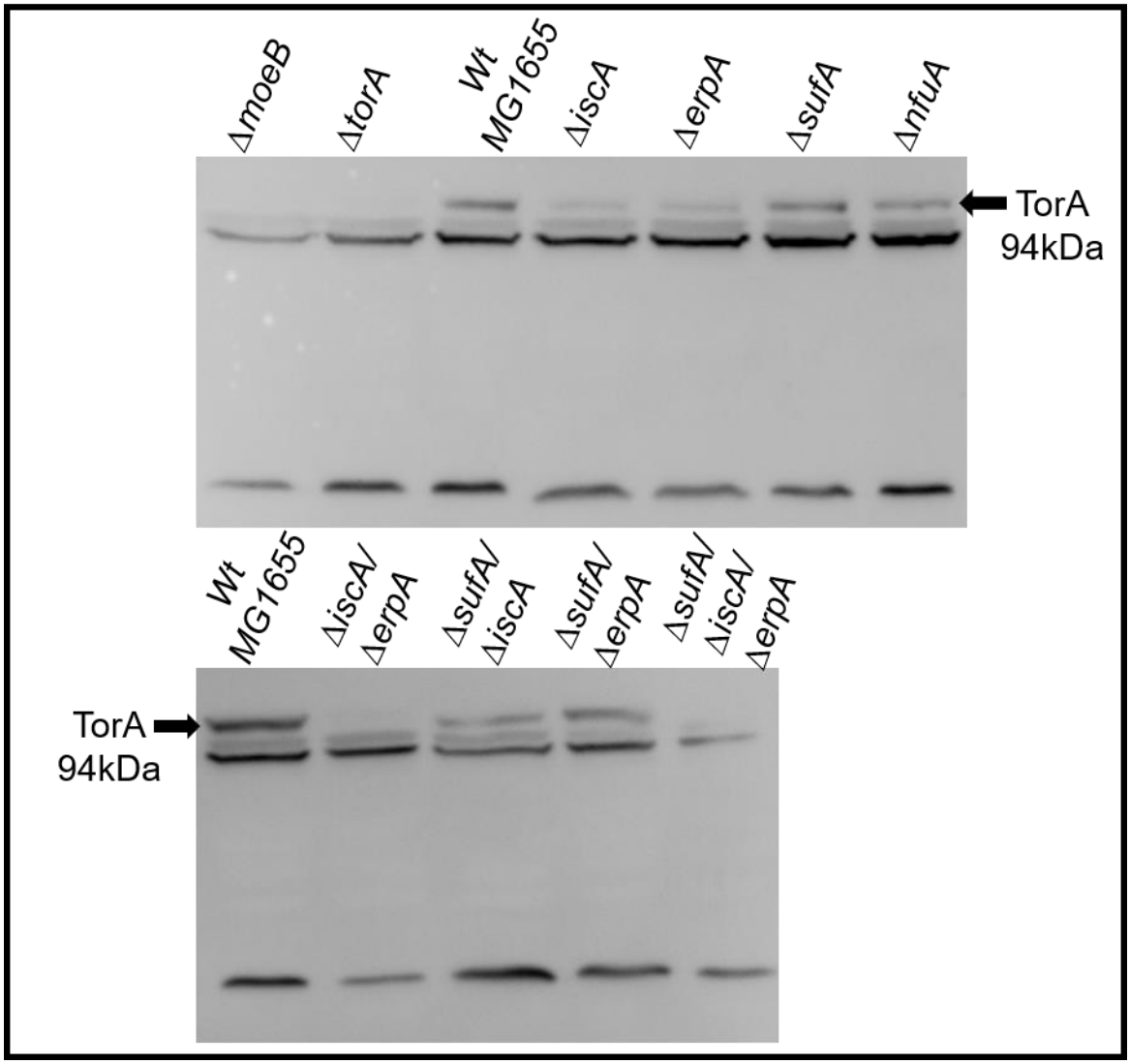

Figure 3-24: Immunodetection of TorA in *E. coli* mutant strains.

50 µg of total protein fractions of the cell extract of Wt MG1655, *ΔmoeB, ΔiscA, ΔerpA, ΔnfuA, ΔsufA, ΔiscA/ΔerpA, ΔiscA/ΔsufA, ΔsufA/ΔerpA, ΔsufA/ΔiscA/ΔerpA* strains were separated by 12% SDS-PAGE and transferred onto a PVDF membrane. A TorA specific antiserum (1:500 dilution) was used and visualized by enhanced chemiluminescence; the *ΔtorA* cell extract served as a negative control; the strains were grown anaerobically in the presence of 15 mM TMAO, and 1 mM mevalonate for 8 h.

The western-blot analysis result (Figure 3-24) shows that the TorA level was remarkably reduced in the deleted strains containing *erpA* and *iscA*, in which the *ΔerpA* and *ΔiscA* single mutant strains showed about ~80% reduction in comparison to the Wt MG1655 strain. Moreover, the TorA amounts in the *ΔsufA/iscA* and *ΔsufA/erpA* double mutant strains were slightly increased as compared to the *ΔerpA* single mutant strain, while no TorA was detected in the *ΔiscA/erpA* double mutant and the *ΔsufA/ΔiscA/ΔerpA* triple mutant strains. In the *ΔsufA* and *ΔnfuA* mutant strains, the levels of TorA remained almost constant compared to in the Wt MG1655 strain.

One possibility is that torCAD expression is regulated by FNR since the expression of the *torCAD* transcript was reduced in the absence of FNR. Therefore, we determined a potential FNR binding site in the *torCAD* promoter region to prove that FNR binds to this site (Figure 3-25). The FNR consensus sequence was mutated with single point mutations and the expression of *torCAD-lacZ* fusion was determined. All the mutated plasmids (mut.1, mut.2, mut.3, mut.4) and the control plasmid (*torCAD-lacZ*) were transformed into the Wt MG1655 and *Δfnr* strains. The cells were cultivated with 15 mM TMAO for 8 h at 37°C.

Figure 3-25: Analysis of predicted FNR binding site at upstream of the *torCAD* operon

FNR binding site in *torCAD* promoter region; (A) the predicting FNR biding site (red) and TorR (blue); the transcriptional starting site atg (green); (B) the point mutation in FNR binding site, the oligonucleotides substitution was performed by mutagenesis to loss of the FNR binding; the TT>>GG substitution for mut.1; the GCT>>AAA substitution for mut.2, the GCT>>GAT substitution for mut.3, the TTGCT>>GGAAA substitution for mut.4 of the consensus sequence

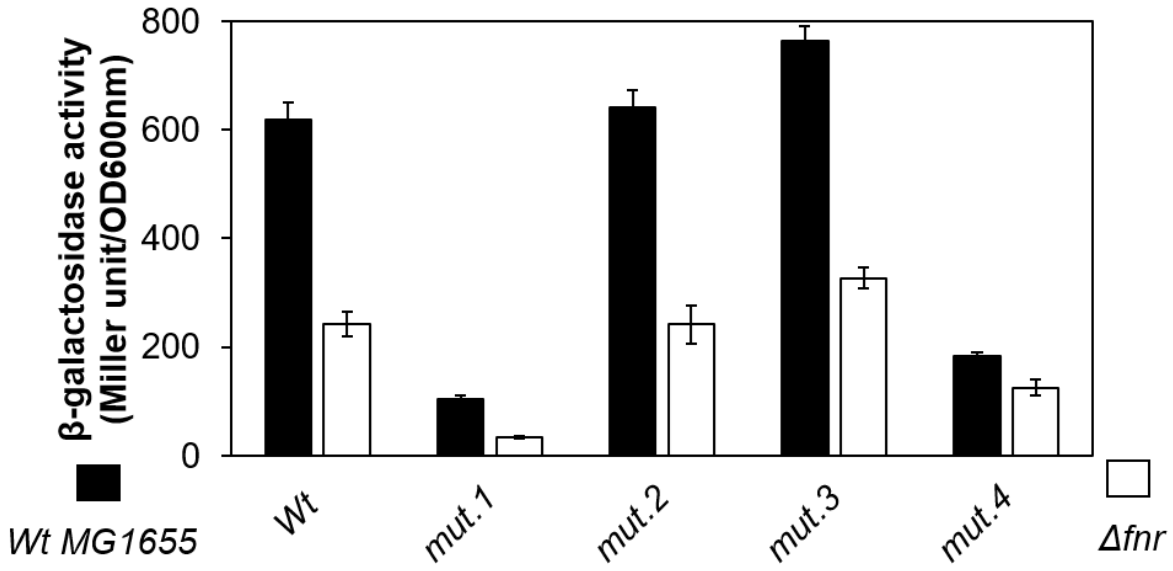

Figure 3-26: Expression of a *PtorCAD-lacZ* fusion in *E. coli* mutant strains

β-galactosidase activities in Miller units were determined for the *PtorCAD-lacZ* fusion in Wt MG1655 (black bars) and *Δfnr (*white bars) strains. The FNR concensor sequence was TTGCT, the mutation of the consensus sequence was denoted as mut.1 (GGGCT), mut.2 (TTAAA), mut.3 (TTGAT), and mut.4 (GGAAA). The strains were grown anaerobically with 15 mM TMAO and 1 mM mevalonate for 8 h; *β*-galactosidase activities were normalized to OD_{600} nm; standard deviations were calculated from three biological replicates.

Figure 3-26 shows that β-galactosidase activity was decreased for Wt MG1655 in mut.1 and mut.4 compared to the Wt MG1655 *torCAD-lacZ*, indicating the importance of the TT sequence in the promoter region since mut.1 and mut.4 were exchanged from the TT to GG. On the other hand, β-galactosidase activity in mut.2 for Wt MG1655 was almost similar to that for Wt MG1655 *torCAD-lacZ*. Increased β-galactosidase activity was observed for the Wt MG1655 mut.3 compared to the Wt *torCAD-lacZ* strain since the mutation of C to A on the sequence leads to generation of the exact FNR consensus sequence (TTGAT). It also indicates that the A in TTGAT plays a role in FNR binding since β-galactosidase activity was slightly enhanced compared to the Wt MG1655 *torCAD-lacZ*. Moreover, activity for *torCAD-lacZ* in the *Δfnr* strain also decreased compared to Wt MG1655 *torCAD-lacZ*.

3.4 Expression and purification of periplasmic aldehyde oxidase (PaoABC) from different *E. coli* mutant strains

Periplasmic aldehyde oxidase (PaoABC) belongs to the xanthine oxidase (XO) family of molybdoenzymes, and contains MCD as a form of Moco, FAD, and two [2Fe-2S] clusters along with an additional [4Fe-4S] cluster. The goal of the experiment was to identify the Fe-S cluster carrier proteins that insert the different types of Fe-S cluster for the maturation of EcPaoABC. Therefore, we expressed *E. coli paoABCD* in the selected *E. coli* mutant strains in Wt MG1655, *ΔerpA*, *ΔiscA*, *ΔsufA*, and *ΔnfuA*, purified, and characterized the enzymes.

3.4.1 Expression of EcPaoABC in *E. coli* mutant strains

The expression of periplasmic aldehyde oxidase was performed using the plasmid *pMN100*, which was constructed in the *pTrcHis* vector, in which the *paoABCD* genes were cloned from *E. coli*, using NdeI-SalI restriction sites (Neumann et al., 2009). The expression was performed in Wt MG1655 and other single mutant strains *ΔerpA*, *ΔiscA*, *ΔsufA*, and Δ*nufA*. The expression of the protein leads to the formation of N-terminal 6x-His fusion to PaoA. The protein was purified by IMAC using Ni^{++}-nitrilotriacetic acid (NTA).

The strains were cultivated aerobically at 22°C for 24 h for the expression of *paoABCD*. The cells were harvested by centrifugation, and the cell pellets were resuspended in a phosphate buffer, pH 8.0. Cell lysis was performed in 2 cycles at 1.35 kBar pressure and the crude extract was isolated by centrifugation, which was used for the IMAC purification. Elution was carried out by using a phosphate buffer containing 250 mM imidazole. The eluted fractions were analyzed by 12% SDS-polyacrylamide gel electrophoresis. The eluted fractions after Ni^{++}-NTA affinity chromatography were further dialyzed overnight at 4°C into a Tris buffer, pH7.5.

3.4.2 Size exclusion chromatography (SEC)

Size exclusion chromatography was the last step of purification. This step was performed using a Superose-6 gel filtration column, and further, the eluted fractions were analyzed by 12% SDS-PAGE.

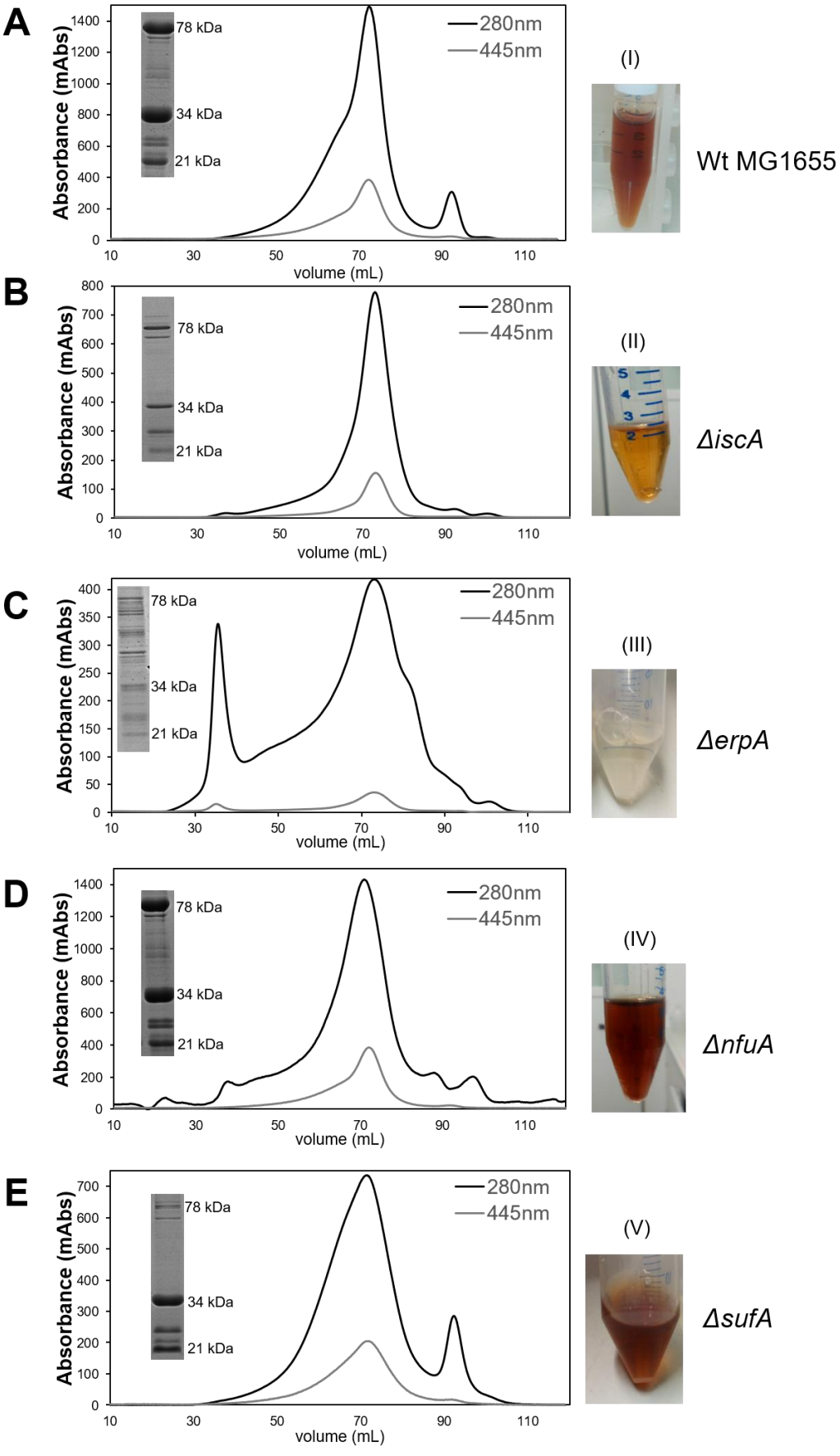
A
Absorbance (mAbs)
volume (mL)
78 kDa
34 kDa
21 kDa
280nm
445nm
(I)
Wt MG1655
B
(II)
ΔiscA
C
(III)
ΔerpA
D
(IV)
ΔnfuA
E
(V)
ΔsufA

Figure 3-27: Gel filtration chromatograms of the purified EcPaoABC expressed in different *E. coli* mutant strains

The elution profiles (absorbance at 280 nm and 445 nm) and analysis of the purity after the analytical gel filtration chromatography of EcPaoABC expressed in (A) Wt MG1655, (B) *ΔiscA,* (C) *ΔerpA,* (D) *ΔnfuA,* and (E) *ΔsufA* mutant strains; the elution of the protein was performed using 50 mM Tris, 1 mM EDTA and 200 mM NaCl, pH 7.5 by superose-6 gel filtration column on the Äkta system; the purity of EcPaoABC was analyzed using 12% SDS-PAGE gel; the eluted EcPaoABC that expressed in Wt MG1655 (I), *ΔiscA* (II)*, ΔnfuA* (III)*, ΔsufA* (IV) and *ΔerpA* (V)

Figure 3-27 shows that the elution profiles of expressed PaoABC in Wt MG1655, as well as in the *ΔiscA*, *ΔnfuA*, and *ΔsufA* mutant strains, show a prominent peak after 70 mL and another minor peak at around 90 mL (except for *ΔerpA*-expressed PaoABC). The presence of the subunits was also confirmed from the respective bands after separation by SDS-PAGE around 78 kDa, 34 kDa, and 21 kDa corresponding to PaoC, PaoB, and PaoA, respectively. Additional bands in the SDS-PAGE gel also indicate the presence of minor impurities. However, the *ΔsufA* mutant-strain-expressed PaoABC shows only a weak band at 78 kDa for PaoC.

While the elution profile of PaoABC from the *ΔerpA* strain shows two significant peaks at around 30-40 mL and 50-85 mL respectively, elution of trimeric PaoABC corresponded to the peak at 70 mL. The first peak, around 30-40 mL indicated aggregation of the protein.

3.4.3 Characterization of periplasmic aldehyde oxidase

3.4.3.1 UV-Vis spectroscopy

The typical UV-Vis spectra of periplasmic aldehyde oxidase show the characteristic features of other molybdoflavo-enzymes, where aromatic amino acids are absorbed at 280 nm, FAD at 445 nm, and the [2Fe-2S] cluster at 550 nm. The absorption spectra were recorded from 250 nm to 800 nm.

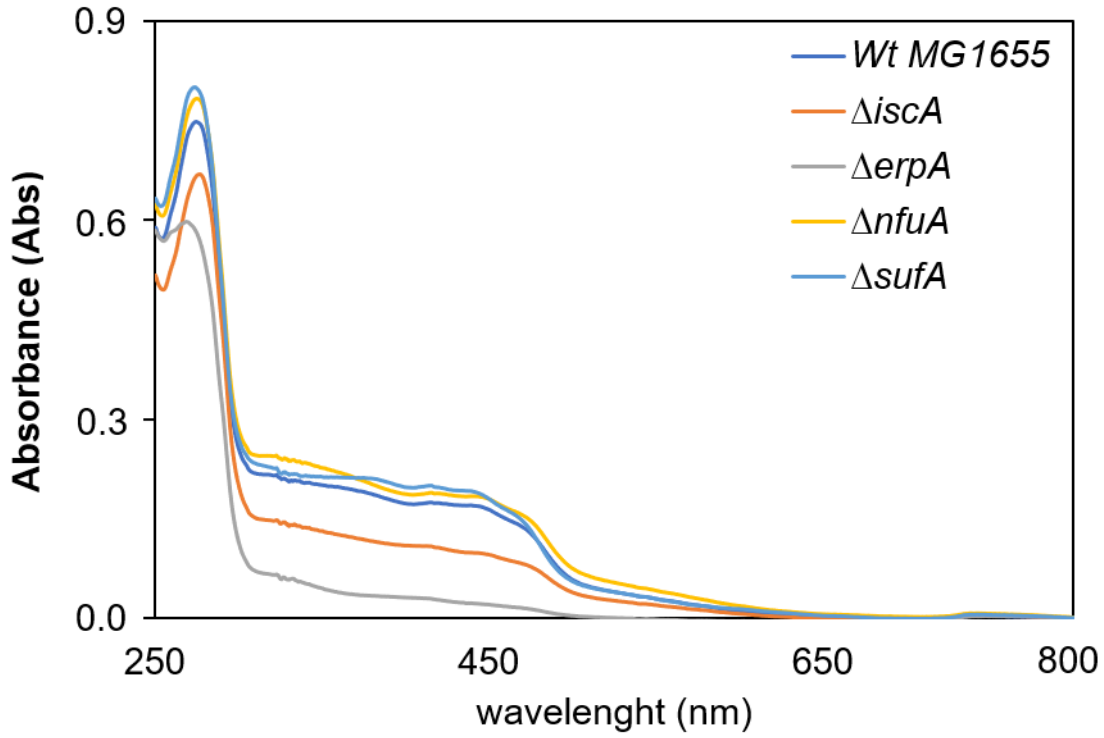

Figure 3-28: Analysis of UV-visible spectrum from purified EcPaoABC expressed in different *E. coli* mutant strains

The UV-visible spectrum (250 nm to 800 nm) for characterization of purified EcPaoABC that expressed in Wt MG1655, *ΔiscA, ΔerpA, ΔnfuA,* and *ΔsufA* strains; the concentration of purified EcPaoABC was 10 µM, and the spectrum was recorded at room temperature using 50 mM Tris, 1 mM EDTA, pH 7.5

Table 3-1: The absorbance ratio between 280 nm and 445 nm of purified EcPaoABC expressed in *E. coli* mutant strains

Strains	Ratio (280/445)
Wt MG1655	4.28
ΔiscA	6.66
ΔerpA	25.88
ΔnfuA	4.16
ΔsufA	4.10

Based on previous knowledge regarding closely related enzymes such as xanthine oxidase (XO), a way to determine the purity of the protein and with cofactors saturation are the absorbance ratios at A280/A445. The ratio between A280/A450 of 5.0 or less for the recombinant enzyme indicates a high purity. A ratio of A280/A450 higher than 5 indicates impurities in the sample (Alfaro et al., 2009; Hartmann et al., 2012). The spectra (Figure 3-28) of purified enzymes show that PaoABC expression in the Wt MG1655, *ΔnfuA*, and *ΔsufA* strains was quite similar because their respective FAD shoulders at 445 nm were well visible and comparable to each other, and where the ratio of A280/A445 was around 4.28, 4.16, and 4.10, respectively. This suggests that the quality of PaoABC that was expressed in the *ΔnfuA* and *ΔsufA* strains was identical to the quality in Wt MG1655. The paoABC in the *ΔiscA* and *ΔerpA* strains show a relatively weak FAD shoulder at 445 nm compared to the Wt MG1655 one, in which the ratio of A280/A445 was 6.66 and 25.88, respectively. This indicates that PaoABC in the *ΔerpA* strain had a significant lack of purity and high contamination along with a low FAD content in the enzyme in comparison to Wt MG1655. However, PaoABC in the *ΔiscA* strain showed a ratio of 6.66 (A280/A445), indicating that it was significantly less contaminated as compared to the PaoABC in the *ΔerpA* strain, but relatively more impure than in Wt MG1655.

3.4.3.2 Metal content determination by ICP-OES

The metal content of the purified PaoABC was quantified using inductively coupled plasma optical emission spectrometry (ICP-OES). The experiment was conducted to estimate the iron and molybdenum content reflecting both Moco and Fe-S clusters in the enzyme. The measurement was conducted using a reference standard (Solution XVI, Merck) for the exact quantification of both elements. The concentration used of PaoABC for ICP-OES analysis was around 10 µM. The concentration of the elements was calculated to a percentage scale of saturation values of cofactors, considering 1 molybdenum and 8 iron atoms (in the two [2Fe-2S] clusters and the single [4Fe-4S] cluster).

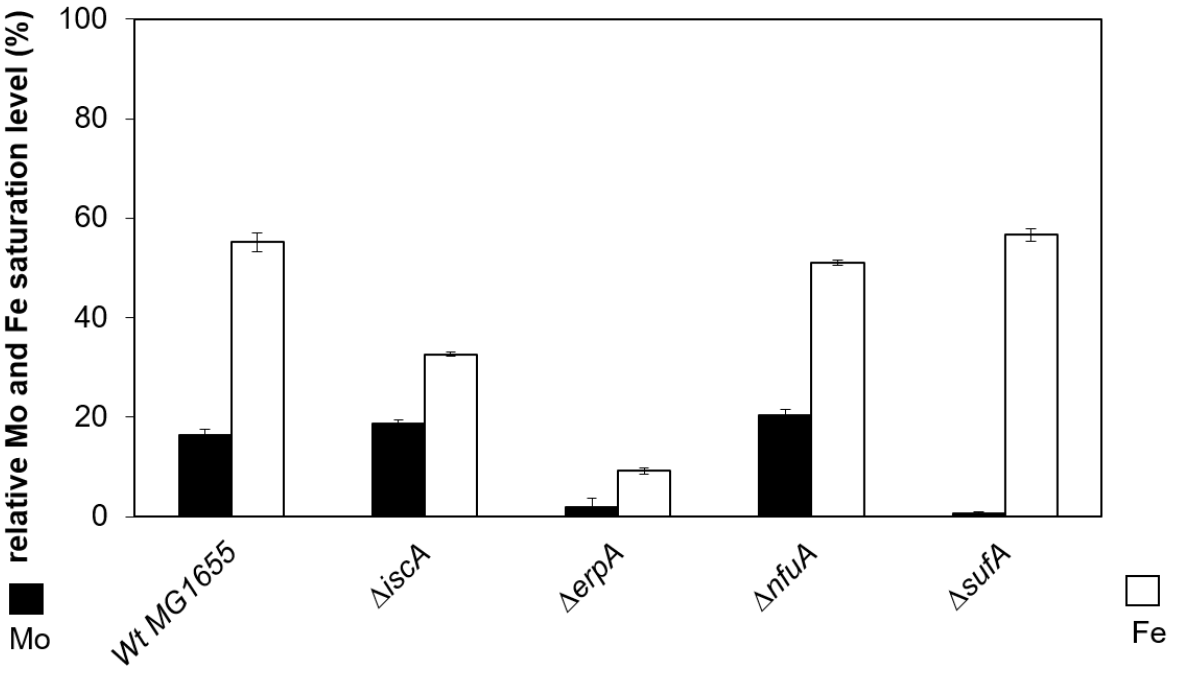

Figure 3-29: Analysis of relative molybdenum and iron saturation from EcPaoABC expressed in different *E. coli* mutant strains

The ICP-OES analysis for the determination of relative molybdenum (black bars) and iron (white bars) saturation of EcPaoABC that expressed in Wt MG1655, *ΔiscA, ΔerpA, ΔnfuA,* and *ΔsufA* strains; the concentration of purified EcPaoABC was 10 µM; the following wavelengths were used to analyze for iron: 238.204 nm, 238.562 nm, 259.939 nm and for molybdate: 203.84 nm, 202.031 nm, 204.597 nm. A baseline was measured using 50 mM Tris, 1 mM EDTA, pH 7.5; the iron and molybdenum concentrations were determined by using the Standard XVI (Merck); Standard deviations were calculated from three biological replicates

Figure 3-29 show that the molybdenum saturation of expressed PaoABC in the *ΔnfuA* and *ΔiscA* strains was quite similar compared to Wt MG1655, with a saturation of 18-20%. This low molybdenum saturation of the enzyme implies that the majority of the purified PaoABC was in a Moco-free form. However, the molybdenum saturation of expressed PaoABC was significantly reduced in the *ΔerpA* strain and almost undetectable in the *ΔsufA* strain. Moreover, the iron saturation of expressed PaoABC in the *ΔerpA* strain was significantly reduced to ~85% compared to saturation in Wt MG1655. The iron saturation of PaoABC in Wt MG1655 was around ~56%, which indicates that 44% of the enzyme was in iron-free form. Furthermore, the iron saturation of PaoABC was almost unaltered in the *ΔnfuA* and *ΔsufA* strains compared to in the Wt MG1655. The iron saturation of expressed PaoABC in the *ΔiscA* strain was reduced to ~40% compared to that in the Wt MG1655 one. The lack of iron in *ΔerpA*- and *ΔiscA*-expressed PaoABC suggests that these play an essential role in the maturation of PaoABC.

3.4.3.3 Quantification of Moco content in purified EcPaoABC

The Moco content was determined from the purified PaoABC in Wt MG1655 and in the *ΔiscA*, *ΔerpA*, *ΔnfuA*, and *ΔsufA* strains. In addition, the cellular Moco content was also analyzed for the same strains under the aerobic condition. The Moco was measured as FormA, the fluorescence derivatives of Moco produced by oxidation using I_2 and KI.

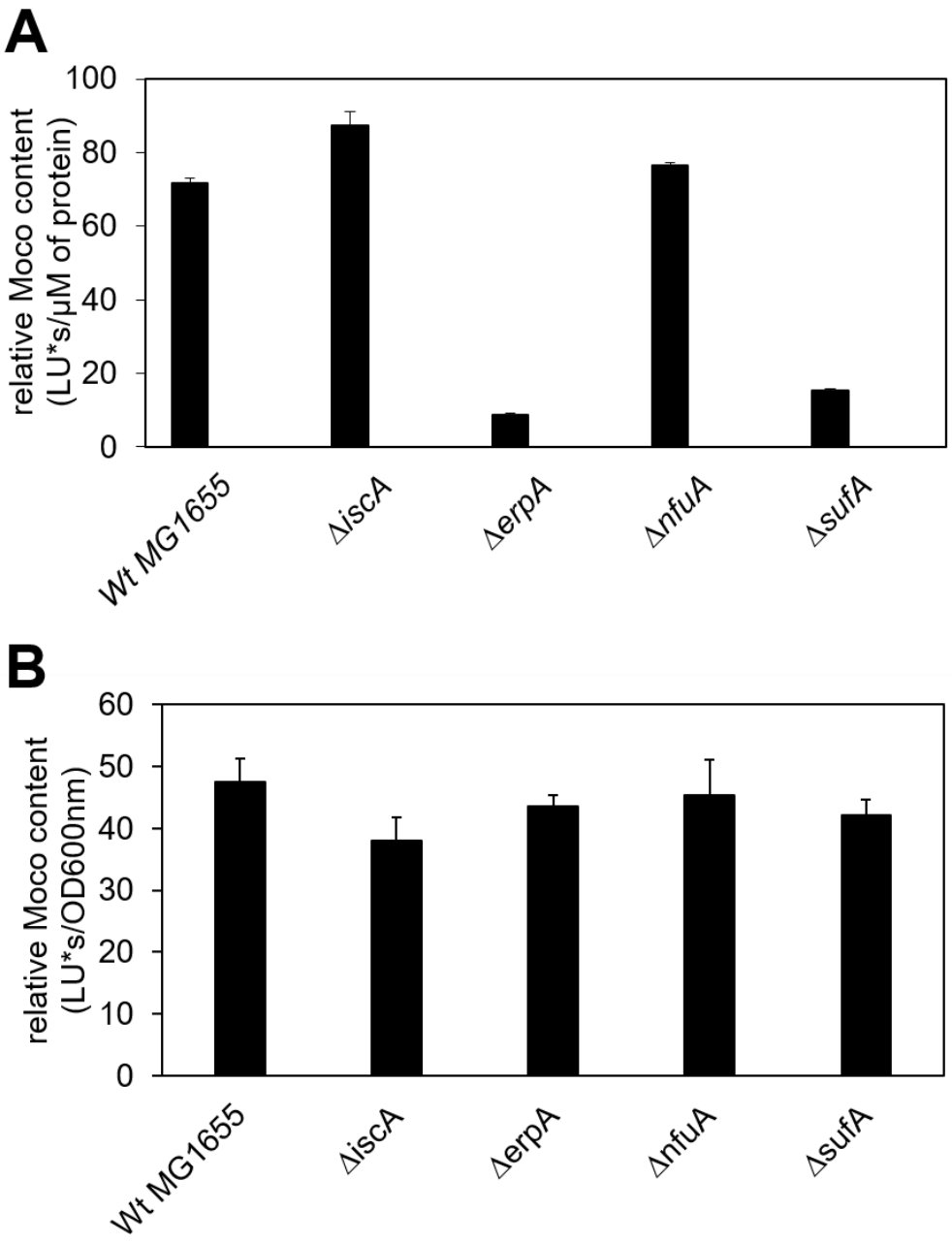

Figure 3-30: Analysis of relative Moco content from purified EcPaoABC (A) and cell extract (B) in different *E. coli* mutant strains

Relative Moco content was quantified from the purified EcPaoABC (A) and cell extract (B) was determined in Wt MG1655, *ΔiscA, ΔerpA, ΔnfuA,* and *ΔsufA* strains. FormA (Moco) was

monitored by fluorescence of extinction at 383 nm and an emission at 450 nm using HPLC; the relative amount of Moco were normalized to protein concentration (µM) and OD_{600} nm for the purified EcPaoABC and cell extract, respectively. Standard deviations were calculated from three biological replicates

Figure 3-30 show that the Moco content of expressed PaoABC in the *ΔiscA* and *ΔnfuA* strains was almost similar to that of Wt MG1655. However, the Moco content of expressed PaoABC in the *ΔerpA* and *ΔsufA* strains was significantly reduced to ~88% and ~81%, respectively, compared to the Wt MG1655.

However, the overall Moco content in the cell extract was almost identical for all the mutant strains compared to the Wt MG1655 strain under aerobic conditions, which suggests that sufficient Moco was produced in the cells but could not be delivered into the apo-PaoABC. Moreover, the reduced Moco content of expressed PaoABC in the *ΔsufA* strain is reflected in a very weak band of PaoC from the purified enzyme after SEC, which belongs to the Moco domain.

3.4.3.4 Quantification of FAD content in purified EcPaoABC

The FAD content was quantified for Wt MG1655 and for the *ΔiscA*, *ΔerpA*, *ΔnfuA*, and *ΔsufA* strains' expressed purified PaoABC enzyme.

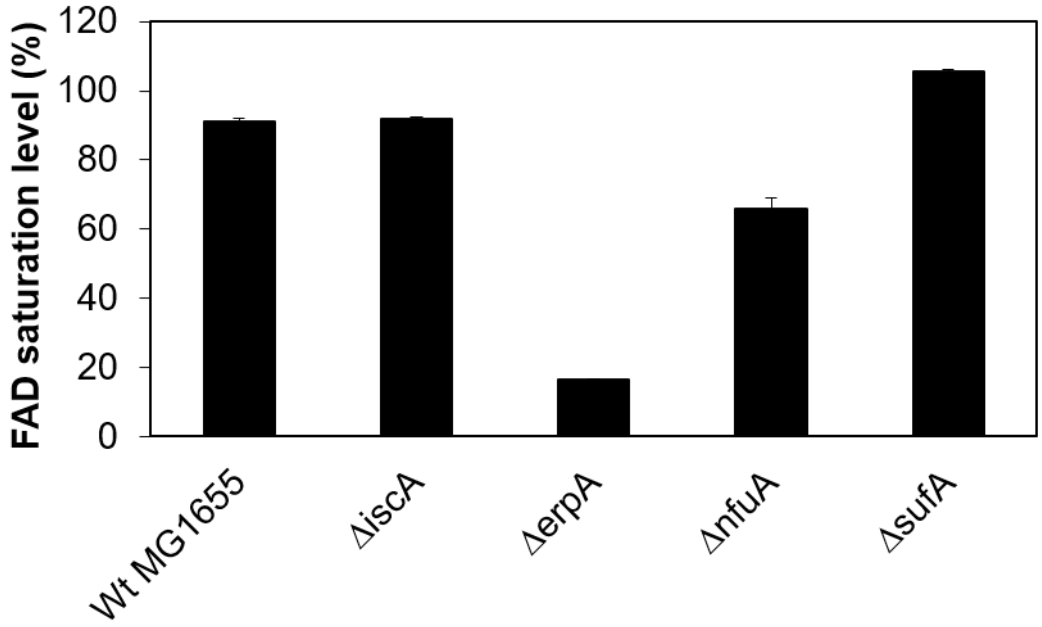

Figure 3-31: Analysis of relative FAD content from EcPaoABC expressed in different *E. coli* mutant strains

The quantification of FAD cofactor from purified EcPaoABC expressed in Wt MG1655, *ΔiscA, ΔerpA, ΔnfuA, ΔsufA* mutant strains; the concentration of purified protein was 10 µM, and measurement was performed using 50 mM Tris, 1 mM EDTA, pH 7.5. Standard deviations were calculated from three biological replicates

Figure 3-31 shows that the FAD content of expressed PaoABC was comparable in Wt MG1655 and in the *ΔiscA*, *ΔnfuA*, and *ΔsufA* strains. This was also reflected in the FAD spectra that contain the FAD shoulder peak at 445 nm. In contrast, the FAD spectra of expressed PaoABC in the *ΔerpA* strain show a significantly weak shoulder at 445 nm, which reflected a reduction in FAD content by about ~85% compared to the Wt MG1655. Moreover, the FAD content of expressed PaoABC in the *ΔnfuA* strain was also slightly reduced to around ~15% compared to the Wt MG1655.

3.4.3.5 Enzyme activity of purified EcPaoABC

The enzyme activity was determined from the expressed PaoABC in the Wt MG1655 and in the *ΔiscA*, *ΔerpA*, *ΔnfuA*, and *ΔsufA* strains, where benzaldehyde was used as a substrate, and oxygen as a terminal electron acceptor. About 5 µM purified PaoABC was used in the enzymatic reaction.

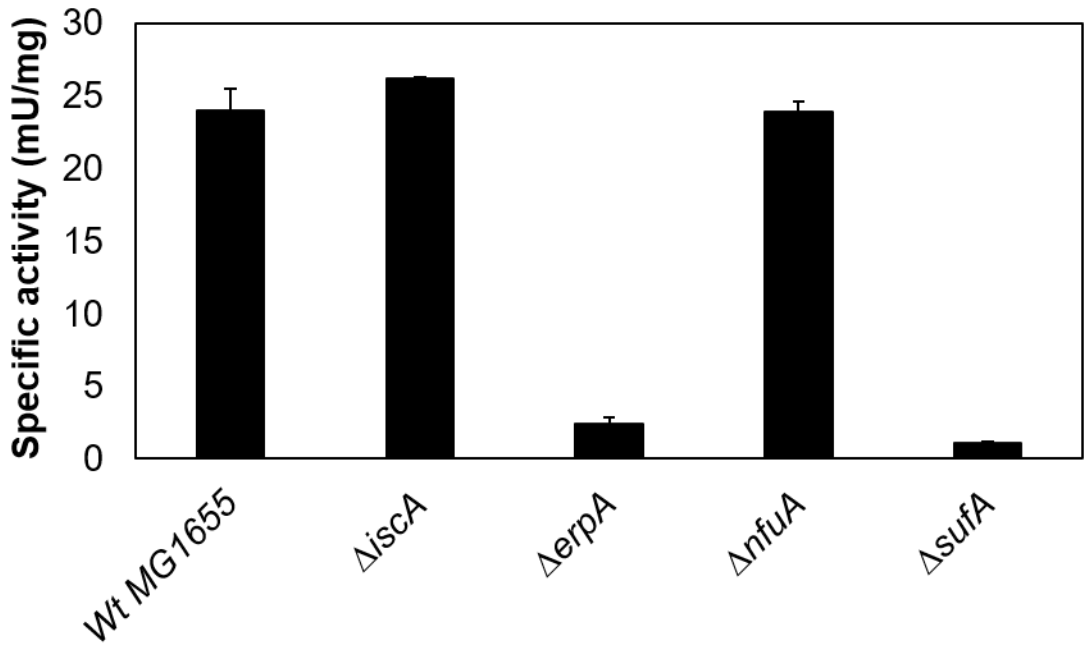

Figure 3-32: Analysis of the specific activity from purified EcPaoABC expressed in different *E. coli* mutant strains

The specific activity from purified EcPaoABC expressed in Wt MG1655, *ΔiscA, ΔerpA, ΔnfuA, ΔsufA* mutant strains was determined; the benzaldehyde and oxygen were used as a substrate

and terminal electron acceptor for this reaction; 5 µM purified EcPaoABC was used, and the reaction was performed at room temperature. Standard deviations were calculated from three biological replicates

Figure 3-32 shows that the specific activity of expressed PaoABC in the *ΔiscA* and *ΔnfuA* strains was comparable to that of the Wt MG1655. Moreover, the specific activity of expressed PaoABC in the *ΔerpA* strains was significantly decreased to almost ~90% compared to Wt MG1655, since the expressed PaoABC from the *ΔerpA* strain shows a lack of Fe, Mo, and FAD content. However, the specific activity of expressed PaoABC in the *ΔsufA* strain was almost undetectable based on the lack of Moco.

3.4.3.6 CD spectroscopy of purified EcPaoABC

CD spectroscopy was carried out to determine the presence of [2Fe-2S] and [4Fe-4S] clusters in purified PaoABC expressed in Wt MG1655 and in the *ΔiscA*, *ΔerpA*, *ΔnfuA*, and *ΔsufA* strains. The experiment was conducted using purified PaoABC, in which the spectrum was recorded using a 50 mM Tris buffer; 1mM EDTA pH 7.5 at room temperature in the range of 300-600 nm as an average of 3 runs with the sensitivity set to standard. The slit width was set to 1 nm and the delay time to 3 seconds.

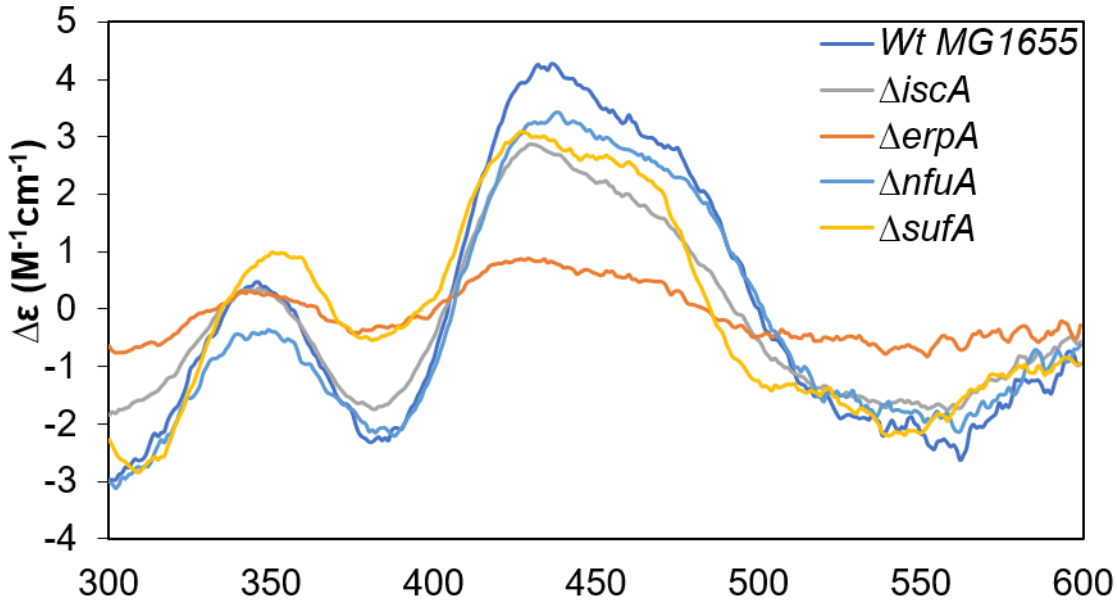

Figure 3-33: Analysis of CD spectra from purified EcPaoABC expressed in different *E. coli* mutant strains

CD spectra of purified EcPaoABC expressed in Wt MG1655, *ΔiscA, ΔerpA, ΔnfuA, ΔsufA* mutant strains; the concentration of purified protein was 10 µM, and measurement was performed at room temperature in the range of 300-600 nm using 50 mM Tris, 1 mM EDTA, pH 7.5

Figure 3-33 show that the negative signals at 350-400 nm, 520-580 nm, and the intense positive signal at 400-500 nm were observed for the expressed PaoABC in Wt MG1655 and in the *ΔiscA*, *ΔnfuA*, and *ΔsufA* strains. Moreover, the peak transition was visible at 374 nm, 434 nm, 470 nm, and 552 nm for purified PaoABC. Furthermore, the peak intensity around 400 nm to 500 nm for PaoABC expressed in the *ΔiscA*, *ΔnfuA*, and *ΔsufA* strains was slightly reduced compared to with the Wt MG1655. Peak intensity at around 400-500 nm was significantly reduced for PaoABC expressed in the *ΔerpA* strain compared to Wt MG1655. Moreover, the peak shift at 520-580 nm remained relatively unaltered for the PaoABC expressed in the *ΔerpA* strain. The peak shift at 434 nm and 470 nm revealed the presence of [2Fe-2S] clusters (Schumann et al., 2008), which was very prominent for the PaoABC expressed in Wt MG1655 and in the *ΔiscA*, *ΔnfuA*, and *ΔsufA* strains, although not for the *ΔerpA* strain. This indicates the absence of Fe-S clusters in the PaoABC-expressed *ΔerpA* strain.

3.5 Expression and purification of xanthine dehydrogenase from *R. capsulatus*

The xanthine dehydrogenase from *R. capsulatus* belongs to the xanthine oxidase (XO) family of molybdoenzymes, which is a heterotetrameric enzyme that contains Mo-MPT as a form of Moco, FAD, and two [2Fe-2S] clusters. The objective of the experiment was to identify the Fe-S cluster carrier proteins that insert [2Fe-2S] clusters for the maturation of RcXDH. Therefore, we expressed *R. capsulatus xdhABC* in the *E. coli* Wt MG1655, and in the *ΔerpA*, *ΔiscA*, *ΔsufA*, and *ΔnfuA* mutant strains, purified, and characterized the enzymes.

3.5.1 Expression of RcXDH in mutant strains

The expression of RcXDH was performed in the *E. coli* Wt MG1655 and the mutant strains. The overexpression was performed using the plasmid *pSL207*, constructed in the *pTrcHis* vector, where the *xdhABC* operon from *R. capsulatus* was cloned, using the NdeI-HindIII restriction sites (Leimkühler et al., 2003). The expression was performed aerobically at 30°C for 24 h at 130 rpm. The cells were harvested by centrifugation and resuspended using a phosphate buffer, pH 8.0. Further, purification was carried out by IMAC and followed by the gel.

3.5.2 Ni-NTA affinity and size exclusion chromatography

After cell lysis, the crude extract was separated by centrifugation, further used for IMAC purification. The crude extract was incubated with a Ni^{++}-NTA matrix, in which 0.5 mL of the matrix was used per liter of cell culture. Elution was performed using 250 mM imidazole-containing phosphate buffer, where the eluted XDH fractions were a brown color, and no significant exceptions were visible for different mutant strains that expressed RcXDH in comparison to the Wt MG1655 eluent. After Ni^{++}-NTA affinity chromatography, the eluted fractions were further dialyzed overnight at 4°C into a Tris buffer, pH7.5.

Size exclusion chromatography was the last step of purification. This step was performed using a Superose-6 gel filtration column, and further, the eluted fractions were analyzed by 12% SDS-PAGE.

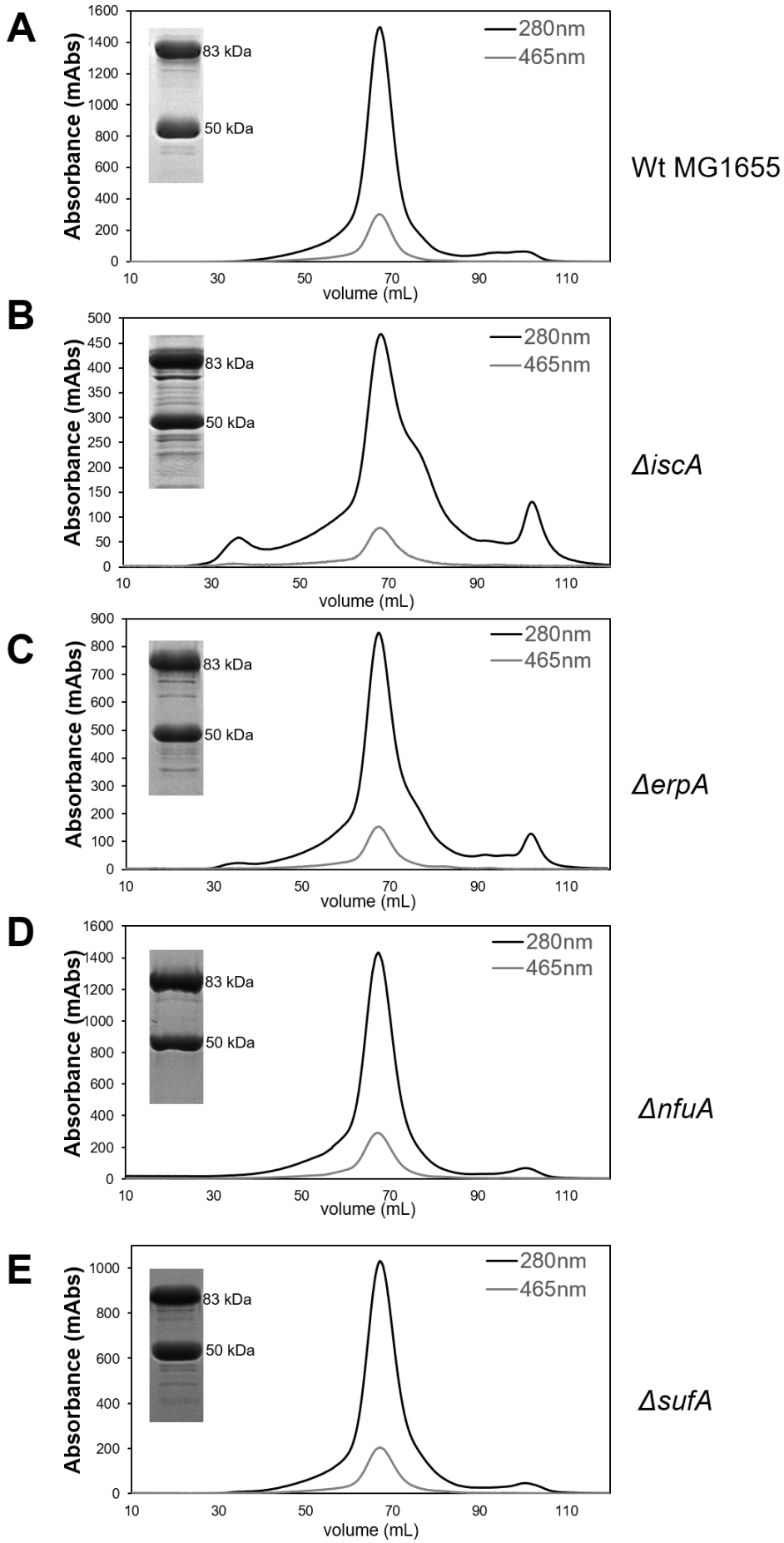
A
B
C
D
E
Absorbance (mAbs)
volume (mL)
280nm
465nm
83 kDa
50 kDa
Wt MG1655
ΔiscA
ΔerpA
ΔnfuA
ΔsufA

Figure 3-34: Gel filtration chromatograms of the purified RcXDH expressed in different *E. coli* mutant strains

The elution profiles (absorbance at 280 nm and 445 nm) and analysis of the purity after the analytical gel filtration chromatography of RcXDH expressed in (A) Wt MG1655, (B) *ΔiscA,* (C) *ΔerpA,* (D) *ΔnfuA,* and (E) *ΔsufA* mutant strains; the elution of the protein was performed using 50 mM Tris, 1 mM EDTA, 2.5 mM DTT and 200 mM NaCl, pH 7.5 by superose-6 gel filtration column on the Äkta system; the purity of RcXDH was analyzed using 12% SDS-PAGE gel.

Figure 3-34 shows that the elution profiles of expressed XDH in the *E. coli* Wt MG1655 and in the *ΔiscA*, *ΔerpA*, *ΔnfuA*, and *ΔsufA* mutant strains show a prominent peak after 65 mL and another minor peak at around ~100 mL. The protein eluted between 60-80 mL, where the heterotetrameric XDH form elutes. Fractions of XDH heterotetrameric in the *ΔiscA* strain showed an additional minor peak at 35 mL, which indicates the presence of aggregated proteins. The SDS-PAGE analysis shows two bands around 83 kDa and 50 kDa corresponding to the sizes of XdhA, and XdhB, respectively. SDS-PAGE also indicated minor impurities, with the exception of expressed XDH in the *ΔiscA* mutant strain that contains some additional minor bands. This indicates that the purified XDH from the *ΔiscA* mutant strains contained more contaminants than the purified XDH from the Wt MG1655.

3.5.3 Characterization of purified RcXDH

3.5.3.1 UV-Vis spectroscopy

The typical UV-Vis spectra for the XDH enzyme show absorption at 280 nm for the aromatic amino acids and 550 nm for two [2Fe-2S] clusters, FAD at 465 nm. The absorption spectra were recorded from 250 nm to 800 nm using a UV-visible spectrometer.

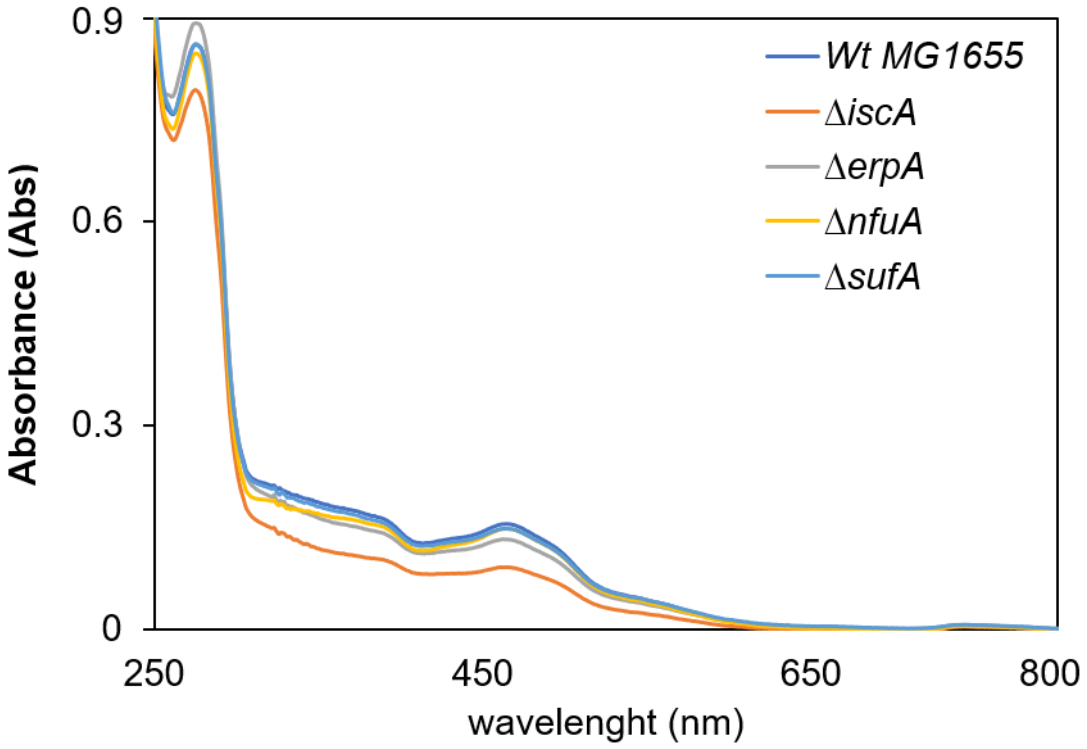

Figure 3-35: Analysis of UV-visible spectrum from purified RcXDH expressed in different *E. coli* mutant strains

The UV-visible spectrum (250 nm to 800 nm) for characterization of purified RcXDH that expressed in Wt MG1655, *ΔiscA, ΔerpA, ΔnfuA,* and *ΔsufA* strains; the concentration of purified EcPaoABC was 10 µM, and the spectrum was recorded at room temperature using 50 mM Tris, 2.5 mM DTT, 1 mM EDTA, pH 7.5

Table 3-2: The absorbance ratio between 280 nm and 445 nm of purified RcXDH expressed in *E. coli* mutant strains

Strains	Ratio (280/445)
Wt MG1655	5.5
ΔiscA	8.6
ΔerpA	6.1
ΔnfuA	5.6
ΔsufA	5.7

The high purity of metalloflavoproteins can be reflected in their absorption ratio between 280 nm and 465 nm, which should be around 5.0 (Leimkühler et al., 2003). The spectra of purified XDH enzyme shows that the Wt MG1655-, *ΔnfuA*-, and *ΔsufA*-expressed XDH were quite similar since the FAD peak shoulder at 465 nm was well visible and the

shoulders were comparable to each other, with the ratio of A280/A465 in the same range at around 5.5, 5.6 and 5.7 respectively. The FAD shoulder was also observed for expressed XDH in the *ΔerpA* strains, in which the ratio of A280/A465 was 6.1, which is higher compared to the Wt MG1655. This indicates that the quality of XDH expressed in the *ΔerpA*, *ΔnfuA*, and *ΔsufA* strains was quite similar to that of Wt MG1655. The expressed XDH in the *ΔiscA* strain shows a relatively weaker FAD shoulder at 465 nm compared to the Wt MG1655, with ratio of A280/A465 at 8.6. This indicates that the expressed XDH in the *ΔiscA* strain was comparatively less purified and more contaminated than in the Wt MG1655.

3.5.3.2 Metal content determination by ICP-OES

The iron and molybdenum content were quantified for the expressed XDH in the Wt MG1655, and in the *ΔiscA*, *ΔerpA*, *ΔnfuA*, and *ΔsufA* strains using inductively coupled plasma optical emission spectrometry (ICP-OES). The concentration of the elements was calculated to a percentage scale of saturation values of cofactors, considering 1 molybdenum and 4 iron atoms (in the two [2Fe-2S] clusters).

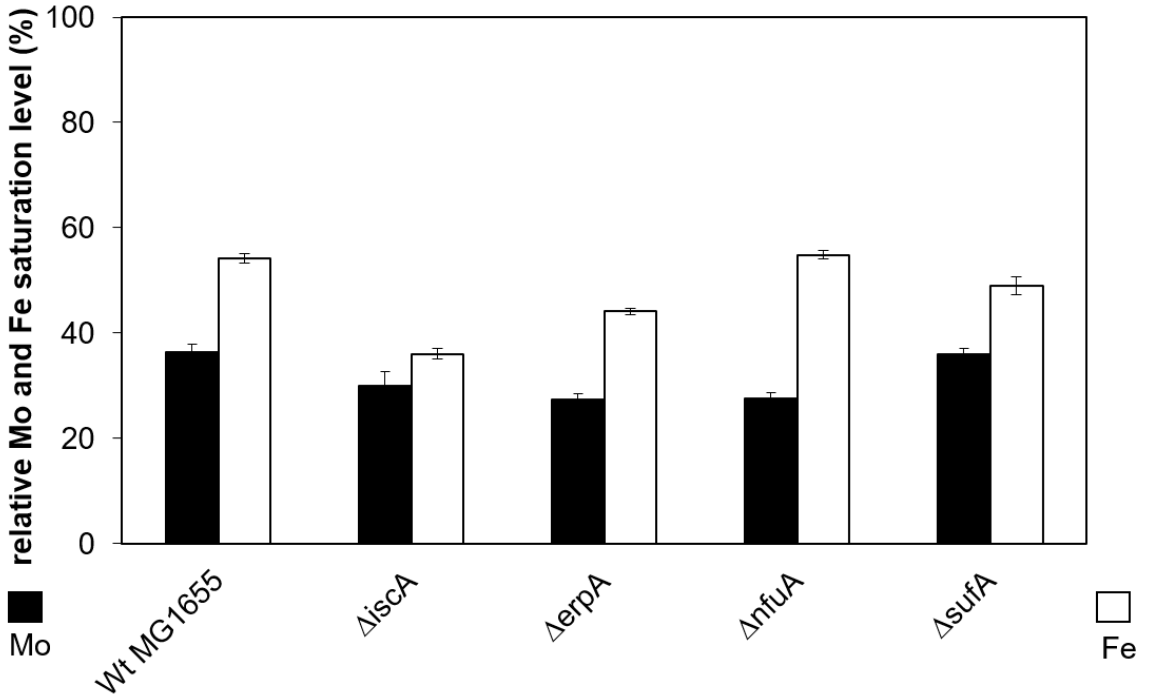

Figure 3-36: Analysis of relative molybdenum and iron saturation from RcXDH expressed in different *E. coli* mutant strains

The ICP-OES analysis for the determination of relative molybdenum (black bars) and iron (white bars) saturation of RcXDH that expressed in Wt MG1655, *ΔiscA, ΔerpA, ΔnfuA,* and

ΔsufA strains; the concentration of purified RcXDH was 10 µM; the following wavelengths were used to analyze for iron: 238.204 nm, 238.562 nm, 259.939 nm and for molybdate: 203.84 nm, 202.031 nm, 204.597 nm. A baseline was measured using 50 mM Tris, 2.5 mM DTT, 1 mM EDTA, pH 7.5; the iron and molybdenum concentrations were determined by using the Standard XVI (Merck); Standard deviations were calculated from three biological replicates

Figure 3-36 show that the molybdenum saturation of expressed XDH in the *ΔsufA* strain was comparable to that of the Wt MG1655, which was around ~35%. This 35% molybdenum saturation implies that most purified XDH was in its Moco-free form. However, this number was slightly reduced for the expressed XDH in the *ΔiscA*, *ΔerpA*, and *ΔnfuA* strains, where the molybdenum saturation was ~30%, ~26%, and ~25%, respectively. On the other hand, the iron saturation of the expressed XDH in the *ΔiscA* and *ΔerpA* strain was significantly decreased around ~34% and ~16% compared to in the Wt MG1655. The iron saturation of expressed XDH in the Wt MG1655 strain was around ~55%, indicating around ~45% of the XDH was in its iron-free form. Furthermore, the iron saturation of expressed XDH in the *ΔnfuA* and *ΔsufA* strains was comparable to that of the Wt MG1655.

3.5.3.3 Quantification of Moco content in purified RcXDH

The Moco content was determined from the Wt MG1655, and from the *ΔiscA*, *ΔerpA*, *ΔnfuA*, and *ΔsufA* strains expressed purified XDH enzyme. The Moco was measured as FormA, the fluorescence derivatives of Moco, produced by oxidation using I_2 and KI.

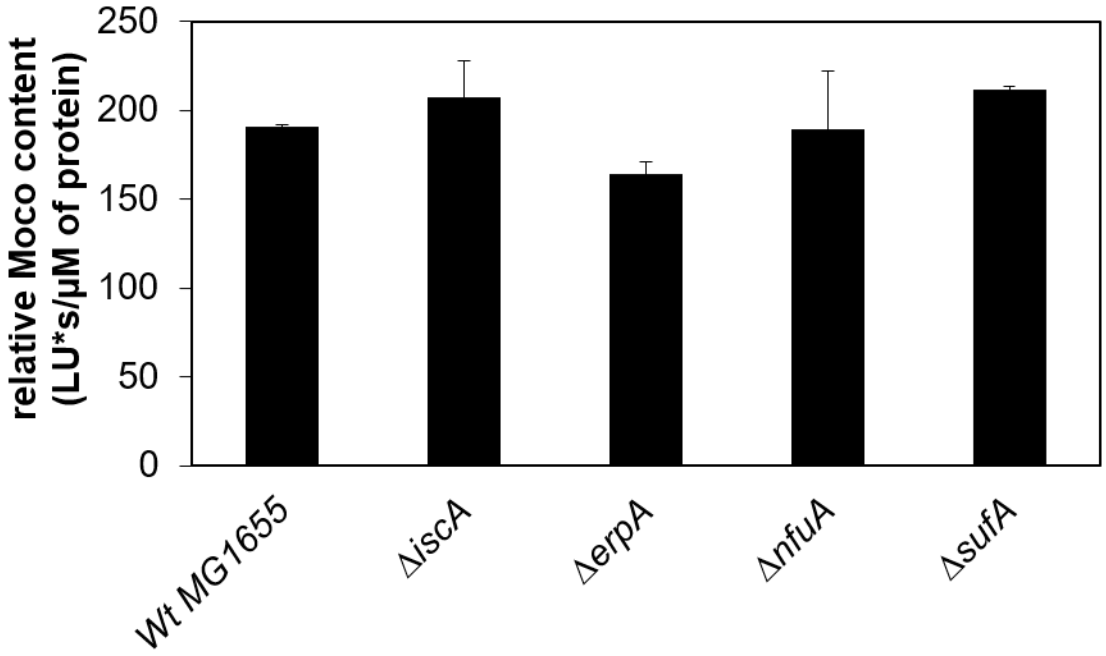

Figure 3-37: Analysis of relative Moco content from purified RcXDH expressed in different *E. coli* mutant strains

Relative Moco content was quantified from the purified RcXDH was determined in Wt MG1655, *ΔiscA, ΔerpA, ΔnfuA,* and *ΔsufA* strains. FormA (Moco) was monitored by fluorescence of extinction at 383 nm and an emission at 450 nm using HPLC; the relative amount of Moco were normalized to protein concentration (µM) and OD_{600} nm for the purified EcPaoABC and cell extract, respectively. Standard deviations were calculated from three biological replicates

Figure 3-37 shows that the Moco content of expressed XDH in the *ΔiscA*, *ΔnfuA*, and *ΔsufA* strains was unaltered compared to the Wt MG1655. However, the Moco content slightly reduced to ~10% for the expressed XDH in the *ΔerpA* strains compared to the Wt MG1655. Therefore, no significant change was observed in the Moco content of purified XDH for all the mutant strains compared to that in Wt MG1655.

3.5.3.4 Quantification of FAD content in purified RcXDH

The FAD content of purified XDH enzyme was detected from the absorbance at 465 nm by UV-visible spectra and quantified.

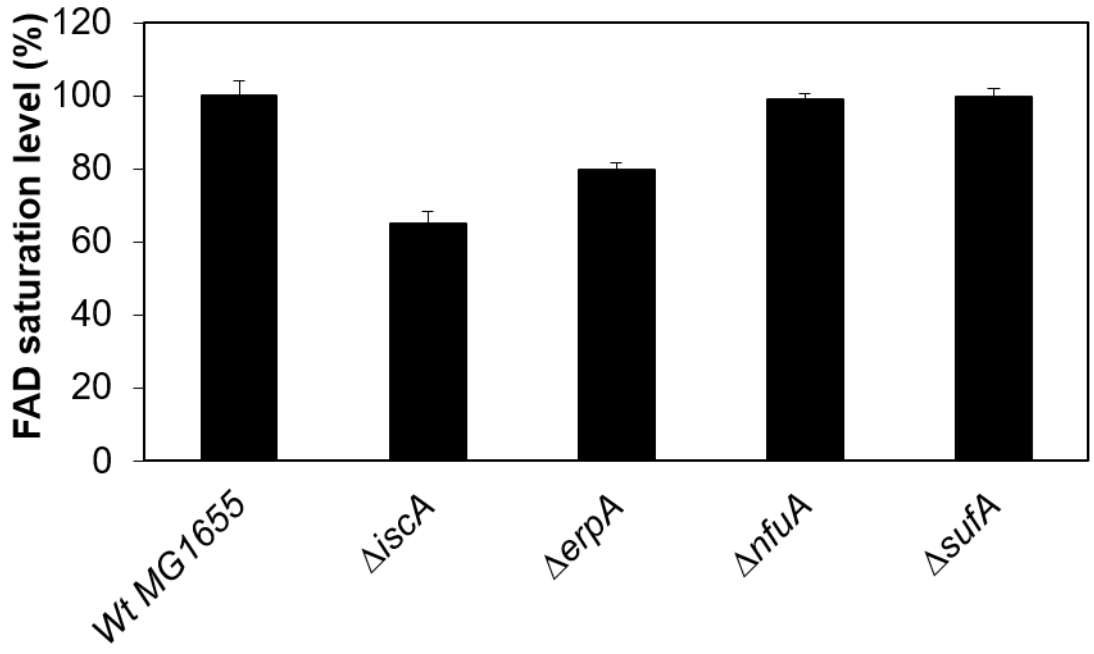

Figure 3-38: Analysis of relative FAD content from RcXDH expressed in different *E. coli* mutant strains

The quantification of FAD cofactor from purified RcXDH expressed in Wt MG1655, *ΔiscA, ΔerpA, ΔnfuA, ΔsufA* mutant strains; the concentration of purified protein was 10 µM, and measurement was performed using 50 mM Tris, 2.5 mM DTT, 1 mM EDTA, pH 7.5. Standard deviations were calculated from three biological replicates

Figure 3-38 shows that the FAD content of expressed XDH in the Wt MG1655, *ΔnfuA*, and *ΔsufA* strains was comparable. This was also reflected in the FAD shoulder at 465 nm. However, the FAD spectra of expressed XDH in the *ΔerpA* strains show a slightly weaker shoulder at 465 nm, reflecting a reduced FAD content about ~20% compared to the Wt MG1655. Moreover, the FAD content of expressed XDH in the *ΔiscA* strains was around ~36% compared to that of Wt MG1655. This was also reflected in the FAD shoulder of expressed XDH in the *ΔiscA* strain at 465 nm.

3.5.3.5 Enzyme activity of purified RcXDH

Enzyme activity was determined from purified XDH from the Wt MG1655, and from the *ΔiscA*, *ΔerpA*, *ΔnfuA*, and *ΔsufA* strains, where NAD^+ was used as a substrate. About 5 µM purified XDH was used in the enzymatic reaction.

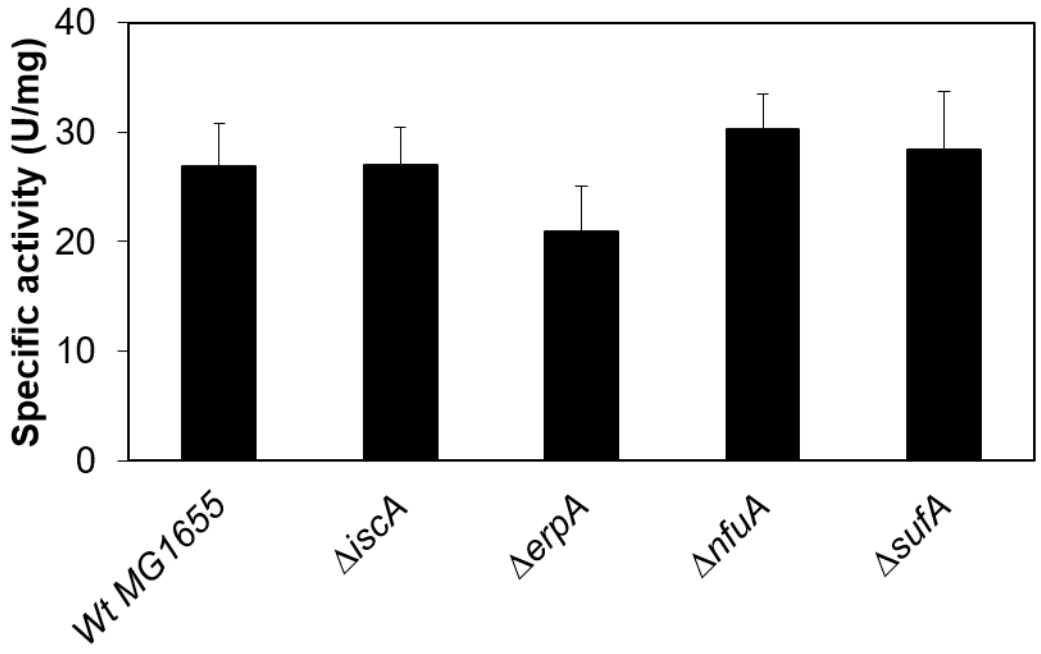

Figure 3-39: Analysis of the specific activity from purified RcXDH expressed in different *E. coli* mutant strains

The specific activity from purified RcXDH expressed in Wt MG1655, *ΔiscA, ΔerpA, ΔnfuA, ΔsufA* mutant strains was determined*;* the NAD and xanthine were used as a substrate and terminal electron acceptor for this reaction; 5 µM purified RcXDH was used, and the reaction was performed at room temperature. Standard deviations were calculated from three biological replicates

Figure 3-39 shows that the specific activity of purified XDH in the *ΔiscA*, *ΔnfuA*, and *ΔsufA* strains was comparable to that of the Wt MG1655. Moreover, the specific activity of purified XDH in the Δ*erpA* strain was slightly reduced to almost ~10% compared to Wt MG1655.

3.5.3.6 CD spectroscopy of purified RcXDH

CD spectroscopy was carried out to determine the presence of [2Fe-2S] clusters in purified XDH that expressed in Wt MG1655, and in the *ΔiscA*, *ΔerpA*, *ΔnfuA,* and *ΔsufA* strains. The experiment was performed using purified XDH, in which the spectrum was recorded using a 50 mM Tris buffer, 1 mM EDTA; pH 7.5 at room temperature in the range of 300-600 nm as an average of 3 runs with the sensitivity set to standard. The slit width was set to 1 nm and the delay time to 3 seconds.

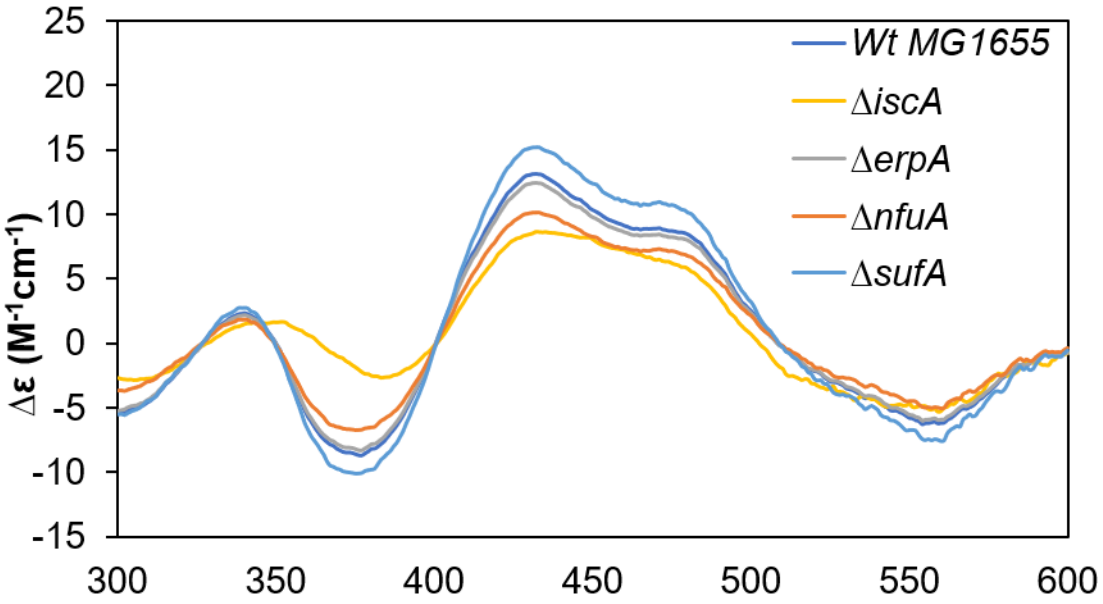

Figure 3-40: Analysis of CD spectra from purified RcXDH expressed in different *E. coli* strains

CD spectra for purified RcXDH expressed in Wt MG1655, *ΔiscA, ΔerpA, ΔnfuA, ΔsufA* mutant strains; the concentration of purified protein was 10 µM, and measurement was performed at room temperature in the range of 300-600 nm using 50 mM Tris, 2.5 mM DDT, 1 mM EDTA, pH 7.5

Figure 3-40 shows that all the spectrum characteristics are identical to a typical xanthine dehydrogenase CD spectrum (Schumann et al., 2008). Negative signals at 350-400 nm, 520-580 nm, and a strong positive signal at 400-500 nm were observed for the expressed XDH in the Wt MG1655, and in the *ΔerpA*, *ΔnfuA*, and *ΔsufA* strains. Meanwhile, the XDH expressed in the *ΔiscA* strain shows less intense negative signals at 350-400 nm, whereas the other signal transitions were similar as compared to Wt MG1655. The peak transition was visible at 374 nm, 434 nm, 470 nm, and 552 nm for purified XDH expressed from the Wt MG1655, and from the *ΔerpA*, *ΔnfuA*, and *ΔsufA* mutant strains. However, the peak intensity at 434 nm and 470 nm was slightly decreased for XDH expressed in the *ΔiscA* mutant strain compared to that of Wt MG1655. The peak shift at 434 nm and 470 nm indicated the presence of [2Fe-2S] clusters (Schumann et al., 2008).

4 Discussion

4.1 Fe-S cluster insertion into MoaA and FNR under anaerobic nitrate respiratory conditions

In the first part of this study, the Fe-S cluster carrier proteins that are involved in MoaA maturation were identified under nitrate and TMAO respiration. Together, ErpA and IscA are involved in [4Fe-4S] cluster insertion into the MoaA. Moreover, relatively weak FNR regulation in Moco biosynthesis was also determined in our study based on the unaltered Moco content in the *fnr* deleted strain. We were unable to detect the Fe-S cluster carrier proteins that were involved in the insertion of Fe-S clusters into nitrate reductase. [4Fe-4S]-FNR is required for the expression of the *narGHJI* operon. In our study, we were able to identify ErpA as the FNR maturation protein by inserting the Fe-S cluster into it under nitrate respiratory conditions. Moreover, exogenous expression of *sufA* and *iscA* revealed that both could complement ErpA in FNR maturation under the growth conditions tested.

4.1.1 Cross-talk between Fe-S and Moco biosynthesis

The Fe-S cluster assembly in *E. coli* involves two core systems: the iron–sulfur cluster (ISC) and sulfur mobilization (SUF). The ISC system is a housekeeping system that works under normal cellular conditions (L. Zheng et al., 1998). The SUF system is activated under conditions of iron starvation and oxidative stress (Outten, Djaman, and Storz, 2004; Ayala-Castro, Saini, and Outten, 2008; Tanaka et al., 2016). To date, about 165 Fe-S clusters containing proteins have been identified in *E. coli* (Roche et al., 2013). Among these, one important protein is MoaA. MoaA is involved in Moco biosynthesis, whereby MoaA catalyzes the formation of cPMP from 5'GTP in the first step of Moco biosynthesis (Hanzelmann & Schindelin, 2004). MoaA belongs to the superfamily of radical/S-adenoslymethionine (SAM) enzymes (Broderick et al., 2014), that use a [4Fe-4S] cluster to reductively cleave SAM. MoaA consists of two [4Fe-4S] cluster-binding domains, one at the C-terminus and another at the N-terminus (Yokoyama & Leimkuhler, 2015). The [4Fe-4S] cluster located in the N-terminus binds to the C-X3-C-X2-C motif and initiates the electron transfer for SAM cleavage.

4.1.2 MoaA maturation under anaerobic conditions

4.1.2.1 Mevalonate is required for cell growth and respiration

The cells were cultivated for 8 h anaerobically with potassium nitrate or TMAO. Despite the growth defects of some mutant strains such as the *erpA*-deleted ones, all the strains reached the late-exponential phase after around 7-8 h of cultivation. The exponential phase was chosen for harvesting since most of the growth-related genes are activated in this phase (A Ishihama, 1997; Loewen & Hengge-Aronis, 1994). Moreover, the cell population is more homogenous in the exponential phase than in the stationary phase, where heterogeneity and cell diversity increase and lead to cell death (Kolter, Siegele, and Tormo, 1993; Ishihama, 1999; Makinoshima et al., 2003). This is why, in our study, the cells were harvested after 8 h of growth to acquire the most homogenous results.

According to evolutionary considerations and phylogenetic study, A-type carrier proteins in *E. coli* such as ErpA belong to the ATC-I and IscA family members, and SufA is classified as ATC-II. It has been reported that the ATC-I family members can directly interact with the target apo-protein, whereas the members in ATC-II are able to interact with scaffold proteins (Daniel Vinella et al., 2009).

It has been reported that the deletion of A-type carrier protein ErpA can be lethal for the strains in the presence of oxygen or other terminal electron acceptors such as nitrate, fumarate, and TMAO (Loiseau et al., 2007), which negatively influence the growth of *ΔerpA* and other double mutant or triple mutants such as *ΔiscA*/*ΔerpA*, *ΔsufA*/*ΔerpA*, and *ΔsufA*/*ΔiscA*/*ΔerpA* (Loiseau et al., 2007). Aerobic and anaerobic respiration depends on the requirement of quinones as electron carriers, which are derived from isopentenyl diphosphate (IPP). Deletion of *erpA* and *iscA* leads to lack of maturation of the IspG/H enzymes (Daniel Vinella et al., 2009), which are essential for the biosynthesis of isopentenyl diphosphate (IPP) (Gräwert et al., 2004; Wolff et al., 2003). To avoid growth deficiency, the mutant strains were introduced with the eukaryotic mevalonate-dependent pathway for biosynthesis of IPP (Gräwert et al., 2004; Wolff et al., 2003). In this study, the mutants can respire and are viable under nitrate respiratory conditions in the presence of mevalonate.

4.1.2.2 Fe-S clusters insertion into MoaA under nitrate respiratory conditions

Under nitrate respiratory conditions, a significant reduction in cellular Moco content was observed in the *ΔiscA* and *ΔerpA* single mutant strains, which indicates their involvement in Fe-S cluster insertion into MoaA. Completely devoid Moco content in the *ΔiscA/ΔerpA* double mutant strain indicated that ErpA and IscA together are involved in the maturation of MoaA. SufA did not play any role in the maturation of MoaA under anaerobic conditions at the cellular level since the Moco content was unaltered in the *ΔsufA* strain. Under nitrate respiratory conditions, SufA was unable to substitute either ErpA or IscA or both in MoaA maturation despite the exogenous expression of *sufA*. SufA is a Fe-S cluster carrier protein, which belongs to the *suf*-operon system. It has been previously reported that the SUF system is employed for Fe-S cluster biosynthesis under oxidative stress or in iron starvation conditions (Outten, Djaman, and Storz, 2004; Ayala-Castro, Saini, and Outten, 2008; Tanaka et al., 2016). The apo-IscR protein induces *suf*-operon expression (Giel et al., 2006a; Yeo et al., 2006; Lee, Yeo, and Roe, 2008). In the presence of oxygen, SufA receives Fe-S clusters from the SufBCD complex and further transfers them to ErpA or other carrier proteins for insertion into target apo-proteins (Roche et al., 2013). Therefore, under anaerobic respiration in the presence of nitrate, the role of SufA plays only a minor role in Fe-S cluster transfer to MoaA. The Moco content after exogenous expression of *iscA* indicated that IscA is able to replace the role of ErpA in MoaA maturation. Moreover, ErpA can also replace the function of IscA in Moco biosynthesis. The analysis of gene expression showed similar observations. The transcription level of *erpA* in the *ΔiscA* strain and respective double mutant strains such as *ΔnfuA/ΔiscA* and *ΔsufA/ΔiscA* was increased around ~2.6-4.6-fold. Moreover, *iscA* expression was also increased around ~3-fold in the absence of *erpA* in the *ΔerpA* single and the *ΔsufA/ΔerpA* double mutant strains. The higher Moco content in double mutant strains can be based on the increased level of *erpA* and *iscA* in the *iscA* and *erpA* deleted strains. These observations indicate that IscA and ErpA are able to replace each other's functions in the maturation of MoaA at the cellular level under nitrate respiratory conditions.

NfuA did not play any role in Fe-S cluster transfer into MoaA since the Moco content was identical for the *ΔnfuA* strain and for the *ΔnfuA/ΔiscA* double mutant as it was for the Wt MG1655 strain. The role of NfuA is probably more specialized in the repair of damaged or oxidized Fe-S clusters in the presence of oxygen, as suggested by a recent study by Py and coworkers (Py et al., 2018a). It has been reported that under aerobic respiration, NfuA

and ErpA interact with each other, where NfuA is presumed to assist ErpA under severely unfavorable conditions by interacting directly with the client protein for Fe-S cluster delivery (Py et al., 2018a). Moreover, a recent study has shown a specific role played by a NfuA carrier protein in inserting an auxiliary [4Fe-4S] cluster into LipA. In LipA, this auxiliary [4Fe-4S] cluster is sacrificed during catalysis to supply the sulfur atoms to synthesize lipoic acid (McCarthy et al., 2019; McCarthy & Booker, 2017). The specific function for NfuA in Fe-S cluster insertion for LipA is distinct from the [4Fe-4S] cluster insertion by ErpA and IscA into MoaA, which allows for a more rapid exchange of the inactive Fe-S cluster in LipA. Conclusively, our study shows that SufA and NfuA do not play any role in transferring Fe-S clusters into MoaA under anaerobic conditions.

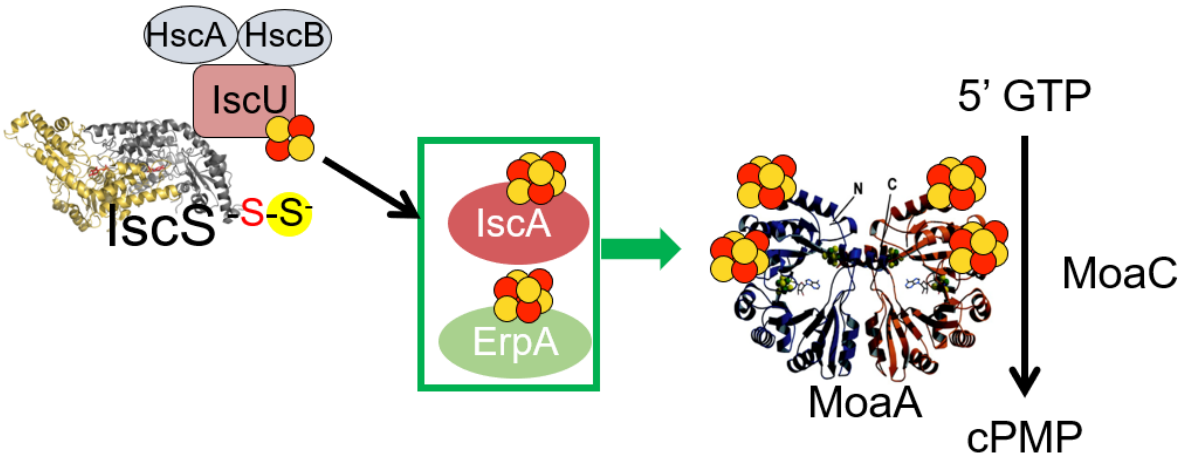

Figure 4-1: The insertion of Fe-S clusters into the MoaA in *E. coli* under nitrate respiratory conditions

MoaA catalyzes the conversion of 5'GTP to cPMP in the first step of Moco biosynthesis; active MoaA requires ErpA and IscA, which insert [4Fe-4S] clusters under anaerobic nitrate respiratory conditions, whereby the Fe-S cluster is released from the scaffold protein IscU by the chaperones HscA and HscB, and further delivered into IscA and ErpA for insertion into MoaA; IscS: PDB – 3LVM; MoaA:PDB – 1TV7

Under anaerobic respiration, the expression of MoaA is partly dependent on the regulatory protein, FNR, which positively regulates the expression of the *moa* operon by binding to the promoter site (Zupok et al., 2019). The *moa* operon was overexpressed in the strains to avoid regulation based on the inactivation of FNR. Immunodetection of MoaC confirmed overexpression of this operon in all the mutant strains. The *moa* operon expression ensured the presence of Moco biosynthesis enzymes in sufficient quantity in all the strains. No significant difference was obtained for exogenous *moa*-operon expression compared to the results of the chromosomal *moa* operon for all the strains. Reduced Moco content

was observed in the *ΔiscA/ΔerpA* double mutant strain in both chromosomal and exogenous *moa*-operon expression, which indicates the necessity of both ErpA and IscA in the maturation of MoaA. Similar Moco content was observed for the other mutants, such as *ΔnfuA* and *ΔsufA*, which suggests that no significant role is played by NfuA and SufA in MoaA maturation.

MoaA maturation was also investigated in our study under TAMO respiratory conditions. TMAO was used to induce the production of TMAO reductase under anaerobic conditions. TMAO reductase belongs to the DMSO reductase family of molybdoenzymes, and contains the bis-MGD cofactor as a form of Moco but no Fe-S clusters (Czjzek et al., 1998). Under TMAO respiration, no significant difference in Moco content was observed in the mutant strains as compared to the nitrate respiratory condition since no Moco was detectable in the *ΔiscA/ΔerpA* double and *ΔsufA*/*ΔiscA/ΔerpA* triple mutant strains. The role of ErpA and IscA was again obvious, since under these conditions the Moco content was reduced to ~ 60% of the Wt MG1655 strain. Conclusively, together ErpA and IscA are involved in the maturation of MoaA by inserting Fe-S clusters into it.

4.1.3 FNR regulatory network under anaerobic nitrate respiratory conditions

4.1.3.1 The influence of FNR on the expression of the *moa* operon

The *moa*-operon expression is dependent on FNR (Zupok et al., 2019) since FNR is a global regulator under anaerobic conditions (Green & Guest, 1993). FNR acts as a transcriptional factor by binding to the promoter site. It has been reported that FNR binds at the -46 to -33 region, upstream of the *moa* operon (Zupok et al., 2019; Anderson et al., 2000).

In our study, the expression of the *moa* operon was analyzed by β-galactosidase activity. It seems that deletion of *erpA* and *iscA* has a slight influence on *moa*-operon expression, with ~15% and ~20% reduction of activity compared to in the Wt MG1655 strain. Moreover, deletion of *nfuA* and *sufA* did not influence *moa*-operon expression. However, it has also been reported that FNR is not entirely essential for *moa*-operon expression (Zupok et al., 2019), which was indicated from the partially reduced β-galactosidase activity (~40%) in the *Δfnr* strain from our study. The maturation of FNR requires a [4Fe-4S] cluster under anaerobic conditions, where ErpA and iscA might be involved in the insertion of Fe-S clusters into it. This is also reflected in the partially reduced expression

of the *moa* operon in the *erpA* and *iscA* mutant strains. Moreover, similar Moco content in the *Δfnr* strain compared to in Wt MG1655 is probably based on the dual regulation of FNR in Moco biosynthesis, whereby FNR upregulates the *moa* operon and downregulates the *moe* operon.

4.1.3.2 The influence of FNR on the expression of the *narGHJI* operon

In this study, the nitrate reductase activity in all the mutant strains was relatively consistent except for the *erpA*- and *iscA*-deleted mutants based on reduced Moco content. However, nitrate reductase activity in the *ΔerpA* and *ΔsufA/ΔerpA* strains was not detectable despite the presence of Moco. This indicates that ErpA is involved in the maturation of NarGHI either by inserting Fe-S clusters into it or by involving other regulations in the expression of nitrate reductase. Holo-FNR activates the expression of *narGHI* (Lamberg & Kiley, 2000; Melville & Gunsalus, 1996); therefore, the absence of [4Fe-4S] leads to an absence of *narGHI* expression. The undetectable nitrate reductase activity and *narG* transcription in the *Δfnr* strain showed that FNR is required for the expression of *narGHI*. These results are consistent with those of Patricia Kiley and coworkers (Mettert et al., 2008), who also showed that *narG* expression was undetected in the *Δfnr* strain. Nitrate reductase activity was restored in the *Δfnr* strain by exogenous expression of *narGHJI*. Regulation based on FNR was avoided by overexpressing the *narGHJI* plasmid in all the mutant strains. Nitrate reductase activity was partially restored by ~50% in *erpA*-deleted strains after exogenous *narGHJI* expression. Partial nitrate reductase activity in *erpA*-deleted strains can be explained based on a reduced Moco content. This result indicates that ErpA is not essential for producing active nitrate reductase, but it might play a role in the expression of *narGHI*. Therefore, the undetectable nitrate reductase activity in the *ΔerpA* strain indicates that ErpA is required for the maturation of FNR by inserting [4Fe-4S] cluster into it. Completely devoid *narG* transcription in the *ΔerpA* and *Δfnr* strains confirms the necessity of ErpA for the expression of *narGHI* under nitrate respiratory conditions.

We were able to show that IscA is also involved in the maturation of MoaA, but its role in FNR maturation is still not evident. Nitrate reductase activity in the *ΔiscA* strain was reduced to ~80% compared to the Wt MG1655 strain, where the activity was not influenced by the expression of the *fnr* plasmid. The reduced nitrate reductase activity in the *ΔiscA* strain is probably based on two major reasons: firstly, the reduced Moco content in the *ΔiscA* strain since IscA is involved in MoaA maturation; secondly, IscA might insert Fe-S clusters into NarGHI since the optimum expression of *narGHI* was achieved by ErpA

based on FNR maturation. Furthermore, the detected *narG* transcription also confirmed the optimum expression of *narGHI* in the *ΔiscA* strain. This result is also consistent with findings from Kiley and coworkers, who showed no significant impact of *narG* expression in the *iscA*-deleted strain (Mettert et al., 2008). However, they did not report findings about *narG* expression in the *ΔerpA* strain, whereas we have shown the essential role of ErpA in *narGHJI* expression under anaerobic nitrate respiratory conditions. The reduced (~20%) and restored (~60%) nitrate reductase activity before and after exogenous *narGHJI* expression in the *ΔiscA* strain strongly indicates that IscA might be one of the candidates involved in the maturation of nitrate reductase enzyme, since deletion of IscA might negatively influence the maturation of nitrate reductase enzyme at the cellular level.

4.1.3.3 Maturation of NarGHI is still not evident

Completely devoid expression of nitrate reductase in the *ΔiscA/ΔerpA* and *ΔsufA*/*ΔiscA/ΔerpA* strains is based on the absence of Moco content in these strains. That the partial restoration of nitrate reductase activity in the *ΔiscA* and *ΔerpA* strains is based on their limited Moco content does not represent confirmation of the maturation of NarGHI by IscA or ErpA. Therefore, Fe-S cluster insertion can be performed by either ErpA or IscA or by other proteins that might replace each other at the cellular level under nitrate respiratory conditions. Our results are in contrast to Pinske and Sawers' study (Pinske and Sawers, 2012a, 2012b; Jaroschinsky, Pinske, and Sawers, 2017). It was concluded that ErpA and IscA are involved in the maturation of nitrate reductase by inserting Fe-S clusters into it. However, the study of Pinske and Sawers did not consider the reduced Moco content in the *ΔerpA* and *ΔiscA* strains since nitrate reductase activity depends not only on Fe-S clusters but also on the presence of Moco as a form of bis-MGD. Moreover, in our studies, we have shown the restoration of nitrate reductase activity despite the absence of an ErpA or IscA protein. The carrier proteins are involved in Fe-S cluster insertion into NarGHI can be analyzed by in vitro interaction study of purified NarGHI with carrier proteins such as ErpA, IscA or others using gel filtration.

4.1.3.4 The insertion of Fe-S clusters into FNR under anaerobic conditions

It has been previously reported that the FNR protein is essential and regulates the expression of many hundreds of genes under anaerobic conditions (Kang et al., 2005; Salmon et al., 2003). FNR directly regulates the expression of the *moa* and *narGHJI*

operon under nitrate respiratory conditions (Lamberg & Kiley, 2000; Melville & Gunsalus, 1996; Unden et al., 2002; Zupok et al., 2019). Therefore, it is crucial to understand how the Fe-S cluster is delivered to FNR for its maturation. Because our study has shown that the presence of ErpA is essential for the expression of nitrate reductase (*narGHI*) but not for its activity, it can be assumed that ErpA probably regulates the expression of *narGHI* indirectly by inserting the Fe-S cluster into MoaA and FNR. *PpepT-lacZ* was used to analyze the maturation of FNR in Wt MG1655 and in all the mutant strains. FNR activates the expression of *pepT* (Constantinidou et al., 2006; Dahl et al., 2013).

Under nitrate respiratory conditions, ErpA seems the most important Fe-S cluster carrier protein for the activation of FNR by inserting Fe-S clusters into it, since no transcription was detected for *pepT* in the *erpA*-deleted strain at the cellular level. Under this experimental condition, IscA or SufA was unable to replace ErpA. However, the exogenous coexpression of *psufA* and *piscA* with *pepT-lacZ* in the *erpA*-deleted strain showed that SufA and IscA are able to compensate for the role of ErpA in FNR activation. This result is consistent with findings from a previous study (D Vinella et al., 2013). The essential role of ErpA was replaced by SufA if sufficiently produced in cells. This was reflected in the partial (~50%) restoration of nitrate reductase activity in the *ΔerpA* strain based on the reduced Moco content. Complete restoration of FNR activity was achieved after the overexpression of *erpA* in the *ΔiscA/ΔerpA* strain, which was also reflected in the increased nitrate reductase activity in this strain. However, FNR activity was slightly lower in the *ΔiscA/ΔerpA* strain after the exogenous expression of *sufA* and *iscA* as compared to *erpA*. These observations suggest that ErpA is the most preferred Fe-S cluster carrier protein in FNR maturation under nitrate respiratory conditions.

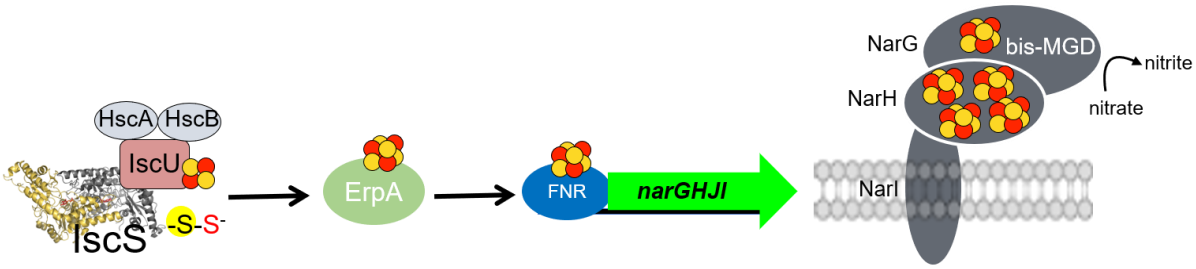

Figure 4-2: The insertion of Fe-S clusters into FNR under nitrate respiratory conditions

Holo-FNR activates the expression of *narGHJI* by binding at the promoter site. The activation of FNR requires a [4Fe-4S] cluster, which is inserted by ErpA under nitrate respiratory conditions. The Fe-S cluster is released from the scaffold protein IscU by the chaperones HscA and HscB, and further delivered into ErpA for insertion into FNR; IscS: PDB – 3LVM

Transcription of *pepT* was reduced to around ~60% in the absence of IscA compared to in the Wt MG1655 strain; these results are consistent with fidings from Kiley and coworkers (Mettert et al., 2008). They have shown that under fermentative conditions, the IscSUAhscBAfdx plays a significant role in Fe-S cluster insertion into FNR since the deletion of the *isc* operon leads to a significant reduction in *ydfZ* transcripts. This observation indicates that FNR activation might be slightly dependent on IscA at the cellular level under nitrate respiratory conditions. However, the exogenous *erpA* and *sufA* expression showed complete restoration of FNR activity in the *ΔiscA* strain. These results are consistent with the previous study (Mettert et al., 2008), in which the expression of SUF was able to rescue FNR activity in the *isc*-operon-deleted strain. This was reflected in the relatively enhanced nitrate reductase activity after *erpA* overexpression in the *ΔiscA* strain. However, the unaltered nitrate reductase activity after the *sufA* exogenous expression was based on the limited Moco content since SufA was unable to replace IscA or ErpA in MoaA maturation under nitrate respiratory conditions. Moreover, Kiley and her team have shown that FNR activity is unaltered in the *ΔsufA* or *ΔsufABCDSE* strains. This result is also consistent with our studies as an unaltered *pepT* expression was observed in the *ΔsufA* strain. However, the role of ErpA under anaerobic nitrate respiratory conditions for FNR maturation is not mentioned by Kiley and her team (Mettert et al., 2008). In contrast, we have shown that ErpA is an essential and most favorable Fe-S cluster carrier protein in FNR maturation. IscA or SufA can replace ErpA when produced sufficiently at the cellular level under nitrate respiratory conditions.

4.1.3.5 Autoregulation of *fnr* expression

The expression is *fnr* is autoregulated by [4Fe-S]-FNR, whereby holo-FNR binds to the promoter region for regulating the transcription of its own expression (Mettert & Kiley, 2007). This might explain the high accumulation of apo-FNR in the *Δfnr* strain. Similar results were obtained for *erpA*- and *iscA*-deleted strains. Since we have identified that ErpA performed FNR maturation under the nitrate respiratory condition, the deletion of this gene leads to inhibition of cluster transfer into apo-FNR and disrupts the regulation of *fnr* expression. This indicates high apo-FNR accumulation in the *ΔerpA*, *ΔiscA*, and *Δfnr* strains under anaerobic nitrate respiratory conditions.

4.1.4 The dominant expression of the *isc* operon compared to the *suf* operon under nitrate respiratory conditions

4.1.4.1 The expression of *iscR* under nitrate respiratory conditions

The expression of IscR was performed in all the strains using *piscR-lacZ* (Dahl et al., 2013) to determine the expression of the *isc* operon and compare it to the *suf* operon under nitrate respiratory conditions in different mutant strains.

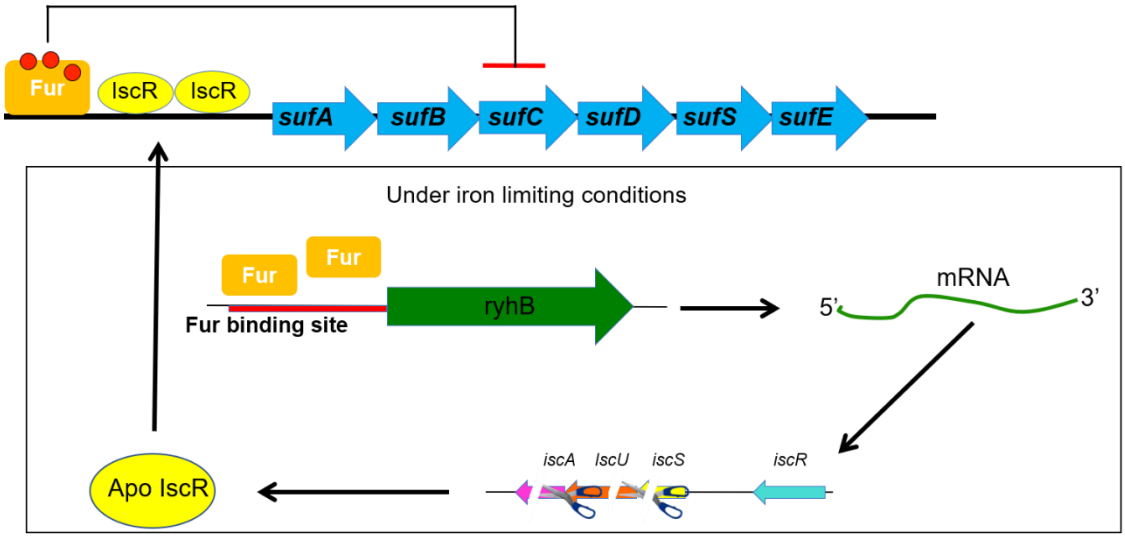

Figure 4-3: Model for apo-IscR regulation of the *suf* operon and degradation of the *isc* operon in the presence of iron

In the presence of iron, the isc operon expression is downregulated by Fur and a small mRNA *rhyB*; where *rhyB* binds at the upstream of *iscSUA* and cleaves the respective genes. The intact *iscR* is upregulated the *suf* operon for Fe-S cluster biosynthesis. The Fe^{2+}-Fur downregulated the expression of *suf* operon.

The unaltered *iscR* expression in the *ΔsufA* strain compared to in the Wt MG1655 strain is consistent with the findings from Frédéric Barras and coworkers (D Vinella et al., 2013), although Vinella et al. 2013 did not show *iscR* expression in the *nfuA*-deleted strain. However, *iscR* expression was significantly increased when *erpA* or *iscA* or both were deleted in our study. These results are also consistent with previous studies (Mettert & Kiley, 2014; D Vinella et al., 2013) that reported similar observations for *iscR* expression under anaerobic fermentative conditions, as distinct from our nitrate respiratory conditions. These showed an increased *iscR* expression based on the maturation of IscR (D Vinella et al., 2013). The relatively higher expression of *iscR* in *ΔerpA* and *ΔiscA, a*s well as in other *erpA*- or *iscA*-deleted double mutant strains, was due to the accumulation of apo-

IscR, since deletion of *erpA* or *iscA* leads to an inhibition in the transfer of Fe-S clusters into *iscR* (D Vinella et al., 2013). As a result, most of the IscR remain in their apo form. The apo-IscR is unable to bind to the promoter site of the *isc* operon and fails to regulate the repression of *iscR* expression since *iscR* is autoregulated by [2Fe-2S]-IscR (Fleischhacker et al., 2012; Giel et al., 2006, 2013; Roche et al., 2013).

On the other hand, *iscR* expression was significantly reduced in the *Δfnr* strain compared to the Wt MG1655 strain, which can be explained by the regulation of Fur. Fur plays an essential role in the low expression of *iscR* in the *Δfnr* mutant strain. Fur is a sensor for iron where, under iron-limiting conditions, it allows the transcription of *rhyB*, a small single-stranded RNA, which further degrades *iscSUA* and allow IscR to recruit the *suf* operon for transcription (Schwartz et al., 2001; Giel et al., 2006; Yeo et al., 2006; Lee, Yeo, and Roe, 2008). Fur protein expression was increased in the *Δfnr* strain since Fur negatively regulates FNR (Kumar & Shimizu, 2011). However, under nitrate respiratory conditions and the presence of all the Fe-S cluster carrier proteins, holo-IscR represses IscR expression, since the *iscR* expression is regulated by [2Fe-2S]-IscR (Fleischhacker et al., 2012; Giel et al., 2006, 2013; Roche et al., 2013). This leads to reduced IscR accumulation in the *Δfnr* strain.

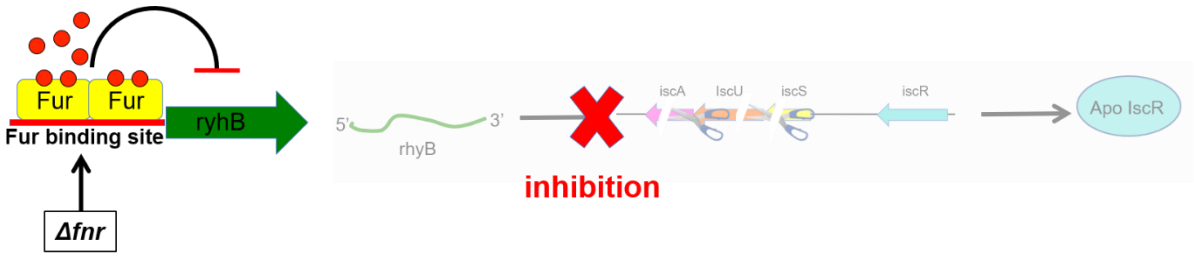

Figure 4-4: Analysis of iscR expression in the *Δfnr* strain under anaerobic nitrate respiratory conditions

iscR expression in the *Δfnr* strain is regulated by *rhyB* where, in the *Δfnr* strain, Fe^{2+}-Fur inhibit the expression of *rhyB* and, followed by the intact *isc* operon. The accumulation of apo-IscR is reduced

4.1.4.2 Expression of the *suf* operon under nitrate respiratory conditions

SufA acts as an Fe-S carrier protein, which belongs to the *suf* operon that consists of *sufABCDSE* genes (Chahal et al., 2009; Takahashi & Tokumoto, 2002; Wollers et al., 2010), expressed under oxidative stress or iron starvation conditions for Fe-S cluster

biosynthesis. Apo-IscR induces *suf* operon expression (Giel et al., 2006; Lee, Yeo, and Roe, 2008). Under aerobic conditions, SufA receives Fe-S clusters from the $SufBC_2D$ complex and deliveres them to the apo-enzymes. Under anaerobic nitrate respiratory conditions, it seems that SufA does not play any significant role in Fe-S cluster insertion either into MoaA or into FNR. This is reflected in the unaltered Moco content and *pepT* transcripts in the *ΔsufA* strain compared to in the Wt MG1655. To understand the role of SufA in Fe-S cluster insertion, *sufA* expression was analyzed in all the mutant strains and compared to the Wt MG1655 strain using a *psuf-lacZ* fusion, an immunoblot analysis using a SufS-derived antiserum and qRT-PCR. The *suf* operon transcription was almost consistent in all the mutant strains as in the Wt MG1655 strain, except for the *ΔiscA* and *Δfnr* strains. In the *ΔiscA* strain, *sufA* expression was downregulated compared to in the Wt MG1655 strain. The lower transcription of the *psufA-lacZ* fusion in the *ΔiscA* strain might be due to dose effects based on the higher copy number of the plasmid *pGE593*. On the other hand, *sufA* expression was not detectable in the *Δfnr* strain based on the Fur regulation. Fur plays a significant role in regulating the *suf* operon since the operon is negatively regulated by the Fe^{2+}-Fur protein (Outten, Djaman, and Storz, 2004; Lee, Yeo, and Roe, 2008; Mettert and Kiley, 2014), which allows indirect regulation of the *suf* operon in the absence of *fnr*. *fur* expression is increased in the absence of FNR based on the negative regulation of FNR in *fur* expression (Kumar & Shimizu, 2011), which leads the Fur protein to reduce the expression of the *suf* operon. As a result, *sufA* was not detectable in the *Δfnr* strain under nitrate respiratory conditions.

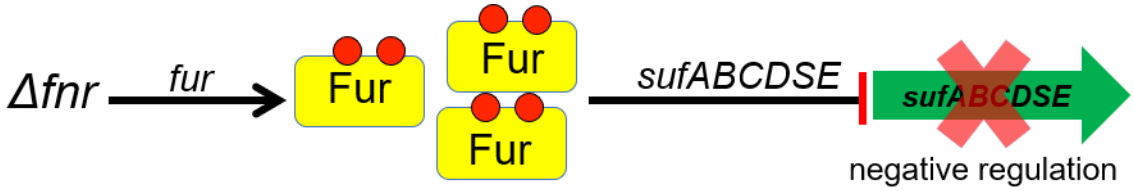

Figure 4-5: Analysis of the expression of the *suf* operon in the *Δfnr* strain under nitrate respiratory conditions

The downregulation of the *suf* operon in the *Δfnr* strain is regulated by Fe^{2+}-Fur and *rhyB* where, in the *Δfnr* strain, Fe^{2+}-Fur downregulates the expression of *rhyB,* and apo-IscR accumulation is reduced; this leads to inhibition of the recruitment of the *suf* operon by apo-IscR

Similar results were obtained using qRT-PCR, where *sufA* transcription was almost identical in all the mutant strains compared to in the Wt MG1655 strain. Moreover, the undetectable transcription of *sufA* in the *Δfnr* strain was also consistent as we also

observed for *PsufA-lacZ*. Patricia Kiley and her team have reported that *sufA* expression was increased ~2-3-fold as compared to the wild-type strain in the absence of both the *isc* operon and *fnr* under anaerobic fermentative conditions containing 0.2% glucose. This was explained as a result of the overlapping functions of the A-type carrier protein because SufA can replace the functions of IscA (Mettert et al., 2008). In contrast, under the nitrate respiratory condition, we have shown that *sufA* expression was slightly reduced or identical in the *ΔiscA* strain, and no expression was detected in the *Δfnr* strain. Our results were not consistent with previous observations based on differing experimental conditions (Mettert et al., 2008). Kiley and coworkers cultivated cells without nitrate, but in an M9 minimal-glucose medium, which induces fermentation in cells. Consequently, *fnr* is repressed since the expression of *fnr* is repressed by glucose under anaerobic conditions (Stephen Spiro & Guest, 1987). FNR repression was shown in our study, where nitrate reductase activity in the Wt MG1655 strain was reduced around ~80% in the presence of 0.2% glucose compared to when glucose was absent. This observation indicates that the presence of glucose significantly represses the expression of *narGHI* through FNR. Moreover, it has been reported that IscA and SufA paralogues are necessary for assembling and transferring [4Fe-4S] clusters in to the enzymes of multiple physiological pathways and for complementing each other's functions (Lu et al., 2008; Tan et al., 2009). This observation was also contradicted in our study. The previous studies were also performed under aerobic conditions in the presence of glucose and without nitrate, which represses FNR protein expression (Lu et al., 2008; Tan et al., 2009). As a result, the *suf* operon was induced and took part in the assembly of Fe-S clusters.

Under anaerobic nitrate respiratory conditions, both the *isc* and *suf* operons were expressed. However, the expression of the *suf* operon seems much lower in our study than the fermentation conditions used by Kiley and coworkers (Mettert et al., 2008). They have reported that the expression of *sufA* is increased in *iscA*- and *fnr*-deleted strains (Mettert et al., 2008). The expression of *sufA* using *PsufA-lacZ* fusion in the mutant strains was reduced around ~20-fold compared to the expression of *iscR* by *PiscR-lacZ* fusion. This observation also underlines the importance of the ISC system under nitrate respiratory conditions, in contrast to the SUF system.

Immunodetection of SufS and analysis of the gene expression of *iscA* were also carried out in our study to determine the expression of the *suf* operon, since the *suf* operon consists of *sufABCDSE* genes. Immunodetection by SufS-derived antisera also confirmed an almost identical amount of SufS in all the mutant strains, except for the *ΔiscA* strain

and the *ΔsufA/ΔiscA* double mutant strain, where the SufS was slightly reduced. These results are also consistent with the previous *sufA* expression results by *psufA-lacZ* and qRT-PCR in our study. Moreover, the slightly reduced expression of *sufA* was observed for *psufA-lacZ* or in qRT-PCR and SufS in the immunoblot analysis for *ΔiscA* and *ΔerpA* and for other double mutant strains in our study. Overall, this limited expression of *sufA* in the mutants reflects that SufA could not replace the functions of IscA or ErpA under anaerobic nitrate respiratory conditions. Therefore, the role of SufA as an Fe-S cluster carrier is not involved in the maturation of FNR under anaerobic nitrate respiratory conditions. Similar results were obtained for MoaA, where SufA was unable to complement ErpA and IscA in their roles.

4.1.5 The influence of iron content in *erpA*- and *iscA*-deleted strains under nitrate respiratory conditions

In the assembly of Fe-S clusters, the source of the iron donor is still elusive. It has been proposed that CyaY-frataxin homologs in eukaryotes and IscX can be the potential donor of iron in Fe-S cluster biosynthesis (Huynen et al., 2001; Kim et al., 2014). However, both of these have shown weak binding to iron under physiological conditions. Deletion of *iscx* and *cyaY* resulted in a very slight decreased activity of Fe-S cluster containing enzymes. Huangen Ding and coworkers have shown that IscA or SufA might be functioning as an iron chaperone, where deletion of either one can lead to the accumulation of a red-colored cysteine desulfurases in wild-type *E. coli* (Yang et al., 2015), reflecting the depletion of intracellular iron for Fe-S cluster assembly. This leads to impede sulfur delivery by IscS, and result in the accumulation of red IscS in *E. coli* cells (Yang et al., 2015). In our studies, Moco biosynthesis was significantly impaired in *ΔiscA* and *ΔerpA* strains based on the reduced Fe-S cluster insertion into MoaA. The iron content determination in the *ΔiscA* and *ΔerpA* strains confirmed the presence of sufficient iron. This indicates the availability of iron for Fe-S cluster assembly. Therefore, reduced Moco content in the *ΔiscA* and *ΔerpA* strains was based on impaired MoaA activity based on the lack of Fe-S cluster transfer into it. ErpA and IscA are involved in Fe-S cluster insertion into MoaA rather than acting as iron donors.

4.2 Regulation of *torCAD* expression under anaerobic TMAO respiratory conditions

Under anaerobic conditions, TMAO reductase catalyzes the formation of TMA. TMAO is an alternative terminal electron acceptor like nitrate under anaerobic conditions (Wissenbach, Kröger, and Unden, 1990; Wissenbach, Ternes, and Unden, 1992; McCrindle, Kappler, and McEwan, 2005). Unlike nitrate reductase, TMAO reductase does not contain any Fe-S clusters as a cofactor, but both contain bis-MGD as form of Moco (Czjzek et al., 1998). The devoid TMAOR reductase activity in the *ΔiscA/ΔerpA* and *ΔsufA/ΔiscA/ΔerpA* strains was based on inactive MoaA because ErpA and IscA are involved together in the maturation of MoaA under TMAO and nitrate respiratory conditions. The reduced TMAO reductase activity in the *ΔerpA* strain was due to the partially active MoaA. This was identical to the Moco content under nitrate respiratory conditions for the *ΔerpA* strain. So far, it has been reported that under the anaerobic condition, the TMAO reductase expression is independent of FNR regulation (Pascal, Burini, and Chippaux, 1984; Iuchi and Lin, 1988; Spiro and Guest, 1990). Therefore, it was important to determine TMAOR activity in the *Δfnr* strain. The result was unexpected since the TMAOR activity was reduced around ~65% for the *fnr*-deleted strain compared to the Wt MG1655 strain. This observation indicates the requirement of FNR for the complete expression of *torCAD*. Therefore, it was essential to determine *torA* expression in all the mutant strains. The *torCAD* expression was remarkably reduced in the *ΔiscA*, *ΔerpA*, and *Δfnr* mutant strains compared to in the Wt MG1655, which was also reflected from TMAOR activity in the former strains. These observations suggest that *torCAD* expression is regulated by FNR. The relatively lower expression of *torCAD* in *erpA*- and *iscA*-deleted strains might be based on the reduced Moco content. The reduced TMAOR enzyme production level in these strains was confirmed by immunodetection of TorA. The devoid expression of *torCAD* in *ΔiscA/ΔerpA* and in the *ΔsufA/ΔiscA/ΔerpA* strain was due to the lack of Moco production by these strains, reflected in the undetected TorA protein in the immunoblot analysis. TorA was probably not produced by the cells because, this way, cells conserve energy to prevent the unnecessary production of apo-enzymes that will not be functional due to the absence of cofactors. So far, it has been shown in our studies that *torCAD* expression is significantly reduced in the *Δfnr* strain, which indicates that the presence of FNR protein influences expression of the *torCAD* level.

In our study, we showed that the absence of FNR negatively influences TMAOR activity by reducing *torCAD* expression. FNR might bind at the promoter site and activate

transcription of the operon. By analyzing the upstream sequence of the *torCAD* operon around the +34 to +48 region, the TTGCTCATTAAGAT sequence has been identified as the FNR binding site correlated with the FNR consensus sequence (Eiglmeier et al., 1989; Gerasimova et al., 2001). Reduced β-galactosidase activity was observed in consensus sequence substitution of TTGTC by GGGTC, indicating a lack of *torCAD* expression. The substitution of TT by GG had a substantial impact on β-galactosidase activity compared to GCT by AAA. However, the significant loss of β-galactosidase activity in Wt MG1655 and in the *Δfnr* strain for the substitution of TT by GG compared to *torCAD-lacZ* in the *Δfnr* strain indicated that TT might not be involved in FNR binding; instead, this sequence is essential for the polymerase- or sigma-factor binding for transcription. Therefore, the removal of TT probably leads to disruption of polymerase binding for transcription. However, the *fnr*-deleted strain might still negatively influence *torCAD*-operon expression through another regulatory protein, NarL. NarL functions as a repressor in *torCAD* expression (Iuchi & Lin, 1987a). The *narL* expression is increased in the absence of FNR since NarL negatively regulates the expression of *fnr*.

4.3 Model for Fe-S clusters insertion under nitrate and TMAO respiratory conditions

Overall, we want to summarize our results in the following model, whereby we investigated Fe-S cluster insertion into MoaA and FNR under anaerobic respiratory conditions. Under this condition, the ISC system plays a major role in Fe-S cluster assembly, since the SUF system is activated under oxidative stress and iron-limiting conditions. The [2Fe-2S] clusters are assembled on the scaffold protein IscU and passed to IscA and further to ErpA, which delivers it to the target protein. It is believed that the [4Fe-4S] clusters are assembled on these proteins. In our study, we mainly analyzed the Fe-S cluster insertion into MoaA for Moco biosynthesis and FNR, the major transcriptional regulator under the anaerobic condition. Under both nitrate and TMAO respiratory conditions, IscA and ErpA insert Fe-S clusters into MoaA, since the reduced Moco content was obtained in *erpA*- and *iscA*-deleted strains and the *ΔiscA*/*ΔerpA* double mutant strain was completely devoid of Moco. Moreover, SufA is unable to substitute the roles of both proteins under these conditions. For FNR maturation, ErpA is the major A-type carrier protein, a role that is not substituted by IscA and SufA under cellular conditions of nitrate respiration. Completely devoid *narG* transcription in the *ΔerpA* strain indicates that the expression of *narGHI* is indirectly regulated by ErpA via the maturation of FNR. Moco insertion into apo-NarG is

performed after the insertion of Fe-S clusters into the enzymes. The pathway of Fe-S cluster carrier proteins into nitrate reductase still need to be determined. Probably ErpA or IscA are also involved in this step, as suggested by Pinske and Sawers. Therefore, FNR targets operons coding for Fe-S cluster-containing enzymes that are not expressed in the absence of A-type carrier proteins. This might be a way for the cell to conserve energy to prevent the unnecessary production of apo-enzymes that will not be functional when either Fe-S clusters or A-type carrier proteins are absent.

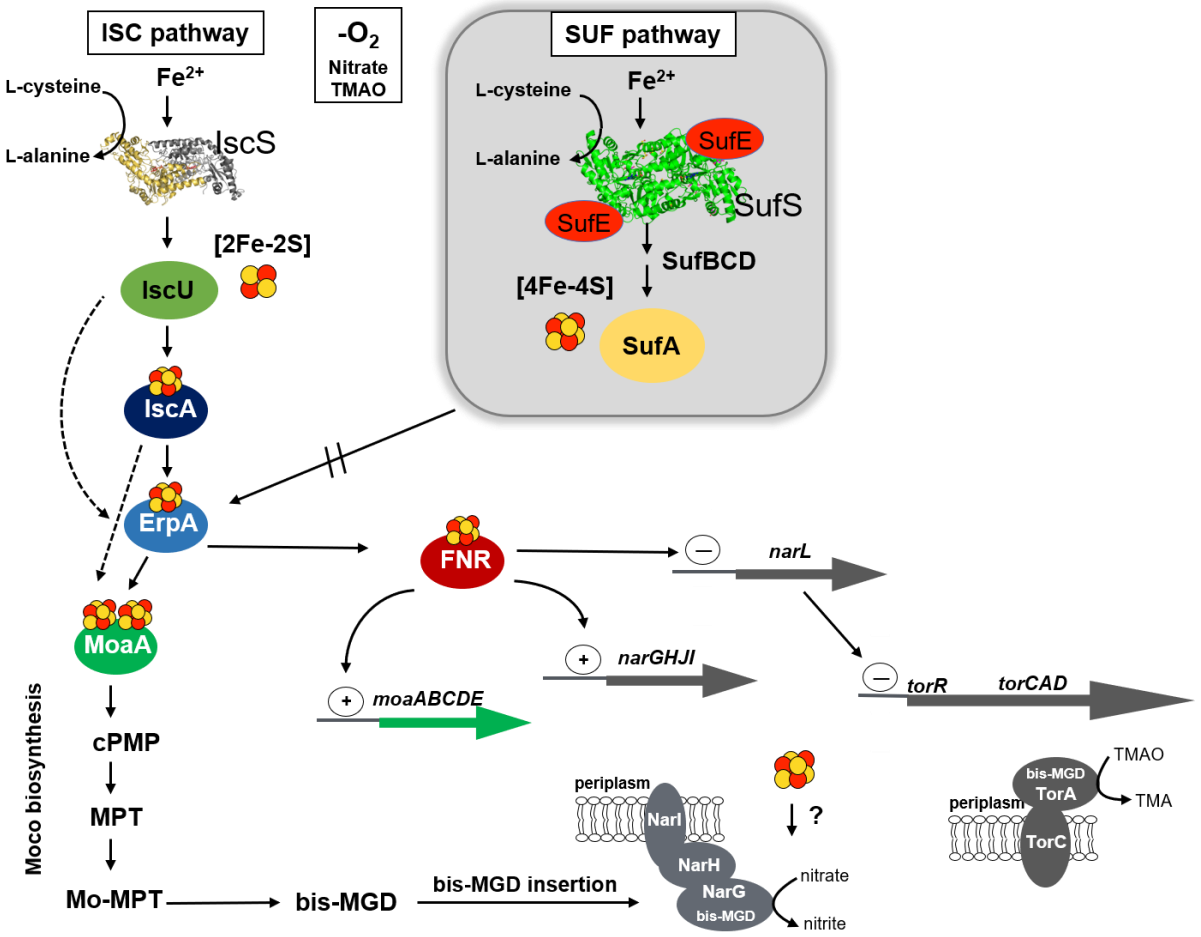

Figure 4-6: Model for Fe-S cluster insertion into MoaA and FNR under anaerobic nitrate and TMAO respiratory conditions

The ISC system plays a major role in Fe-S cluster biosynthesis, whereas the SUF system is generally expressed under oxidative stress and iron-limiting conditions. The [2Fe-2S] clusters are assembled on IscU and pass to IscA and further to ErpA, which delivers it to the target protein (the dotted line shows that IscU is also able to directly supply the [4Fe-4S] clusters to ErpA). Both IscA and ErpA can insert Fe-S clusters into MoaA. SufA is unable to substitute the roles of both proteins under these conditions partially, based on a low expression. For FNR maturation, ErpA is the major A-type carrier protein, a role that is not substituted by IscA and SufA under cellular conditions of nitrate respiration. FNR activates transcription of the *narGHJI* operon and the *moaABCDE* operon. Moco, in general, is inserted into apo-molybdoenzymes, like NarG and TorA, after the insertion of Fe-S clusters into the enzyme.

The proteins that insert Fe-S clusters into NarGHI were not investigated in this study. The deletion of *fnr* contributes to the low expression of the torCAD operon via NarL, since NarL acts as a repressor of the *torCAD* operon under TMAO respiratory conditions; IscS: PDB – 3LVM; SufS: PDB – 6O10

FNR indirectly regulates the expression of *torCAD*, which is reflected in significantly reduced TMAO reductase activity and *torCAD* expression in the *Δfnr* strain. Deletion of *fnr* contributes to the low expression of the *torCAD* operon via another regulator protein, NarL (Iuchi & Lin, 1987a). The deletion of *fnr* upregulates the expression of *narL*, whereby NarL acts as a repressor of the *torCAD* operon under TMAO respiratory conditions and reduces the expression of *torCAD*.

A similar model of Fe-S cluster insertion has been reported by Fédéric Barras and coworkers in the maturation of IspG and IspH. They have shown that the Fe-S cluster is directly transferred into ErpA and IscA from IscU under the anaerobic condition (Daniel Vinella et al., 2009). ErpA is the most preferred Fe-S cluster carrier protein in the maturation of IspG/H, and IscA can also insert the Fe-S clusters directly or via ErpA (Daniel Vinella et al., 2009). This is consistent with our findings, as we have shown that ErpA and IscA are involved in the maturation of MoaA under anaerobic respiratory conditions. Moreover, the apo-FNR maturation model from Patricia Kiley and her team show a major involvement of the Isc pathway in FNR maturation under anaerobic conditions (Mettert et al., 2008). In our study, we have additionally shown that ErpA is necessary for the maturation of FNR and this role cannot be taken over by IscA for *pepT* and *narG* expression.

4.4 Fe-S cluster insertion in MoaA under aerobic conditions

So far in our study, we have been able to quantify the Moco content, nitrate reductase activity, and TMAO reductase activity under anaerobic nitrate and TMAO respiratory conditions. However, under the aerobic condition in the presence of nitrate, both the Moco content and nitrate reductase activity were significantly reduced, at around ~80% as compared to under anaerobic conditions. This significant reduction is mainly based on FNR regulation since FNR activity is directly regulated by oxygen or oxidative stress conditions. Under aerobic conditions, FNR dimer inactivates via oxidation of [4Fe-4S] to a [2Fe-2S] cluster and apo-FNR is formed. Apo-FNR is unable to influence *moa*-operon and *narGHI* expression, which was reflected in reduced Moco content and nitrate reductase activity. Moreover, the requirement of nitrate reductase is significantly reduced in the

presence of oxygen as compared to under anaerobic conditions. This leads to reduce the expression of nitrate reductase and consequently, the biosynthesis of Moco is also significantly reduced as Moco is no longer required for cellular respiration. Under aerobic conditions, no alteration in Moco content and nitrate reductase activity was observed for the mutant strains compared to the Wt strain. This suggests that ErpA and IscA are not involved in MoaA maturation under the aerobic condition, as observed under anaerobic nitrate respiratory conditions.

4.5 Maturation of EcPaoABC and RcXDH

In this part of the study, we investigated Fe-S cluster insertion into the *E. coli* periplasmic aldehyde oxidase (PaoABC) and *R. capsulatus* xanthine dehydrogenase (XDH). The overexpression, purification, and characterizations of the enzymes from different mutant strains showed that ErpA is involved in the maturation of PaoABC by inserting Fe-S clusters into it. However, we were unable to determine whether ErpA is able to insert the [2Fe-2S] or [4Fe-4S] cluster or both into PaoABC. Moreover, the XDH from mutant strains showed no significant difference in activity.

4.5.1 ErpA is essential for the maturation of EcPaoABC

The aerobically expressed PaoABC from Wt MG1655 and other mutant strains were purified by Ni^{++}-NTA and followed by size exclusion chromatography (SEC). A similar purity was achieved after the SEC of expressed PaoABC in the *ΔiscA*, *ΔnfuA*, and *ΔsufA* strains as with the Wt MG1655 strain. The SDS-PAGE analysis of purified protein showed clear bands at 78 kDa, 34 kDa, and 21 kDa for the PaoC, PaoB, and PaoA with minor bands of impurities. This result was also reflected in the almost identical chromatograms of the expressed PaoABC from the Wt MG1655, *ΔiscA*, *ΔnfuA*, and *ΔsufA* strains. However, the chromatogram of expressed PaoABC from the *ΔerpA* strain showed the elution of the aggregated protein. This observation indicates poor expression of PaoABC, which contained relatively high impurities or contaminants, as confirmed by many irrelevant SDS-PAGE analysis bands. The poor expression and high impurities of PaoABC in the absence of ErpA were also reflected in the purity analysis by UV-visible spectra. The purity of molybdoflavo-enzymes is determined from the absorbance ratio of A280/A445. The significantly high value of ~26 for the absorption ratio of A280/A445 suggests that purified PaoABC expressed in the *ΔerpA* strain contains remarkably high impurities and extremely poor cofactor loading, since the ideal ratio is less than 5.0 for the

other molybdometalloflavo-enzymes (Hartmann et al., 2012). These observations were also correlated with the eluted dark brown color of PaoABC from the Wt MG1655, *ΔiscA*, *ΔnfuA*, and *ΔsufA* strains. The color indicates the presence of flavin cofactor (Michaelis, Schubert, and Smythe, 1936), together with Fe-S clusters (Adinolfi et al., 2009b). However, the transparent color for eluted PaoABC from the *ΔerpA* strain also reflected poor cofactor loading into the enzyme. This result is correlated to the insignificant FAD shoulder in UV-visible spectra with extremely reduced flavin content for PaoABC expressed in the *ΔerpA* strain compared to in the Wt MG1655 strain. Moreover, poor Fe-S cluster loading was obtained in the expressed PaoABC from the *ΔerpA* strain, which is reflected in significantly reduced (~85%) iron saturation of expressed PaoABC compared to the expressed PaoABC from the Wt MG1655 strain. This observation indicates the failure of insertion of [2Fe-2S] or [4Fe-4S] clusters or both in the absence of ErpA. Moreover, overall iron saturation of PaoABC expressed in the Wt MG1655, *ΔnfuA*, and *ΔsufA* strains was reduced around ~40% compared to the previously reported by Neumann et al. (2009), which was 101% for PaoABC that was expressed in the *ΔmobAB* strain. A slight reduction in iron saturation of expressed PaoABC in the *ΔiscA* strain suggests the importance of IscA as an Fe-S cluster carrier protein in the maturation of PaoABC. However, this does not affect enzyme activity, which was reflected in the unaltered specific activity of PaoABC expressed in the *ΔiscA* strain compared to in the Wt MG1655 strain.

Furthermore, overall molybdenum saturation was significantly lower for the expressed PaoABC in all the strains in our study. It has been reported that the purified PaoABC overexpressed in *ΔmobAB* strain showed ~58% molybdenum saturation (Neumann, Mittelstädt, et al., 2009), whereas it was around ~20% in our study. The significantly reduced molybdenum saturation might be based on the different expression strains (Neumann, Mittelstädt, et al., 2009), where the production of bis-MGD is inhibited in the *ΔmobAB* strain since MobA and MobB are involved in the conversion of bis-MGD from Mo-MPT (Lake et al., 2000; Palmer et al., 1996). Therefore, all the Mo-MPT is converted into MCD. In contrast, Mo-MTP might be converted into both bis-MGD and MCD in our study, which further reduced the overall molybdenum saturation. Molybdenum saturation was remarkably reduced to ~85% for the expressed PaoABC in the *ΔerpA* strain compared to in the Wt MG1655 strain, which was consistent with the reduced Moco content (~88%) in the same strain. These results were correlated to poor expression of the enzyme based on a significantly reduced iron saturation and flavin content in the absence of ErpA, as mentioned above. However, similar molybdenum saturation and

Moco content of the expressed PaoABC from the *ΔiscA* strain compared to from the Wt MG1655 strain was obtained despite the slightly reduced iron saturation. A significant reduction in molybdenum saturation and Moco content for PaoABC expressed in the *ΔsufA s*train was also observed.

A similar Moco content from the cell extract of the Wt MG1655, *ΔiscA*, *ΔerpA, ΔsufA* and *ΔnfuA* strains was obtained, based on the unperturbed Moco content in the analyzed strains, under aerobic conditions. Therefore ErpA, IscA, NfuA, and SufA do not play any significant role in the maturation of MoaA. Under anaerobic conditions, however, ErpA and IscA insert Fe-S clusters into MoaA. Moreover, the cellular Moco content of the *ΔsufA* strain was unperturbed, compared to the Wt MG1655 strain. In contrast to these findings, no Moco was detected from the expressed PaoABC in the *ΔsufA* strain.

In our study, the significantly reduced iron content of expressed PaoABC in the *ΔerpA* strain led to identifying the different forms of Fe-S clusters since the purified PaoABC contained both [2Fe-2S] and [4Fe-4S] clusters. The significant reduction in the peak intensity of CD spectra of PaoABC expressed in the *ΔerpA* strain compared to the Wt MG1655 strain confirmed the absence of [2Fe-2S] clusters, as has also been reported for XDH (Schumann et al., 2008). We were not able to detect the presence of [4Fe-4S] clusters in our study, since no significant difference in the signal transition was obtained in the presence or absence of [4Fe-4S] in CD spectra. Similar CD spectra of expressed PaoABC in the Wt MG1655, *ΔnfuA*, and *ΔiscA* strains were obtained, indicating that IscA and NfuA might not play a role in the maturation of PaoABC.

The significant reduction in FAD, iron saturation and Fe-S clusters loading to the expressed PaoABC in the *ΔerpA* strain reflects the poor expression, structural integrity, and folding of the enzyme. Since insertion of the Fe-S cluster occurs before the Moco insertion, this indicates that ErpA is necessary for insertion of both [2Fe-2S] and [4Fe-4S] clusters into PaoABC. Moreover, it has been reported that [4Fe-4S] clusters are required for the structural integrity of the PaoB subunit, since the removal of one of the four coordinating cysteine residues hampers the formation of stable protein (Correia et al., 2016). The significantly reduced Moco loading of the expressed PaoABC in the *ΔsufA* strain might indicate the lack of [4Fe-4S] cluster insertion, as Fe-S cluster insertion is prioritized over Moco insertion in vivo. Moreover, CD spectra show that SufA is not essential for inserting [2Fe-2S] clusters in RcXDH, but probably plays an important role in [4Fe-4S] insertion into PaoABC. Conclusively, ErpA is essential for EcPaoABC maturation

by inserting [2Fe-2S] together with [4Fe-4S] clusters. In addition, SufA is involved in [4Fe-4S] clusters' insertion into EcPaoABC.

4.5.2 Purification of RcXDH from *E. coli* mutant strains

Xanthine dehydrogenase (XDH) from *R. capsulatus* was heterologously expressed in the *E. coli* mutant strains in our study. The purity of the expressed XDH in the *ΔerpA*, *ΔnfuA*, and *ΔsufA* strains was almost identical to that in the Wt MG1655 strain, where the SDS-PAGE gel showed two clear bands at 83.0 kDa and 50.0 kDa for the XdhB and XdhA subunit, respectively. However, the expressed XDH in the *ΔiscA* strain showed relatively more contaminations than the Wt MG1655 strain. The purity was also confirmed from the UV-visible spectra of XDH expressed from the mutant strains using the FAD-characterized peak shoulder at 465nm (Leimkühler et al., 2003). The identical peak shoulder at 465 nm was obtained for purified XDH that expressed in the Wt MG1655, *ΔerpA*, *ΔnfuA*, and *ΔsufA* strains, with the exception of the *ΔiscA* strain. The cofactor loading into the expressed enzyme in all the strains was ideal for the molybdoflavo-proteins, which was reflected in the absorbance ratio (A280/A465) of around 5.0. This result is consistent with Leimkühler et al., 2003, where the purified XDH from the *ΔmobAB s*train has been reported with an absorbance ratio (A280/A465) of 5.23. This observation suggests that the expressed XDH in all the strains was optimally loaded with FAD and [2Fe-2S] clusters. However, the poor flavin loading of expressed XDH from the *ΔiscA* strain was reflected in the relatively high A280/A465 ratio of around ~8.6. This was confirmed by the 36%-reduced flavin content of the expressed XDH in the *ΔiscA* strain compared to in the Wt MG1655 strain.

Moreover, the molybdenum saturation in purified enzymes showed that most of the XDH was in Moco-free form, and around ~38% of XDH contained Mo-MPT as a cofactor. This was significantly lower compared to the MPT content reported by Schumann et al. (2008), which was around ~95%. This significant low Moco content might be based on the different expression strain, since Schumann *et al.*, 2008 used *ΔmobAB* strain for expressing RcXDH. The molybdenum saturation was 30% reduced for the XDH expressed in the *ΔerpA* and *ΔnfuA* strains. This result also accorded with the slightly reduced Moco content for XDH expressed in the *ΔerpA* strain. On the other hand, the overall iron saturation of purified XDH expressed in the Wt MG1655 was around 55%, significantly lower compared to the 95% saturation reported by Schumann et al. (2008). Moreover, the reduced (~ 36%) iron saturation of the expressed XDH from the *ΔiscA* strain compared to the Wt MG1655

strain might negatively influence FAD loading into the enzyme since the flavin content was also reduced significantly in the absence of IscA. Moreover, a similar CD-spectra signal transition obtained at 434 nm and at 470 nm for XDH expressed in all the strains suggests the presence of [2Fe-2S] clusters, which Schumann et al. (2008) had also reported.

In our study, we were not able to determine the *E. coli* Fe-S cluster carrier protein that inserts [2Fe-2S] clusters into RcXDH, with the exception of the *iscA*-deleted strain based on the reduced iron saturation and FAD content. It might be due to the heterologous system of expression, since XDH from *R. capsulatus* was expressed in the *E. coli* strain in our study. This leads to the maturation of RcXDH in a non-native system, which indicates that the carrier proteins involved in RcXDH maturation are only present in *R. capsulatus.* This might be the reason why we were unable to detect the Fe-S cluster-inserting protein for RcXDH in *E. coli*.

4.6 Model for Fe-S clusters insertion into EcPaoABC and RcXDH under aerobic respiratory conditions

Overall, we want to summarize our results in the following model, where we investigated Fe-S cluster insertion into MoaA, EcPaoABC, and RcXDH under aerobic respiratory conditions. Under this condition, the SUF system plays a major role in Fe-S cluster assembly, whereas the ISC system is only involved to a minor extent, since the *isc* operon is generally cleaved by Fur/*rhyB* expression in the presence of oxygen that leads to oxidation of the Fe-S cluster. The [2Fe-2S] clusters were assembled on the scaffold protein SufBCD or IscU and passed to A-type carrier proteins for delivery of the cluster to the target protein. It is believed that the [4Fe-4S] clusters are assembled on these carrier proteins. In our study, we mainly analyzed Fe-S cluster insertion into MoaA for Moco biosynthesis, *E. coli* periplasmic aldehyde oxidase (EcPaoABC) and *R. capsulatus* xanthine dehydrogenase (RcXDH) under aerobic conditions. The maturation of EcPaoABC is performed by ErpA and SufA. ErpA inserts both [2Fe-2S] and [4Fe-4S] clusters into PaoA and PaoB based on the poor expression, significantly reduced iron content and devoid Fe-S cluster signals in CD spectra of the expressed PaoABC in the *ΔerpA* strain. In addition, SufA inserts [4Fe-4S] clusters into PaoB in the maturation of EcPaoABC. The maturation of RcXDH and MoaA still needs to be determined. However, it seems that ErpA, IscA, SufA, and NfuA are not involved in the maturation of RcXDH and MoaA. Therefore, other Fe-S cluster carrier proteins such as BolA, GrxA/B/C/D, and Mrp might be involved in the maturation of these enzymes under aerobic conditions.

Our model for the maturation of EcPaoABC under the aerobic condition is consistent with the model reported by Fédéric Barras and coworkers in the maturation of IspG and IspH (Daniel Vinella et al., 2009). They have shown ErpA can directly transfer the Fe-S cluster into IspG/H, whereas IscA requires ErpA under aerobic conditions. We have shown that SufA is involved in the insertion of the [4Fe-4S] cluster into EcPaoABC, which is also consistent with the previously reported study, which has shown that the maturation of IspG/H is performed by SufA under conditions of oxidative stress (Daniel Vinella et al., 2009).

It has been reported that Fe-S cluster insertion into a Mocs1A-MoaA homolog of humans has not been investigated so far (R R. Mendel et al., 2020). In human, Mosc1A and Mocs1B are involved in the formation of 5'GTP to cPMP, which is produced and localized in mitochondria (Hanzelmann et al., 2004). However, Moco is formed in the cytoplasm. Therefore, cPMP is transported into the cytoplasm via Atm3 transporter, which is a homolog of ABC transporter, namely ABCB7 in human (Gerber et al., 2008; Teschner et al., 2010).

It has been reported that the assembled [2Fe-2S] cluster in mitochondria is further transferred to GLRX5 via chaperone proteins and can be directly delivered into the target apoprotein (Lill, 2020). However, since GLRX5 is not essential, the protein function can be bypassed by direct transfer of [2Fe-2S] to ISCU2 (R R. Mendel et al., 2020). However, in case of [4Fe-4S] clusters insertion into Mocs1A, It is believed that the [4Fe-4S] cluster insertion is performed by mitochondrial A-type ISC proteins like IscA1, IscA2, and IBA57 (Beilschmidt et al., 2017; Ulrich Mühlenhoff et al., 2011; Sheftel et al., 2012). It has also been reported that the GLRX5 transfer the [2Fe-2S] clusters into IscA1/2 to assemble the [4Fe-4S] cluster. However, the mechanism by which these proteins assist the fusion of the two [2Fe-2S] clusters to one [4Fe-4S] cluster (R R. Mendel et al., 2020) is still unclear. Recently it has been shown that mitochondrial [4Fe-4S] cluster biosynthesis and trafficking is a dynamic system involving other proteins such as Nfu1, Ind1 and BolA3 (Maio & Rouault, 2020).

However, Fe-S cluster assembly is also taken place in the cytosol. It has been reported that the mitochondrial ISC system is essential for the cytosolic Fe-S cluster assembly (CIA) (Netz et al., 2014; Paul & Lill, 2015), where mitochondrial ISC machinery generates a sulfur-containing factor, which is exported to the cytosol via ABCB7 transporter for cytosolic Fe-S cluster assembly by the CIA machinery (Biederbick et al., 2006; Gerber et al., 2008; Kispal et al., 1999; Stehling et al., 2008). The trafficking of [4Fe-4S] clusters

from CIA machinery is performed by CIA targeting complex (CTC), which is composed of CIAO1, CIAO2B, and MMS19 (Gari et al., 2012; Srinivasan et al., 2007). This complex is able to perform specific interaction to the target apoprotein like aldehyde oxidase or aconitase and deliver the cluster.

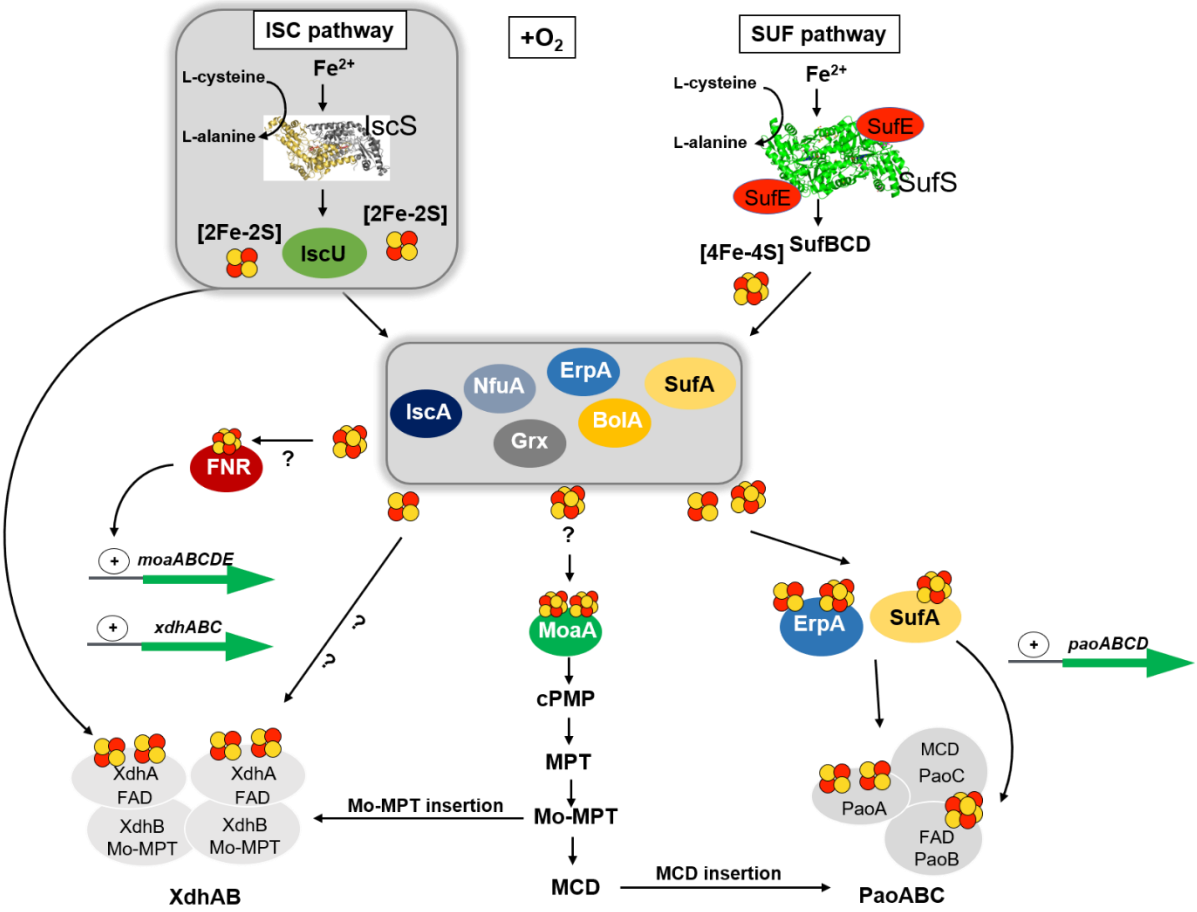

Figure 4-7: Model for Fe-S cluster insertion into RcXDH and EcPaoABC under aerobic respiratory conditions

Under aerobic conditions, the SUF system plays a major role in Fe-S cluster biosynthesis, whereas the ISC system is only involved to a minor extent, since the *isc* operon is generally cleaved by Fur/*rhyB* expression in the presence of oxygen that leads to oxidation of the Fe-S cluster. The mRNA of *isc* operon is generally cleaved by Fur/*rhyB* expresson under oxidative stress and iron-limiting conditions. The assembled [2Fe-2S] and [4Fe-4S] clusters on the SufBCD complex were further passed to ErpA, which is involved in the maturation of PaoABC by inserting both [2Fe-2S] and [4Fe-4S] clusters. Moreover, SufA might be required only for [4Fe-4S] clusters. The Fe-S cluster carrier protein that is involved in [2Fe-2S] cluster insertion into XDH was not identified from our study. Under aerobic conditions, the insertion of Fe-S clusters into MoaA and FNR remained undetected. FNR activates the transcription of the *moaABCDE* operon. Moco, in general, is inserted into apo-molybdoenzymes, like PaoC and XdhB, after the insertion of Fe-S clusters into the enzyme; ; IscS: PDB – 3LVM; SufS:PDB – 6O10

5 Outlook

This study mostly focused on the connections between Fe-S clusters and Moco biosynthesis under anaerobic conditions. We have investigated the Fe-S clusters insertion into MoaA, which is performed by IscA and ErpA at the cellular level under anaerobic nitrate and TMAO respiration conditions. However, the most preferred Fe-S cluster carrier protein in MoaA maturation at the cellular level has not been determined from our study. Therefore, it is important to identify a hierarchy of Fe-S cluster carrier proteins in the maturation of MoaA in the future. Moreover, we were not able to show any interaction between IscA and ErpA to MoaA since we only perform *in-vivo* maturation of MoaA based on the Moco content. Therefore, further studies can be carried out by analyzing the interaction of MoaA to Fe-S cluster carrier proteins IscA and ErpA *in-vivo* by using fluorescence resonance energy transfer (FRET) and bacterial two-hybrid system (B2H). Moreover, *in-vitro* interaction can also be performed using the purified proteins by microscale thermophoresis. Therefore, it is necessary to optimize the expression and purification of the *E. coli* MoaA enzyme in the future. Moreover, *in vivo* MoaA maturation under aerobic conditions is still unknown. Therefore, further studies are necessary to identify the Fe-S cluster carrier proteins in the maturation of MoaA under aerobic conditions. This can be performed by creating double and triple mutants in different combinations using Fe-S cluster carrier proteins such as ErpA, NfuA, IscA, BolA, SufA, GrxA/B/C/D, and Mrp.

The Fe-S cluster insertion into molybdoenzymes such as nitrate reductase (NR), Format dehydrogenase (Fdh) and Xanthine dehydrogenase (XDH) in *E. coli* is still unclear. It has been reported that deletion of *erpA* and *iscA* strongly reduced the specific activity of Fdh-N and nitrate reductase enzyme. However, the study of Pinske and Sawers did not consider the reduced Moco content of the *ΔerpA* and *ΔiscA* strains since ErpA and IscA are involved in MoaA maturation in Moco biosynthesis (Pinske & Sawers, 2012a). Therefore, further investigations are necessary to identify the Fe-S cluster carrier proteins in the maturation of nitrate reductase under anaerobic respiratory conditions. Moreover, the Fe-S clusters insertion into other Fe-S clusters containing molybdoenzymes such as FdhF and XDH needs to be studied in the future.

It has been reported that the TMAO reductase is managed to escape the FNR regulation (Pascal et al., 1984; S Spiro & Guest, 1990). Our study shows that TMAO reductase activity is significantly reduced based on the low expression of *torCAD* in *fnr* deleted

strains. Although. Moreover, the FNR binding site at the *torCAD* promoter region was not identified in our study. Therefore, further studies are necessary to understand the indirect regulations of FNR via ArcA, NarL and Fe-S cluster biosynthesis, which are negatively influencing the expression of *torCAD* operon.

6 References

Adamec, J., Rusnak, F., Owen, W. G., Naylor, S., Benson, L. M., Gacy, A. M., & Isaya, G. (2000). Iron-dependent self-assembly of recombinant yeast frataxin: Implications for Friedreich ataxia. *American Journal of Human Genetics*, *67*(3), 549–562. https://doi.org/10.1086/303056

Adinolfi, S., Iannuzzi, C., Prischi, F., Pastore, C., Iametti, S., Martin, S. R., Bonomi, F., & Pastore, A. (2009a). Bacterial frataxin CyaY is the gatekeeper of iron-sulfur cluster formation catalyzed by IscS. *Nature Structural & Molecular Biology*, *16*(4), 390–396. https://doi.org/10.1038/nsmb.1579

Adinolfi, S., Iannuzzi, C., Prischi, F., Pastore, C., Iametti, S., Martin, S. R., Bonomi, F., & Pastore, A. (2009b). Bacterial frataxin CyaY is the gatekeeper of iron-sulfur cluster formation catalyzed by IscS. *Nature Structural and Molecular Biology*, *16*(4), 390–396. https://doi.org/10.1038/nsmb.1579

Agar, J. N., Krebs, C., Frazzon, J., Huynh, B. H., Dean, D. R., & Johnson, M. K. (2000). IscU as a scaffold for iron-sulfur cluster biosynthesis: Sequential assembly of [2Fe-2S] and [4Fe-4S] clusters in IscU. *Biochemistry*, *39*(27), 7856–7862. https://doi.org/10.1021/bi000931n

Aldea, M., Garrido, T., Hernandez-Chico, C., Vicente, M., & Kushner, S. R. (1989). *Induction of a growth-phase-dependent promoter triggers transcription of bolA, an Escherichia coli morphogene*. EMBO Journal. https://doi.org/10.1002/j.1460-2075.1989.tb08573.x

Alfaro, J. F., Joswig-Jones, C. A., Ouyang, W., Nichols, J., Crouch, G. J., & Jones, J. P. (2009). Purification and mechanism of human aldehyde oxidase expressed in Escherichia coli. *Drug Metabolism and Disposition*, *37*(12), 2393–2398. https://doi.org/10.1124/dmd.109.029520

Althaus, E. W., Outten, C. E., Olson, K. E., Cao, H., & O'Halloran, T. V. (1999). The ferric uptake regulation (Fur) repressor is a zinc metalloprotein. *Biochemistry*, *38*(20), 6559–6569. https://doi.org/10.1021/bi982788s

Anderson, L. A., McNairn, E., Lubke, T., Pau, R. N., & Boxer, D. H. (2000). ModE-dependent molybdate regulation of the molybdenum cofactor operon moa in

Escherichia coli. *Journal of Bacteriology*, *182*(24), 7035–7043. http://www.ncbi.nlm.nih.gov/pubmed/11092866

Andrews, S. C., Robinson, A. K., & Rodríguez-Quiñones, F. (2003). Bacterial iron homeostasis. In *FEMS Microbiology Reviews* (Vol. 27, Issues 2–3, pp. 215–237). Elsevier. https://doi.org/10.1016/S0168-6445(03)00055-X

Angelini, S., Gerez, C., Choudens, S. O. De, Sanakis, Y., Fontecave, M., Barras, F., & Py, B. (2008). NfuA, a new factor required for maturing Fe/S proteins in Escherichia coli under oxidative stress and iron starvation conditions. *Journal of Biological Chemistry*, *283*(20), 14084–14091. https://doi.org/10.1074/jbc.M709405200

Ansaldi, M., Bordi, C., Lepelletier, M., & Méjean, V. (1999). TorC apocytochrome negatively autoregulates the trimethylamine N-oxide (TMAO) reductase operon in Escherichia coli. *Molecular Microbiology*, *33*(2), 284–295. https://doi.org/10.1046/j.1365-2958.1999.01468.x

Ansaldi, M., Théraulaz, L., Baraquet, C., Panis, G., & Méjean, V. (2007). Aerobic TMAO respiration in Escherichia coli. *Molecular Microbiology*, *66*(2), 484–494. https://doi.org/10.1111/j.1365-2958.2007.05936.x

Åslund, F., Nordstrand, K., Beradt, K. D., Nikkola, M., Bergman, T., Ponstingl, H., Jörnvall, H., Otting, G., & Holmgren, A. (1996). Glutaredoxin-3 from Escheriehia coli: Amino acid sequence, 1H and 15N NME assignments, and structural analysis. *Journal of Biological Chemistry*, *271*(12), 6736–6745. https://doi.org/10.1074/jbc.271.12.6736

Ayala-Castro, C., Saini, A., & Outten, F. W. (2008). Fe-S cluster assembly pathways in bacteria. *Microbiology and Molecular Biology Reviews : MMBR*, *72*(1), 110–125, table of contents. https://doi.org/10.1128/MMBR.00034-07

Baba, T., Ara, T., Hasegawa, M., Takai, Y., Okumura, Y., Baba, M., Datsenko, K. A., Tomita, M., Wanner, B. L., & Mori, H. (2006). Construction of Escherichia coli K-12 in-frame, single-gene knockout mutants: The Keio collection. *Molecular Systems Biology*, *2*. https://doi.org/10.1038/msb4100050

Bags, A., & Neilands, J. B. (1987). Ferric Uptake Regulation Protein Acts as a

Repressor, Employing Iron(II) as a Cofactor To Bind the Operator of an Iron Transport Operon in Escherichia coli. *Biochemistry*, *26*(17), 5471–5477. https://doi.org/10.1021/bi00391a039

Baraquet, C., Théraulaz, L., Guiral, M., Lafitte, D., Méjean, V., & Jourlin-Castelli, C. (2006). TorT, a member of a new periplasmic binding protein family, triggers induction of the Tor respiratory system upon trimethylamine N-oxide electron-acceptor binding in Escherichia coli. *Journal of Biological Chemistry*, *281*(50), 38189–38199. https://doi.org/10.1074/jbc.M604321200

Beedham, C. (2010). Xanthine Oxidoreductase and Aldehyde Oxidase. In *Comprehensive Toxicology, Second Edition* (Vol. 4, pp. 185–205). Elsevier Inc. https://doi.org/10.1016/B978-0-08-046884-6.00410-3

Begas, P., Liedgens, L., Moseler, A., Meyer, A. J., & Deponte, M. (2017). Glutaredoxin catalysis requires two distinct glutathione interaction sites. *Nature Communications*, *8*(1), 1–13. https://doi.org/10.1038/ncomms14835

Behshad, E., Parkin, S. E., & Bollinger, J. M. (2004). Mechanism of cysteine desulfurase Slr0387 from Synechocystis sp. PCC 6803: Kinetic analysis of cleavage of the persulfide intermediate by chemical reductants. *Biochemistry*, *43*(38), 12220–12226. https://doi.org/10.1021/bi049143e

Beilschmidt, L. K., De Choudens, S. O., Fournier, M., Sanakis, I., Hograindleur, M. A., Clémancey, M., Blondin, G., Schmucker, S., Eisenmann, A., Weiss, A., Koebel, P., Messaddeq, N., Puccio, H., & Martelli, A. (2017). ISCA1 is essential for mitochondrial Fe4S4 biogenesis in vivo. *Nature Communications*, *8*(1), 1–12. https://doi.org/10.1038/ncomms15124

Beinert, H. (2000a). A tribute to sulfur. *European Journal of Biochemistry*, *267*(18), 5657–5664. https://doi.org/10.1046/j.1432-1327.2000.01637.x

Beinert, H. (2000b). Iron-sulfur proteins: ancient structures, still full of surprises. *Journal of Biological Inorganic Chemistry : JBIC : A Publication of the Society of Biological Inorganic Chemistry*, *5*(1), 2–15. http://www.ncbi.nlm.nih.gov/pubmed/10766431

Beinert, H. (2000c). Iron-sulfur proteins: Ancient structures, still full of surprises. In

Journal of Biological Inorganic Chemistry (Vol. 5, Issue 1, pp. 2–15). Springer Verlag. https://doi.org/10.1007/s007750050002

Beinert, H., Holm, R. H., & Munck, E. (1997). Iron-sulfur clusters: nature's modular, multipurpose structures. *Science*, *277*(5326), 653–659. http://www.ncbi.nlm.nih.gov/pubmed/9235882

Berks, B. C., Ferguson, S. J., Moir, J. W. B., & Richardson, D. J. (1995). Enzymes and associated electron transport systems that catalyse the respiratory reduction of nitrogen oxides and oxyanions. In *BBA - Bioenergetics* (Vol. 1232, Issue 3, pp. 97–173). Biochim Biophys Acta. https://doi.org/10.1016/0005-2728(95)00092-5

Berks, B. C., Palmer, T., & Sargent, F. (2005). Protein targeting by the bacterial twin-arginine translocation (Tat) pathway. In *Current Opinion in Microbiology* (Vol. 8, Issue 2, pp. 174–181). Elsevier Ltd. https://doi.org/10.1016/j.mib.2005.02.010

Bertero, M. G., Rothery, R. A., Palak, M., Hou, C., Lim, D., Blasco, F., Weiner, J. H., & Strynadka, N. C. (2003). Insights into the respiratory electron transfer pathway from the structure of nitrate reductase A. *Nature Structural Biology*, *10*(9), 681–687. https://doi.org/10.1038/nsb969

Biederbick, A., Stehling, O., Rösser, R., Niggemeyer, B., Nakai, Y., Elsässer, H.-P., & Lill, R. (2006). Role of Human Mitochondrial Nfs1 in Cytosolic Iron-Sulfur Protein Biogenesis and Iron Regulation. *Molecular and Cellular Biology*, *26*(15), 5675–5687. https://doi.org/10.1128/mcb.00112-06

Bilder, P. W., Ding, H., & Newcomer, M. E. (2004). Crystal Structure of the Ancient, Fe-S Scaffold IscA Reveals a Novel Protein Fold. *Biochemistry*, *43*(1), 133–139. https://doi.org/10.1021/bi035440s

Blanc, B., Gerez, C., & Ollagnier de Choudens, S. (2015). Assembly of Fe/S proteins in bacterial systems. Biochemistry of the bacterial ISC system. In *Biochimica et Biophysica Acta - Molecular Cell Research* (Vol. 1853, Issue 6, pp. 1436–1447). Elsevier. https://doi.org/10.1016/j.bbamcr.2014.12.009

Blasco, F., Dos Santos, J. P., Magalon, A., Frixon, C., Guigliarelli, B., Santini, C. L., & Giordano, G. (1998). NarJ is a specific chaperone required for molybdenum

cofactor assembly in nitrate reductase A of Escherichia coli. *Molecular Microbiology*, *28*(3), 435–447. https://doi.org/10.1046/j.1365-2958.1998.00795.x

Blasco, F., Pommier, J., Augier, V., Chippaux, M., & Giordano, G. (1992). Involvement of the narJ or narW gene product in the formation of active nitrate reductase in Escherichia coli. *Molecular Microbiology*, *6*(2), 221–230. https://doi.org/10.1111/j.1365-2958.1992.tb02003.x

Bolstad, H. M., Botelho, D. J., & Wood, M. J. (2010). Proteomic analysis of protein-protein interactions within the cysteine sulfinate desulfinase Fe-S cluster biogenesis system. *Journal of Proteome Research*, *9*(10), 5358–5369. https://doi.org/10.1021/pr1006087

Bolstad, H. M., & Wood, M. J. (2010). An in vivo method for characterization of protein interactions within sulfur trafficking systems of E. coli. *Journal of Proteome Research*, *9*(12), 6740–6751. https://doi.org/10.1021/pr100920r

Bonomi, F., Iametti, S., Morleo, A., Ta, D., & Vickery, L. E. (2008). Studies on the mechanism of catalysis of iron-sulfur cluster transfer from IscU[2Fe2S] by HscA/HscB chaperones. *Biochemistry*, *47*(48), 12795–12801. https://doi.org/10.1021/bi801565j

Bonomi, F., Iametti, S., Morleo, A., Ta, D., & Vickery, L. E. (2011). Facilitated transfer of IscU-[2Fe2S] clusters by chaperone-mediated ligand exchange. *Biochemistry*, *50*(44), 9641–9650. https://doi.org/10.1021/bi201123z

Boutigny, S., Saini, A., Baidoo, E. E. K., Yeung, N., Keasling, J. D., & Butland, G. (2013). Physical and functional interactions of a monothiol glutaredoxin and an iron sulfur cluster carrier protein with the sulfur-donating radical S-adenosyl-L-methionine enzyme MiaB. *Journal of Biological Chemistry*, *288*(20), 14200–14211. https://doi.org/10.1074/jbc.M113.460360

Boyd, E. S., Thomas, K. M., Dai, Y., Boyd, J. M., & Outten, F. W. (2014). Interplay between Oxygen and Fe-S Cluster Biogenesis: Insights from the Suf Pathway. In *Biochemistry* (Vol. 53, Issue 37, pp. 5834–5847). American Chemical Society. https://doi.org/10.1021/bi500488r

Boyd, J. M., Drevland, R. M., Downs, D. M., & Graham, D. E. (2009). Archaeal

ApbC/Nbp35 homologs function as iron-sulfur cluster carrier proteins. *Journal of Bacteriology*, *191*(5), 1490–1497. https://doi.org/10.1128/JB.01469-08

Boyd, J. M., Pierik, A. J., Netz, D. J. A., Lill, R., & Downs, D. M. (2008). Bacterial ApbC can bind and effectively transfer iron-sulfur clusters. *Biochemistry*, *47*(31), 8195–8202. https://doi.org/10.1021/bi800551y

Boyd, J. M., Sondelski, J. L., & Downs, D. M. (2009). Bacterial apbC protein has two biochemical activities that are required for in vivo function. *Journal of Biological Chemistry*, *284*(1), 110–118. https://doi.org/10.1074/jbc.M807003200

Bradley, M. D., Beach, M. B., de Koning, A. P. J., Pratt, T. S., & Osuna, R. (2007). Effects of Fis on Escherichia coli gene expression during different growth stages. *Microbiology*, *153*(9), 2922–2940. https://doi.org/10.1099/mic.0.2007/008565-0

Braman, J., Papworth, C., & Greener, A. (1996). Site-directed mutagenesis using double-stranded plasmid DNA templates. In *Methods in molecular biology (Clifton, N.J.)* (Vol. 57, pp. 31–44). Methods Mol Biol. https://doi.org/10.1385/0-89603-332-5:31

Broderick, J. B., Duffus, B. R., Duschene, K. S., & Shepard, E. M. (2014). Radical S-adenosylmethionine enzymes. In *Chemical Reviews* (Vol. 114, Issue 8, pp. 4229–4317). American Chemical Society. https://doi.org/10.1021/cr4004709

Brokx, S. J., Rothery, R. A., Zhang, G., Ng, D. P., & Weiner, J. H. (2005). Characterization of an Escherichia coli Sulfite Oxidase Homologue Reveals the Role of a Conserved Active Site Cysteine in Assembly and Function †. *Biochemistry*, *44*(30), 10339–10348. https://doi.org/10.1021/bi050621a

Brondijk, T. H. C., Nilavongse, A., Filenko, N., Richardson, D. J., & Cole, J. A. (2004). NapGH components of the periplasmic nitrate reductase of Escherichia coli K-12: Location, topology and physiological roles in quinol oxidation and redox balancing. *Biochemical Journal*, *379*(1), 47–55. https://doi.org/10.1042/BJ20031115

Burschel, S., Kreuzer Decovic, D., Nuber, F., Stiller, M., Hofmann, M., Zupok, A., Siemiatkowska, B., Gorka, M., Leimkühler, S., & Friedrich, T. (2019). Iron-sulfur

cluster carrier proteins involved in the assembly of Escherichia coli NADH:ubiquinone oxidoreductase (complex I). *Molecular Microbiology*, *111*(1), 31–45. https://doi.org/10.1111/mmi.14137

Carey, J. N., Mettert, E. L., Roggiani, M., Myers, K. S., Kiley, P. J., & Goulian, M. (2018). Regulated Stochasticity in a Bacterial Signaling Network Permits Tolerance to a Rapid Environmental Change. *Cell*, *173*(1), 196-207.e14. https://doi.org/10.1016/j.cell.2018.02.005

Carpenter, L. J., Archer, S. D., & Beale, R. (2012). Ocean-atmosphere trace gas exchange. *Chemical Society Reviews*, *41*(19), 6473–6506. https://doi.org/10.1039/c2cs35121h

Chahal, H. K., Dai, Y., Saini, A., Ayala-Castro, C., & Outten, F. W. (2009). The SufBCD Fe-S scaffold complex interacts with sufa for Fe-s cluster transfer. *Biochemistry*, *48*(44), 10644–10653. https://doi.org/10.1021/bi901518y

Chandramouli, K., & Johnson, M. K. (2006). HscA and HscB stimulate [2Fe-2S] cluster transfer from IscU to apoferredoxin in an ATP-dependent reaction. *Biochemistry*, *45*(37), 11087–11095. https://doi.org/10.1021/bi061237w

Chandramouli, K., Unciuleac, M. C., Naik, S., Dean, D. R., Boi, H. H., & Johnson, M. K. (2007). Formation and properties of [4Fe-4S] clusters on the IscU scaffold protein. *Biochemistry*, *46*(23), 6804–6811. https://doi.org/10.1021/bi6026659

Chang, L., Wei, L. I. C., Audia, J. P., Morton, R. A., & Schellhorn, H. E. (1999). Expression of the Escherichia coli NRZ nitrate reductase is highly growth phase dependent and is controlled by RpoS, the alternative vegetative sigma factor. *Molecular Microbiology*, *34*(4), 756–766. https://doi.org/10.1046/j.1365-2958.1999.01637.x

Chiang, R. C., Cavicchioli, R., & Gunsalus, R. P. (1992). Identification and characterization of narQ, a second nitrate sensor for nitrate-dependent gene regulation in Escherichia coli. *Molecular Microbiology*, *6*(14), 1913–1923. https://doi.org/10.1111/j.1365-2958.1992.tb01364.x

Clegg, R. A. (1976). Purification and some properties of nitrate reductase (EC 1.7.99.4) from Escherichia coli K12. *Biochemical Journal*, *153*(3), 533–541.

https://doi.org/10.1042/bj1530533

Cole, J. (2006). Nitrate reduction to ammonia by enteric bacteria: redundancy, or a strategy for survival during oxygen starvation? *FEMS Microbiology Letters*, *136*(1), 1–11. https://doi.org/10.1111/j.1574-6968.1996.tb08017.x

Coleman, K. J., Cornish-Bowden, A., & Cole, J. A. (1978). *Purification and properties of nitrite reductase from Escherichia coli K12*. Biochemical Journal. https://doi.org/10.1042/bj1750483

Compan, I., & Touati, D. (1994). Anaerobic activation of arcA transcription in Escherichia coli: roles of Fnr and ArcA. *Molecular Microbiology*, *11*(5), 955–964. https://doi.org/10.1111/j.1365-2958.1994.tb00374.x

Constantinidou, C., Hobman, J. L., Griffiths, L., Patel, M. D., Penn, C. W., Cole, J. A., & Overton, T. W. (2006). A reassessment of the FNR regulon and transcriptomic analysis of the effects of nitrate, nitrite, NarXL, and NarQP as Escherichia coli K12 adapts from aerobic to anaerobic growth. *Journal of Biological Chemistry*, *281*(8), 4802–4815. https://doi.org/10.1074/jbc.M512312200

Correia, M. A. S., Otrelo-Cardoso, A. R., Schwuchow, V., Sigfridsson Clauss, K. G. V., Haumann, M., Romão, M. J., Leimkühler, S., & Santos-Silva, T. (2016). The Escherichia coli Periplasmic Aldehyde Oxidoreductase Is an Exceptional Member of the Xanthine Oxidase Family of Molybdoenzymes. *ACS Chemical Biology*, *11*(10), 2923–2935. https://doi.org/10.1021/acschembio.6b00572

Cowart, R. E. (2002). Reduction of iron by extracellular iron reductases: Implications for microbial iron acquisition. *Archives of Biochemistry and Biophysics*, *400*(2), 273–281. https://doi.org/10.1016/S0003-9861(02)00012-7

Cox, J. C., & Knight, R. (1981). Trimethylamine N-oxide (TMAO) reductase activity in chlorate-resistant or respiration-deficient mutants of Escherichia coli. In *FEMS Microbiology Letters* (Vol. 12). https://doi.org/10.1111/j.1574-6968.1981.tb07651.x

Cox, J. C., Madigan, M. T., Favinger, J. L., & Gest, H. (1980). Redox mechanisms in “oxidant-dependent” hexose fermentation by Rhodopseudomonas capsulata. *Archives of Biochemistry and Biophysics*, *204*(1), 10–17.

https://doi.org/10.1016/0003-9861(80)90002-8

Crack, J. C., Green, J., Thomson, A. J., & Brun, N. E. L. (2014). Iron-sulfur clusters as biological sensors: The chemistry of reactions with molecular oxygen and nitric oxide. *Accounts of Chemical Research*, *47*(10), 3196–3205. https://doi.org/10.1021/ar5002507

Crack, J. C., Thomson, A. J., & Le Brun, N. E. (2017). Mass spectrometric identification of intermediates in the O2-driven [4Fe-4S] to [2Fe-2S] cluster conversion in FNR. *Proceedings of the National Academy of Sciences of the United States of America*, *114*(16), E3215–E3223. https://doi.org/10.1073/pnas.1620987114

Cupp-Vickery, J. R., Peterson, J. C., Ta, D. T., & Vickery, L. E. (2004). Crystal Structure of the Molecular Chaperone HscA Substrate Binding Domain Complexed with the IscU Recognition Peptide ELPPVKIHC. *Journal of Molecular Biology*, *342*(4), 1265–1278. https://doi.org/10.1016/j.jmb.2004.07.025

Cupp-Vickery, J. R., Silberg, J. J., Ta, D. T., & Vickery, L. E. (2004). Crystal structure of IscA, an iron-sulfur cluster assembly protein from Escherichia coli. *Journal of Molecular Biology*, *338*(1), 127–137. https://doi.org/10.1016/j.jmb.2004.02.027

Cupp-Vickery, J. R., Urbina, H., & Vickery, L. E. (2003). Crystal structure of IscS, a cysteine desulfurase from Escherichia coli. *Journal of Molecular Biology*, *330*(5), 1049–1059. https://doi.org/10.1016/S0022-2836(03)00690-9

Czjzek, M., Dos Santos, J. P., Pommier, J., Giordano, G., Méjean, V., & Haser, R. (1998). Crystal structure of oxidized trimethylamine N-oxide reductase from Shewanella massilia at 2.5 Å resolution. *Journal of Molecular Biology*, *284*(2), 435–447. https://doi.org/10.1006/jmbi.1998.2156

Dagert, M., & Ehrlich, S. D. (1979). Prolonged incubation in calcium chloride improves the competence of Escherichia coli cells. *Gene*, *6*(1), 23–28. https://doi.org/10.1016/0378-1119(79)90082-9

Dahl, J. U., Radon, C., Buhning, M., Nimtz, M., Leichert, L. I., Denis, Y., Jourlin-Castelli, C., Iobbi-Nivol, C., Mejean, V., & Leimkuhler, S. (2013). The sulfur

carrier protein TusA has a pleiotropic role in Escherichia coli that also affects molybdenum cofactor biosynthesis. *The Journal of Biological Chemistry*, *288*(8), 5426–5442. https://doi.org/10.1074/jbc.M112.431569

Dahl, J. U., Radon, C., Bühning, M., Nimtz, M., Leichert, L. I., Denis, Y., Jourlin-Castelli, C., Iobbi-Nivol, C., Méjean, V., & Leimkühler, S. (2013). The sulfur carrier protein tusa has a pleiotropic role in escherichia coli that also affects molybdenum cofactor biosynthesis. *Journal of Biological Chemistry*, *288*(8), 5426–5442. https://doi.org/10.1074/jbc.M112.431569

Daniels, J. N., Wuebbens, M. M., Rajagopalan, K. V., & Schindelin, H. (2008). Crystal structure of a molybdopterin synthase-precursor Z complex: Insight into its sulfur transfer mechanism and its role in molybdenum cofactor deficiency. *Biochemistry*, *47*(2), 615–626. https://doi.org/10.1021/bi701734g

Datsenko, K. A., & Wanner, B. L. (2000). One-step inactivation of chromosomal genes in Escherichia coli K-12 using PCR products. *Proceedings of the National Academy of Sciences of the United States of America*, *97*(12), 6640–6645. https://doi.org/10.1073/pnas.120163297

Desnoyers, G., Morissette, A., Prévost, K., & Massé, E. (2009). Small RNA-induced differential degradation of the polycistronic mRNA iscRSUA. *EMBO Journal*, *28*(11), 1551–1561. https://doi.org/10.1038/emboj.2009.116

Dixon, S. J., & Stockwell, B. R. (2014). The role of iron and reactive oxygen species in cell death. In *Nature Chemical Biology* (Vol. 10, Issue 1, pp. 9–17). Nat Chem Biol. https://doi.org/10.1038/nchembio.1416

Dow, J. M., Grahl, S., Ward, R., Evans, R., Byron, O., Norman, D. G., Palmer, T., & Sargent, F. (2014). Characterization of a periplasmic nitrate reductase in complex with its biosynthetic chaperone. *FEBS Journal*, *281*(1), 246–260. https://doi.org/10.1111/febs.12592

Dubourdieu, M., & DeMoss, J. A. (1992). The narJ gene product is required for biogenesis of respiratory nitrate reductase in Escherichia coli. *Journal of Bacteriology*, *174*(3), 867–872. https://doi.org/10.1128/jb.174.3.867-872.1992

Eiglmeier, K., Honoré, N., Iuchi, S., Lin, E. C. C., & Cole, S. T. (1989). Molecular

genetic analysis of FNR-dependent promoters. *Molecular Microbiology*, *3*(7), 869–878. https://doi.org/10.1111/j.1365-2958.1989.tb00236.x

Enoch, H. G., & Lester, R. L. (1975). *The purification and properties of formate dehydrogenase and nitrate reductase from Escherichia coli*. Journal of Biological Chemistry. https://doi.org/10.1016/s0021-9258(19)40989-7

Fernandes, A. P., Fladvad, M., Berndt, C., Andrésen, C., Lillig, C. H., Neubauer, P., Sunnerhagen, M., Holmgren, A., & Vlamis-Gardikas, A. (2005). A novel monothiol glutaredoxin (Grx4) from Escherichia coli can serve as a substrate for thioredoxin reductase. *Journal of Biological Chemistry*, *280*(26), 24544–24552. https://doi.org/10.1074/jbc.M500678200

Fillat, M. F. (2014). The fur (ferric uptake regulator) superfamily: Diversity and versatility of key transcriptional regulators. In *Archives of Biochemistry and Biophysics* (Vol. 546, pp. 41–52). Academic Press. https://doi.org/10.1016/j.abb.2014.01.029

Fleischhacker, A. S., Stubna, A., Hsueh, K. L., Guo, Y., Teter, S. J., Rose, J. C., Brunold, T. C., Markley, J. L., Münck, E., & Kiley, P. J. (2012). Characterization of the [2Fe-2S] cluster of Escherichia coli transcription factor IscR. *Biochemistry*, *51*(22), 4453–4462. https://doi.org/10.1021/bi3003204

Flint, D. H. (1996). Escherichia coli contains a protein that is homologous in function and N-terminal sequence to the protein encoded by the nifS gene of Azotobacter vinelandii and that can participate in the synthesis of the Fe-S cluster of dihydroxy-acid dehydratase. *Journal of Biological Chemistry*, *271*(27), 16068–16074. https://doi.org/10.1016/s0021-9258(18)48580-8

Fontecave, M. (2006). Iron-sulfur clusters: Ever-expanding roles. *Nature Chemical Biology*, *2*(4), 171–174. https://doi.org/10.1038/nchembio0406-171

Forget, P. (1974). The Bacterial Nitrate Reductases: Solubilization, Purification and Properties of the Enzyme A of Escherichia coli K 12. *European Journal of Biochemistry*, *42*(2), 325–332. https://doi.org/10.1111/j.1432-1033.1974.tb03343.x

Frey, A. G., Palenchar, D. J., Wildemann, J. D., & Philpott, C. C. (2016). A

glutaredoxin-BolA complex serves as an iron-sulfur cluster chaperone for the cytosolic cluster assembly machinery. *Journal of Biological Chemistry*, *291*(43), 22344–22356. https://doi.org/10.1074/jbc.M116.744946

Frey, P. A., Hegeman, A. D., & Ruzicka, F. J. (2008). The Radical SAM Superfamily. *Critical Reviews in Biochemistry and Molecular Biology*, *43*(1), 63–88. https://doi.org/10.1080/10409230701829169

Frey, P. A., & Reed, G. H. (2012). *The Ubiquity of Iron*. https://doi.org/10.1021/cb300323q

Furrer, J. L., Sanders, D. N., Hook-Barnard, I. G., & McIntosh, M. A. (2002). Export of the siderophore enterobactin in Escherichia coli: Involvement of a 43 kDa membrane exporter. *Molecular Microbiology*, *44*(5), 1225–1234. https://doi.org/10.1046/j.1365-2958.2002.02885.x

Fuss, J. O., Tsai, C. L., Ishida, J. P., & Tainer, J. A. (2015). Emerging critical roles of Fe-S clusters in DNA replication and repair. In *Biochimica et Biophysica Acta - Molecular Cell Research* (Vol. 1853, Issue 6, pp. 1253–1271). Elsevier. https://doi.org/10.1016/j.bbamcr.2015.01.018

Gari, K., Ortiz, A. M. L., Borel, V., Flynn, H., Skehel, J. M., & Boulton, S. J. (2012). MMS19 links cytoplasmic iron-sulfur cluster assembly to DNA metabolism. *Science*, *337*(6091), 243–245. https://doi.org/10.1126/science.1219664

Genest, O., Ilbert, M., Méjean, V., & Iobbi-Nivol, C. (2005). TorD, an essential chaperone for TorA molybdoenzyme maturation at high temperature. *Journal of Biological Chemistry*, *280*(16), 15644–15648. https://doi.org/10.1074/jbc.M501119200

Genest, O., Méjean, V., & Iobbi-Nivol, C. (2009). Multiple roles of TorD-like chaperones in the biogenesis of molybdoenzymes. In *FEMS Microbiology Letters* (Vol. 297, Issue 1, pp. 1–9). FEMS Microbiol Lett. https://doi.org/10.1111/j.1574-6968.2009.01660.x

Genest, O., Neumann, M., Seduk, F., Stöcklein, W., Méjean, V., Leimkühler, S., & Iobbi-Nivol, C. (2008). Dedicated metallochaperone connects apoenzyme and molybdenum cofactor biosynthesis components. *Journal of Biological*

Chemistry, *283*(31), 21433–21440. https://doi.org/10.1074/jbc.M802954200

Genest, O., Seduk, F., Théraulaz, L., Méjean, V., & Iobbi-Nivol, C. (2006). Chaperone protection of immature molybdoenzyme during molybdenum cofactor limitation. *FEMS Microbiology Letters*, *265*(1), 51–55. https://doi.org/10.1111/j.1574-6968.2006.00468.x

Gerasimova, A. V., Rodionov, D. A., Mironov, A. A., & Gelfand, M. S. (2001). *Computer analysis of regulatory signals in bacterial genomes. Fnr binding sites*. Molecular Biology. https://doi.org/10.1023/A:1013286202014

Gerber, S., Comellas-Bigler, M., Goetz, B. A., & Locher, K. P. (2008). Structural basis of trans-inhibition in a molybdate/tungstate ABC transporter. *Science*, *321*(5886), 246–250. https://doi.org/10.1126/science.1156213

Giel, J. L., Nesbit, A. D., Mettert, E. L., Fleischhacker, A. S., Wanta, B. T., & Kiley, P. J. (2013). Regulation of iron-sulphur cluster homeostasis through transcriptional control of the Isc pathway by [2Fe-2S]-IscR in Escherichia coli. *Molecular Microbiology*, *87*(3), 478–492. https://doi.org/10.1111/mmi.12052

Giel, J. L., Rodionov, D., Liu, M., Blattner, F. R., & Kiley, P. J. (2006). IscR-dependent gene expression links iron-sulphur cluster assembly to the control of O2-regulated genes in Escherichia coli. *Molecular Microbiology*, *60*(4), 1058–1075. https://doi.org/10.1111/j.1365-2958.2006.05160.x

Goldsmith-Fischman, S., Kuzin, A., Edstrom, W. C., Benach, J., Shastry, R., Xiao, R., Acton, T. B., Honig, B., Montelione, G. T., & Hunt, J. F. (2004). The SufE sulfur-acceptor protein contains a conserved core structure that mediates interdomain interactions in a variety of redox protein complexes. *Journal of Molecular Biology*, *344*(2), 549–565. https://doi.org/10.1016/j.jmb.2004.08.074

Gon, S., Giudici-Orticoni, M. T., Méjean, V., & Iobbi-Nivol, C. (2001). Electron Transfer and Binding of the c-Type Cytochrome TorC to the Trimethylamine N-Oxide Reductase in Escherichia coli. *Journal of Biological Chemistry*, *276*(15), 11545–11551. https://doi.org/10.1074/jbc.M008875200

Gon, S., Jourlin-Castelli, C., Théraulaz, L., & Méjean, V. (2001). An unsuspected autoregulatory pathway involving apocytochrome TorC and sensor TorS in

Escherichia coli. *Proceedings of the National Academy of Sciences of the United States of America*, *98*(20), 11615–11620. https://doi.org/10.1073/pnas.211330598

Gon, S., Patte, J. C., Mejean, V., & Iobbi-Nivol, C. (2000). The torYZ (yecK bisZ) operon encodes a third respiratory trimethylamine N-oxide reductase in Escherichia coli. *Journal of Bacteriology*, *182*(20), 5779–5786. https://doi.org/10.1128/JB.182.20.5779-5786.2000

Gonzales, M. F., Brooks, T., Pukatzki, S. U., & Provenzano, D. (2013). Rapid protocol for preparation of electrocompetent Escherichia coli and Vibrio cholerae. *Journal of Visualized Experiments*, *80*, 50684. https://doi.org/10.3791/50684

Gräwert, T., Kaiser, J., Zepeck, F., Laupitz, R., Hecht, S., Amslinger, S., Schramek, N., Schleicher, E., Weber, S., Haslbeck, M., Buchner, J., Rieder, C., Arigoni, D., Bacher, A., Eisenreich, W., & Rohdich, F. (2004). IspH protein of Escherichia coli: Studies on iron-sulfur cluster implementation and catalysis. *Journal of the American Chemical Society*, *126*(40), 12847–12855. https://doi.org/10.1021/ja0471727

Green, J., & Guest, J. R. (1993). A role for iron in transcriptional activation by FNR. *FEBS Letters*, *329*(1–2), 55–58. https://doi.org/10.1016/0014-5793(93)80192-w

Green, J., Sharrocks, A. D., Green, B., Geisow, M., & Guest, J. R. (1993). Properties of FNR proteins substituted at each of the five cysteine residues. *Molecular Microbiology*, *8*(1), 61–68. https://doi.org/10.1111/j.1365-2958.1993.tb01203.x

Grunden, A. M., & Shanmugam, K. T. (1997). Molybdate transport and regulation in bacteria. In *Archives of Microbiology* (Vol. 168, Issue 5, pp. 345–354). Springer. https://doi.org/10.1007/s002030050508

Gunsalus, R. P., & Park, S. J. (1994). Aerobic-anaerobic gene regulation in Escherichia coli: control by the ArcAB and Fnr regulons. *Research in Microbiology*, *145*(5–6), 437–450. https://doi.org/10.1016/0923-2508(94)90092-2

Gupta, V., Sendra, M., Naik, S. G., Chahal, H. K., Huynh, B. H., Outten, F. W.,

Fontecave, M., & De Choudens, S. O. (2009). Native escherichia coli SufA coexpressed with SufBCDSE purifies as a [2Fe-2S] protein and acts as an Fe-S transporter to Fe-S target enzymes. *Journal of the American Chemical Society*, *131*(17), 6149–6153. https://doi.org/10.1021/ja807551e

Hanahan, D. (1983). Studies on transformation of Escherichia coli with plasmids. *Journal of Molecular Biology*, *166*(4), 557–580. https://doi.org/10.1016/S0022-2836(83)80284-8

Hanzelmann, P., Hernandez, H. L., Menzel, C., Garcia-Serres, R., Huynh, B. H., Johnson, M. K., Mendel, R. R., & Schindelin, H. (2004). Characterization of MOCS1A, an oxygen-sensitive iron-sulfur protein involved in human molybdenum cofactor biosynthesis. *The Journal of Biological Chemistry*, *279*(33), 34721–34732. https://doi.org/10.1074/jbc.M313398200

Hanzelmann, P., & Schindelin, H. (2004). Crystal structure of the S-adenosylmethionine-dependent enzyme MoaA and its implications for molybdenum cofactor deficiency in humans. *Proceedings of the National Academy of Sciences of the United States of America*, *101*(35), 12870–12875. https://doi.org/10.1073/pnas.0404624101

Hänzelmann, P., & Schindelin, H. (2006). Binding of 5′-GTP to the C-terminal FeS cluster of the radical S-adenosylmethionine enzyme MoaA provides insights into its mechanism. *Proceedings of the National Academy of Sciences of the United States of America*, *103*(18), 6829–6834. https://doi.org/10.1073/pnas.0510711103

Hartmann, T., Terao, M., Garattini, E., Teutloff, C., Alfaro, J. F., Jones, J. P., & Leimkühler, S. (2012). The impact of single nucleotide polymorphisms on human aldehyde oxidase. *Drug Metabolism and Disposition*, *40*(5), 856–864. https://doi.org/10.1124/dmd.111.043828

Hasona, A., Self, W. T., & Shanmugam, K. T. (2001). Transcriptional regulation of the moe (molybdate metabolism) operon of Escherichia coli. *Archives of Microbiology*, *175*(3), 178–188. http://www.ncbi.nlm.nih.gov/pubmed/11357510

Havelius, K. G. V., Reschke, S., Horn, S., Döring, A., Niks, D., Hille, R., Schulzke, C., Leimkühler, S., & Haumann, M. (2011). Structure of the molybdenum site in

YedY, a sulfite oxidase homologue from escherichia coli. *Inorganic Chemistry*, *50*(3), 741–748. https://doi.org/10.1021/ic101291j

Hermsdorf, C. L. (1978). Tripeptide-Specific Aminopeptidase from Escherichia coli AJ0051†. *Biochemistry*, *17*(16), 3370–3376. https://doi.org/10.1021/bi00609a030

Hidese, R., Mihara, H., & Esaki, N. (2011). Bacterial cysteine desulfurases: Versatile key players in biosynthetic pathways of sulfur-containing biofactors. In *Applied Microbiology and Biotechnology* (Vol. 91, Issue 1, pp. 47–61). Appl Microbiol Biotechnol. https://doi.org/10.1007/s00253-011-3336-x

Hille, R. (1996). The mononuclear molybdenum enzymes. *Chemical Reviews*, *96*(7), 2757–2816. https://doi.org/10.1021/cr950061t

Hille, R. (2002). Molybdenum and tungsten in biology. In *Trends in Biochemical Sciences* (Vol. 27, Issue 7, pp. 360–367). Trends Biochem Sci. https://doi.org/10.1016/S0968-0004(02)02107-2

Hille, R. (2007). Xanthine oxidoreductase. In *xPharm: The Comprehensive Pharmacology Reference* (pp. 1–10). Elsevier Inc. https://doi.org/10.1016/B978-008055232-3.60496-9

Hille, R., Hall, J., & Basu, P. (2014). The mononuclear molybdenum enzymes. *Chemical Reviews*, *114*(7), 3963–4038. https://doi.org/10.1021/cr400443z

Hoff, K. G., Cupp-Vickery, J. R., & Vickery, L. E. (2003). Contributions of the LPPVK Motif of the Iron-Sulfur Template Protein IscU to Interactions with the Hsc66-Hsc20 Chaperone System. *Journal of Biological Chemistry*, *278*(39), 37582–37589. https://doi.org/10.1074/jbc.M305292200

Hover, B. M., Loksztejn, A., Ribeiro, A. A., & Yokoyama, K. (2013). Identification of a cyclic nucleotide as a cryptic intermediate in molybdenum cofactor biosynthesis. *Journal of the American Chemical Society*, *135*(18), 7019–7032. https://doi.org/10.1021/ja401781t

Hover, B. M., Tonthat, N. K., Schumacher, M. A., & Yokoyama, K. (2015). Mechanism of pyranopterin ring formation in molybdenum cofactor biosynthesis. *Proceedings of the National Academy of Sciences of the United States of*

America, *112*(20), 6347–6352. https://doi.org/10.1073/pnas.1500697112

Hover, B. M., & Yokoyama, K. (2015). C-terminal glycine-gated radical initiation by GTP 3′,8-cyclase in the molybdenum cofactor biosynthesis. *Journal of the American Chemical Society*, *137*(9), 3352–3359. https://doi.org/10.1021/ja512997j

Hullo, M. F., Auger, S., Soutourina, O., Barzu, O., Yvon, M., Danchin, A., & Martin-Verstraete, I. (2007). Conversion of methionine to cysteine in Bacillus subtilis and its regulation. *Journal of Bacteriology*, *189*(1), 187–197. https://doi.org/10.1128/JB.01273-06

Huynen, M. A., Snel, B., Bork, P., & Gibson, T. J. (2001). The phylogenetic distribution of frataxin indicates a role in iron-sulfur cluster protein assembly. *Human Molecular Genetics*, *10*(21), 2463–2468. https://doi.org/10.1093/hmg/10.21.2463

Imlay, J. A. (2003). Pathways of Oxidative Damage. *Annual Review of Microbiology*, *57*(1), 395–418. https://doi.org/10.1146/annurev.micro.57.030502.090938

Iobbi-Nivol, C., Crooke, H., Griffiths, L., Grove, J., Hussain, H., Pommier, J., Mejean, V., & Cole, J. A. (1994). A reassessment of the range of c-type cytochromes synthesized by Escherichia coli K-12. *FEMS Microbiology Letters*, *119*(1–2), 89–94. https://doi.org/10.1111/j.1574-6968.1994.tb06872.x

Iobbi-Nivol, C., & Leimkühler, S. (2013). Molybdenum enzymes, their maturation and molybdenum cofactor biosynthesis in Escherichia coli. *Biochimica et Biophysica Acta - Bioenergetics*, *1827*(8–9), 1086–1101. https://doi.org/10.1016/j.bbabio.2012.11.007

Ishihama, A. (1997). Adaptation of gene expression in stationary phase bacteria. *Current Opinion in Genetics and Development*, *7*(5), 582–588. https://doi.org/10.1016/S0959-437X(97)80003-2

Ishihama, Akira. (1999). Modulation of the nucleoid, the transcription apparatus, and the translation machinery in bacteria for stationary phase survival. In *Genes to Cells* (Vol. 4, Issue 3, pp. 135–143). Genes Cells. https://doi.org/10.1046/j.1365-2443.1999.00247.x

Iuchi, S., & Lin, E. C. C. (1987a). The narL gene product activates the nitrate reductase operon and represses the fumarate reductase and trimethylamine N-oxide reductase operons in Escherichia coli. *Proceedings of the National Academy of Sciences of the United States of America*, *84*(11), 3901–3905. https://doi.org/10.1073/pnas.84.11.3901

Iuchi, S., & Lin, E. C. C. (1987b). The narL gene product activates the nitrate reductase operon and represses the fumarate reductase and trimethylamine N-oxide reductase operons in Escherichia coli. *Proceedings of the National Academy of Sciences of the United States of America*, *84*(11), 3901–3905. https://doi.org/10.1073/pnas.84.11.3901

Iuchi, S., & Lin, E. C. C. (1988). arcA (dye), a global regulatory gene in Escherichia coli mediating repression of enzymes in aerobic pathways. *Proceedings of the National Academy of Sciences of the United States of America*, *85*(6), 1888–1892. https://doi.org/10.1073/pnas.85.6.1888

Ize, B., Coulthurst, S. J., Harzixanthis, K., Caldelari, I., Buchanan, G., Barclay, E. C., Richardson, D. J., Palmer, T., & Sargent, F. (2009). Remnant signal peptides on non-exported enzymes: Implications for the evolution of prokaryotic respiratory chains. *Microbiology*, *155*(12), 3992–4004. https://doi.org/10.1099/mic.0.033647-0

Jack, R. L., Buchanan, G., Dubini, A., Hatzixanthis, K., Palmer, T., & Sargent, F. (2004). Coordinating assembly and export of complex bacterial proteins. *EMBO Journal*, *23*(20), 3962–3972. https://doi.org/10.1038/sj.emboj.7600409

Jacobson, M. R., Cash, V. L., Weiss, M. C., Laird, N. F., Newton, W. E., & Dean, D. R. (1989). Biochemical and genetic analysis of the nifUSVWZM cluster from Azotobacter vinelandii. *MGG Molecular & General Genetics*, *219*(1–2), 49–57. https://doi.org/10.1007/BF00261156

Jang, S., & Imlay, J. A. (2010). Hydrogen peroxide inactivates the Escherichia coli Isc iron-sulphur assembly system, and OxyR induces the Suf system to compensate. *Molecular Microbiology*, *78*(6), 1448–1467. https://doi.org/10.1111/j.1365-2958.2010.07418.x

Jaroschinsky, M., Pinske, C., & Sawers, R. G. (2017). Differential effects of isc

operon mutations on the biosynthesis and activity of key anaerobic metalloenzymes in Escherichia coli. *Microbiology (United Kingdom)*, *163*(6), 878–890. https://doi.org/10.1099/mic.0.000481

Jervis, A. J., Crack, J. C., White, G., Artymiuk, P. J., Cheesman, M. R., Thomson, A. J., Brun, N. E. L., & Green, J. (2009). The O2 sensitivity of the transcription factor FNR is controlled by Ser24 modulating the kinetics of [4Fe-4S] to [2Fe-2S] conversion. *Proceedings of the National Academy of Sciences of the United States of America*, *106*(12), 4659–4664. https://doi.org/10.1073/pnas.0804943106

Johnson, D. C., Dean, D. R., Smith, A. D., & Johnson, M. K. (2005). Structure, function, and formation of biological iron-sulfur clusters. *Annual Review of Biochemistry*, *74*, 247–281. https://doi.org/10.1146/annurev.biochem.74.082803.133518

Johnson, J. L., & Rajagopalan, K. V. (1982). Structural and metabolic relationship between the molybdenum cofactor and urothione. *Proceedings of the National Academy of Sciences of the United States of America*, *79*(22 I), 6856–6860. https://doi.org/10.1073/pnas.79.22.6856

Jourlin, C., Bengrine, A., Chippaux, M., & Méjean, V. (1996). An unorthodox sensor protein (TorS) mediates the induction of the tor structural genes in response to trimethylamine N-oxide in Escherichia coli. *Molecular Microbiology*, *20*(6), 1297–1306. https://doi.org/10.1111/j.1365-2958.1996.tb02648.x

Jourlin, C., Simon, G., Lepelletier, M., Chippaux, M., & Méjean, V. (1995). Conservation of cis-acting elements within the tor regulatory region among different Enterobacteriaceae. *Gene*, *152*(1), 53–57. https://doi.org/10.1016/0378-1119(94)00772-K

Kalman, L. V., & Gunsalus, R. P. (1990). Nitrate- and molybdenum-independent signal transduction mutations in narX that alter regulation of anaerobic respiratory genes in Escherichia coli. *Journal of Bacteriology*, *172*(12), 7049–7056. https://doi.org/10.1128/jb.172.12.7049-7056.1990

Kang, Y., Weber, K. D., Qiu, Y., Kiley, P. J., & Blattner, F. R. (2005). Genome-wide expression analysis indicates that FNR of Escherichia coli K-12 regulates a

large number of genes of unknown function. *Journal of Bacteriology*, *187*(3), 1135–1160. https://doi.org/10.1128/JB.187.3.1135-1160.2005

Kato, S. I., Mihara, H., Kurihara, T., Takahashi, Y., Tokumoto, U., Yoshimura, T., & Esaki, N. (2002). Cys-328 of IscS and Cys-63 of IscU are the sites of disulfide bridge formation in a covalently bound IscS/IscU complex: Implications for the mechanism of iron-sulfur cluster assembly. *Proceedings of the National Academy of Sciences of the United States of America*, *99*(9), 5948–5952. https://doi.org/10.1073/pnas.082123599

Kaufmann, P., Duffus, B. R., Mitrova, B., Iobbi-Nivol, C., Teutloff, C., Nimtz, M., Jänsch, L., Wollenberger, U., & Leimkühler, S. (2018). Modulating the Molybdenum Coordination Sphere of Escherichia coli Trimethylamine N-Oxide Reductase. *Biochemistry*, *57*(7), 1130–1143. https://doi.org/10.1021/acs.biochem.7b01108

Kessler, D. (2006). Enzymatic activation of sulfur for incorporation into biomolecules in prokaryotes. In *FEMS Microbiology Reviews* (Vol. 30, Issue 6, pp. 825–840). FEMS Microbiol Rev. https://doi.org/10.1111/j.1574-6976.2006.00036.x

Khoroshilova, N., Beinert, H., & Kiley, P. J. (1995). Association of a polynuclear iron-sulfur center with a mutant FNR protein enhances DNA binding. *Proceedings of the National Academy of Sciences of the United States of America*, *92*(7), 2499–2503. https://doi.org/10.1073/pnas.92.7.2499

Kim, J. H., Bothe, J. R., Frederick, R. O., Holder, J. C., & Markley, J. L. (2014). Role of IscX in iron-sulfur cluster biogenesis in Escherichia coli. *Journal of the American Chemical Society*, *136*(22), 7933–7942. https://doi.org/10.1021/ja501260h

Kim, J. H., Frederick, R. O., Reinen, N. M., Troupis, A. T., & Markley, J. L. (2013). [2Fe-2S]-Ferredoxin binds directly to cysteine desulfurase and supplies an electron for iron-sulfur cluster assembly but is displaced by the scaffold protein or bacterial frataxin. *Journal of the American Chemical Society*, *135*(22), 8117–8120. https://doi.org/10.1021/ja401950a

Kim, J. H., Tonelli, M., Frederick, R. O., Chow, D. C., & Markley, J. L. (2012). Specialized Hsp70 chaperone (HscA) binds preferentially to the disordered

form, whereas J-protein (HscB) binds preferentially to the structured form of the iron-sulfur cluster scaffold protein (IscU). *The Journal of Biological Chemistry*, *287*(37), 31406–31413. https://doi.org/10.1074/jbc.M112.352617

Kim, J. H., Tonelli, M., & Markley, J. L. (2012). Disordered form of the scaffold protein IscU is the substrate for iron-sulfur cluster assembly on cysteine desulfurase. *Proceedings of the National Academy of Sciences of the United States of America*, *109*(2), 454–459. https://doi.org/10.1073/pnas.1114372109

Kispal, G., Csere, P., Prohl, C., & Lill, R. (1999). The mitochondrial proteins Atm1p and Nfs1p are essential for biogenesis of cytosolic Fe/S proteins. *EMBO Journal*, *18*(14), 3981–3989. https://doi.org/10.1093/emboj/18.14.3981

Kolter, R., Siegele, D. A., & Tormo, A. (1993). The stationary phase of the bacterial life cycle. In *Annual Review of Microbiology* (Vol. 47, pp. 855–874). Annual Reviews Inc. https://doi.org/10.1146/annurev.mi.47.100193.004231

Körner, H., Sofia, H. J., & Zumft, W. G. (2003). Phylogeny of the bacterial superfamily of Crp-Fnr transcription regulators: Exploiting the metabolic spectrum by controlling alternative gene programs. In *FEMS Microbiology Reviews* (Vol. 27, Issue 5, pp. 559–592). Elsevier. https://doi.org/10.1016/S0168-6445(03)00066-4

Köster, W. (2001). ABC transporter-mediated uptake of iron, siderophores, heme and vitamin B12. *Research in Microbiology*, *152*(3–4), 291–301. https://doi.org/10.1016/S0923-2508(01)01200-1

Krewulak, K. D., & Vogel, H. J. (2008). Structural biology of bacterial iron uptake. In *Biochimica et Biophysica Acta - Biomembranes* (Vol. 1778, Issue 9, pp. 1781–1804). Biochim Biophys Acta. https://doi.org/10.1016/j.bbamem.2007.07.026

Kumar, R., & Shimizu, K. (2011). Transcriptional regulation of main metabolic pathways of cyoA, cydB, fnr, and fur gene knockout Escherichia coli in C-limited and N-limited aerobic continuous cultures. *Microbial Cell Factories*, *10*. https://doi.org/10.1186/1475-2859-10-3

Kuper, J., Llamas, A., Hecht, H. J., Mendel, R. R., & Schwarz, G. (2004). Structure of the molybdopterin-bound Cnx1G domain links molybdenum and copper

metabolism. *Nature*, *430*(7001), 803–806. https://doi.org/10.1038/nature02681

Lake, M. W., Temple, C. A., Rajagopalan, K. V., & Schindelin, H. (2000). The crystal structure of the Escherichia coli MobA protein provides insight into molybdopterin guanine dinucleotide biosynthesis. *Journal of Biological Chemistry*, *275*(51), 40211–40217. https://doi.org/10.1074/jbc.M007406200

Lamberg, K. E., & Kiley, P. J. (2000). FNR-dependent activation of the class II dmsA and narG promoters of Escherichia coli requires FNR-activating regions 1 and 3. *Molecular Microbiology*, *38*(4), 817–827. https://doi.org/10.1046/j.1365-2958.2000.02172.x

Lange, H., Kaut, A., Kispal, G., & Lill, R. (2000). A mitochondrial ferredoxin is essential for biogenesis of cellular iron-sulfur proteins. *Proceedings of the National Academy of Sciences of the United States of America*, *97*(3), 1050–1055. https://doi.org/10.1073/pnas.97.3.1050

Layer, G., Aparna Gaddam, S., Ayala-Castro, C. N., Choudens, S. O. De, Lascoux, D., Fontecave, M., & Outten, F. W. (2007). SufE transfers sulfur from SufS to SufB for iron-sulfur cluster assembly. *Journal of Biological Chemistry*, *282*(18), 13342–13350. https://doi.org/10.1074/jbc.M608555200

Layer, G., Ollagnier-De Choudens, S., Sanakis, Y., & Fontecave, M. (2006). Iron-sulfur cluster biosynthesis: Characterization of escherichia coli CYaY as an iron donor for the assembly of [2Fe-2S] clusters in the scaffold IscU. *Journal of Biological Chemistry*, *281*(24), 16256–16263. https://doi.org/10.1074/jbc.M513569200

Lazazzera, B. A., Beinert, H., Khoroshilova, N., Kennedy, M. C., & Kiley, P. J. (1996). DNA binding and dimerization of the Fe-S-containing FNR protein from Escherichia coli are regulated by oxygen. *The Journal of Biological Chemistry*, *271*(5), 2762–2768. http://www.ncbi.nlm.nih.gov/pubmed/8576252

Lee, C., Lee, S. M., Mukhopadhyay, P., Kim, S. J., Lee, S. C., Ahn, W. S., Yu, M. H., Storz, G., & Ryu, S. E. (2004). Redox regulation of OxyR requires specific disulfide bond formation involving a rapid kinetic reaction path. *Nature Structural and Molecular Biology*, *11*(12), 1179–1185. https://doi.org/10.1038/nsmb856

Lee, J. H., Yeo, W. S., & Roe, J. H. (2004). Induction of the sufA operon encoding Fe-S assembly proteins by superoxide generators and hydrogen peroxide: Involvement of OxyR, IHF and an unidentified oxidant-responsive factor. *Molecular Microbiology*, *51*(6), 1745–1755. https://doi.org/10.1111/j.1365-2958.2003.03946.x

Lee, K. C., Yeo, W. S., & Roe, J. H. (2008). Oxidant-responsive induction of the suf operon, encoding a Fe-S assembly system, through Fur and IscR in Escherichia coli. *Journal of Bacteriology*, *190*(24), 8244–8247. https://doi.org/10.1128/JB.01161-08

Leimkühler, S. (2017). Shared function and moonlighting proteins in molybdenum cofactor biosynthesis. In *Biological Chemistry* (Vol. 398, Issue 9, pp. 1009–1026). Walter de Gruyter GmbH. https://doi.org/10.1515/hsz-2017-0110

Leimkühler, S. (2020). The biosynthesis of the molybdenum cofactors in <scp> *Escherichia coli* </scp>. *Environmental Microbiology*, *22*(6), 2007–2026. https://doi.org/10.1111/1462-2920.15003

Leimkühler, S., Hodson, R., George, G. N., & Rajagopalan, K. V. (2003). Recombinant Rhodobacter capsulatus xanthine dehydrogenase, a useful model system for the characterization of protein variants leading to xanthinuria I in humans. *Journal of Biological Chemistry*, *278*(23), 20802–20811. https://doi.org/10.1074/jbc.M303091200

Leimkuhler, S., & Iobbi-Nivol, C. (2016). Bacterial molybdoenzymes: old enzymes for new purposes. *FEMS Microbiology Reviews*, *40*(1), 1–18. https://doi.org/10.1093/femsre/fuv043

Leimkühler, S., Kern, M., Solomon, P. S., McEwan, A. G., Schwarz, G., Mendel, R. R., & Klipp, W. (1998). Xanthine dehydrogenase from the phototrophic purple bacterium Rhodobacter capsulatus is more similar to its eukaryotic counterparts than to prokaryotic molybdenum enzymes. In *Molecular Microbiology* (Vol. 27, Issue 4, pp. 853–869). Mol Microbiol. https://doi.org/10.1046/j.1365-2958.1998.00733.x

Leimkühler, S., & Klipp, W. (1999). Role of XDHC in molybdenum cofactor insertion into xanthine dehydrogenase of Rhodobacter capsulatus. *Journal of*

Bacteriology, *181*(9), 2745–2751. https://doi.org/10.1128/jb.181.9.2745-2751.1999

Leimkühler, S., & Neumann, M. (2011). The role of system-specific molecular chaperones in the maturation of molybdoenzymes in bacteria. In *Biochemistry Research International* (Vol. 2011). Biochem Res Int. https://doi.org/10.1155/2011/850924

Leimkuhler, S., & Rajagopalan, K. V. (2001). A sulfurtransferase is required in the transfer of cysteine sulfur in the in vitro synthesis of molybdopterin from precursor Z in Escherichia coli. *The Journal of Biological Chemistry*, *276*(25), 22024–22031. https://doi.org/10.1074/jbc.M102072200

Leimkuhler, S., Wuebbens, M. M., & Rajagopalan, K. V. (2001). Characterization of Escherichia coli MoeB and its involvement in the activation of molybdopterin synthase for the biosynthesis of the molybdenum cofactor. *The Journal of Biological Chemistry*, *276*(37), 34695–34701. https://doi.org/10.1074/jbc.M102787200

Leimkuhler, S., Wuebbens, M. M., & Rajagopalan, K. V. (2011). The History of the Discovery of the Molybdenum Cofactor and Novel Aspects of its Biosynthesis in Bacteria. *Coordination Chemistry Reviews*, *255*(9–10), 1129–1144. https://doi.org/10.1016/j.ccr.2010.12.003

Leipe, D. D., Wolf, Y. I., Koonin, E. V., & Aravind, L. (2002). Classification and evolution of P-loop GTPases and related ATPases. *Journal of Molecular Biology*, *317*(1), 41–72. https://doi.org/10.1006/jmbi.2001.5378

Li, D. S., Ohshima, K., Jiralerspong, S., Bojanowski, M. W., & Pandolfo, M. (1999). Knock-out of the cyaY gene in Escherichia coli does not affect cellular iron content and sensitivity to oxidants. *FEBS Letters*, *456*(1), 13–16. https://doi.org/10.1016/S0014-5793(99)00896-0

Li, H., Mapolelo, D. T., Randeniya, S., Johnson, M. K., & Outten, C. E. (2012). Human glutaredoxin 3 forms [2Fe-2S]-bridged complexes with human BolA2. *Biochemistry*, *51*(8), 1687–1696. https://doi.org/10.1021/bi2019089

Li, J., Kustu, S., & Stewart, V. (1994). In vitro interaction of nitrate-responsive

regulatory protein NarL with DNA target sequences in the fdnG, narG, narK and frdA operon control regions of Escherichia coli K-12. *Journal of Molecular Biology*, *241*(2), 150–165. https://doi.org/10.1006/jmbi.1994.1485

Lill, R. (2009). Function and biogenesis of iron-sulphur proteins. In *Nature* (Vol. 460, Issue 7257, pp. 831–838). Nature. https://doi.org/10.1038/nature08301

Lill, R. (2020). From the discovery to molecular understanding of cellular iron-sulfur protein biogenesis. In *Biological Chemistry* (Vol. 401, Issues 6–7, pp. 855–876). De Gruyter. https://doi.org/10.1515/hsz-2020-0117

Lill, R., Dutkiewicz, R., Elsasser, H. P., Hausmann, A., Netz, D. J., Pierik, A. J., Stehling, O., Urzica, E., & Muhlenhoff, U. (2006). Mechanisms of iron-sulfur protein maturation in mitochondria, cytosol and nucleus of eukaryotes. *Biochimica et Biophysica Acta*, *1763*(7), 652–667. https://doi.org/10.1016/j.bbamcr.2006.05.011

Lima, C. D. (2002). Analysis of the E. coli NifS CsdB protein at 2.0 Å reveals the structural basis for perselenide and persulfide intermediate formation. *Journal of Molecular Biology*, *315*(5), 1199–1208. https://doi.org/10.1006/jmbi.2001.5308

Liu, G., Li, Z., Chiang, Y., Acton, T., Montelione, G. T., Murray, D., & Szyperski, T. (2009). High-quality homology models derived from NMR and X-ray structures of E. coli proteins YgdK and Suf E suggest that all members of the YgdK/Suf E protein family are enhancers of cysteine desulfurases. *Protein Science*, *14*(6), 1597–1608. https://doi.org/10.1110/ps.041322705

Liu, M. T. W., Wuebbens, M. M., Rajagopalan, K. V., & Schindelin, H. (2000). Crystal structure of the gephyrin-related molybdenum cofactor biosynthesis protein MogA from Escherichia coli. *Journal of Biological Chemistry*, *275*(3), 1814–1822. https://doi.org/10.1074/jbc.275.3.1814

Loewen, P. C., & Hengge-Aronis, R. (1994). The role of the sigma factor σ(S) (katF) in bacterial global regulation. In *Annual Review of Microbiology* (Vol. 48, pp. 53–80). Annual Reviews Inc. https://doi.org/10.1146/annurev.mi.48.100194.000413

Loiseau, L., Gerez, C., Bekker, M., Ollagnier-de Choudens, S., Py, B., Sanakis, Y., Teixeira de Mattos, J., Fontecave, M., & Barras, F. (2007). ErpA, an iron sulfur

(Fe S) protein of the A-type essential for respiratory metabolism in Escherichia coli. *Proceedings of the National Academy of Sciences of the United States of America*, *104*(34), 13626–13631. https://doi.org/10.1073/pnas.0705829104

Loiseau, L., Ollagnier-de-Choudens, S., Nachin, L., Fontecave, M., & Barras, F. (2003). Biogenesis of Fe-S cluster by the bacterial suf system. SufS and SufE form a new type of cysteine desulfurase. *Journal of Biological Chemistry*, *278*(40), 38352–38359. https://doi.org/10.1074/jbc.M305953200

Lu, J., Yang, J., Tan, G., & Ding, H. (2008). Complementary roles of SufA and IscA in the biogenesis of iron-sulfur clusters in Escherichia coli. *Biochemical Journal*, *409*(2), 535–543. https://doi.org/10.1042/BJ20071166

Madsen, E. L. (2011). Microorganisms and their roles in fundamental biogeochemical cycles. In *Current Opinion in Biotechnology* (Vol. 22, Issue 3, pp. 456–464). Curr Opin Biotechnol. https://doi.org/10.1016/j.copbio.2011.01.008

Maio, N., & Rouault, T. A. (2020). Outlining the Complex Pathway of Mammalian Fe-S Cluster Biogenesis. In *Trends in Biochemical Sciences* (Vol. 45, Issue 5, pp. 411–426). Elsevier Ltd. https://doi.org/10.1016/j.tibs.2020.02.001

Makinoshima, H., Aizawa, S. I., Hayashi, H., Miki, T., Nishimura, A., & Ishihama, A. (2003). Growth phase-coupled alterations in cell structure and function of Escherichia coli. *Journal of Bacteriology*, *185*(4), 1338–1345. https://doi.org/10.1128/JB.185.4.1338-1345.2003

Malkin, R., & Rabinowitz, J. C. (1966). The reconstitution of clostridial ferredoxin. *Biochemical and Biophysical Research Communications*, *23*(6), 822–827. https://doi.org/10.1016/0006-291X(66)90561-4

Massé, E., & Gottesman, S. (2002). A small RNA regulates the expression of genes involved in iron metabolism in Escherichia coli. *Proceedings of the National Academy of Sciences of the United States of America*, *99*(7), 4620–4625. https://doi.org/10.1073/pnas.032066599

Massé, E., Vanderpool, C. K., & Gottesman, S. (2005). Effect of RyhB small RNA on global iron use in Escherichia coli. *Journal of Bacteriology*, *187*(20), 6962–6971.

https://doi.org/10.1128/JB.187.20.6962-6971.2005

McCarthy, E. L., & Booker, S. J. (2017). Destruction and reformation of an iron-sulfur cluster during catalysis by lipoyl synthase. *Science*, *358*(6361), 373–377. https://doi.org/10.1126/science.aan4574

McCarthy, E. L., Rankin, A. N., Dill, Z. R., & Booker, S. J. (2019). The A-type domain in Escherichia coli NfuA is required for regenerating the auxiliary [4Fe– 4S] cluster in Escherichia coli lipoyl synthase. *Journal of Biological Chemistry*, *294*(5), 1609–1617. https://doi.org/10.1074/jbc.RA118.006171

McCrindle, S. L., Kappler, U., & McEwan, A. G. (2005). Microbial dimethylsulfoxide and trimethylamine-N-oxide respiration. In *Advances in Microbial Physiology* (Vol. 50, pp. 147–198). Adv Microb Physiol. https://doi.org/10.1016/S0065-2911(05)50004-3

Mehta, A. P., Abdelwahed, S. H., & Begley, T. P. (2013). Molybdopterin biosynthesis: Trapping an unusual purine ribose adduct in the MoaA-catalyzed reaction. *Journal of the American Chemical Society*, *135*(30), 10883–10885. https://doi.org/10.1021/ja4041048

Méjean, V., Lobbi-Nivol, C., Lepelletier, M., Giordano, G., Chippaux, M., & Pascal, M. -C. (1994). TMAO anaerobic respiration in Escherichia coli: involvement of the tor operon. *Molecular Microbiology*, *11*(6), 1169–1179. https://doi.org/10.1111/j.1365-2958.1994.tb00393.x

Melville, S. B., & Gunsalus, R. P. (1996). Isolation of an oxygen-sensitive FNR protein of Escherichia coli: Interaction at activator and repressor sites of FNR-controlled genes. *Proceedings of the National Academy of Sciences of the United States of America*, *93*(3), 1226–1231. https://doi.org/10.1073/pnas.93.3.1226

Mendel, R R., Hercher, T. W., Zupok, A., Hasnat, M. A., & Leimkühler, S. (2020). The requirement of inorganic Fe-S clusters for the biosynthesis of the organometallic molybdenum cofactor. In *Inorganics* (Vol. 8, Issue 7, pp. 1–23). MDPI AG. https://doi.org/10.3390/inorganics8070043

Mendel, R R, & Leimkuhler, S. (2015). The biosynthesis of the molybdenum

cofactors. *Journal of Biological Inorganic Chemistry : JBIC : A Publication of the Society of Biological Inorganic Chemistry*, *20*(2), 337–347. https://doi.org/10.1007/s00775-014-1173-y

Mendel, Ralf R. (2013). The molybdenum cofactor. In *Journal of Biological Chemistry* (Vol. 288, Issue 19, pp. 13165–13172). Elsevier. https://doi.org/10.1074/jbc.R113.455311

Mettert, E. L., & Kiley, P. J. (2007). Contributions of [4Fe-4S]-FNR and integration host factor to fnr transcriptional regulation. *Journal of Bacteriology*, *189*(8), 3036–3043. https://doi.org/10.1128/JB.00052-07

Mettert, E. L., & Kiley, P. J. (2014). Coordinate regulation of the Suf and Isc Fe-S cluster biogenesis pathways by IscR is essential for viability of Escherichia coli. *Journal of Bacteriology*, *196*(24), 4315–4323. https://doi.org/10.1128/JB.01975-14

Mettert, E. L., & Kiley, P. J. (2015). Fe-S proteins that regulate gene expression. *Biochimica et Biophysica Acta*, *1853*(6), 1284–1293. https://doi.org/10.1016/j.bbamcr.2014.11.018

Mettert, E. L., Outten, F. W., Wanta, B., & Kiley, P. J. (2008). The Impact of O2 on the Fe-S Cluster Biogenesis Requirements of Escherichia coli FNR. *Journal of Molecular Biology*, *384*(4), 798–811. https://doi.org/10.1016/j.jmb.2008.09.080

Michaelis, L., Schubert, M. P., & Smythe, C. V. (1936). POTENTIOMETRIC STUDY OF THE FLAVINS. *Journal of Biological Chemistry*, *116*(2), 587–607. https://doi.org/10.1016/s0021-9258(18)74634-6

Mihara, H., Kurihara, T., Yoshimura, T., & Esaki, N. (2000). Kinetic and mutational studies of three NifS homologs from Escherichia coli: Mechanistic difference between L-cysteine desulfurase and L- selenocysteine lyase reactions. *Journal of Biochemistry*, *127*(4), 559–567. https://doi.org/10.1093/oxfordjournals.jbchem.a022641

Mihara, H., Kurihara, T., Yoshimura, T., Soda, K., & Esaki, N. (1997). Cysteine sulfinate desulfinase, a NIFS-like protein of Escherichia coli with selenocysteine lyase and cysteine desulfurase activities. Gene cloning, purification, and

characterization of a novel pyridoxal enzyme. *Journal of Biological Chemistry*, *272*(36), 22417–22424. https://doi.org/10.1074/jbc.272.36.22417

Mihara, H., Maeda, M., Fujii, T., Kurihara, T., Hata, Y., & Esaki, N. (1999). A nifS-like gene, csdB, encodes an Escherichia coli counterpart of mammalian selenocysteine lyase. Gene cloning, purification, characterization and preliminary X-ray crystallographic studies. *Journal of Biological Chemistry*, *274*(21), 14768–14772. https://doi.org/10.1074/jbc.274.21.14768

Miralles-Robledillo, J. M., Torregrosa-Crespo, J., Martínez-Espinosa, R. M., & Pire, C. (2019). DMSO reductase family: Phylogenetics and applications of extremophiles. *International Journal of Molecular Sciences*, *20*(13). https://doi.org/10.3390/ijms20133349

Moore, L. J., & Kiley, P. J. (2001). Characterization of the dimerization domain in the FNR transcription factor. *The Journal of Biological Chemistry*, *276*(49), 45744–45750. https://doi.org/10.1074/jbc.M106569200

Mueller, E. G. (2006). Trafficking in persulfides: Delivering sulfur in biosynthetic pathways. *Nature Chemical Biology*, *2*(4), 185–194. https://doi.org/10.1038/nchembio779

Mühlenhoff, U, Gerber, J., Richhardt, N., & Lill, R. (2003). Components involved in assembly and dislocation of iron-sulfur clusters on the scaffold protein Isu1p. *EMBO Journal*, *22*(18), 4815–4825. https://doi.org/10.1093/emboj/cdg446

Mühlenhoff, Ulrich, Richter, N., Pines, O., Pierik, A. J., & Lill, R. (2011). Specialized function of yeast Isa1 and Isa2 proteins in the maturation of mitochondrial [4Fe-4S] proteins. *Journal of Biological Chemistry*, *286*(48), 41205–41216. https://doi.org/10.1074/jbc.M111.296152

Myers, K. S., Yan, H., Ong, I. M., Chung, D., Liang, K., Tran, F., Keles, S., Landick, R., & Kiley, P. J. (2013). Genome-scale analysis of escherichia coli FNR reveals complex features of transcription factor binding. *PLoS Genetics*, *9*(6), e1003565. https://doi.org/10.1371/journal.pgen.1003565

Myers, K. S., Yan, H., Ong, I. M., Chung, D., Liang, K., Tran, F., Keleş, S., Landick, R., & Kiley, P. J. (2013). Genome-scale Analysis of Escherichia coli FNR

Reveals Complex Features of Transcription Factor Binding. *PLoS Genetics*, *9*(6), e1003565. https://doi.org/10.1371/journal.pgen.1003565

Nagahara, N., Matsumura, T., Okamoto, R., & Kajihara, Y. (2009). Protein Cysteine Modifications: (1) Medicinal Chemistry for Proteomics. *Current Medicinal Chemistry*, *16*(33), 4419–4444. https://doi.org/10.2174/092986709789712880

Najmudin, S., González, P. J., Trincão, J., Coelho, C., Mukhopadhyay, A., Cerqueira, N. M. F. S. A., Romão, C. C., Moura, I., Moura, J. J. G., Brondino, C. D., & Romão, M. J. (2008). Periplasmic nitrate reductase revisited: A sulfur atom completes the sixth coordination of the catalytic molybdenum. *Journal of Biological Inorganic Chemistry*, *13*(5), 737–753. https://doi.org/10.1007/s00775-008-0359-6

Neilands, J. B. (1981). Microbial Iron Compounds. *Annual Review of Biochemistry*, *50*(1), 715–731. https://doi.org/10.1146/annurev.bi.50.070181.003435

Netz, D. J. A., Mascarenhas, J., Stehling, O., Pierik, A. J., & Lill, R. (2014). Maturation of cytosolic and nuclear iron-sulfur proteins. In *Trends in Cell Biology* (Vol. 24, Issue 5, pp. 303–312). Elsevier Ltd. https://doi.org/10.1016/j.tcb.2013.11.005

Neumann, M., Mittelstädt, G., Iobbi-Nivol, C., Saggu, M., Lendzian, F., Hildebrandt, P., & Leimkühler, S. (2009). A periplasmic aldehyde oxidoreductase represents the first molybdopterin cytosine dinucleotide cofactor containing molybdo-flavoenzyme from Escherichia coli. *FEBS Journal*, *276*(10), 2762–2774. https://doi.org/10.1111/j.1742-4658.2009.07000.x

Neumann, M., Mittelstadt, G., Seduk, F., Iobbi-Nivol, C., & Leimkuhler, S. (2009). MocA is a specific cytidylyltransferase involved in molybdopterin cytosine dinucleotide biosynthesis in Escherichia coli. *The Journal of Biological Chemistry*, *284*(33), 21891–21898. https://doi.org/10.1074/jbc.M109.008565

Neumann, M., Stöcklein, W., Walburger, A., Magalon, A., & Leimkühler, S. (2007a). Identification of a Rhodobacter capsulatus L-cysteine desulfurase that sulfurates the molybdenum cofactor when bound to XdhC and before its insertion into xanthine dehydrogenase. *Biochemistry*, *46*(33), 9586–9595. https://doi.org/10.1021/bi700630p

Neumann, M., Stöcklein, W., Walburger, A., Magalon, A., & Leimkühler, S. (2007b). Identification of a Rhodobacter capsulatus L-cysteine desulfurase that sulfurates the molybdenum cofactor when bound to XdhC and before its insertion into xanthine dehydrogenase. *Biochemistry*, *46*(33), 9586–9595. https://doi.org/10.1021/bi700630p

Nichols, J. D., & Rajagopalan, K. V. (2005). In Vitro Molybdenum Ligation to Molybdopterin Using Purified Components. *Journal of Biological Chemistry*, *280*(9), 7817–7822. https://doi.org/10.1074/jbc.M413783200

Nichols, J., & Rajagopalan, K. V. (2002). Escherichia coli MoeA and MogA. Function in metal incorporation step of molybdenum cofactor biosynthesis. *The Journal of Biological Chemistry*, *277*(28), 24995–25000. https://doi.org/10.1074/jbc.M203238200

Ollagnier-de-Choudens, S., Sanakis, Y., & Fontecave, M. (2004). SufA/IscA: Reactivity studies of a class of scaffold proteins involved in [Fe-S] cluster assembly. *Journal of Biological Inorganic Chemistry*, *9*(7), 828–838. https://doi.org/10.1007/s00775-004-0581-9

Outten, F. W., Djaman, O., & Storz, G. (2004). A suf operon requirement for Fe-S cluster assembly during iron starvation in Escherichia coli. *Molecular Microbiology*, *52*(3), 861–872. https://doi.org/10.1111/j.1365-2958.2004.04025.x

Outten, F. W., Wood, M. J., Muñoz, F. M., & Storz, G. (2003). The SufE Protein and the SufBCD Complex Enhance SufS Cysteine Desulfurase Activity as Part of a Sulfur Transfer Pathway for Fe-S Cluster Assembly in Escherichia coli. *Journal of Biological Chemistry*, *278*(46), 45713–45719. https://doi.org/10.1074/jbc.M308004200

Palchevskiy, V., & Finkel, S. E. (2006). Escherichia coli competence gene homologs are essential for competitive fitness and the use of DNA as a nutrient. *Journal of Bacteriology*, *188*(11), 3902–3910. https://doi.org/10.1128/JB.01974-05

Palmer, T., Santini, C. L., Iobbi-Nivol, C., Eaves, D. J., Boxer, D. H., & Giordano, G. (1996). Involvement of the narJ and mob gene products in distinct steps in the biosynthesis of the molybdoenzyme nitrate reductase in Escherichia coli. *Molecular Microbiology*, *20*(4), 875–884. https://doi.org/10.1111/j.1365-

2958.1996.tb02525.x

Pascal, M. C., Burini, J. F., & Chippaux, M. (1984). Regulation of the trimethylamine N-oxide (TMAO) reductase in Escherichia coli: Analysis of tor::Mu d1 operon fusion. *MGG Molecular & General Genetics*, *195*(1–2), 351–355. https://doi.org/10.1007/BF00332770

Paul, V. D., & Lill, R. (2015). Biogenesis of cytosolic and nuclear iron-sulfur proteins and their role in genome stability. In *Biochimica et Biophysica Acta - Molecular Cell Research* (Vol. 1853, Issue 6, pp. 1528–1539). Elsevier. https://doi.org/10.1016/j.bbamcr.2014.12.018

Petersen, L., & Downs, D. M. (1996). Mutations in apbC (mrp) prevent function of the alternative pyrimidine biosynthetic pathway in Salmonella typhimurium. *Journal of Bacteriology*, *178*(19), 5676–5682. https://doi.org/10.1128/jb.178.19.5676-5682.1996

Pinske, C., & Sawers, R. G. (2012a). A-type carrier protein ErpA is essential for formation of an active formate-nitrate respiratory pathway in Escherichia coli K-12. *Journal of Bacteriology*, *194*(2), 346–353. https://doi.org/10.1128/JB.06024-11

Pinske, C., & Sawers, R. G. (2012b). Delivery of iron-sulfur clusters to the hydrogen-oxidizing [NiFe]-hydrogenases in Escherichia coli requires the A-type carrier proteins ErpA and IscA. *PloS One*, *7*(2), e31755. https://doi.org/10.1371/journal.pone.0031755

Pitterle, D. M., Johnson, J. L., & Rajagopalan, K. V. (1993). In vitro synthesis of molybdopterin from precursor Z using purified converting factor. Role of protein-bound sulfur in formation of the dithiolene. *Journal of Biological Chemistry*, *268*(18), 13506–13509. https://doi.org/10.1016/s0021-9258(19)38678-8

Pitterle, D. M., & Rajagopalan, K. V. (1989). Two proteins encoded at the chlA locus constitute the converting factor of Escherichia coli chlA1. *Journal of Bacteriology*, *171*(6), 3373–3378. https://doi.org/10.1128/jb.171.6.3373-3378.1989

Pitterle, D. M., & Rajagopalan, K. V. (1993). The biosynthesis of molybdopterin in

Escherichia coli. Purification and characterization of the converting factor. *Journal of Biological Chemistry*, *268*(18), 13499–13505. https://doi.org/10.1016/s0021-9258(19)38677-6

Pohl, T., Walter, J., Stolpe, S., Soufo, J. H. D., Grauman, P. L., & Friedrich, T. (2007). Effects of the deletion of the Escherichia coli frataxin homologue CyaY on the respiratory NADH:ubiquinone oxidoreductase. *BMC Biochemistry*, *8*. https://doi.org/10.1186/1471-2091-8-13

Pommier, J., Mejean, V., Giordano, G., & Iobbi-Nivol, C. (1998). TorD, a cytoplasmic chaperone that interats with the unfolded trimethylamine N-oxide reductase enzyme (TorA) in Escherichia coli. *Journal of Biological Chemistry*, *273*(26), 16615–16620. https://doi.org/10.1074/jbc.273.26.16615

Prischi, F., Konarev, P. V., Iannuzzi, C., Pastore, C., Adinolfi, S., Martin, S. R., Svergun, D. I., & Pastore, A. (2010). Structural bases for the interaction of frataxin with the central components of iron-sulphur cluster assembly. *Nature Communications*, *1*(7). https://doi.org/10.1038/ncomms1097

Py, B., & Barras, F. (2010). Building Feg-S proteins: Bacterial strategies. In *Nature Reviews Microbiology* (Vol. 8, Issue 6, pp. 436–446). Nature Publishing Group. https://doi.org/10.1038/nrmicro2356

Py, B., Gerez, C., Angelini, S., Planel, R., Vinella, D., Loiseau, L., Talla, E., Brochier-Armanet, C., Garcia Serres, R., Latour, J. M., Ollagnier-de Choudens, S., Fontecave, M., & Barras, F. (2012). Molecular organization, biochemical function, cellular role and evolution of NfuA, an atypical Fe-S carrier. *Molecular Microbiology*, *86*(1), 155–171. https://doi.org/10.1111/j.1365-2958.2012.08181.x

Py, B., Gerez, C., Huguenot, A., Vidaud, C., Fontecave, M., Ollagnier de Choudens, S., & Barras, F. (2018a). The ErpA/NfuA complex builds an oxidation-resistant Fe-S cluster delivery pathway. *The Journal of Biological Chemistry*, *293*(20), 7689–7702. https://doi.org/10.1074/jbc.RA118.002160

Py, B., Gerez, C., Huguenot, A., Vidaud, C., Fontecave, M., Ollagnier de Choudens, S., & Barras, F. (2018b). The ErpA/NfuA complex builds an oxidation-resistant Fe-S cluster delivery pathway. *Journal of Biological Chemistry*, *293*(20), 7689–7702. https://doi.org/10.1074/jbc.RA118.002160

Py, B., Moreau, P. L., & Barras, F. (2011). Fe-S clusters, fragile sentinels of the cell. In *Current Opinion in Microbiology* (Vol. 14, Issue 2, pp. 218–223). Elsevier Current Trends. https://doi.org/10.1016/j.mib.2011.01.004

Rabin, R. S., Collins, L. A., & Stewart, V. (1992). In vivo requirement of integration host factor for nar (nitrate reductase) operon expression in Escherichia coli K-12. *Proceedings of the National Academy of Sciences of the United States of America*, *89*(18), 8701–8705. https://doi.org/10.1073/pnas.89.18.8701

Rabin, R. S., & Stewart, V. (1993). Dual response regulators (NarL and NarP) interact with dual sensors (NarX and NarQ) to control nitrate- and nitrite-regulated gene expression in Escherichia coli K-12. *Journal of Bacteriology*, *175*(11), 3259–3268. https://doi.org/10.1128/jb.175.11.3259-3268.1993

Rajagopalan, & V., K. (1996). Biosynthesis of the molybdenum cofactor. *Escherichia Coli and Salmonella Typhimurium*, 674–679. https://ci.nii.ac.jp/naid/10011704404

Rajagopalan, K. V., Johnson, J. L., & Hainline, B. E. (1982). The pterin of the molybdenum cofactor. *Federation Proceedings*, *41*(9), 2608–2612. http://www.ncbi.nlm.nih.gov/pubmed/6953016

Rajagopalan, K. V, & Johnson, J. L. (1992). The pterin molybdenum cofactors. *The Journal of Biological Chemistry*, *267*(15), 10199–10202. http://www.ncbi.nlm.nih.gov/pubmed/1587808

Raulfs, E. C., O'Carroll, I. P., Dos Santos, P. C., Unciuleac, M. C., & Dean, D. R. (2008). In vivo iron-sulfur cluster formation. *Proceedings of the National Academy of Sciences of the United States of America*, *105*(25), 8591–8596. https://doi.org/10.1073/pnas.0803173105

Reinhart, F., Achebach, S., Koch, T., & Unden, G. (2008). Reduced apo-fumarate nitrate reductase regulator (ApoFNR) as the major form of FNR in aerobically growing Escherichia coli. *Journal of Bacteriology*, *190*(3), 879–886. https://doi.org/10.1128/JB.01374-07

Reschke, S., Sigfridsson, K. G., Kaufmann, P., Leidel, N., Horn, S., Gast, K., Schulzke, C., Haumann, M., & Leimkuhler, S. (2013). Identification of a bis-

molybdopterin intermediate in molybdenum cofactor biosynthesis in Escherichia coli. *The Journal of Biological Chemistry*, *288*(41), 29736–29745. https://doi.org/10.1074/jbc.M113.497453

Rivers, S. L., McNairn, E., Blasco, F., Giordano, G., & Boxer, D. H. (1993). Molecular genetic analysis of the moa operon of Escherichia coli K-12 required for molybdenum cofactor biosynthesis. *Molecular Microbiology*, *8*(6), 1071–1081. https://doi.org/10.1111/j.1365-2958.1993.tb01652.x

Roche, B., Aussel, L., Ezraty, B., Mandin, P., Py, B., & Barras, F. (2013). Iron/sulfur proteins biogenesis in prokaryotes: formation, regulation and diversity. *Biochimica et Biophysica Acta*, *1827*(3), 455–469. https://doi.org/10.1016/j.bbabio.2012.12.010

Roggiani, M., & Goulian, M. (2015). Oxygen-dependent cell-to-cell variability in the output of the Escherichia coli tor phosphorelay. *Journal of Bacteriology*, *197*(12), 1976–1987. https://doi.org/10.1128/JB.00074-15

Rothery, R. A., Bertero, M. G., Cammack, R., Palak, M., Blasco, F., Strynadka, N. C. J., & Weiner, J. H. (2004). The Catalytic Subunit of Escherichia coli Nitrate Reductase A Contains a Novel [4Fe-4S] Cluster with a High-Spin Ground State. *Biochemistry*, *43*(18), 5324–5333. https://doi.org/10.1021/bi049938l

Rothery, R. A., Blasco, F., Magalon, A., Asso, M., & Weiner, J. H. (1999). The hemes of Escherichia coli nitrate reductase A (NarGHI): Potentiometric effects of inhibitor binding to NarI. *Biochemistry*, *38*(39), 12747–12757. https://doi.org/10.1021/bi990533o

Rothery, R. A., Blasco, F., Magalon, A., & Weiner, J. H. (2001). *The diheme cytochrome b subunit (NarI) of Escherichia coli nitrate reductase A (NarGHI): Structure, function, and interaction with quinols*. Journal of Molecular Microbiology and Biotechnology. https://pubmed.ncbi.nlm.nih.gov/11321583/

Rudolph, M. J., Wuebbens, M. M., Rajagopalan, K. V., & Schindelin, H. (2001). Crystal structure of molybdopterin synthase and its evolutionary relationship to ubiquitin activation. *Nature Structural Biology*, *8*(1), 42–46. https://doi.org/10.1038/83034

Saini, A., Mapolelo, D. T., Chahal, H. K., Johnson, M. K., & Outten, F. W. (2010). SufD and SufC ATPase activity are required for iron acquisition during in vivo Fe-S cluster formation on SufB. *Biochemistry*, *49*(43), 9402–9412. https://doi.org/10.1021/bi1011546

Salmon, K., Hung, S. pin, Mekjian, K., Baldi, P., Hatfield, G. W., & Gunsalus, R. P. (2003). Global gene expression profiling in Escherichia coli K12: The effects of oxygen availability and FNR. *Journal of Biological Chemistry*, *278*(32), 29837–29855. https://doi.org/10.1074/jbc.M213060200

Santos, J. M., Lobo, M., Matos, A. P. A., De Pedro, M. A., & Arraiano, C. M. (2002). The gene bolA regulates dacA (PBP5), dacC (PBP6) and ampC (AmpC), promoting normal morphology in Escherichia coli. *Molecular Microbiology*, *45*(6), 1729–1740. https://doi.org/10.1046/j.1365-2958.2002.03131.x

Schrag, J. D., Huang, W., Sivaraman, J., Smith, C., Plamondon, J., Larocque, R., Matte, A., & Cygler, M. (2001). The crystal structure of Escherichia coli MoeA, a protein from the molybdopterin synthesis pathway. *Journal of Molecular Biology*, *310*(2), 419–431. https://doi.org/10.1006/jmbi.2001.4771

Schroder, I., Darie, S., & Gunsalus, R. P. (1993). Activation of the Escherichia coli nitrate reductase (narGHJI) operon by NarL and Fnr requires integration host factor. *Journal of Biological Chemistry*, *268*(2), 771–774. https://doi.org/10.1016/s0021-9258(18)53999-5

Schumann, S., Saggu, M., Möller, N., Anker, S. D., Lendzian, F., Hildebrandt, P., & Leimkühler, S. (2008). The mechanism of assembly and cofactor insertion into Rhodobacter capsulatus xanthine dehydrogenase. *Journal of Biological Chemistry*, *283*(24), 16602–16611. https://doi.org/10.1074/jbc.M709894200

Schwartz, C. J., Giel, J. L., Patschkowski, T., Luther, C., Ruzicka, F. J., Beinert, H., & Kiley, P. J. (2001). IscR, an Fe-S cluster-containing transcription factor, represses expression of escherichia coli genes encoding Fe-S cluster assembly proteins. *Proceedings of the National Academy of Sciences of the United States of America*, *98*(26), 14895–14900. https://doi.org/10.1073/pnas.251550898

Sekowska, A., Danchin, A., & Risler, J. L. (2000). Phylogeny of related functions: The case of polyamine biosynthetic enzymes. *Microbiology*, *146*(8), 1815–1828.

https://doi.org/10.1099/00221287-146-8-1815

Shanmugam, K. T., Stewart, V., Gunsalus, R. P., Boxer, D. H., Cole, J. A., Chippaux, M., DeMoss, J. A., Giordano, G., Lin, E. C., & Rajagopalan, K. V. (1992). Proposed nomenclature for the genes involved in molybdenum metabolism in Escherichia coli and Salmonella typhimurium. *Molecular Microbiology*, *6*(22), 3452–3454. https://doi.org/10.1111/j.1365-2958.1992.tb02215.x

Sheftel, A. D., Wilbrecht, C., Stehling, O., Niggemeyer, B., Elsässer, H. P., Mühlenhoff, U., & Lill, R. (2012). The human mitochondrial ISCA1, ISCA2, and IBA57 proteins are required for [4Fe-4S] protein maturation. *Molecular Biology of the Cell*, *23*(7), 1157–1166. https://doi.org/10.1091/mbc.E11-09-0772

Shi, R., Proteau, A., Villarroya, M., Moukadiri, I., Zhang, L., Trempe, J.-F., Matte, A., Armengod, M. E., & Cygler, M. (2010). Structural Basis for Fe–S Cluster Assembly and tRNA Thiolation Mediated by IscS Protein–Protein Interactions. *PLoS Biology*, *8*(4), e1000354. https://doi.org/10.1371/journal.pbio.1000354

Shimomura, Y., Wada, K., Fukuyama, K., & Takahashi, Y. (2008). The Asymmetric Trimeric Architecture of [2Fe-2S] IscU: Implications for Its Scaffolding during Iron-Sulfur Cluster Biosynthesis. *Journal of Molecular Biology*, *383*(1), 133–143. https://doi.org/10.1016/j.jmb.2008.08.015

Silberg, J. J., & Vickery, L. E. (2000). Kinetic characterization of the ATPase cycle of the molecular chaperone Hsc66 from Escherichia coli. *Journal of Biological Chemistry*, *275*(11), 7779–7786. https://doi.org/10.1074/jbc.275.11.7779

Simmonds, S., Szeto, K. S., & Fletterick, C. (1976). Soluble Tri- and Dipeptidases in Escherichia coli K-12. *Biochemistry*, *15*(2), 261–271. https://doi.org/10.1021/bi00647a004

Simon, G., Mejean, V., Jourlin, C., Chippaux, M., & Pascal, M. C. (1994). The torR gene of Escherichia coli encodes a response regulator protein involved in the expression of the trimethylamine N-oxide reductase genes. *Journal of Bacteriology*, *176*(18), 5601–5606. https://doi.org/10.1128/jb.176.18.5601-5606.1994

Sodergren, E. J., Hsu, P. Y., & DeMoss, J. A. (1988). *Roles of the narJ and narI*

gene products in the expression of nitrate reductase in Escherichia coli. The Journal of Biological Chemistry. https://doi.org/10.1016/s0021-9258(18)37572-0

Sofia, H. J., Chen, G., Hetzler, B. G., Reyes-Spindola, J. F., & Miller, N. E. (2001). Radical SAM, a novel protein superfamily linking unresolved steps in familiar biosynthetic pathways with radical mechanisms: Functional characterization using new analysis and information visualization methods. *Nucleic Acids Research*, *29*(5), 1097–1106. https://doi.org/10.1093/nar/29.5.1097

Spiro, S, & Guest, J. R. (1990). FNR and its role in oxygen-regulated gene expression in Escherichia coli. *FEMS Microbiology Letters*, *75*(4), 399–428. https://doi.org/10.1111/j.1574-6968.1990.tb04109.x

Spiro, Stephen, & Guest, J. R. (1987). Regulation and Over-expression of the fnr Gene of Escherichia coli. *Microbiology*, *133*(12), 3279–3288. https://doi.org/10.1099/00221287-133-12-3279

Srinivasan, V., Netz, D. J. A., Webert, H., Mascarenhas, J., Pierik, A. J., Michel, H., & Lill, R. (2007). Structure of the Yeast WD40 Domain Protein Cia1, a Component Acting Late in Iron-Sulfur Protein Biogenesis. *Structure*, *15*(10), 1246–1257. https://doi.org/10.1016/j.str.2007.08.009

Stehling, O., Netz, D. J. A., Niggemeyer, B., Rösser, R., Eisenstein, R. S., Puccio, H., Pierik, A. J., & Lill, R. (2008). Human Nbp35 Is Essential for both Cytosolic Iron-Sulfur Protein Assembly and Iron Homeostasis. *Molecular and Cellular Biology*, *28*(17), 5517–5528. https://doi.org/10.1128/mcb.00545-08

Stevenson, C. E. M., Sargent, F., Buchanan, G., Palmer, T., & Lawson, D. M. (2000). Crystal structure of the molybdenum cofactor biosynthesis protein MobA from Escherichia coli at near-atomic resolution. *Structure*, *8*(11), 1115–1125. https://doi.org/10.1016/S0969-2126(00)00518-9

Stewart, V. (1982). Requirement of Fnr and NarL functions for nitrate reductase expression in Escherichia coli K-12. *Journal of Bacteriology*, *151*(3), 1320–1325. https://doi.org/10.1128/jb.151.3.1320-1325.1982

Stewart, V. (1988). Nitrate respiration in relation to facultative metabolism in enterobacteria. In *Microbiological Reviews* (Vol. 52, Issue 2, pp. 190–232).

American Society for Microbiology (ASM). https://doi.org/10.1128/mmbr.52.2.190-232.1988

Stintzi, A., Barnes, C., Xu, J., & Raymond, K. N. (2000). Microbial iron transport via a siderophore shuttle: A membrane ion transport paradigm. *Proceedings of the National Academy of Sciences of the United States of America*, *97*(20), 10691–10696. https://doi.org/10.1073/pnas.200318797

Sussman, A. J., & Gilvarg, C. (1970). *Peptidases in Escherichia coli K-12 capable of cleaving lysine homopeptides.* Journal of Biological Chemistry. https://doi.org/10.1016/s0021-9258(18)62564-5

Sutton, V. R., Mettert, E. L., Beinert, H., & Kiley, P. J. (2004). Kinetic analysis of the oxidative conversion of the [4Fe-4S]2+ cluster of FNR to a [2Fe-2S]2+ cluster. *Journal of Bacteriology*, *186*(23), 8018–8025. https://doi.org/10.1128/JB.186.23.8018-8025.2004

Takahashi, Y., & Tokumoto, U. (2002). A third bacterial system for the assembly of iron-sulfur clusters with homologs in archaea and plastids. *The Journal of Biological Chemistry*, *277*(32), 28380–28383. https://doi.org/10.1074/jbc.C200365200

Tan, G., Lu, J., Bitoun, J. P., Huang, H., & Ding, H. (2009). IscA/SufA paralogues are required for the [4Fe-4S] cluster assembly in enzymes of multiple physiological pathways in Escherichia coli under aerobic growth conditions. *Biochemical Journal*, *420*(3), 463–472. https://doi.org/10.1042/BJ20090206

Tanaka, N., Kanazawa, M., Tonosaki, K., Yokoyama, N., Kuzuyama, T., & Takahashi, Y. (2016). Novel features of the ISC machinery revealed by characterization of Escherichia coli mutants that survive without iron-sulfur clusters. *Molecular Microbiology*, *99*(5), 835–848. https://doi.org/10.1111/mmi.13271

Tapley, T. L., Cupp-Vickery, J. R., & Vickery, L. E. (2006). Structural determinants of HscA peptide-binding specificity. *Biochemistry*, *45*(26), 8058–8066. https://doi.org/10.1021/bi0606187

Temple, C. A., Graf, T. N., & Rajagopalan, K. V. (2000). Optimization of expression

of human sulfite oxidase and its molybdenum domain. *Archives of Biochemistry and Biophysics*, *383*(2), 281–287. https://doi.org/10.1006/abbi.2000.2089

Teschner, J., Lachmann, N., Schulze, J., Geisler, M., Selbach, K., Santamaria-Araujo, J., Balk, J., Mendel, R. R., & Bittner, F. (2010). A novel role for Arabidopsis mitochondrial ABC transporter ATM3 in molybdenum cofactor biosynthesis. *Plant Cell*, *22*(2), 468–480. https://doi.org/10.1105/tpc.109.068478

Thome, R., Gust, A., Toci, R., Mendel, R., Bittner, F., Magalon, A., & Walburger, A. (2012). A sulfurtransferase is essential for activity of formate dehydrogenases in Escherichia coli. *The Journal of Biological Chemistry*, *287*(7), 4671–4678. https://doi.org/10.1074/jbc.M111.327122

Tokumoto, U., & Takahashi, Y. (2001). Genetic analysis of the isc operon in Escherichia coli involved in the biogenesis of cellular iron-sulfur proteins. *Journal of Biochemistry*, *130*(1), 63–71. https://doi.org/10.1093/oxfordjournals.jbchem.a002963

Tsai, C. L., & Barondeau, D. P. (2010). Human frataxin is an allosteric switch that activates the Fe-S cluster biosynthetic complex. *Biochemistry*, *49*(43), 9132–9139. https://doi.org/10.1021/bi1013062

Unden, G., Achebach, S., Holighaus, G., Tran, H. Q., Wackwitz, B., & Zeuner, Y. (2002). *Control of FNR function of Escherichia coli by O2 and reducing conditions*. Journal of Molecular Microbiology and Biotechnology. https://pubmed.ncbi.nlm.nih.gov/11931557/

Unden, G., & Bongaerts, J. (1997). Alternative respiratory pathways of Escherichia coli: Energetics and transcriptional regulation in response to electron acceptors. In *Biochimica et Biophysica Acta - Bioenergetics* (Vol. 1320, Issue 3, pp. 217–234). Biochim Biophys Acta. https://doi.org/10.1016/S0005-2728(97)00034-0

Vinella, D, Loiseau, L., de Choudens, S. O., Fontecave, M., & Barras, F. (2013). In vivo [Fe-S] cluster acquisition by IscR and NsrR, two stress regulators in Escherichia coli. *Molecular Microbiology*, *87*(3), 493–508. https://doi.org/10.1111/mmi.12135

Vinella, Daniel, Brochier-Armanet, C., Loiseau, L., Talla, E., & Barras, F. (2009).

Iron-sulfur (Fe/S) protein biogenesis: Phylogenomic and genetic studies of A-type carriers. *PLoS Genetics*, *5*(5), e1000497. https://doi.org/10.1371/journal.pgen.1000497

Vivas, E., Skovran, E., & Downs, D. M. (2006). Salmonella enterica strains lacking the frataxin homolog cyaY show defects in Fe-S cluster metabolism in vivo. *Journal of Bacteriology*, *188*(3), 1175–1179. https://doi.org/10.1128/JB.188.3.1175-1179.2006

Wada, K., Hasegawa, Y., Gong, Z., Minami, Y., Fukuyama, K., & Takahashi, Y. (2005). Crystal structure of Escherichia coli SufA involved in biosynthesis of iron-sulfur clusters: Implications for a functional dimer. *FEBS Letters*, *579*(29), 6543–6548. https://doi.org/10.1016/j.febslet.2005.10.046

Wahl, R. C., & Rajagopalan, K. V. (1982). Evidence for the inorganic nature of the cyanolyzable sulfur of molybdenum hydroxylases. *Journal of Biological Chemistry*, *257*(3), 1354–1359. https://doi.org/10.1016/s0021-9258(19)68199-8

Wang, F., Lv, H., Zhao, B., Zhou, L., Wang, S., Luo, J., Liu, J., & Shang, P. (2019). Iron and leukemia: New insights for future treatments. In *Journal of Experimental and Clinical Cancer Research* (Vol. 38). BioMed Central Ltd. https://doi.org/10.1186/s13046-019-1397-3

Wayne Outten, F. (2015). Recent advances in the Suf Fe-S cluster biogenesis pathway: Beyond the Proteobacteria. In *Biochimica et Biophysica Acta - Molecular Cell Research* (Vol. 1853, Issue 6, pp. 1464–1469). Elsevier. https://doi.org/10.1016/j.bbamcr.2014.11.001

WESTLEY, J., ADLER, H., WESTLEY, L., & NISHIDA, C. (1983). The sulfurtransferases. *Fundamental and Applied Toxicology*, *3*(5), 377–382. https://doi.org/10.1016/s0272-0590(83)80008-6

Wing, H. J., Williams, S. M., & Busby, S. J. W. (1995). Spacing requirements for transcription activation by Escherichia coli FNR protein. *Journal of Bacteriology*, *177*(23), 6704–6710. https://doi.org/10.1128/jb.177.23.6704-6710.1995

Wissenbach, U., Kröger, A., & Unden, G. (1990). The specific functions of menaquinone and demethylmenaquinone in anaerobic respiration with

fumarate, dimethylsulfoxide, trimethylamine N-oxide and nitrate by Escherichia coli. *Archives of Microbiology*, *154*(1), 60–66. https://doi.org/10.1007/BF00249179

Wissenbach, U., Ternes, D., & Unden, G. (1992). An Escherichia coli mutant containing only demethylmenaquinone, but no menaquinone: effects on fumarate, dimethylsulfoxide, trimethylamine N-oxide and nitrate respiration. *Archives of Microbiology*, *158*(1), 68–73. https://doi.org/10.1007/BF00249068

Wolff, M., Seemann, M., Tse Sum Bui, B., Frapart, Y., Tritsch, D., Garcia Estrabot, A., Rodríguez-Concepción, M., Boronat, A., Marquet, A., & Rohmer, M. (2003). Isoprenoid biosynthesis via the methylerythritol phosphate pathway: The (E)-4-hydroxy-3-methylbut-2-enyl diphosphate reductase (LytB/IspH) from Escherichia coli is a [4Fe-4S] protein. *FEBS Letters*, *541*(1–3), 115–120. https://doi.org/10.1016/S0014-5793(03)00317-X

Wollers, S., Layer, G., Garcia-Serres, R., Signor, L., Clemancey, M., Latour, J. M., Fontecave, M., & De Choudens, S. O. (2010). Iron-sulfur (Fe-S) cluster assembly: The SufBCD complex is a new type of Fe-S scaffold with a flavin redox cofactor. *Journal of Biological Chemistry*, *285*(30), 23331–23341. https://doi.org/10.1074/jbc.M110.127449

Wu, S. P., Mansy, S. S., & Cowan, J. A. (2005). Iron-sulfur cluster biosynthesis. Molecular chaperone DnaK promotes IscU-bound [2Fe-2S] cluster stability and inhibits cluster transfer activity. *Biochemistry*, *44*(11), 4284–4293. https://doi.org/10.1021/bi0483007

Wuebbens, M. M., & Rajagopalan, K. V. (1995). Investigation of the early steps of molybdopterin biosynthesis in Escherichia coli through the use of in vivo labeling studies. *Journal of Biological Chemistry*, *270*(3), 1082–1087. https://doi.org/10.1074/jbc.270.3.1082

Wuebbens, M. M., & Rajagopalan, K. V. (2003). Mechanistic and mutational studies of Escherichia coli molybdopterin synthase clarify the final step of molybdopterin biosynthesis. *Journal of Biological Chemistry*, *278*(16), 14523–14532. https://doi.org/10.1074/jbc.M300453200

Xiang, S., Nichols, J., Rajagopalan, K. V., & Schindelin, H. (2001). The crystal

structure of Escherichia coli MoeA and its relationship to the multifunctional protein gephyrin. *Structure*, *9*(4), 299–310. https://doi.org/10.1016/S0969-2126(01)00588-3

Yang, J., Tan, G., Zhang, T., White, R. H., Lu, J., & Ding, H. (2015). Deletion of the proposed iron chaperones IscA/SufA results in accumulation of a red intermediate cysteine desulfurase IscS in Escherichia coli. *Journal of Biological Chemistry*, *290*(22), 14226–14234. https://doi.org/10.1074/jbc.M115.654269

Yeo, W. S., Lee, J. H., Lee, K. C., & Roe, J. H. (2006). IscR acts as an activator in response to oxidative stress for the suf operon encoding Fe-S assembly proteins. *Molecular Microbiology*, *61*(1), 206–218. https://doi.org/10.1111/j.1365-2958.2006.05220.x

Yeung, N., Gold, B., Liu, N. L., Prathapam, R., Sterling, H. J., Willams, E. R., & Butland, G. (2011). The E. coli monothiol glutaredoxin GrxD forms homodimeric and heterodimeric FeS cluster containing complexes. *Biochemistry*, *50*(41), 8957–8969. https://doi.org/10.1021/bi2008883

Yokoyama, K., & Leimkuhler, S. (2015). The role of FeS clusters for molybdenum cofactor biosynthesis and molybdoenzymes in bacteria. *Biochimica et Biophysica Acta*, *1853*(6), 1335–1349. https://doi.org/10.1016/j.bbamcr.2014.09.021

Zhang, L., Nelson, K. J., Rajagopalan, K. V., & George, G. N. (2008). Structure of the molybdenum site of Escherichia coli trimethylamine N-oxide reductase. *Inorganic Chemistry*, *47*(3), 1074–1078. https://doi.org/10.1021/ic701956f

Zhang, Y., & Gladyshev, V. N. (2008). Molybdoproteomes and Evolution of Molybdenum Utilization. *Journal of Molecular Biology*, *379*(4), 881–899. https://doi.org/10.1016/j.jmb.2008.03.051

Zhao, Z., Rothery, R. A., & Weiner, J. H. (2003). Transient kinetic studies of heme reduction in Escherichia coli nitrate reductase A (NarGHI) by menaquinol. *Biochemistry*, *42*(18), 5403–5413. https://doi.org/10.1021/bi027221x

Zheng, L., Cash, V. L., Flint, D. H., & Dean, D. R. (1998). Assembly of iron-sulfur clusters. Identification of an iscSUA-hscBA-fdx gene cluster from Azotobacter

vinelandii. *The Journal of Biological Chemistry*, *273*(21), 13264–13272. http://www.ncbi.nlm.nih.gov/pubmed/9582371

Zheng, L., White, R. H., Cash, V. L., & Dean, D. R. (1994). Mechanism for the Desulfurization of L-Cysteine Catalyzed by the nifS Gene Product. *Biochemistry*, *33*(15), 4714–4720. https://doi.org/10.1021/bi00181a031

Zheng, L., White, R. H., Cash, V. L., Jack, R. F., & Dean, D. R. (1993). Cysteine desulfurase activity indicates a role for NIFS in metallocluster biosynthesis. *Proceedings of the National Academy of Sciences of the United States of America*, *90*(7), 2754–2758. https://doi.org/10.1073/pnas.90.7.2754

Zheng, M., Wang, X., Templeton, L. J., Smulski, D. R., LaRossa, R. A., & Storz, G. (2001). DNA microarray-mediated transcriptional profiling of the Escherichia coli response to hydrogen peroxide. *Journal of Bacteriology*, *183*(15), 4562–4570. https://doi.org/10.1128/JB.183.15.4562-4570.2001

Zupok, A., Gorka, M., Siemiatkowska, B., Skirycz, A., & Leimkühler, S. (2019). Iron-dependent regulation of molybdenum cofactor biosynthesis genes in Escherichia coli. *Journal of Bacteriology*, *201*(17). https://doi.org/10.1128/JB.00382-19

7 Appendix

Table 7-1: The list of oligonucleotides was used for this study

sufA_ver_rev	CCAGGTTTTGACATCGTCAGT
moeB_ver_for	GAATGGGTGGAAGTAGAACCGT
moeB_ver_rev	CGTCTTATCAGGCCTGGAGGT
moeB_del_for (Cm)	GGCGAATGGGTGGAAGTAGAACCGTTTAACGCGTTGTTCGGAGG CCTGTAGTGTAGGCTGGAGCTGCTTC
moeB_del_rev (Cm)	TGCTGATGACGTGGCGGAGTGCCGCGTCTTATCAGGCCTGGAG GTGGCAAATGGGAATTAGCCATGGTCC
sufA_del_for (Cm)	TATCACTAACATGCTGTTATACGCTGAAAGCGATGAAGTGAGGTA AATCGGTGTAGGCTGGAGCTGCTTC
sufA_del_rev (Cm)	CCAGGTTTTGACATCGTCAGTTGCTTCAGTATTACGAGACATAGT ACCGCATGGGAATTAGCCATGGTCC
fnr_del_for (Cm)	CTAAAAAGATGTTAAAATTGACAAATATCAATTACGGCTTGAGCAG ACCTGTGTAGGCTGGAGCTGCTTC
fnr_del_rev (Cm)	TCAGAAAAATTTAATGATATGACAGAAGGATAGTGAGTTATGCGG AAAAAATGGGAATTAGCCATGGTCC
erpA_for_qPCR	TAACCCGAATCTGAAATTACGCG
erpA_rev_qPCR	GTATAATCAACGGAACCGCC
iscA_for_qPCR	TCTGGGCGTGAGAACCTCCG
iscA_rev_qPCR	AGCTGCGTACCGTCCAGAAA
sufA_for_qPCR	GTATGGTCGGCGTGCGCTTA
sufA_rev_qPCR	CGTGCCATCAATAAACGGCATCG
narG_for_qPCR	ACAAACTGCCGGTGAAACGC
narG_rev_qPCR	CACATCGTCATAGCTGGTTG
rrsa_qPCR_for	CTC TTG CCA TCG GAT GTG CCC A
rrsa_qPCR_rev	CCA GTG TGG CTG GTC ATC CTC TCA
torCAD (mut.1) TT to GG_for	CAGTGCCGCTGTTCATATGGGCTCATTAAGATCGC
torCAD (mut.1) TT to GG_rev	GCGATCTTAATGAGCCCATATGAACAGCGGCACTG
torCAD (mut.2) GCT to AAA_for	CAGTGCCGCTGTTCATATTTAAACATTAAGATCGC
torCAD (mut.2) GCT to AAA_rev	GCGATCTTAATGTTTAAATATGAACAGCGGCACTG
torCAD (mut.3) GCT to GAT_for	CAGTGCCGCTGTTCATATTTGATCATTAAGATCGCTTC
torCAD (mut.3) GCT to GAT_rev	GAAGCGATCTTAATGATCAAATATGAACAGCGGCACTG
torCAD (mut.4) TTGCT to GGAAA_for	CAGTGCCGCTGTTCATATGGAAACATTAAGATCGCTTC
torCAD (mut.4) TTGCT to GGAAA_rev	GAAGCGATCTTAATGTTTCCATATGAACAGCGGCACTG
iscA_cloning_for_NdeI	GCTCATATGCTGACGCTTTTTATCGCAACTCTCTACTG
iscA_cloning_rev_XhoI	GCCTCTCGAGTCAAACGTGGAAGCTTTCGCCG

moaABCDE_cloning_for_HINDIII	GCAAAGCTTCTGACGCTTTTTATCGCAACTCTCTACTG
moaABCDE_cloning_rev_XhoI	GCCTCTCGAGAACTACCAGCGTTTTGCCGCCTGCTG
sufA_cloning_for_BamHI	GCATGGATCCCTGACGCTTTTTATCGCAACTCTCTACTG
sufA_cloning_rev_XhoI	GCCTCTCGAGTTAGATACTAAAGGAAGAACCGCAAC
erpA_cloning_for_BamHI	GCATGGATCCCTGACGCTTTTTATCGCAACTCTCTACTG
erpA_cloning_rev_XhoI	GCCTCTCGAGCTATACCCCAAAGCTTTCGCCAC